



The Neoproterozoic tectonic evolution of the western Jiagenen Orogenic Belt and its Early Paleozoic-Mesozoic tectonic reworking

Chaolei Yan

► To cite this version:

Chaolei Yan. The Neoproterozoic tectonic evolution of the western Jiagenen Orogenic Belt and its Early Paleozoic-Mesozoic tectonic reworking. Earth Sciences. Université d'Orléans; Nanjing University (China), 2018. English. NNT : 2018ORLE2041 . tel-02436748

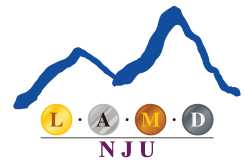
HAL Id: tel-02436748

<https://theses.hal.science/tel-02436748>

Submitted on 13 Jan 2020

HAL is a multi-disciplinary open access archive for the deposit and dissemination of scientific research documents, whether they are published or not. The documents may come from teaching and research institutions in France or abroad, or from public or private research centers.

L'archive ouverte pluridisciplinaire **HAL**, est destinée au dépôt et à la diffusion de documents scientifiques de niveau recherche, publiés ou non, émanant des établissements d'enseignement et de recherche français ou étrangers, des laboratoires publics ou privés.



ÉCOLE DOCTORALE
ENERGIE, MATERIAUX, SCIENCES DE LA TERRE ET DE L'UNIVERS
Institut des Sciences de la Terre d'Orléans
School of Earth Sciences and Engineering, Nanjing University

THÈSE EN COTUTELLE INTERNATIONALE présentée par:

Chaolei YAN

soutenue le **29 Octobre 2018**

pour obtenir le grade de

Docteur de l'Université d'Orléans et de l'Université de Nanjing

Discipline / Spécialité: Sciences de la Terre / Géodynamique

**The Neoproterozoic tectonic evolution of the western
Jiangnan Orogenic Belt and its Early Paleozoic-Mesozoic
tectonic reworking**

THÈSE dirigée par:

Cheng LI

Michel FAURE

Professeur, Nanjing University

Professeur, Université d'Orléans

RAPPORTEURS:

Zhenmin JIN

Mingguo ZHAI

Professeur, China University of Geoscience

Professeur, Institute of Geology and Geophysics, CAS

JURY (*y reporter tous les membres de jury présents à la soutenance*):

Zhenmin JIN

Mingguo ZHAI

Bruno SCAILLET

Hanlin CHEN

Wei LIN

Cheng LI

Yan CHEN

Liangshu SHU

Professeur, China University of Geoscience

Professeur, Institute of Geology and Geophysics, CAS

Directeur de Recherche, CNRS

Professeur, Zhejiang University

Professeur, Institute of Geology and Geophysics, CAS

Professeur, Nanjing University

Professeur, Université d'Orléans

Professeur, Nanjing University

Abstract

The South China Block is composed of two distinct tectonic domains: the Yangtze and Cathaysia blocks. The Jiangnan Orogenic Belt, marking the Neoproterozoic northeast-trending collisional suture of the Cathaysia Block with the Yangtze Block, is located at the southeastern margin of the Yangtze Block and separated from the Cathaysia Block to the southeast by the Jiangshan-Shaoxing fault zone.

In the Jiangnan Orogenic Belt, some geological facts are well recognised by geologists. An ophiolitic belt is exposed in the Dexing-Shexian area, the eastern Jiangnan region, named the northeast Jiangxi ophiolite, with an age cluster of 1.0-0.85 Ga. It is mainly composed of harzburgites, gabbros, blueschists and spilites. Besides, some mafic and intermediate rocks are identified in the Jiangnan region with apparent age cluster of 900-850 Ma. Moreover, peraluminous granitic plutons are sporadically exposed along the Jiangnan Orogenic Belt. In the Jiangnan Orogenic Belt, the oldest exposed strata belong to the Sibao group (equivalent to the Fanjingshan, Lengjiayi, lower Shuangqiaoshan, Shangxi and Shuangxiwu groups), which is unconformably covered by the Danzhou group (equivalent to the Xiajiang, Banxi, upper Shuangqiaoshan, Likou and Heshangzhen groups).

However, since [Guo et al. \(1984\)](#) firstly established the subduction mechanism in the Proterozoic and proposed the Jiangnan arc-basin system, there is no agreement on the tectonic evolution of the Jiangnan Orogenic Belt in the Neoproterozoic period. Over the past decades, advancements in research on the Jiangnan Orogenic Belt and Cathaysia Block led to the proposal of several tectonic models which also led to new controversies on the evolution of these two regions, as well as the timing of the collision of the Yangtze and Cathaysia blocks. There are mainly three kinds of hypotheses proposed by researchers.

Several geodynamic models

1. [Li et al. \(2002\)](#) suggested that the orogeny occurred at ca. 1.0, and was followed by a mantle plume activity ca. 825 Ma, on the basis of their geochronological and geochemical results. An ancient metamorphism in the South China Block was proposed with the consideration of 1300-1000 Ma zircon overgrowths and 1007 ± 14 Ma granitic gneiss of the samples from the Cathaysia Block, thus it was interpreted that a Grenvillian continental collision between the

Yangtze and Cathaysia blocks, which was named the Sibao Orogeny (equals to the Jiangnan Orogeny). Together with the muscovite $^{40}\text{Ar}/^{39}\text{Ar}$ results of the Tianli schists with ages ranging between 1042 ± 7 Ma and 1015 ± 4 Ma, it was proposed that the depositional age of the protolith of Tianli schist was older than 1042 Ma, as well as the Sibao Orogeny was older than the 1.0 Ga. Abundant granitoids and mafic-ultramafic intrusions were reported in the South China Block. The two major phases of widespread bimodal magmatism during the Neoproterozoic were dated at 830-795 Ma and 780-745 Ma. Geochemical studies of the mafic rocks display high $\epsilon\text{Nd}(\text{T})$ values of 3.3 to 5.3, therefore it was suggested that these magmatic rocks were derived from a mantle source. As a consequence, it was proposed that the South China Block was formed owing to the Sibao orogeny which brought the Yangtze and Cathaysia blocks together at ca. 1.0 Ga, and it subsequently underwent extensive continental rifting related to mantle plume or superplume activities beneath Rodinia since ca. 825 Ma.

2. However, another tectonic evolution model was proposed by [Zhou et al. \(2004\)](#). The authors mainly focused on the derivation of the mafic rocks in the Jiangnan Orogenic Belt and the depositional age of the Sibao group. A large amount of mafic rocks with high-Mg geochemical features, dated at ca. 830 Ma, was reported in the Jiangnan Orogenic Belt. Some researchers thought that they were generated from the mantle source, whereas, [Zhou et al. \(2004, 2009\)](#) pointed out that they were not related to the mantle plume but displayed arc-like geochemical features. Thus, the mafic rocks were thought to be the products of magmatism at a convergent plate boundary rather than derived from mantle plume. Another episode of the Neoproterozoic mafic magmatism was identified at 770-750 Ma, with the $\epsilon\text{Hf}(\text{t})$ values of 2.6-6.7, suggesting a post-collision extension event, only on the geochemical bases. Besides, typical S-type granite with high ACNK value (1.10-1.87) was dated at ca. 825 Ma. This magmatism was interpreted as the result of the collision between the Yangtze and Cathaysia blocks ([Wang et al., 2006](#)). Additionally, the dating of detrital zircons suggested a maximum depositional age of the Sibao group (and its equivalents), and Danzhou group (and its equivalents) at ca. 872 Ma and ca. 800 Ma, respectively, which indicates that the orogeny should be finished before ca. 800 Ma. As a consequence, the Early Neoproterozoic tectonic evolution of the Jiangnan Orogenic Belt suggested that: (1) the Neoproterozoic pillow lava and komatitic basalt were formed during the island arc magmatism (ca. 878–822 Ma) coeval with the sedimentation of the Sibao group; (2) the northwest-ward

subduction of the oceanic crust (before ca. 866–835Ma) with a peak at 866 Ma; (3) the sedimentation in the back-arc basin was at ca. 872–835Ma; (4) the collision between the Yangtze and Cathaysia blocks took place at ca. 835–820 Ma; (5) the post-collision extension occurred after ca. 820 Ma.

3. Meanwhile, another group hold divergent perspectives, due to numerous investigations on the detrital zircon, intermediate-mafic rocks, metamorphism, S-type granites and A-type granites carried out by Yao et al. (2017) The detrital zircon age spectra analysis on the Dengshan group (equals to the Sibao group) shows an age cluster at 1000–820 Ma with a peak at 850 Ma. Besides, the works on the intermediate-mafic rocks, e.g., Longsheng gabbro and diabase, Daolinshan dolerite and andesite, Shijiao diorite and gabbro, yielded apparent age of 880–860 Ma, which were interpreted as subduction-related products. Moreover, a metamorphic event was revealed by the Wanyuan paragneiss with a concordant weighted age of 860 Ma (zircon metamorphic rim, U-Pb method). The S-type granites in the Yuanbaoshan display the average of 830 Ma, indicating a collision event between the Yangtze and Cathaysia blocks. Whereas the A-type granites in the eastern Jiangnan Orogenic Belt give the crystallization age of 790 Ma, which complies with the Nanhua rifting event in the South China Block. Integrating the previous studies on the ca. 1.0 Ga ophiolites in the NE Jiangxi province, these authors proposed a tectonic evolution of the Jiangnan Orogenic Belt as following. The subduction of the Paleo South China Ocean occurred during the 1000–860 Ma, afterwards, the assembly of the Yangtze and Cathaysia blocks resulted in the Jiangnan Orogeny at ca. 860–800 Ma. Subsequently, the Jiangnan region was in a rifting setting since 800 Ma.

Existing problems

In spite of the various scenario proposed to explain the Neoproterozoic tectonic evolution of the Jiangnan Orogeny, there are still some problems to be clarified.

I) **What is the geological meaning and the depositional age of the Sibao group?** In the above mentioned tectonic evolution models, a few authors paid attention to the geological significance of the Sibao group. People essentially focused on the ages and source affinities of the mafic rocks, but ignored the geological meaning of the Sibao sediments. As it was coeval with the subduction of the Paleo-South China Ocean and the collision of the Yangtze and Cathaysia blocks, the Sibao group probably records the entire processes of the oceanic crust subduction and

Jiangnan Orogeny. If this assumption is accepted, the Sibao group should be initially deposited from ca. 1.0 Ga, however, [Wang et al. \(2007\)](#) and [Zhou et al. \(2009\)](#) used the youngest zircon grains to constrain the maximum depositional age of the Sibao group between 872 Ma and 860 Ma. Nevertheless, the meaning of the analysed samples is questionable. According to the stratigraphic columns of the Sibao group, the sampling localities for the oldest Sibao strata are more than 2.5 kilometers above the apparent bottom of the Sibao group, thus, these rocks cannot be utilized for determining the depositional age of the earliest (and lowermost part) of the Sibao group.

II) When did the Jiangnan Orogeny took place? Many perspectives have been studied on this subject. [Li et al. \(2002\)](#) proposed that the orogeny took place in the Mesoproterozoic according to the 1.3-1.0 Ga zircon overgrowth rims, and ca. 1.0 Ga metamorphic rocks in the Sichuan and Hainan, respectively. However, the results are not convincing, as Sichuan was located in the western margin of the Yangtze Block, those samples probably were not involved within the Jiangnan Orogeny, which is located in the southeastern margin of the Yangtze Block. Meanwhile, the Hainan block was recognised as an independent block, away from the Cathaysia Block ([Wang et al., 2015](#)), therefore, it had no relationship with the assembly of the Yangtze and Cathaysia blocks. The Neoproterozoic angular unconformities are thought as the marks of the orogeny. Recently, the detrital zircon analysis showed that the maximum age of the Danzhou group (the strata above the unconformity) is around 800 Ma, thus it was suggested as the upper limit of the Jiangnan Orogeny. With the consideration of the ca. 860-825 Ma mafic rocks and 830 Ma S-type granites, some researchers hold the view that the subduction was ongoing during the 860-830 Ma and the orogeny occurred at 830-800 Ma. However, there are some queries for this kind of model. (1) The angular unconformity can certainly be recognised as the consequence of the orogeny, we can qualitatively estimate that the orogeny finished before the sedimentation of the conglomerates, but the upper limit of the orogeny have to be further constrained by other evidence; (2) How can the subduction related mafic rocks at 860-825 Ma be coeval with the continental reworked peraluminous granites at 830 Ma? This is a paradox in the tectonic evolution model. According to the identification of the Cathodoluminescence (CL) images of the zircons from the mafic rocks, we found that some authors confused the acidic magma zircons as those observed in the mafic magmas. The mafic magma zircon should display broad band features rather than the clear oscillatory zoning as the granitic ones. Furthermore, the $\epsilon_{\text{Hf}}(t)$ values of the mafic zircons are

negative which is not the case for those zircons. Therefore, we should revisit the previously recognised 860-825 Ma mafic rocks and make a new interpretation of the Jiangnan Orogeny.

III) What is the emplacement mechanism of the post collisional granitic plutons? As the S-type granite is generally recognized as produced by partial melting and crystallization of crustal rocks, and it is commonly accepted as a syn- to late orogenic product. Peraluminous plutonism is recognised as the indication of the ending of the orogeny. However, so far, nobody paid attention to the emplacement mechanism of the peraluminous magma, which can provide another vision on the evolution of the orogeny. Therefore, to study the emplacement mechanism of the Neoproterozoic peraluminous magma in the Jiangnan region would be beneficial to understand the Jiangnan Orogeny.

IV) What is the geological evolution of the Jiangnan Belt after the collision? Usually, it was accepted that the South China underwent a rifting episode, called the Nanhua rift, during the 800-750 Ma period. After the Nanhua rifting, the entire South China was in a depositional setting until to 460 Ma, since then the Cathaysia block experienced an intraplate tectonic event, represented by N (or NW)-ward continental subduction, but the Yangtze block was in a stable depositional environment. The heterogeneity of the two blocks might probably be due to the difference in the rigidity of the Paleo- to Mesoproterozoic basement. Moreover, how the posterior tectonic events affected the Jiangnan Orogenic Belt deserves investigations.

In order to solve these problems, we choose the Neoproterozoic unconformity and S-type granite as targets to give a more precise and comprehensive understanding of the evolution of the Jiangnan Orogenic Belt from Neoproterozoic to Triassic.

Time constraints on the closure of the Paleo-South China Ocean and the Neoproterozoic assembly of the Yangtze and Cathaysia blocks: insight from detrital zircon analyses

The Early Neoproterozoic angular unconformity is well developed in the Jiangnan Orogenic Belt, but poorly exposed. We have visited almost all of the exposure of the Sibao and Danzhou groups (and their equivalents) in the western part of the Jiangnan Orogenic Belt, and then choose the best outcropped unconformities as study targets. We collected sandstone samples from four localities: Fanjingshan, Guizhou Province, Sanfang, Guangxi Province, Madiyi, Hunan Province and Yueyang, Hunan Province. The Danzhou group (and its equivalents) unconformably covered

on the Sibao group (and its equivalents), with distinct differences in deformation style. The Sibao group and its equivalents are deformed with N-S and NE-SW trending fold axes. Tight folds with vertical axes are also common at the outcrop scale. On the contrary to the Sibao group, the Danzhou group and its equivalents display gentle folds.

Thirteen representative samples were collected for the major and trace element analyses. In the Hf–La/Th plot, most samples of the Sibao group and its equivalents cluster around the average compositions of andesite, TTG, felsic volcanic rock and granite, which are the source provider for the Sibao group and its equivalents. In the plot of tectonic setting discriminant, all samples of the Sibao group and its equivalents drop in the active continental margin field, suggesting that the Sibao group and its equivalents were more likely deposited in an active continental margin. The prominent trace and rare earth elements characters of the Sibao group and its equivalents show distinct enrichment in light rare earth elements (LREE) with respect to heavy rare earth elements (HREE), and yield strong negative Ba, Sr and Nb anomalies. These features suggest that the top sequence of the Sibao group sediments was derived from an upper crustal source. The results yield that the bottom sequence of the Danzhou group inherited the bulk geochemical signature of the Sibao group and its equivalents, which indicates that the Sibao sediments supplied the material deposited in the Danzhou group.

We have collected a set of samples from the Sibao and Danzhou groups (and equivalents) from above and below the unconformity surface of the Fanjingshan, Sanfang and Madiyi areas for the detrital zircon age spectra analysis. The results of the six samples indicate that there are both similarity and dissimilarity between their detrital zircon spectra.

The age spectra among the Sibao group and its equivalents are consistent, with an age cluster at 1000–830 Ma, and display a distinct peak at ca. 855 Ma. The age spectra of the Danzhou group are also comparable, the data mostly range between 1000–780 Ma with at least two peaks, at 850 Ma and 790 Ma. Concerning the comparison between two different strata sequence, the Sibao and the Danzhou groups have a high similarity, showing that their detrital zircon ages are mostly concentrated within 1000 Ma. Moreover, in the interval of 1000–830 Ma, these two groups are particularly matched, not only with consistent steps, but also with the same age peak at 850 Ma.

However, when comparing the spectra among the individual sample with same period, we find that the sample of Danzhou group in the Sanfang area shows a distinct difference with other

two samples in the other areas. Apart from the two peaks at 850 Ma and 790 Ma as the others, it additionally displays a minor peak at 997 Ma, and shows the age marks at 2.5 Ga and ca. 1.8-1.6 Ga. Furthermore, comparing the age spectra of different groups, the Danzhou group and equivalents record more detrital zircon age information of 2.5 Ga and 2.0-1.5 Ga, moreover, the information of 800-780 Ma was only recorded in the Danzhou group, but not in the Sibao group, with a significant peak at 795 Ma.

The comparison of the detrital zircon age spectra of the Sibao and the Danzhou groups indicates that a magmatism occurred at a peak of 850 Ma and lasted until 820 Ma. However, during the period of 820-800 Ma, magmatism was rare in the Jiangnan region. Since 800 Ma, the magmatism in the Jiangnan region became active again, which is generally considered as related with the Nanhua Rifting.

Furthermore, in order to trace the detrital zircon age spectra information of the Yangtze block, Jiangnan Orogenic Belt, and the Cathaysia block, we have collected nearly 10,000 groups of data from previous studies, to carry out a statistical analysis of detrital zircon age distribution of these three regions. The detrital zircons are mainly collected from the following areas: Yangtze block (northern Guizhou, northern Hunan and Hubei), Jiangnan Orogenic Belt (Anhui, Jiangxi, Hunan, northwestern Guangxi, northeastern Guizhou) and Cathaysia block (Fujian, Guangdong), southeastern Hunan and southeastern Guangxi). The analytic results yield that the detrital zircon age spectrum of the Jiangnan Orogenic Belt is quite similar to that of the Yangtze block, but significantly different from that of the Cathaysia block. In the age spectra of the Yangtze Block and the Jiangnan Orogenic Belt, the ages are mainly distributed between 1000-820 Ma, with a peak range of 850-830 Ma. However, the spectrum of the Cathaysia Block is quite different from the other two, it clearly shows the age cluster of 1.5-1.0 Ga, which is missing in the Yangtze Block and the Jiangnan Orogenic Belt. In the range of 1000-820 Ma, the Cathaysia Block presents multiple peaks, including 970, 960, 930 and 840 Ma, which makes differences from the other two. Therefore, we can qualitatively determine that the Cathaysia Block was independent from the Yangtze Block at ca. 1.0 Ga.

The regional geological data show that the 1.0-0.88 Ga mafic rocks are sporadically outcropped in the Jiangnan region, and they are recognised as oceanic crust fragments and island-arc magmatic rocks, which indicate that the Paleo South China Ocean was in the

subduction. The age spectrum of detrital zircon can also be used for tracing the evolution of the Jiangnan region. Since ca. 1.0 Ga, the age trace of detrital zircon spectra of the Yangtze and Jiangnan regions has been increasingly changed, reflecting the magmatism acceleration in the Jiangnan region. However, such feature is not seen in the spectrum of the Cathaysia Block, indicating that the Cathaysia Block was still not close to the subduction zone at that time. By the comparison of the detrital zircon age spectra of the Yangtze, Jiangnan and Cathaysia regions, it is obvious that the age spectra of detrital zircon in these regions have a synchronous and rapid increase since 865 Ma, with peaks at around 840 Ma. And, it is worth noting that during the period of 865-820 Ma, the amount of detrital zircons in the Jiangnan region is approximately equal to the sum of those of the Yangtze and Cathaysia regions. Concerning the regional geological facts, 850-820 Ma S-type granites are distributed along the Jiangnan orogenic belt. Such granites are generally considered as the products of orogeny. Therefore, we suggest that the collision between the Yangtze and the Cathaysia blocks started at 865 Ma and ended at 820 Ma. During this period, an orogeny occurred throughout the whole Jiangnan area, volumes of peraluminum crustal granites were produced with a peak of magmatism at ca. 840-820 Ma. Due to the orogeny, the Jiangnan region uplifted, and it is the reason why many zircon information on 865-820 Ma can be recorded on both sides of the Yangtze and Cathaysia blocks.

Consequently, using the detrital zircon age spectrum analysis method to compare different strata in the same area, and comparing the contemporaneous strata in different regions, as well as combined with reliable geological evidence, we propose that the subduction of the Paleo South China Ocean initially occurred at ca. 1.0 Ga and lasted until ca. 865 Ma. Afterwards, the Yangtze and Cathaysia blocks collided to form the Jiangnan Orogenic Belt, and the Jiangnan orogeny lasted to 820 Ma. Afterwards, the Jiangnan Orogenic Belt was in a tectonic quiescence, without significant magmatism. Since 800 Ma, the Jiangnan region began to break owing to the Nanhua rifting. During the Neoproterozoic tectonic evolution of Jiangnan region, the sedimentation of the Sibao group can be divided into two stages, namely the oceanic crust subduction stage and the continent-continent collision one. Shortly after the beginning of the Nanhua rifting, the Jiangnan region entered into the sedimentary stage and the Danzhou group was formed.

The construction mechanism of the Sanfang-Yuanbaoshan granite plutons: insights from the Geological observation, Geochronology, AMS and Bouger gravity

modelling

Magmatic rock is an important constituent part of the continent crust, and magmatic activity plays a significant role in the recycling of crustal material and crust-mantle interaction. Therefore, it is essential to study the magmatism in order to obtain a better understanding of the magmatic process and the crustal evolution. Several aspects, such as: i) magma generation, ii) differentiation, iii) transport and ascent, and iv) emplacement, must be distinguished in the magmatic evolution. The magma emplacement is the last but an essential stage of the process. During the emplacement, some features documented both in the pluton and its country rocks reflect the interaction between the magma and the country rocks as well as the space needed for the magma emplacement. S-type granite is considered as a kind of granite produced by partial melting and crystallization of Al-rich rocks, such as crustal orthogneiss and pelitic sediments forming the lower to middle continental crust. It is commonly accepted that peraluminous magma is a syn- to post-orogenic product formed by the melting of the thickened orogenic root. However, S-type granite may also emplace in an intracontinental setting (e.g., most of the post-orogenic plutons in the Early Paleozoic orogen of SE China), and also in an active continental margin (for instance in the central Andes). In the Jiangnan Orogenic Belt, the peraluminous granite plutons crop out sporadically from east to west. In order to better constrain the Neoproterozoic evolution of the Jiangnan Orogeny, studies on the emplacement of the Neoproterozoic granite plutons along the Jiangnan Orogenic Belt as well as the detailed consideration of the pluton construction, syn-magmatic and syn (post)-tectonic events are necessary. Consequently, we choose the Sanfang and Yuanbaoshan plutons, located in the western part of the Jiangnan Orogenic Belt, as the study target to decipher the late stage of the evolution of the Jiangnan orogeny. We have carried out field observations, microscopic observations, geochronology, isotopy, rock magnetic investigations and gravity modelling methods to obtain a good understanding of the evolution processes of the plutons. The Sanfang pluton stands at a varying elevation ranging from ca. 200 meters to ca. 1800 meters, however, the elevation of the Yuanbao pluton attains to ca. 2000 meters. The granitic rocks of these two plutons mainly consist of quartz, plagioclase, K-feldspar, biotite and muscovite, thus they belong to a porphyritic monzogranite. According to the field observation, the granite plutons can be generally divided into two parts, namely, undeformed and deformed ones. The elevation of ca. 700 meters seems like the separatrix of the undeformed and deformed granites. Below the 700 meters, the

granites are visually isotropic and massive, but above the separatrix, the quartz and feldspar are deformed to augen, original magmatic structures are modified to gneissic structures. The deformation increases with the elevation. Neoproterozoic strata are well exposed in the Sanfang-Yuanbaoshan area, including the Sibao group, Danzhou group and Sinian strata. Generally, the Sinian strata and Danzhou group display broad and gentle folds. However, the Sibao group shows tight folds. Based on our field observations and thin-section investigations, the degrees of the metamorphism and deformation of the Sibao group are positively correlated to the elevation, this is comparable to the deformation of the granites.

In order to reveal the crystallization age and source of the magma, two samples were collected from the Sanfang and Yuanbaoshan plutons, respectively. Most of the data indicate U-Pb ages comprised between 820 to 850 Ma, with an average of 830 ± 2 Ma and 830 ± 5 Ma, respectively. More than half of the U-Pb dated zircons from the Sanfang granite were chosen for in-situ Hf isotopic analysis. The results show negative $\epsilon_{\text{Hf}}(t)$ values, ranging from -1.89 to -11.15, with an average of -4.63. Correspondingly, on the $\epsilon_{\text{Hf}}(t)$ versus U-Pb age plot, the two model ages ($T_{\text{DM}2}$) mainly concentrate on 1828–2143 Ma. These results indicate that the analyzed granitic rock was derived from the partial melting of Paleoproterozoic continental basement rocks, the involvement of a mantle component in the granitic magma was negligible.

Nine samples from the Sanfang pluton were selected for magnetic mineralogical analysis. This study reveals that magnetic susceptibility carriers in the Sanfang granite pluton are composed of ferromagnetic minerals, such as (titano) magnetite in multidomaine and hematite, with paramagnetic minerals, such as biotite, muscovite and feldspar. The magnetic fabrics of these minerals are comparable to the petrographic ones. Therefore, the Anisotropy of Magnetic Susceptibility (AMS) measurements will be an effective way to obtain the information of the petrofabrics of granite as well as the knowledge on the pluton emplacement. A total of 352 granitic oriented cores from 55 sites (35 and 20 for the Sanfang and Yuanbaoshan plutons, respectively) were sampled for the AMS study. According to the anisotropy degree (P_J), these two plutons can be grouped into two units, namely, magmatic and post-solidus ones, which correspond to the undeformed and deformed granites, respectively. For the magmatic one, the granites are "nearly isotropic". The microscopic observations show that the quartz grains are euhedral with very slightly undulose extinction. The biotites in the granites are magmatic without any post-solidus

deformation. These evidence suggests that the granite did not experienced a post-solidus deformation. Furthermore, 96% of the P_j values are lower than 1.1, which indicates that the magnetic fabrics are probably acquired during the magma crystalization, in agreement with the macroscopic and microscopic observations presented above. Therefore, we propose that the magnetic fabrics in this domain are primary, i.e. without any post-solidus overprint of posterior geological events. Therefore, they can be utilized for the interpretation of the magma flow and emplacement process.

In the western part of the Sanfang pluton, the magmatic foliations are consistently dipping to the E with steep angles (31-60 degrees), even near vertical angles (61-90°) for 2 sites. It is worthy to note that this general N-S oriented strike of foliations is consistent with the orientation of fold axes of the country rocks, i.e. the Sibao group. According to the magmatic lineations, this zone can be divided into two units, i.e., the lineations in the southern one mainly plunging in the E-W with steep angle, and those in the northern one mostly plunging in the N-S with gentle angles (0-30°). It may reflect that the magmatic lineations in the southern part are mainly dominated by the vertical and E-W directions, while those of the northern unit by the horizontal and meridional directions. In the central-southern part of the Sanfang pluton, the westward dipping magmatic foliations with steep angles and mainly W-dipping lineation possibly imply that the magma dominantly flowed steeply and accreted in the E-W direction. In the central-southern and a small fraction of northern parts of the Yuanbaoshan pluton, the strikes of the magmatic foliations are almost N-S directed with steep and even vertical angles, whereas the magmatic lineations are consistently N-S directed with gentle angles, suggesting that the magma might vertically ascend and gently or horizontally flow in the N-S direction (present coordinates). In addition, the shape parameter plot shows the ratio of about 1:1 between the oblate and prolate shapes, indicating the magmatic foliations and lineations were developed at a weak stress field, and thus we can speculate that the migration of magma. Moreover, the residual Bouguer gravity anomaly data show that the roots of the Sanfang and Yuanbaoshan plutons are located in their southern and central parts, respectively. The interpreted profiles suggest that these two plutons are constructed by the E-W lateral accumulation of N-S oriented dykes and the shape of two plutons are both N-S elongated tange- or sill-like, their thicknesses decrease northwards.

Consequently, we propose that the magma: (1) intruded into probably pre-existing

tectonically weak zones in the Sibao group; (2) ascended with steep to vertical angle and E-W laterally accumulated by N-S oriented dykes; (3) dominantly flowed from south to north with gentle angle to form the tongue- and/or sill-shaped plutons.

Early Paleozoic to Triassic geological events in the Sanfang-Yuanbaoshan area: insights from Argon isotopic records

By integrating the field observations, microscopic investigations and AMS studies, we find that the upper part (ca. 700 m above sea level) of the Sanfang-Yuanbaoshan plutons has experienced a post-solidus deformation, probably due to a posterior tectonic event, with foliations consistently dipping to the W in both of the granites and country rocks, and coherent lineations directed in the sub E-W. All of the kinematic indicators, i.e., shear band, augen structure, mica fish, S-C fabric and pressure shadows, reveal a top-to-the-W sense of shear. However, the timing of this ductile shearing is poorly constrained. As the muscovite and biotite are common in the plutons, we collect micas from two plutons for argon isotopic analysis, including both of deformed and undeformed muscovite and biotite.

The $^{40}\text{Ar}/^{39}\text{Ar}$ geochronological technique has significantly contributed to the study of crustal deformation, and was proved to be efficient to date deformed rocks by potassium-bearing minerals, e.g., muscovite, biotite, sericite and amphibole. Six samples have been selected for the argon isotopic analysis, including the deformed granites (muscovite and biotite), undeformed granites (biotite) and one mylonite (biotite) sample from country rocks. The argon isotopic analyses on the biotite and muscovite put high resolution $^{40}\text{Ar}/^{39}\text{Ar}$ time-constraints using both conventional step heating and in-situ UV laser techniques. Six single grains (125-250 μm) were analysed by $^{40}\text{Ar}/^{39}\text{Ar}$ step heating, including three granite biotite, two muscovite and one mylonite biotite. All the samples show well defined plateau ages with more than 70% of ^{39}Ar released, which provide the ages ranging from 413 to 392 Ma. As to the in-situ method, all of the analyses were on the sample of A37, collected from the Sanfang pluton. The sample targets were made as rock-chips and biotite aggregations. The biotites show a broad age range from 420 Ma to 240 Ma, with staircase shaped and decreasing trend. However, the muscovite mostly yield a flat release pattern at ca. 420 Ma, whereas only a small fraction of ages display the spectrum like the staircase with the maximum age of 450 Ma.

Many works on $^{40}\text{Ar}/^{39}\text{Ar}$ have been done across the SE South China Block in the

continental scale, including the Wuyi, Yunkai, Jiuling and Xuefengshan areas and yielded two significant age ranges, i.e., 450-390 Ma and 240-190 Ma. The early Paleozoic $^{40}\text{Ar}/^{39}\text{Ar}$ age range has been defined by previous study in ductile décollements and shear zones in the Cathaysia block, which were interpreted as the consequence of the Early Paleozoic intracontinental orogeny. Due to undeformed and unmetamorphosed Cambrian and Ordovician strata, many authors considered that the Jiangnan Orogenic Belt region has not been effected by the Silurian tectonic event. Nevertheless, [Xu et al. \(2015\)](#) and [Li et al. \(2016\)](#) recently reported the early Paleozoic age of micas (449-429 Ma) in the Neoproterozoic strata in the eastern Jiangnan region, i.e., the NE Jiangxi fault belt and eastern Jiuling area. In our study, the older age range of 450-400 Ma from the muscovite located in the shear band plays a first-order importance in both number and quality of our Ar-Ar dating. Our results is comparable with previous ones in the Cathaysia and eastern Jiangnan regions. Therefore, it is reasonable to assume that the muscovite (in our study region, the western Jiangnan Orogenic Belt) were deformed during the same period as those in the Cathaysia and eastern Jiangnan regions. This challenges the idea that the Jiangnan Orogenic Belt has escaped the Early Paleozoic tectonic event.

However, how to match this Paleozoic age with the undeformed Cambrian and Ordovician sedimentary sequence? Many researchers have investigated the rigidity of the Jiangnan Orogenic Belt and Cathaysia block, and reached an agreement that the Cathaysia block was made up by several sub-unit blocks with relatively weak rigidity. It seems that the case is different for the Jiangnan Orogenic Belt. Geophysical investigations show that the Jiangnan Orogenic Belt is underlain by the relatively homogeneous and rigid Yangtze basement. That is probably why we observe rarely the highly metamorphic and strongly deformed rocks in the Jiangnan Orogenic Belt but the 420 Ma $^{40}\text{Ar}/^{39}\text{Ar}$ results cover almost all the Cathaysia block. Meanwhile, all Ar-Ar data showing ca. 420 Ma ages within Proterozoic rocks are located along the Jiangnan Orogenic structures. This possibly indicate that the Jiangnan Orogenic Belt has been modified by the Paleozoic orogenic event, but locally instead of pervasively. In other words, the Paleozoic deformation is just localised in the limited zones, probably the old structures.

The alternative way to explain the age range at about 420 Ma by Ar-Ar dating may consider that this age concerns just a thermal phenomenon instead of deformation one, as the deformation of this age is still rarely observed in the Jiangnan Orogenic Belt, moreover, these observed ages

are from or near the Proterozoic plutons. The deformation is quasi localised around or in the plutons. One of scenario may be proposed as following. During the emplacement of these post-orogenic plutons, the progressive intrusion produced discontinuity and rheological heterogeneity in the crust. The zone where the materials in different reological behaviour (liquid magma, solidified granite and cold sedimentary crust) is where the deformation can easily take place, and this is often in the contact zone between country rocks and plutons. One of this kind of deformation concerns unroofing, i.e., the deformation in the contact zone as a décollement. The shearing band found in Sangfang and Yuanbaoshan may refer to this type of mechanism of deformation. Furthermore, all of this may take place in a depth where the temperature is higher than the mica closure ones. The later Paleozoic orogenic event exhumed plutons, and consequently the age of ca. 420 Ma was recorded by mica when they passed their closure temperature. In other words, the deformation of the shearing band was produced during the construction of the plutons, i.e., the syn-emplacement deformation.

To consider our in-situ biotite results (one sample), intermediate $^{40}\text{Ar}/^{39}\text{Ar}$ ages are progressively distributed between 420 and 240 Ma. They probably imply the mixed signature of partial inheritance and partial thermal overprint of mica. As the results showed, the progressively decreasing ages of biotite go down until to the range of 330-240 Ma. Generally, the closure temperatures of the biotite range from 350-260°C, with a 90°C interval. Assuming that the argon isotopic system in biotite was reset during the period of isobaric cooling, then we can quantitatively estimate the cooling rate of biotite. Using the interval of cooling temperatures (90°C) divided by the age differences (90 and 180 Ma, respectively), we can get the cooling rates of 1.00 °C/Ma and 0.50°C/Ma, respectively. Moreover, the step heating of single mica grains (different samples) yield a positive correlation between the $^{40}\text{Ar}/^{39}\text{Ar}$ age and elevation. Assuming that the closure temperature of the micas were completely induced by the geothermal, and therefore we can make an estimation of cooling rate by the formula with a constant geothermal gradient value of 30°C/Km:

$$R(T) = \frac{\Delta\text{Height}}{\Delta\text{Age}} \times 30 \text{ (}^{\circ}\text{C} \cdot \text{Km}^{-1}\text{)}$$

where the ΔHeight is the height difference, while the ΔAge is the difference of the $^{40}\text{Ar}/^{39}\text{Ar}$ age. In this way, we get the cooling rates of the biotite and muscovite at 0.97°C/Ma and 0.58°C/Ma,

respectively, which are comparable to those of the biotite aggregations. Such progressive decreasing apparent age spectra indicate that the study area was exhumed with a so low rate that this exhumation does not like to be produced by tectonic events since 420 Ma. Hence, it is suggested that the heat was almost sourced from geothermal. According to the slow cooling rates, therefore, we can furthermore infer that the exhumation of the crust was quite slow accommodated by isostatic re-equilibration due to erosion with an average rate interval of 16.7-33.3 meters per million years.

Through the $^{40}\text{Ar}/^{39}\text{Ar}$ analyses on the both deformed and undeformed muscovite and biotite from the Sanfang-Yuanbaoshan plutons, the early Paleozoic to Triassic geological events in this area can be concluded as following: (1) The 420 Ma $^{40}\text{Ar}/^{39}\text{Ar}$ age imply that: i) the shearing band on the upper part of plutons and their roof may be the consequence of the reactivation of Proterozoic structures reactivated by the Paleozoic orogeny; or ii) the exhumation of the study areas by the Paleozoic orogeny; (2) During the 420 Ma to 240 Ma period, the study areas have experienced a slow rate of exhumation which may correspond to the isostatic crustal re-equilibration.

Summary

Accordingly, the major conclusions of this thesis can be summarized as four points:

(1) In the regional view, the subduction of the Paleo-South China Ocean started at ca. 1000 Ma and ended at ca. 865 Ma. Afterwards, the Jiangnan Orogenic Belt was built up due to the assembly of the Yangtze and Cathaysia blocks between ca. 865 and 820 Ma;

(2) The 830 Ma granitic magma intruded into the pre-existing folds and faults in the Sibao group, the tongue- and/or sill-shaped plutons were constructed by an E-W lateral accumulation of N-S oriented dykes with a dominantly northward horizontal magma flow from south to north;

(3) A top-to-the-W ductile shearing event has been identified at the top of the plutons and their sedimentary roof. A coherent mica age of ca. 420 Ma has been obtained from the deformed muscovites of the Sanfang plutons by Ar-Ar dating. Two hypotheses are proposed: i) The shearing band on the upper part of plutons and their roof may be formed during the Early Paleozoic; or ii) The exhumation of the study areas by the Paleozoic orogeny;

(4) During the 420 Ma to 240 Ma period, the study area has experienced a slow rate of exhumation which may correspond to the isostatic crustal re-equilibration.

Our study provides a new look on the Neoproterozoic tectonic evolution of the Jiangnan Orogenic Belt, and a knowledge of the emplacement of the peraluminous magma, furthermore, it firstly detect the early Paleozoic-Mesozoic thermal events in the Sanfang and Yuanbaoshan areas. All of these will contribute to the advance in the understanding of the tectonic evolution of the Jiangnan Orogenic Belt.

Perspectives

In order to better constrain the tectonic evolution of the western Jiangnan Orogenic Belt or even the whole Jiangnan region, more details need to be clarified. Such as the depositional history of the Sibao group and its equivalents, what were the source of the sediments and how the source transported and then deposited? These answers are of great importance for us to have a bulk understanding of the subduction of the Paleo-South China Ocean. Besides, the metamorphism study of the sedimentary rocks, including the Sibao and Danzhou groups and their equivalents, and Sinian strata, would provide a new vision on exploring the significance of the ductile shearing event. Of course, to visit the eastern part of the Jiangnan Orogenic Belt is necessary if we want to have a bulk understanding of the tectonic evolution history of the whole Jiangnan Orogenic Belt.

Keywords: Jiangnan Orogenic Belt; Neoproterozoic unconformity; Sibao group; Danzhou group; S-type granite; Anisotropy of Magnetic Susceptibility; Gravity modelling; Magma emplacement mechanism; Ar-Ar isotopic dating.

Table of Contents

Abstract in English	I
Chapter 1. General introduction	1
1.1 Research status in the Jiangnan Orogenic Belt	1
1.1.1 Introduction of the Jiangnan Orogenic Belt.....	1
1.1.2 Previous study results: several tectonic evolution models of the Early Neoproterozoic period.....	2
1.1.2.1 The ca. 1.0 Ga Jiangnan Orogeny and ca. 825 Ma mantle plume activity.....	2
1.1.2.2 The ca. 880-835 Ma subduction and ca. 830-800 Ma collision.....	3
1.1.2.3 The ca. 1000-860 Ma subduction and ca. 860-800 Ma collision.....	4
1.1.3 The existing problems.....	11
1.1.3.1 What is the geological meaning and the depositional age of the Sibao group?	11
1.1.3.2 When did the Jiangnan Orogeny took place?	11
1.1.3.3 What is the emplacement mechanism of the post collisional granitic plutons?.....	13
1.1.3.4 What is the geological evolution of the Jiangnan Belt after the collision?	13
1.2 Overview of the study	13
1.2.1 Research purpose and contents	13
1.2.2 Research methodology.....	14
1.2.3 Workload of the study	15
1.2.4 Major findings and innovations	15
Chapter 2. Regional pre-Mesozoic geological setting of the South China.....	19
2.1 Tectonic units in the South China Block.....	19
2.1.1 The Yangzte Block	19

2.1.2 The Jiangnan Orogenic Belt	19
2.1.3 The Cathaysia Block.....	20
2.2 Neoproterozoic stratigraphic sequences of the South China Block	24
2.3 Regional angular unconformity in the Jiangnan Orogenic Belt.....	24
2.4 Comparison of the Sibao group (Pt3sb, and its equivalents) and Danzhou group (Pt3dz, and its equivalents) in the Jiangnan Orogenic Belt.....	26
2.5 Ophiolitic mélangé and magmatic events in the Jiangnan Orogenic Belt.....	27
2.6 Nanhua rift.....	28

Chapter 3. Time constraints on the closure of the Paleo–South China

Ocean and the Neoproterozoic assembly of the Yangtze and Cathaysia blocks: insight from new detrital zircon analyses 29

3.1 Introduction	29
3.2 Geological setting.....	30
3.3 Samples collection and analytical procedures.....	30
3.3.1 Sample collection.....	30
3.3.2 Analytical procedures	30
3.4 Analytical results.....	32
3.4.1 Major and trace elements.....	32
3.4.2 Zircon cathodoluminescence images	33
3.4.3 Detrital zircon U–Pb ages	34
3.4.3.1 Sibao group and its equivalents	34
3.4.3.2 Danzhou group and its equivalents	35
3.5 Discussion	39
3.5.1 Comparison of the age spectra between the Sibao and Danzhou groups and geological significance of the detrital zircon ages	39
3.5.2 Comparison of the detrital zircon age spectra of the Neoproterozoic strata in the South China Block.....	41

3.5.3 Significance of the geochemistry and sedimentation record of the Sibao group.....	43
3.5.4 Geodynamic evolution of the South China Block in the Early Neoproterozoic	48
3.6 Conclusions	50
Chapter 4. The construction mechanism of the Neoproterozoic S-type Sanfang-Yuanbaoshan granite plutons in the Jiangnan Orogenic Belt, South China: insights from the Geological observation, Geochronology, AMS and Bouger gravity modelling.....	65
4.1 Introduction of magmatisms of pluton emplacement and research objectives ..	65
4.2 Geological setting.....	68
4.2.1 The Jiangnan Orogenic Belt	68
4.2.2 Sanfang-Yuanbaoshan granite plutons	70
4.3 Field observations	70
4.3.1 Granite plutons.....	71
4.3.2 Country rocks.....	72
4.4 Microscopic observations.....	75
4.4.1 Granite plutons.....	76
4.4.2 Country rocks.....	77
4.5 Magma crystallization age and Hafnium isotopic analysis.....	77
4.5.1 Zircon U-Pb age.....	78
4.5.2 Zircon $\epsilon(\text{Hf})$ analysis	79
4.6 Rock magnetic investigation and results.....	87
4.6.1 Field sampling	87
4.6.2 Magnetic mineralogical analysis	87
4.6.3 AMS parameters	90
4.6.4 AMS results	95
4.7 Gravity modeling.....	98

4.8 Discussion on the construction process of the Sanfang-Yuanbaoshan plutons	104
4.8.1 Origin of the magma and its crystallization age	104
4.8.2 Origins of magnetic fabrics and its tectonic implications	105
4.8.3 Space creation and the mechanism of the magma emplacement.....	106
4.8.4 A top-to-the-W tectonic event	108
4.9 Conclusions	112
Chapter 5. Early Paleozoic to Triassic geological events in the	
 Sanfang-Yuanbaoshan, western Jiangnan region: the	
 Argon isotopic record	113
5.1 Introduction	113
5.2 Geological setting (Late Proterozoic to Triassic).....	114
5.3 Sample collection, description and analytical procedures	116
5.3.1 Sample collection.....	116
5.3.2 Sample description.....	118
5.3.2 Analytical procedure.....	120
5.4 Analytical results.....	122
5.4.1 Step heating	122
5.4.2 In situ UV laser	123
5.5 Discussion	124
5.5.1 Comparison of $^{40}\text{Ar}/^{39}\text{Ar}$ ages from the biotite and muscovite	125
5.5.2 Comparison of the results with previous $^{40}\text{Ar}/^{39}\text{Ar}$ thermochronological studies	126
5.5.3 Significance of the $^{40}\text{Ar}/^{39}\text{Ar}$ thermochronology: two stage events	132
5.5.3.1 Stage I: ductile shearing or crustal uplift in the Early Paleozoic...	132
5.5.3.2 Stage II: slow exhumation after the Early Paleozoic	134
5.6 Conclusions	138
Chapter 6. Conclusions and perspectives	139
6.1 Conclusions: tectonic evolution of the western Jiangnan Orogenic Belt.....	139

6.2 Perspectives	143
References	145
Publications	171
Acknowledgements	173

Chapter 1. General introduction

1.1 Research status in the Jiangnan Orogenic Belt

1.1.1 Introduction of the Jiangnan Orogenic Belt

The South China Block is composed of two distinct tectonic domains: the Yangtze and Cathaysia blocks. The Jiangnan Orogenic Belt, marking the Neoproterozoic northeast-trending collisional suture of the Cathaysia Block with the Yangtze Block, is located at the southeastern margin of the Yangtze Block and separated from the Cathaysia Block to the southeast by the Jiangshan-Shaoxing fault zone ([Figure 1-1; Shu, 2012; Zhao & Cawood, 2012](#)).

In the Jiangnan Orogenic Belt, some geological facts are well accepted by the geologists. An ophiolitic belt is exposed in the Dexing-Shexian area, eastern Jiangnan region, named the northeast Jiangxi ophiolite, with an age cluster of 1.0-0.9 Ga ([Shu et al., 1993; Xin et al., 2007](#)). It is mainly composed of harzburgites, gabbros, blueschists and spilites. Besides, some mafic and intermediate rocks are indentified in the Jiangnan region with two apparent age clusters of 900-860 Ma and 800-750 Ma, respectively ([Chen et al., 2009, 2018; Yao et al., 2014a, b](#)). Moreover, peraluminous granitic plutons are sporadically exposed along the Jiangnan Orogenic Belt. In the Jiangnan Orogenic Belt, the oldest exposed strata belong to the Sibao group (equivalent to the Fanjingshan, Lengjiayi, Shuangqiaoshan, Shangxi and Shuangxiwu groups), which is unconformably covered by the Danzhou group (equivalent to the Xiajiang, Banxi, Dengshan, Likou and Heshangzhen groups).

However, there is no agreement on the tectonic evolution of the Jiangnan Orogenic Belt in the Neoproterozoic period. Over the past decades, advancements in research on the Jiangnan Orogenic Belt and Cathaysia Block led to the proposal of several tectonic models which also led to new controversies on the evolution of these two regions, as well as the timing of the collision of the Yangtze and Cathaysia blocks

(e.g. Li et al., 2007, 2008a, b; Shu, 2006, 2012; Wang et al., 2006, 2007; Yao et al., 2012, 2013, 2014a, b).

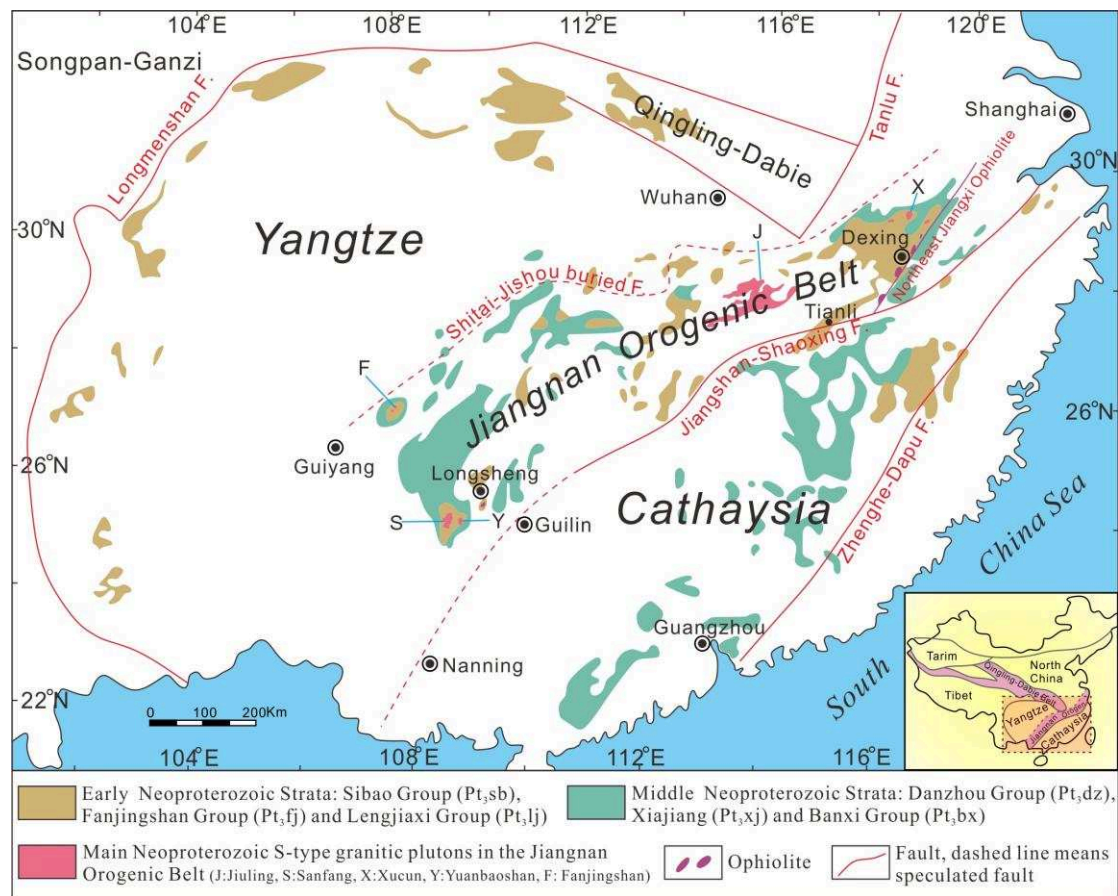


Figure 1-1. Simplified geological map of the South China showing the Yangtze and Cathaysia blocks separated by the Jiangnan Orogenic Belt.

1.1.2 Previous study results: several tectonic evolution models of the Early Neoproterozoic period

Many works have been carried out in the Jiangnan Orogenic Belt by several research teams, the most representative models are as follows (details are quoted in Table 1-1):

1.1.2.1 The ca. 1.0 Ga Jiangnan Orogeny and ca. 825 Ma mantle plume activity

An ancient metamorphism in the South China Block was proposed by Li et al. (2002), with the consideration of 1300-1000 Ma zircon overgrowths and 1007±14 Ma

granitic gneiss of the samples from the Cathaysia Block, thus it was interpreted that a Grenvillian continental collision between the Yangtze and Cathaysia blocks, which was named the Sibao Orogeny (equals to the Jiangnan Orogeny). Together with the muscovite $^{40}\text{Ar}/^{39}\text{Ar}$ results of the Tianli schists with ages ranging between 1042 ± 7 Ma and 1015 ± 4 Ma (Li et al., 2007), it was proposed that the depositional age of the protolith of Tianli schist was older than 1042 Ma, as well as the Sibao Orogeny was older than the 1.0 Ga. However, Ye et al. (2007) suggested that the timing of the Sibao Orogeny should be constrained at 1.0-0.9 Ga, by considering the geological facts of ~1.0 Ga ophiolites and ~0.97 Ga adakitic rocks from the northeastern Jiangxi. Comparing the Sibao Orogeny with other Meso- to Neoproterozoic orogenic belts, it was believed that the Sibao Orogen could be one of the Grenvillian sutures that brought Australia, Yangtze, Cathaysia and Laurentia together at ca. 1.0 Ga (Greentree et al., 2006).

Abundant granitoids and mafic-ultramafic intrusions were reported in the South China Block. The two major phases of widespread bimodal magmatism during the Neoproterozoic were dated at 830-795 Ma and 780-745 Ma, respectively (Li, 1999; Li et al., 2003a, b, 2005; Wang et al., 2009; Yang et al., 2015). Geochemical studies of the mafic rocks display high $\epsilon\text{Nd(T)}$ value of 3.3 to 5.3 and OIB-like features (Zhou et al., 2007), and it was suggested as derived from mantle source.

Therefore, it was proposed that the South China Block was formed owing to the Sibao orogeny which brought the Yangtze and Cathaysia blocks together at ca. 1.0 Ga, and it subsequently underwent extensive continental rifting, called the Nanhua rifting, related to mantle plume or superplume activities beneath Rodinia since ca. 825 Ma.

1.1.2.2 The ca. 880-835 Ma subduction and ca. 830-800 Ma collision

However, a totally different tectonic evolution model was proposed by Zhou et al. (2004) and Wang et al. (2007). The authors mainly focused on the derivation of the mafic rocks in the Jiangnan Orogenic Belt and the depositional age of the Sibao

group.

A quantity of mafic rocks at ca. 830 Ma was reported in the Jiangnan Orogenic Belt with high-Mg geochemical features, some researchers thought they were generated from the mantle source, whereas, [Zhou et al. \(2004, 2009\)](#) pointed out that they were not related to the mantle plume but display arc-like geochemical features. Thus the mafic rocks were thought to be the products of magmatism at a convergent plate boundary rather than derived from mantle plume. Another episode of Neoproterozoic mafic magmatism was identified at 770-750 Ma ([Chen et al., 2018](#)), with the $\epsilon\text{Hf}(t)$ values of 2.6-6.7, suggesting a post-collision extension event, only on the geochemical bases. Besides, typical S-type granite with high ACNK value (1.10-1.87) was dated at ca. 825 Ma ([Wang et al., 2006](#)). This magmatism was interpreted as the result of the collision between the Yangtze and Cathaysia blocks. Additionally, the dating of detrital zircons suggested a maximum depositional age of the Sibao group (and its equivalents), and Danzhou group (and its equivalents) at ca. 872 Ma and ca. 800 Ma, respectively ([Wang et al., 2007](#); [Zhou et al., 2009](#)), which indicates that the orogeny should be finished before at ca. 800 Ma.

As a consequence, the Early Neoproterozoic tectonic evolution of the Jiangnan Orogenic Belt suggested that: (1) the Neoproterozoic pillow lava and komatitic basalt were formed during the island arc magmatism (ca. 878–822 Ma) coeval with the sedimentation of the Sibao group; (2) northwest-ward subduction of the oceanic crust (before ca. 866–835Ma) with a peak at 866 Ma; (3) sedimentation in the back-arc basin was at ca. 872–835Ma; (4) collision between the Yangtze and Cathaysia blocks took place at ca. 835–820 Ma; (5) post-collision extension occurred after ca. 820 Ma.

1.1.2.3 The ca. 1000-860 Ma subduction and ca. 860-800 Ma collision

Meanwhile, another group hold divergent perspectives. Numerous investigations on the detrital zircon, intermediate-mafic rocks, metamorphism, S-type granites and A-type granites have been carried out by [Yao et al. \(2012, 2013, 2014a, b, c, 2015,](#)

2016a, b, 2017). The detrital zircon age spectra analysis on the Dengshan group (equals to the Sibao group) shows an age cluster at 1000-820 Ma with a peak at 850 Ma. Besides, the works on the intermediate-mafic rocks, e.g., Longsheng gabbro and diabase, Daolinshan dolerite and andesite, Shijiao diorite and gabbro, with the apparent age of 880-860 Ma, which are interpreted as subduction related products. Moreover, a metamorphism event is revealed by the Wanyuan paragneiss with a concordant weighted age of 860 Ma (zircon metamorphic rim, U-Pb method). The S-type granites in the Yuanbaoshan display the average of 830 Ma, indicating a collision event between the Yangtze and Cathaysia blocks. Whereas the A-type granites in the eastern Jiangnan Orogenic Belt give the crystallization age of 790 Ma, which complies with the Nanhua rifting event in the South China Block.

Accompanied with the previous studies on the ca. 1.0 Ga ophiolites in the NE Jiangxi province, the authors proposed a tectonic evolution of the Jiangnan Orogenic Belt as following. The subduction of the Paleo South China Ocean occurred during the 1000-860 Ma, afterwards, the assembly of the Yangtze and Cathaysia blocks resulted in the Jiangnan Orogeny at ca. 860–800 Ma. Subsequently, the Jiangnan region was in a rifting setting since 800 Ma.

Table 1-1. Representative models for the tectonic evolution of the Jiangnan Orogenic Belt

Publications	Locations	Results and perspectives	Conclusions
The ca. 1.0 Ga Jiangnan orogeny and ca. 825 Ma mantle plume activity			
Li, X.H., 1999, P.R.	Northern Guangxi	Sanfang and Yuanbaoshan granites with ASI of [1.18, 1.29] and low initial ϵNd values of $[-4.8, -7.6]$, are dated at $826 \pm 10\text{Ma}$ and $824 \pm 4\text{Ma}$, respectively.	Together with previous age determinations of ophiolites, the Neoproterozoic orogeny took place between 1.0 and 0.80 Ga, and likely ended at 0.82 Ga.
Li, Z.X., et al., 2002, Geology.	Hainan; Sichuan	The 1300–1000 Ma zircon overgrowths in sample collected from Hainan; The detrital zircon age spectra can be compared to those of Cathaysia block; The $1007 \pm 14\text{ Ma}$ granitic gneiss is interpreted formed in a foreland fold-and-thrust-belt setting.	Sibao orogen could be one of the Grenvillian sutures that brought Australia, Yangtze, and Cathaysia-Laurentia together by ca. 1000 Ma.
Li, X.H., et al., 2003a, P.R.	South China	The granitoids were essentially coeval with $\sim 825\text{ Ma}$ mafic/ultramafic intrusions in South China	The 825–820 Ma granitoids were formed by extensive crustal anatexis resulting from underplating and intrusion of basaltic magma caused by a mantle plume beneath South China at $\sim 825\text{ Ma}$.
Li, Z.X., et al., 2003b, P.R.	South China	Two major phases of widespread bimodal magmatism during the Neoproterozoic, i.e., ca. 830–795 Ma and ca. 780–745 Ma.	These magmatism as results of a mantle superplume beneath Rodinia, which was responsible for the breakup of the supercontinent during the Neoproterozoic.
Li, W.X., et al., 2005, P.R.	Zhejiang	SHRIMP U–Pb zircon data indicates that the Mamianshan bimodal volcanic rocks were formed at $818 \pm 9\text{ Ma}$. They were derived from an OIB-like mantle source with variable crustal contamination.	A coherent South China Craton was formed during the ca. 1.0 Ga Sibao Orogeny, and it subsequently underwent extensive continental rifting related to mantle plume or superplume activities beneath Rodinia since ca. 825 Ma.
M.R., Greentree, et al., 2006, P.R.	Yunnan	A tuff within the Laowushan Formation yielded a SHRIMP U–Pb zircon age of $1142 \pm 16\text{ Ma}$; Depositional age of the Kunyang Group is ca. 1000–960 Ma.	The Laowushan Formation and the Kunyang Group were deposited during separate basin-forming events.; The peak of Sibao Orogeny is ca. 1000–960 Ma.

Li, Z.X., et al., 2007, P.R.	Jiangxi	In situ UV laser $^{40}\text{Ar}/^{39}\text{Ar}$ results of the muscovites from the Tianli Schists give the ages of 1042 ± 7 Ma to 1015 ± 4 Ma; Muscovite/biotite cooling ages of ca. 968 ± 4 and 942 ± 8 Ma are recorded by deformed and recrystallised muscovite and biotite, respectively.	The depositional age of the protolith of Tianli schist is older than 1042 Ma; The Sibao Orogeny was diachronous: ≥ 1000 Ma in the western Sibao Orogen (Jiangnan Orogyn) and ca. 900 Ma in the eastern part.
Ye, M.F., et al., 2007, P.R.	Zhejiang	The Taohong and Xiqu tonalite–granodiorite stocks dated at 913 ± 15 Ma and 905 ± 14 Ma.	The timing of the Sibao orogenesis is thus believed to be between ~ 1.0 and ~ 0.9 Ga in its eastern segment.
Zhou, J.B., et al., 2007, P.R.	Guangxi and Hunan	The mafic igneous rocks are dated at ~ 765 Ma; Geochemical study shows high $\epsilon\text{Nd}(\text{T})$ value of 3.3 to 5.3 and OIB-type features.	The ~ 765 Ma mafic magmatic rocks were formed in a single continental rift setting related to the plume activities during the breakup of Rodinia.
Wang, X.C., et al., 2009, G.R.	South China	Widespread Neoproterozoic igneous rocks in South China are dated at ca. 825–760 Ma.	The 825-760 Ma igneous rocks are all related with the mantle plume.
Yang, C., et al., 2015, P.R.	Northern Guangxi	The zircons from the Sibao and Danzhou groups are of the similar Hf-O isotopic features.	The regional angular unconformity, separating the Sibao and Danzhou groups, may be related to the mantle plume at ca. 825 Ma.
The ca. 880-835 Ma subduction and ca. 830-800 Ma collision			
Wang, X.L., et al., 2004, P.R.	Northern Hunan	Basalts from Nanqiao are 1272 ± 2 Ma (Zhou et al., 2003), represent the fragments of the oceanic crust; Adesitic rocks in 814 ± 1 Ma (Wang et al., 2003) from Baolinchong, with strong depletions of Nb, Ti and enrichment of LILEs, are arc related; Granites from NE Hunan are post-collisional magmatism products.	Jiangnan orogen formed at 870-820 Ma; The granites are post-collisional products related to the slab breakoff, not to the superplume activities;
Zhou, J.C., et al., 2004, Geoc.J.	Northern Guangxi	Neoproterozoic mafic-ultramafic rocks 828 ± 7 Ma (Li, 1999) show mainly calc-alkaline features.	The mafic-ultramafic rocks are thought to be the products of magmatism of convergent plate boundary rather than derived from mantle plume.

Wang, X.L., et al., 2006, P.R.	Northern Guangxi	Typical S-type granites with high ACNK values (1.10–1.87), and are generally plotted in the collision-related areas in the tectonic discrimination diagrams.	The collision peak between the Yangtze and Cathaysia blocks happened in ca. 870–850 Ma. The 835–800 Ma granitoids and mafic rocks in Northern Guangxi are post- collisional.
Wang, X.L., et al., 2007a, P.R.	Northern Guangxi	The maximum depositional age of the Sibao and Danzhou groups are 860 and 800 Ma, respectively.	Jiangnan orogeny took place at 860–800 Ma
Wang, X.L., et al., 2008, G.R.	Northern Jiangxi	Depositional age for the Shuangqiaoshan Group is ca. 880 Ma; The ca. 800 Ma gabbros display arc-like geochemical features.	The gabbros may generate from the partial melting of juvenile crustal materials resulting from the early subduction
Zhou, J.C., et al., 2009, P.R.	Northern Guizhou	872±3Ma is considered as the maximum depositional age of Sibao group in the Fanjingshan.	(a) northwest-ward subduction of the oceanic crust (before ca. 866–835Ma); (b) sedimentation in the back-arc foreland basin (ca. 872–835Ma); (c) arc magmatism (ca. 878–822 Ma); (d) collision between the Yangtze and Cathaysia Blocks (ca. 835–820 Ma); (e) post-collision (after ca. 820Ma).
Chen, X., et al., 2014, Lithos.	Northern Guangxi	High-Mg diorites (MgO = 6.7–8.9 wt%) were discovered in the southern part of the ca. 830 Ma Dongma Pluton	The existence of subduction-related metasomatism in the western part of the Jiangnan orogen at ca. 830 Ma.
Wang, X.L., et al., 2014, P.R.	Whole Jiangnan	Detrital zircon ages give all of the basement sequences in the Jiangnan Orogen formed within the time span 860–825 Ma, in a tectonic setting that developed from back-arc basin to retro-arc foreland basin.	Final amalgamation of the Yangtze and Cathaysia blocks occurred no older than ca 825 Ma.
Li, J.Y., et al., 2016b, P.R.	Northern Jiangxi	The Anlelin and Xiushui formations were constrained to form in the periods of ca. 845–836 Ma and ca. 835–815 Ma, respectively.	An age gap of about 10 Myr or less between the Neoproterozoic basement sequences and the cover rifting-related sequences in the eastern Jiangnan Orogen
Chen, X., et al., 2018, P.R.	Northern Guangxi	Two episodes of Neoproterozoic mafic magmatism are indentified, namely, 830 Ma in the Baotan and 770 Ma in the Longsheng, which show the $\epsilon_{\text{Hf}}(t)$ values of [-6.3, -2.0] and [2.6, 6.7], respectively.	The two episodes of Neoproterozoic mafic magmatism imply the transition from a subduction regime to a post-orogenic extensional regime in the western segment of the Jiangnan Orogen

The ca. 1000-860 Ma subduction and ca. 860-800 Ma collision

Yao, J.L., et al., 2012, P.R.	Zhejiang	The granodiorite display two peaks at 847 ± 10 Ma and 827 ± 8 Ma with positive $\epsilon_{\text{Hf}}(t)$.	It is the imprint of the breakup of the Rodinia supercontinent in the Yangtze block.
Yao, J.L., et al., 2013, JAES.	Jiangxi; Zhejiang	The detrital zircon age spectrum of Dengshan group (equals to Sibao group) shows a peak at ca. 850 Ma.	The collision occurred at 860-800 Ma; The Yangtze and Cathaysia blocks assembled since 800 Ma.
Yao, J.L., et al., 2014a, JGSL.	Zhejiang	Zircons from the hornblende gneiss yielded weighted mean $^{206}\text{Pb}/^{238}\text{U}$ ages of 879 ± 10 Ma.	The assembly of the Yangtze and Cathaysia blocks was later than the 879 Ma.
Yao, J.L., et al., 2014b, P.R.	Guangxi	The intrusive gabbro is dated at 855 ± 6 Ma, whereas the S-type granite display the ages of 823 ± 6 Ma, 831 ± 5 Ma, 824 ± 6 Ma and 833 ± 6 Ma.	The subduction is interpreted during the 1000-860 Ma, and the collision is constrained at 850-800 Ma.
Yao, J.L., et al., 2014c, P.R.	Zhejiang	The A-type granite in Daolinshan display the age of 790 ± 6 Ma, and arc type dolerite is dated at 863 ± 7 Ma.	The subduction is constrained during the 1000-860 Ma, afterwards, the Jiangnan region was in a rifting setting since 790 Ma.
Yao, J.L., et al., 2015, P.R.	Jiangxi	The andesites yield weighted mean ages of 871-864 Ma, whereas the detrital zircons from the conglomerate yield a major age population of 863–810 Ma.	The subduction should be occurred during the 1000-860 Ma, and the collision is interpreted at 860-810 Ma.
Yao, J.L., et al., 2016a, J.G.	Guangxi	U-Pb zircon age data from the Longsheng gabbros and diabases yield crystallization ages of 869 ± 9 Ma, 867 ± 10 Ma and 863 ± 8 Ma, with positive $\epsilon_{\text{Hf}}(t)$ values.	The mafic rocks occur as exotic blocks derived from the subducting oceanic plate.
Yao, J.L., et al., 2016b, P.R.	Zhejiang	Zircons from quartz diorite and gabbro from the fault zone at Shijiao yield ages of 860-850 Ma, with positive $\epsilon_{\text{Hf}}(t)$ values.	The ca. 860–850 Ma rock suites were generated in a convergent plate margin.

Yao, J.L., et al., 2017, P.R.	Jiangxi	Detrital zircon grains from the Wanyuan paragneiss display metamorphic rims that yield concordant weighted average $^{206}\text{Pb}/^{238}\text{U}$ ages of 860 ± 6 Ma.	The metamorphism event indicates that the collision should take place at 860 ± 6 Ma.
----------------------------------	---------	--	---

1.1.3 The existing problems

Many researchers proposed various scenario to explain the Neoproterozoic tectonic evolution of the Jiangnan Orogeny event, however, there are still some problems to be clarified.

1.1.3.1 What is the geological meaning and the depositional age of the Sibao group?

In the above mentioned tectonic evolution models, few authors paid attention to the geological signification of the Sibao group. People essentially focused on the ages and source affinities of the mafic rocks but ignored the geological meaning of the Sibao sediments. As it was coeval with the subduction of the Paleo-South China Ocean and the collision, the Sibao group probably records the entire processes of the oceanic crust subduction and Jiangnan Orogeny collision.

If this assumption is accepted, the Sibao group should be initially deposited from ca. 1.0 Ga, however, [Wang et al. \(2007\)](#) and [Zhou et al. \(2009\)](#) used the youngest zircon grain to constrain the maximum depositional age of the Sibao group as 860 Ma and 872 Ma, respectively. Nevertheless, the meaning of the analysed samples is questionable. According to the stratigraphic columns of the Sibao group strata, quoted in the references, the sampling localities are more than 2.5 kilometers far away from the base of the Sibao group, these rocks cannot be utilized for delimiting the initial depositional age of the Sibao group.

1.1.3.2 When did the Jiangnan Orogeny took place?

Many perspectives have been suggested for the timing of the Jiangnan Orogeny. [Li et al. \(2002\)](#) proposed that the orogeny took place in the Mesoproterozoic according to the 1.3-1.0 Ga zircon overgrowth rims, and ca. 1.0 Ga metamorphic rocks in the Sichuan and Hainan, respectively. However, the results are not convincing, as Sichuan was located in the western margin of the Yangtze Block, those samples probably were not associated with the Jiangnan Orogeny in the southeastern

margin of the Yangtze Block. Meanwhile, the Hainan block was recognised as an independent block away from the Cathaysia Block (Wang et al., 2015), therefore, it had no relationship with the assembly of the Yangtze and Cathaysia blocks.

The Neoproterozoic angular unconformities are thought as the marks of the orogeny. Recently, the detrital zircon analysis showed that the maximum age of the Danzhou group (the strata above the unconformity) is around 800 Ma (Wang et al., 2007; Yao et al., 2013), thus it was suggested as the upper limit of the Jiangnan Orogeny. With the consideration of the ca. 860-825 Ma mafic rocks and 830 Ma S-type granites, some researchers hold the view that the subduction was ongoing during the 860-830 Ma and the orogeny occurred at 830-800 Ma.

However, there are some queries for this kind of model. (1) The angular unconformities can certainly be recognised as the products of the orogeny, we can qualitatively estimate that the orogeny finished before the sedimentation of the conglomerates, but the upper limit of the orogeny should be further constrained by the other evidence; (2) How can the subduction related mafic rocks at 860-825 Ma be coeval with the continental reworked peraluminous granites at 830 Ma? This is a paradox in the tectonic evolution model. According to the identification of the Cathodoluminescence (CL) images of the zircons from the mafic rocks, we found that some authors confused the acidic magma zircons as those observed in the mafic magmas. The mafic magma zircon should display broad band features rather than the clear oscillatory zoning as the granitic ones (Wu & Zheng, 2004). Furthermore, the $\epsilon_{\text{Hf}}(t)$ values of the mafic zircons are negative which is not the case for those zircons (Chen et al., 2018).

Therefore, we should revisit the previously recognised 860-825 Ma mafic rocks and make a new interpretation of the Jiangnan Orogeny.

1.1.3.3 What is the emplacement mechanism of the post collisional granitic plutons?

As the S-type granite is generally recognized as produced by partial melting and crystallization of crustal rocks, and it is commonly accepted as a product of the post orogeny ([Chappell and White, 2001](#)). It can be recognised as the indication of the ending of the orogeny. However, so far, nobody paid attention to the emplacement mechanism of the peraluminous magma, which can provide another vision on the evolution of the orogeny. Therefore, to study the emplacement mechanism of the Neoproterozoic peraluminous magma in the Jiangnan region would be beneficial to understand the Jiangnan Orogeny.

1.1.3.4 What is the geological evolution of the Jiangnan Belt after the collision?

Usually, it was accepted that the South China underwent a rifting episode, called the Nanhua rift, during the 800-750 Ma period ([Shu, 2012](#); [Yan et al., 2017](#)). After Nanhua rifting, the entire South China was in a depositional setting until to 460 Ma, since then the Cathaysia block experienced extensive and strong intraplate tectonic event, but the Yangtze block was in a stable depositional environment. The heterogeneity of the two blocks might probably be due to the difference in the rigidity of the Paleo- to Mesoproterozoic basement ([Liu, 2017](#); [Shu, 2012](#)). Moreover, how the posterior tectonic events affect the Jiangnan Orogenic Belt is interesting to make investigations.

Moreover, how the posterior tectonic events affect the Jiangnan Orogenic Belt is interesting to make investigations.

1.2 Overview of the study

1.2.1 Research purpose and contents

As the Jiangnan Orogenic Belt plays a key role in the tectonic framework of the South China Block. Over the past decades, advances in research on the Jiangnan

Orogen led authors to propose several controversial tectonic models. Therefore, some issues remain to be clarified, including the timing of the orogeny, the signification of the Sibao group, the emplacement mechanism of the post orogeny magma and the modification of the Jiangnan Orogenic Belt by posterior tectonic events.

The Sibao group is unconformably covered by the Danzhou group in the Jiangnan region. We have visited almost all of the exposure of the Sibao and Danzhou groups in the western part of the Jiangnan Orogenic Belt, and then choose the best outcropped unconformities as study targets.

Meanwhile, the S-type granites are not well exposed except in the Sanfang and Yuanbaoshan areas, the plutons seem like two brothers, with an area of ca. 1000 km² and ca. 300 km², respectively. So they are good targets for the magma emplacement study.

Furthermore, the micas are common in the granites, and we have collected some samples for the argon isotopic analysis to see the undiscovered informations.

1.2.2 Research methodology

Since we have chosen unconformities and S-type granite plutons as the targets, in order to decipher the unclarified scientific problems, some methods have been utilized as following:

(1) Detailed field observations in four areas, including Fanjingshan, Sanfang, Madiyi and Yueyang, from west to east, to get an overview of the Jiangnan Orogenic Belt, and investigate the similarities and differences of the unconformities in different geological units among these areas;

(2) The studies of mineral composition, deformation and metamorphism on the Sibao and Danzhou groups and their equivalents, to recognize their differences;

(3) Geochemical investigation of the Sibao and Danzhou groups, aiming to reveal their protolith source and tectonic setting;

- (4) Cathodoluminescence imaging of zircons, to identify their origin;
- (5) Detrital zircon age spectra analysis from the Sibao and Danzhou groups, to reveal their differences in detritic source. And age spectra comparison among three tectonic units, namely, the Yangtze, Jiangnan and Cathaysia, to understand the subduction and collision processes;
- (6) Geochronological and hafnium isotopic investigation on the Sanfang and Yuanbaoshan granitic plutons, to reveal the crystallization age and source of the magma;
- (7) Magnetic minerals analysis on the granites, to identify carriers of magnetic susceptibility;
- (8) Measurement of the Anisotropy of Magnetic Susceptibility (AMS), to determine the magma flow behaviors and the tectonic setting of pluton emplacement;
- (9) Gravity modelling, to reveal the deep structures of the plutons;
- (10) Ar-Ar isotopic analysis on the micas, to investigate the possible tectonic events posterior to the pluton emplacement.

1.2.3 Workload of the study

Detailed workload can be referred to [Table 1-2](#).

1.2.4 Major findings and innovations

Based on the previous studies, the major findings and innovations in this study are summarized as following:

- (1) The subduction of the Paleo–South China Ocean started at ca. 1000 Ma and ended at ca. 865 Ma. Afterwards, the Jiangnan Orogenic Belt was built up due to the assembly of the Yangtze and Cathaysia blocks between ca. 865 and 820 Ma;
- (2) The deposition environment of the Early Neoproterozoic Sibao group and its equivalents can be divided into two stages. Firstly, they were deposited in an active

continental margin in the period of ca. 1000–865 Ma. Then, their upper part was accumulated in a collisional setting in the period of ca. 865–820 Ma;

(3) The Danzhou group and its equivalents began to deposit since ca. 780 Ma after the Jiangnan Orogeny;

(4) The magnetic fabrics of the Sanfang and Yuanbaoshan plutons can be characterized the primary magmatic fabric and secondary post-solidus one, indicating that the plutons have probably experienced polyphased tectonic events;

(5) The magma of the plutons was derived from crust materials and crystallized at 830 Ma, and intruded probably along pre-existing N-S oriented tectonic (fold/fault) structures in a relatively weak extensional setting.

(6) The gravity anomaly modeling suggests that the plutons might be constructed by an E-W lateral accumulation of N-S oriented dykes, and the magma might flow from south to north horizontally to build tongue- or sill-shaped plutons;

(7) A top-to-the-W ductile shearing event took place after the magma emplacement, however, the timing of it is unclear;

(8) Ar-Ar results of the muscovites and biotites reveal that the ductile shearing event possibly took place during the magma emplacement or at ca. 420 Ma, afterwards, the crust cooled down slowly during the 420 Ma to 240 Ma, probably due to the slow uplift of the crust in the Sanfang-Yuanbaoshan area.

Table 1-2. Workload of the study

Content	Unit	Number	Notes
Field observation	zone	4	Fanjingshan, Sanfang-Yuanbaoshan, Madiyi and Yueyang
	day	>120	More than 120 days, in seven times
Photos	piece	>700	Unconformity, fold, foliation, lineation, kinematic, deformed and undeformed granite, etc.
Thin section	piece	160	Including the orientated and non-orientated samples of Sibao and Danzhou groups, and granites
Major and trace element	sample	12	Including the samples of Sibao and Danzhou groups
Cathodoluminescence	grain	>400	Including the detrital zircons for the Sibao and Danzhou groups, and magmatic zircons for the granites
Zircon U-Pb age	sample	6	Including the detrital zircons for the Sibao and Danzhou groups, and magmatic zircons for the granites
Hafnium isotopic	sample	1	19 spots on the zircons from the Sanfang pluton
AMS measurment	site (core)	55 (352)	35 (228) and 20 (124) samples for the Sanfang and Yuanbaoshan plutons, respectively
Magnetic mineralogical analysis	sample	9	Hysteresis loop curve (3), IRM (4), Thermo-magnetic (2), and EPMA (1)
Density measurment	sample	64	Including the Sibao group, Danzhou group, Sinian strata and Sanfang-Yuanbaoshan granites
Gravity modeling	profile	5	2 E-W directed profiles and 3 N-S profiles across the two plutons
Ar-Ar	sample	17	Including the deformed and undeformed granites, as well as muscovite and biotite

Chapter 2. Regional pre-Mesozoic geological setting of the South China

2.1 Tectonic units in the South China Block

2.1.1 The Yangtze Block

The Yangtze Block is limited to the North China Craton by the Qinlin–Dabie orogen. To the northwest, the Yangtze Block is separated from the Songpan–Ganzi by the Triassic Longmenshan Belt that contains a Proterozoic basement ([Figure 2-1](#); [Zhao & Cawood, 2012](#); [Xue et al., 2017](#)). The Sedimentary cover is well developed in the central part of the Yangtze Block. It is mainly composed of sandstone, conglomerate and tillite in the lower Sinian strata, and carbonate rocks, Cambrian argillaceous shale and graptolite shale in the upper Sinian and Ordovician strata. In the Devonian to Middle Triassic strata, a suit of marine sedimentary structure is developed with carbonate ([Bai & Zhu, 1996](#)). However, the ancient rocks are exposed along the tectonic boundary of the Yangtze Block. The Archean basement beneath the Yangtze Block is revealed based on the geochronology and Hf isotope composition of xenocrystic zircons ([Zhang et al., 2006](#); [Zheng et al., 2006](#)). Paleoproterozoic metamorphism is recorded by the meta-sedimentary rocks of the Kongling complex ([Zhang et al., 2006](#)). Paleo- to Mesoproterozoic strata mainly exposed in the western Yangtze Block, being represented by the ~1.7 Ga Dongchuan and ~1.0 Ga Huili Groups ([Sun et al., 2009](#)).

2.1.2 The Jiangnan Orogenic Belt

The Jiangnan Orogenic Belt locates in the southeastern margin of the Yangtze Block, tracing the northwestward subduction of the Paleo–South China Ocean and the collision between the Yangtze and Cathaysia blocks (e.g., [Charvet, 2013](#); [Guo & Gao, 2017](#); [Guo et al., 1989](#); [Li et al., 2007](#); [Shu, 2012](#); [Shu et al., 1995, 2014, 2015](#); [Wang et al., 2007](#); [Yan et al., 2015](#); [Yao et al., 2014a](#); [Zhao & Cawood, 2012](#)). The Paleo–South China Ocean subducted beneath the Yangtze Block since ca. 1000 Ma ([Wang et al.,](#)

2007, 2008; Yao et al., 2014b), and the final closure of the Paleo–South China Ocean resulted in the collision between the Jiangnan magmatic arc and the Cathaysia Block (Shu, 2012; Wang et al., 2012b). Numerous ultramafic, mafic magmatic (gabbro, diorite), and volcanic rocks, interpreted as ophiolites, dated from ca. 1000 Ma to ca. 870 Ma, distribute along the suture zone (BGMRAH, 1982; BGMRJX, 1984; BGMRZJ, 1989; Xia et al., 2018). In the Dexing–Shexian area of the eastern part of the Jiangnan belt, blueschists are dated at 866 ± 14 Ma by K–Ar on glaucophane (Shu et al, 1994; Shu & Charvet, 1996). The collision led to the important deformation of the Sibao group and its equivalents (see Section 2.2; BGMRGX, 1985; BGMRHN, 1988). Afterwards, the Jiangnan Orogenic Belt was intruded by peraluminous granite plutons dated at ca. 850–830 Ma (e.g., Xucun pluton, Jiuling pluton, Yuanbaoshan pluton, Sanfang pluton; Figure 2-1) along the Jiangnan Orogen (Guo et al., 1989; Xin et al., 2017; Yao et al., 2014b; Zhang et al., 2013 ; Zhou et al., 2009). After the formation of the South China Block, this continent started to rift probably reworking the pre–existing faults related to the Jiangnan Orogeny. The NE–SW striking Nanhua rifting was coeval with the generation of ca. 800 Ma–750 Ma bimodal igneous rocks (Li et al., 2018; Wang & Li, 2003; Xia et al., 2018; Zhang et al., 2018).

However, previous study show the Early Paleozoic tectono-thermal event is not developed in the Jiangnan Orogenic Belt where the Early Paleozoic strata did not experience any significant metamorphism, and only underwent slight brittle deformation, together with weak magmatism (Yan et al., 2017).

2.1.3 The Cathaysia Block

Compared to the Jiangnan Orogenic Belt, the Cathaysia block displays distinct geological features that are characterized by large scaled middle–high–grade metamorphic rocks and several Paleoproterozoic plutons (Figure 2-1; Xu et al., 2007; Yu et al., 2009). Recent studies suggest that the Cathaysia Block experienced poly–phase tectonic and magmatic events, corresponding to the assembly and breakup of the Proterozoic supercontinents Columbia, Rodinia and Gondwana (Li, 1997; Li et

al., 2002, 2003a, b, 2005; Shu, 2012; Shu et al., 2008; Zhao & Cawood, 2012). Among three major Proterozoic distinct tectonic domains in the Cathaysia Block, it exists in the Wuyi domain a Paleo–Mesoproterozoic continental core that is composed of migmatites, gneisses, granitic gneisses, schists, leptynites and leptites, along with minor Neoproterozoic clastic rocks, spilites and basalts (Shu, 2006), whereas the Nanling and Yunkai domains develop Neoproterozoic slates, phyllites, spilites, basalts, rhyolites and clastic rocks (Yu et al., 2009).

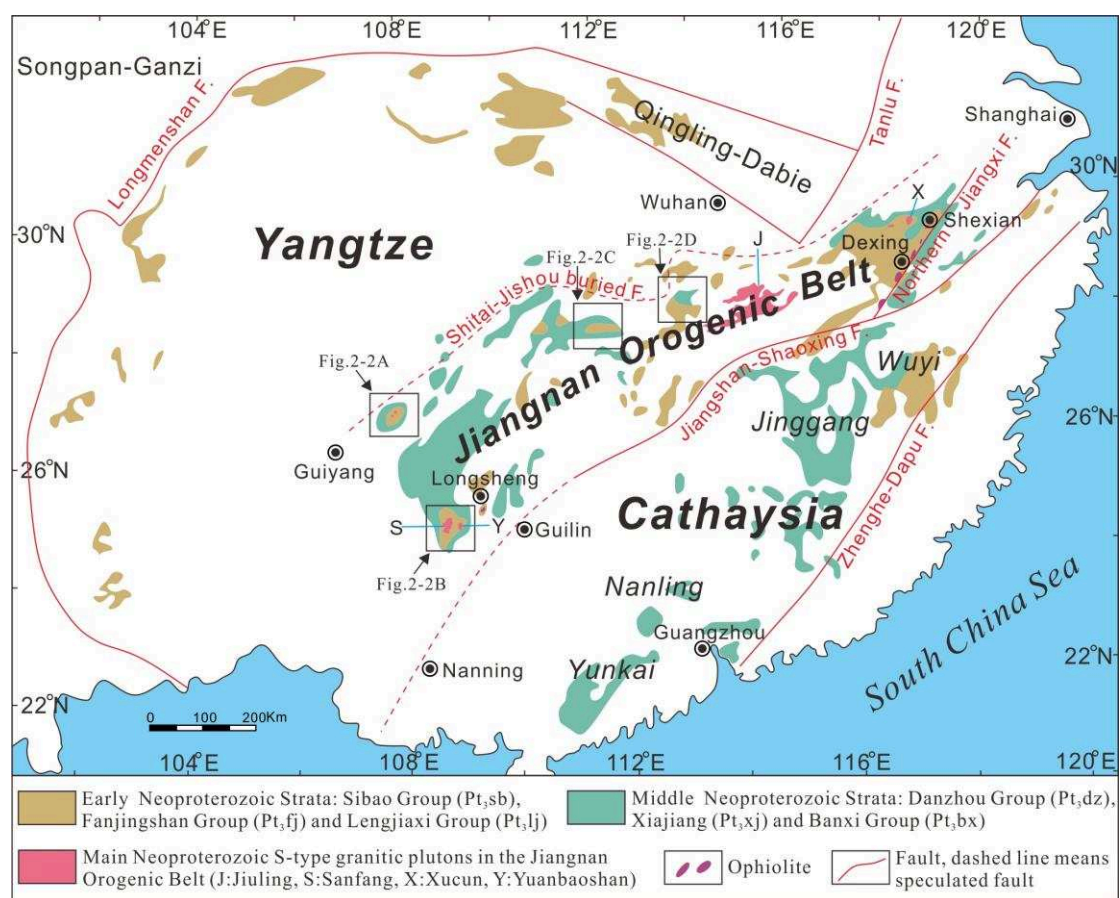


Figure 2-1. Tectonic outline of China and geological sketch map of the Yangtze and Cathaysia blocks.

During the Silurian, extensive folding, thrusting, metamorphism and anatexis developed. The early Paleozoic intracontinental tectono–thermal event in the Cathaysia block (Charvet et al., 2010; Faure et al., 2009; Shu et al., 2014) resulted in large–scale granitic magmatism, strong folding–ductile deformation dated at 440–400

Ma and a regional scale middle Devonian angular unconformity (Shu, 2012; Shu et al., 2008). These features are well recorded in the Wuyi, Jinggang, Nanling and Yunkai areas (Figure 2-1). The maximum shortening can reach up to 67% in the Jinggang and Wuyi belts (Charvet et al., 2010; Shu, 2012; Shu et al., 2008, 2015). Fold axes dominantly strike in the E–W direction. The kinematic analysis in the Jinggang and Wuyi domains shows that the ductile shearing was directed to the S or SE, however, a northwestward vergence may develop in the northwestern part of the belt.

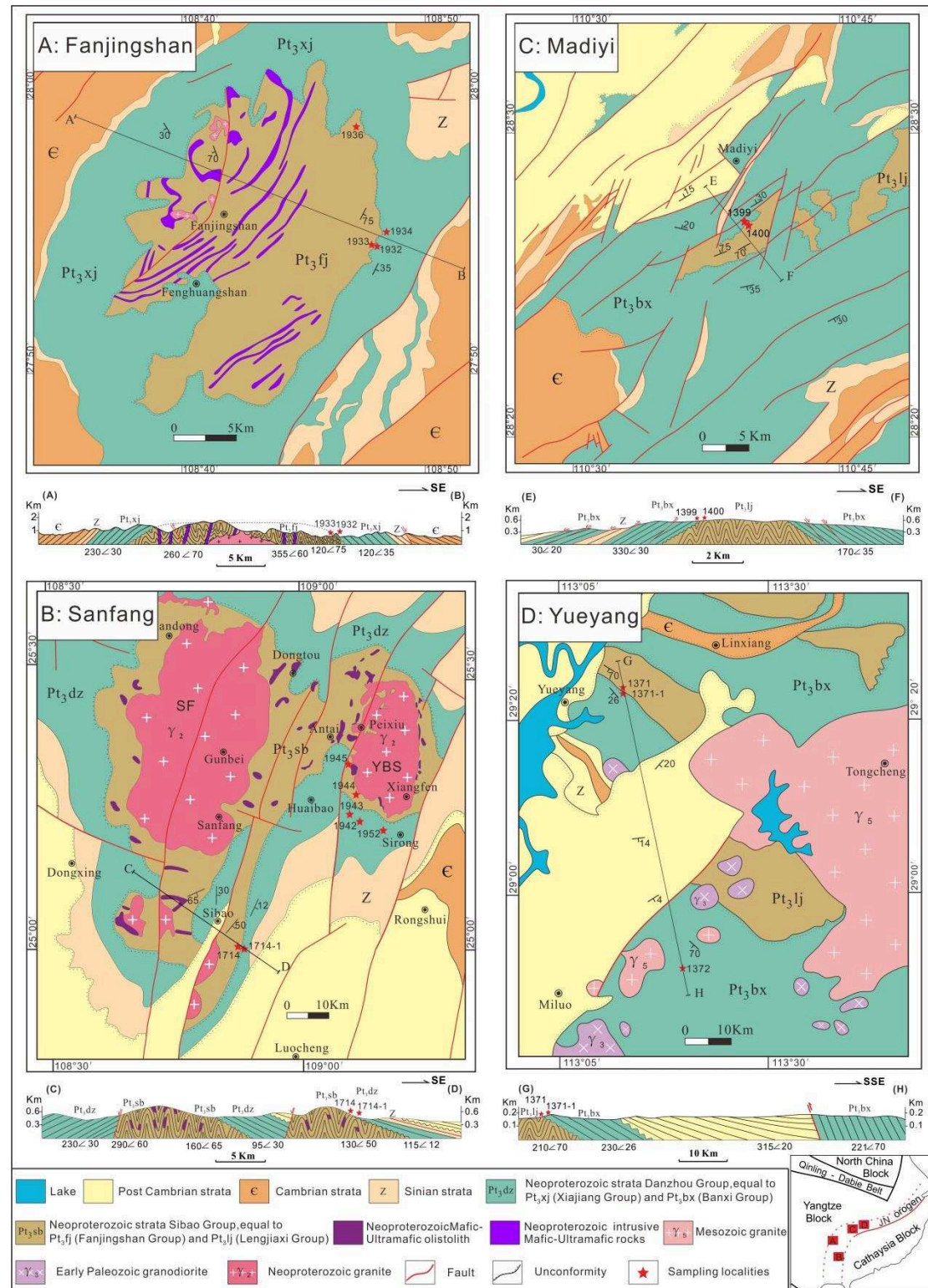


Figure 2-2. Geological sketch maps and cross-sections with sampling locations for (A) the Fanjingshan, (B) Sanfang, (C) Madiyi and (D) Yueyang areas.

2.2 Neoproterozoic stratigraphic sequences of the South China Block

In South China, the early Neoproterozoic strata (contemporary with the Sibao group) distributes geographically in three parts. One part that crops out in the northern and western boundaries of the Yangtze Block ([Figures 2-1 and 2-2](#)) mainly consists of sandstone and mudstone ([Wang & Li, 2003](#)). The second part, exposed within the Jiangnan Orogen, is characterized by greywacke, sandstone, mudstone enclosing mafic and ultramafic blocks. This part is generally interpreted as the result of the assembly of the Paleo–South China Ocean and the Yangtze Block ([Shu et al., 2014](#); [Yao et al., 2014b](#); [Wang et al., 2012a](#); [Zhou et al., 2009](#)). The third part is sporadically exposed in the Cathaysia Block, particularly in the north of the Fujian province. It involves terrigenous clastic rocks interlayered with volcanic rocks ([BGMRFJ, 1985](#); [Xu et al., 2010](#)).

During the middle Neoproterozoic rifting of the unified South China Block, more than 5 km-thick terrigenous and volcano-clastic series were deposited. Although the formation names, such as Banxi, Danzhou and Xiajiang groups, vary depending on the Provinces, they are petrographically and structurally equivalent ([BGMRGX, 1985](#); [BGMRGZ, 1984](#); [BGMRHN, 1988](#)). According to sedimentology, at that time, a littoral-neritic depositional environment characterized the whole South China Block ([Shu, 2012](#)). However, the water depth in the Jiangnan region was deeper than that in the Yangtze and Cathaysia regions ([Wang & Li, 2003](#); [Xu et al., 2010](#)). The middle Neoproterozoic strata are mainly composed of fine grain conglomerate, sandstone and siltstone, and widely exposed in the Jiangnan and the Cathaysia regions but rarely revealed in the Yangtze region ([Zhao & Cawood, 2012](#)).

2.3 Regional angular unconformity in the Jiangnan Orogenic Belt

The Early Neoproterozoic angular unconformity is well developed in the Jiangnan Orogenic Belt, but poorly exposed. The representative outcrops can be traced in Lantian, Anhui province; Yiyang, Jiangxi province; Yueyang and Madiyi, Hunan province; Sibao, Guangxi province; and Fanjingshan, Guizhou province, from

the eastern Jiangnan Orogenic Belt to the western part. The Danzhou group (and its equivalents) unconformably covered on the Sibao group (and its equivalents), with distinct differences in the lithology and deformation style (Figure 2-3).

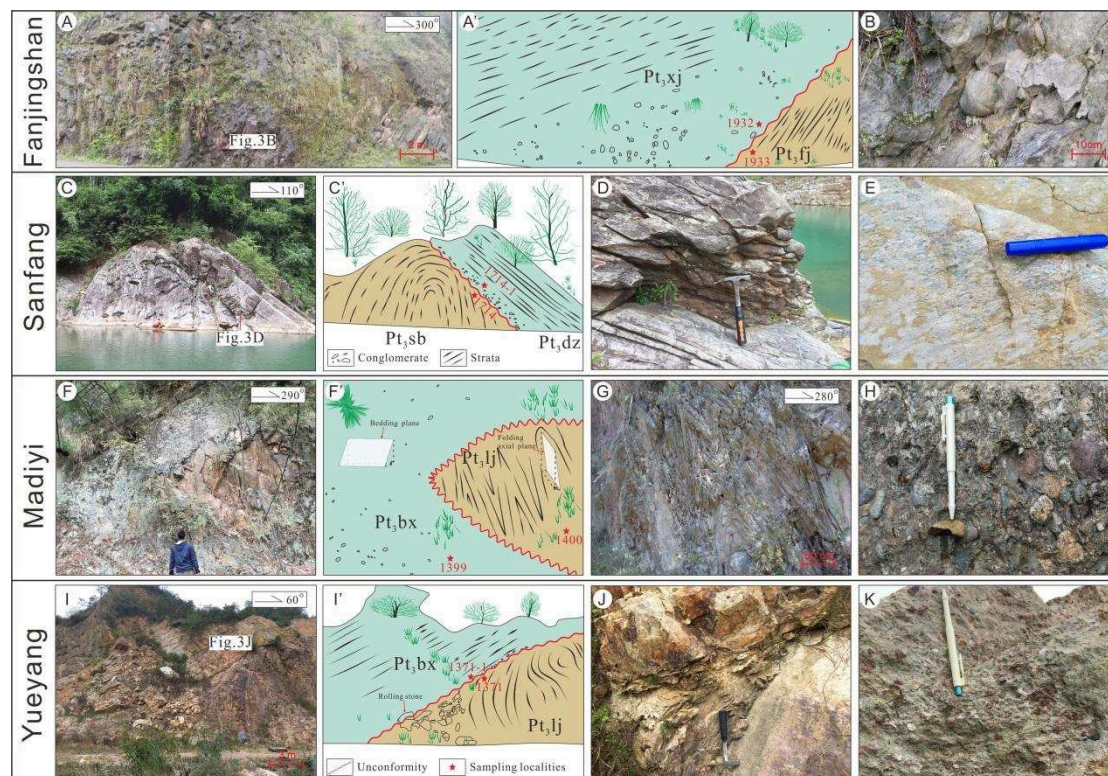


Figure 2-3. Representative field photos and geologic sketches. (A) Unconformity between the Fanjingshan group and the Xiajiang group in the Fanjingshan area; (A') Geologic sketch map of A with the unconformity contact relationship; (B) Conglomerate of the Xiajiang group; (C) Unconformity between the Sibao group and Danzhou group in the Sanfang area; (C') Geologic sketch of C with the unconformity contact relationship; (D, E) Conglomerate of the Danzhou group; (F) Unconformity between the Lengjiaxi group and Banxi group in the Madiyi area; (F') Geologic sketch of F with the unconformity contact relationship; (G) Tight fold in the Lengjiaxi group; (H) Conglomerate of the Banxi group; (I) Unconformity between the Lengjiaxi group and the Banxi group in the Yueyang area; (I') Geologic sketch of I with the unconformity contact relationship; (J) Unconformity contact between the Lengjiaxi group and Banxi group; (K) Conglomerate of the Banxi group.

2.4 Comparison of the Sibao group (Pt3sb, and its equivalents) and Danzhou group (Pt3dz, and its equivalents) in the Jiangnan Orogenic Belt

The early Neoproterozoic and middle Neoproterozoic strata have different names in various places, e.g., the Sibao group, Fanjingshan group, Lengjiayi group, Shuangqiaoshan group, Shangxi group and Shuangxiwu group of the early Neoproterozoic strata were named in the Guangxi province, Guizhou province, Hunan province, Jiangxi province, Anhui province and Zhejiang province, respectively, where the middle Neoproterozoic strata were named the Danzhou group, Xiajiang group, Banxi group, Dengshan group, Likou group and Heshangzhen group, correspondingly (BGMRAH, 1982; BGMRGX, 1985; BGMRGZ, 1984; BGMRHN, 1988; BGMRJX, 1984; BGMRZJ, 1989).

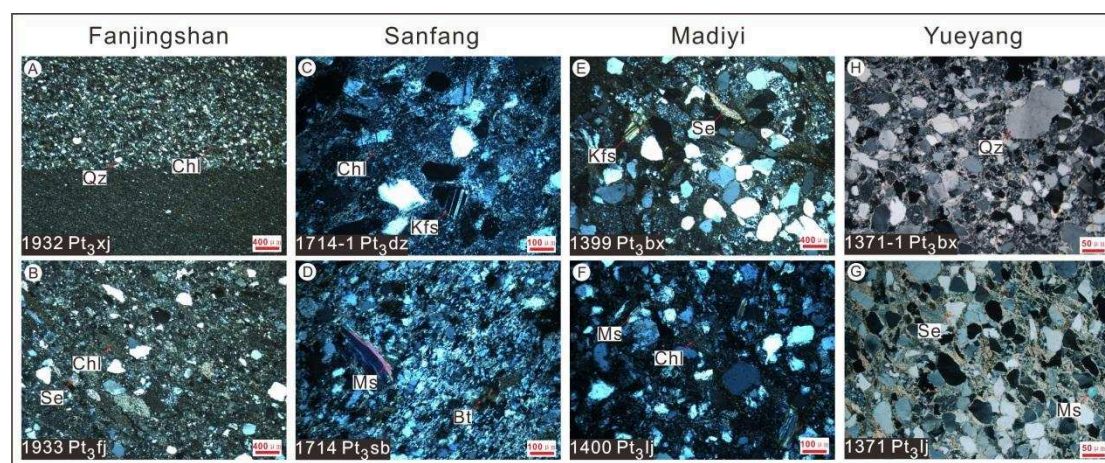


Figure 2-4. Representative thin-section photos of samples. (A) Sample 1932 (blastopsammite) in the Xiajiang group from the Fanjingshan area; (B) Sample 1933 (sandy slate) in the Fanjingshan group from the Fanjingshan area; (C) Sample 1714–1 (blastopsammite) in the Danzhou group from the Sanfang area; (D) Sample 1714 (phyllite) in the Sibao group from the Sanfang area; (E) Sample 1399 (blastopsammite) in the Banxi group from the Madiyi area; (F) Sample 1400 (sandy slate) in the Lengjiayi group from the Madiyi area; (G) Sample 1371–1 (quartz sandstone) in the Banxi group from the Yueyang area; (H) Sample 1371 (sandy slate) in the Lengjiayi group from the Yueyang area.

The Sibao group and its equivalents are deformed by N-S and NE-SW trending fold axes (Figure 2-3). Tight folds with vertical axes are also common at the outcrop scale (Shu, 2012). The deformation is coeval with a low-grade regional metamorphism represented by low greenschist facies metamorphic rocks, such as slate, phyllite, and meta-volcanic rocks. Locally, garnet-biotite micaschist and amphibole schist are observed (Charvet, 2013; Yan et al., 2015; Zhang et al., 2013). These strata were unconformably covered by basal conglomerates of the Middle Neoproterozoic Danzhou group and its equivalents (Figure 2-3; Wang & Li, 2003; Wang et al., 2007). On the contrary to the Sibao group, the Danzhou group and its equivalents display gentle folds and a very low grade metamorphism, or even no metamorphism (Figure 2-4). The Sibao group and its equivalents contain ultramafic and mafic magmatic rocks, and siliceous sedimentary rocks interpreted as olistoliths (Yao et al., 2016).

2.5 Ophiolitic mélange and magmatic events in the Jiangnan Orogenic Belt

Two ophiolitic mélanges in the eastern part of Jiangnan Orogenic Belt are generally accepted by researchers. One is in the NE Jiangxi province, another is located near the Pingxiang–Jiangshan–Shaoxing fault, both of them are thought to be formed in an accretionary complex defining the ophiolitic suture of the Paleo–South China Ocean. The NE Jiangxi ophiolitic rocks yielded Sm–Nd isochron ages of 1034 ± 24 Ma (Chen et al., 1991), and 1024 ± 30 Ma (Zhou et al., 1989), and SHRIMP zircon U–Pb age of 970 ± 21 Ma (Gao et al., 2009), and 968 ± 23 Ma (Li et al., 1994). Recently, Yao et al. (2016) dated a gabbroic block enclosed in an ophiolitic mélange at 869 ± 9 Ma (zircon, LA-ICP-MS) in the Longsheng area, in the western part of the Jiangnan Orogenic Belt (Figure 2-1).

Previous studies indicate that the subduction related rocks are relatively well exposed in the eastern Jiangnan Orogen: plagiogranite (970 ± 21 Ma, zircon SHRIMP U–Pb, NE Jiangxi, Gao et al., 2009; 905 ± 14 Ma, zircon SHRIMP U–Pb, Zhejiang, Ye et al., 2007), andesitic rocks (926 ± 15 Ma, zircon SHRIMP U–Pb, Zhejiang, Li et al., 2009), tonalite (913 ± 15 Ma, zircon SHRIMP U–Pb, Zhejiang, Ye et al., 2007), basalt

(904±8 Ma, zircon SHRIMP U–Pb, Zhejiang, [Chen et al., 2009](#)), rhyolite (891±12 Ma, zircon SHRIMP U–Pb, Zhejiang, [Li et al., 2009](#)), tuff (879±6 Ma, zircon LA–ICP–MS U–Pb, Jiangxi, [Wang et al., 2008](#)), gabbro (875±8 Ma, zircon LA–ICP–MS U–Pb, Jiangxi, [Zhang et al., 2013](#)). However, mafic rocks crop out rarely in the western Jiangnan Orogen: gabbro (869±9 Ma, zircon LA–ICP–MS U–Pb, Guangxi, [Yao et al., 2016](#)).

Several peraluminous granitic plutons crop out along the Jiangnan Orogenic Belt ([Figure 2-1](#)), most of them are dated in the range of 852–825 Ma (e.g., Miaohou at 828±4 Ma, Zhejiang, [Xia et al., 2015](#); Xucun at 852±6, Anhui, [Xue et al., 2010](#); Xiuning at 825±7, Anhui, [Wu et al., 2006](#); Jiuling at 828±8, Jiangxi, [Zhong et al., 2005](#); Yuanbaoshan at 833±6, Guangxi, [Yao et al., 2014a](#); Sanfang at 834±8, Guangxi, [Zhao et al., 2013](#); Nage at 852±5, Guizhou, [Wu et al., 2018](#); Fanjingshan at 838±2, Guizhou, [Wang et al., 2011](#)). These granitoids are interpreted as late- to post-collisional plutons.

2.6 Nanhua rift

A-type granites and contemporaneous mafic intrusions range from 805 Ma to 761 Ma ([Ge et al., 2001](#); [Li et al., 2008b](#); [Wang et al., 2012b](#)). The geochemistry of these rocks is in agreement with an extensional setting of the South China block since the middle Neoproterozoic. A ca. 800–750 Ma bimodal magmatism composed of basalts and rhyolites has been well defined in the Jiangnan and Cathaysia regions.

Chapter 3. Time constraints on the closure of the Paleo–South China Ocean and the Neoproterozoic assembly of the Yangtze and Cathaysia blocks: insight from new detrital zircon analyses

3.1 Introduction

The Jiangnan Orogen plays a key role in the tectonic framework of the South China Block, making the Neoproterozoic northeast–trending collision between the Cathaysia and Yangtze blocks. Over the past decades, advances in research on the Jiangnan Orogen led authors to propose several controversial tectonic models. The presence of remnants of oceanic crust and the well–defined suture zones make the eastern sector of the Jiangnan orogen commonly acknowledged as a collision belt (e.g., [Charvet, 2013](#); [Li et al., 2007](#); [Shu et al., 2014](#); [Zhao & Cawood, 2012](#); [Figure 2-1](#)). However, in the western part of the Jiangnan Orogen, some issues remain to be clarified.

One of the most debated questions is the timing of the collision between the Yangtze and Cathaysia blocks. Some researchers proposed that this collision took place at 1.2–1.0 Ga in the western part, but later in the eastern part at 1.0–0.96 Ga according to the tuff and basin study ([Greentree et al., 2006](#)). [Li et al. \(2007\)](#) proposed that the Jiangnan Orogen was related to the assembly of the Rodinia supercontinent during 1041–1015 Ma by the insight of mica $^{40}\text{Ar}/^{39}\text{Ar}$ dating of the Tianli schist in the Jiangxi Province. While some authors hold the view that the collision between the two blocks should be constrained at 1.0–0.86 Ga owing to the insights of ophiolites, and arc related rocks ([Li et al., 2008a, 2009, 2014](#); [Shu & Charvet 1996](#); [Ye et al., 2007](#); [Zheng et al., 2008](#)). Meanwhile, considering the peak of detrital zircon of the Sibao group (Pt_{3sb}, and its equivalents) as well as the peraluminous granites distributed along the Jiangnan Orogenic Belt, a school of researchers suggested that the collision of the Yangtze and Cathaysia blocks should take place at 850–800 Ma ([Wang et al., 2007, 2008](#); [Yao et al., 2014a, 2014b](#)). Recently, more and more mafic rocks dated at 850–820 Ma, have been

reported in the Jiangnan Orogen (Liu et al., 2015; Sun et al., 2017; Xia et al., 2015; Zhang et al., 2016). These rocks are interpreted as magmatic arc-related, consequently, the authors considered that the collision of the Yangtze and Cathaysia blocks did not started until 820 Ma. However, some authors emphasized the hiatus in sedimentation, and the unconformity between the Sibao group (and its equivalents) and Danzhou group (Pt₃dz, and its equivalents), which resulted from the Jiangnan Orogeny, and proposed that the collision should occur at ca. 830-800 Ma (Su et al., 2008; Zhao & Cawood, 2012).

In order to advance the debate on this topic, we have carried out a detrital zircon dating near the Neoproterozoic unconformity in three distinct localities, and synthesized similar studies by integrating the new and previous data from the Jiangnan Orogen, the Yangtze and Cathaysia blocks, to improve the understanding of the Neoproterozoic tectonic evolution of the Jiangnan Orogenic Belt.

3.2 Geological setting

Detailed geological setting can be referred to the Chapter 2.

3.3 Samples collection and analytical procedures

3.3.1 Sample collection

We collected sandstone samples from both series below and above the unconformity in three localities: Fanjingshan, Guizhou Province, Sanfang, Guangxi Province and Madiyi, Hunan Province (Figures 2-1, 2-2 and 2-3). GPS locations are provided in the Table 3-1.

3.3.2 Analytical procedures

Whole-rock major element contents were analyzed by ARL-9900 X-ray fluorescence spectrometer (XRF) at the Testing Center of Shandong Bureau of China Metallurgical Geology Bureau. The uncertainties reported in this study are 2% for major elements. Trace elements and rare earth elements (REE) were measured by ICP-MS (Finnigan Element II) at the Testing Center of Shandong Bureau of China

Metallurgical Geology Bureau. International standards were used to define the analytical precision and accuracy throughout the analytical processes for ICP–MS. The uncertainties are 5% for trace elements.

Zircons were separated from the crushed rocks using heavy liquid and magnetic techniques and then handpicked under a binocular microscope. The zircon grains were mounted in epoxy resin, and then polished and coated with gold. Cathodoluminescence (CL) images of the zircons were obtained using a JEOL JXA8230 electron probe microanalyzer at the Testing Center of Shandong Bureau of China Metallurgical Geology Bureau.

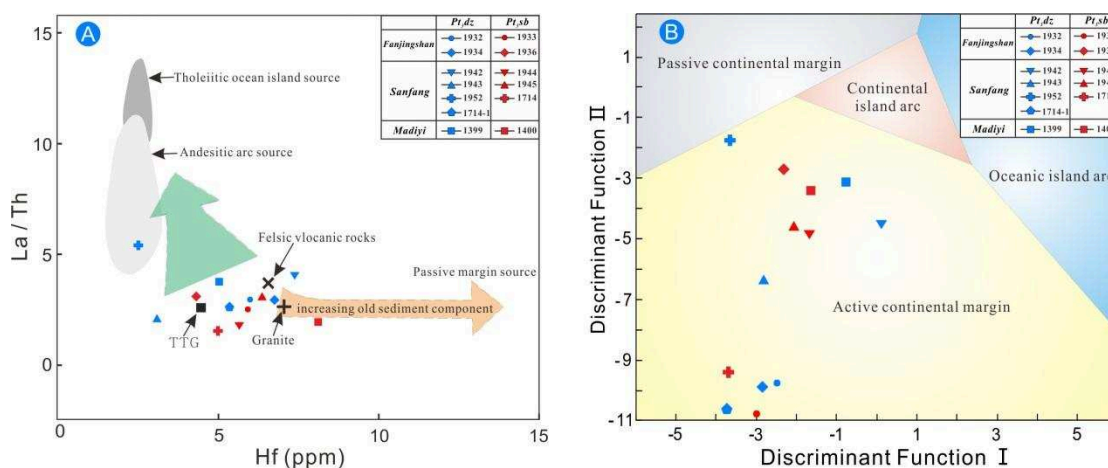


Figure 3-1. (A) Source rock discrimination diagrams for the samples on Hf versus La/Th (modified after (Floyd & Leveridge, 1987)) and (B) Plot of discriminant scores along Function I versus II for various samples (modified after Bhatia, 1983)

The laser ablation (LA)–ICP–MS analysis of zircon U–Pb isotopic compositions was performed at the Testing Center of Shandong Bureau of China Metallurgical Geology Bureau, using a ThermoX2 ICP–MS connected to a GeoLas Pro 193 nm laser ablation system. All analyses were carried out with a spot size of 30 μm or 20 μm and a laser frequency of 10 Hz. Helium was used as the carrier gas to transport the ablated material. The detailed analytical procedure is described in Liu et al. (2010). All measurements were performed using zircon 91500 as the external standard with a $^{206}\text{Pb}/^{238}\text{U}$ age of 1065.4 ± 0.6 Ma (Wiedenbeck et al., 1995). We calibrated elemental

contents with NIST610 as the external standard and ^{29}Si as the internal standard. The U–Pb ages were calculated from the raw signal data using the software ICPMSDataCal (ver.8.4). On account of the ^{204}Pb could not be measured owing to low signal and interference from ^{204}Hg in the gas supply, common lead correction was carried out using the EXCEL program common Pb correction (Andersen, 2002). For zircons older than 1000 Ma, because of large amounts of radiogenic Pb, the $^{207}\text{Pb}/^{206}\text{Pb}$ age is more reliable than $^{206}\text{Pb}/^{238}\text{U}$, whereas for zircons younger than 1000 Ma, as a result of the low content of radiogenic Pb and uncertainty of common Pb correction, the $^{206}\text{Pb}/^{238}\text{U}$ age is more reliable.

Table 3-1. GPS locations of samples and petrological description

Samples	Area	GPS locations	Period of strata	Rock type
1932	Fanjingshan	N27°54.523', E108°48.073'	Pt3xj	Blastopsammite
1933		N27°54.524', E108°48.070'	Pt3fj	Sandy slate
1934		N27°55.011', E108°48.252'	Pt3xj	Blastopsammite
1936		N27°59.141', E108°47.219'	Pt3fj	Sandy slate
1942	Sanfang	N25°14.122', E109°07.432'	Pt3dz	Sandy slate
1943		N25°14.876', E109°06.790'	Pt3dz	Sandy slate
1944		N25°17.053', E109°07.491'	Pt3sb	Muddy phyllite
1945		N25°20.017', E109°05.961'	Pt3sb	Muddy phyllite
1952		N25°12.566', E109°09.349'	Pt3dz	Blastopsammite
1714-1		N25°00.741', E108°52.674'	Pt3dz	Blastopsammite
1714		N25°00.741', E108°52.673'	Pt3sb	Phyllite
1399	Madiyi	N28°25.482', E110°39.877'	Pt3bx	Blastopsammite
1400		N28°25.481', E110°39.878'	Pt3lj	Sandy slate
1371-1	Yueyang	N29°43.875', E113°17.449'	Pt3bx	Quartz sandstone
1371		N29°43.885', E113°17.447'	Pt3lj	Sandy slate

3.4 Analytical results

3.4.1 Major and trace elements

The analytical results of major and trace elements of 13 representative samples are given in Table 3-2. Slate and phyllite of the Sibao group and its equivalents show high SiO_2 (72.2–79.8 wt%), intermediate Al_2O_3 (6.2–13.1 wt%). However, sandstone, blastopsammite and slate of the Danzhou group and its equivalents yield lower SiO_2 (66.2–77.1 wt%) and higher Al_2O_3 (7.3–16.0 wt%). These two suites of strata have

similar content in Fe_2O_3 , MgO and K_2O . The most intuitive character of all samples analyzed for geochemistry is that they display similar chondrite-normalized steep rare earth element (REE) patterns revealing obvious enrichment in light rare earth element (LREE) with respect to heavy rare earth element (HREE; Figure 3-2A). LREE/HREE values range from 6.15 to 16.28, and $(\text{La}/\text{Yb})_{\text{N}}$ vary from 3.26 to 14.20 with an average of 8.18. All the samples reveal distinct negative Eu anomalies (Eu/Eu^* value of 0.31–0.70, with an average of 0.53). On the upper crust normalized spidergrams (Figure 3-2B), all samples exhibit strong negative Ba, Sr and Nb anomalies and the enrichment of Rb, Th and U, suggesting that the sedimentary rocks were derived from the upper crustal source (Sun & McDonough, 1989; Taylor & McLennan, 1981).

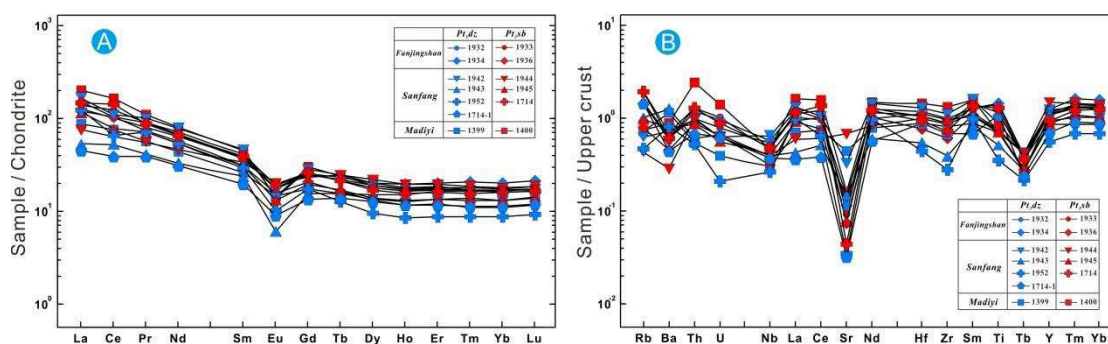


Figure 3-2. Distribution of (A) rare earth elements and (B) trace elements for the samples derived from the Jiangnan Orogen. The normalization values for (A) and (B) are taken from Sun & McDonough (1989) and McDonough & Sun (1995), respectively.

3.4.2 Zircon cathodoluminescence images

Representative cathodoluminescence (CL) images of detrital zircons of the six samples are shown in Figure 3-3. In majority, the zircon grains are subhedral and euhedral, revealing that they are near source accumulation. Most of zircon grains display clear oscillatory zoning with granitic zircon feature, while three of them show broad banded structure with mafic zircon characters (1933–12, 1933–32, 1714–32). Some zircon grains reveal thin luminescent overgrowth rims that appear bright in the CL images. Interestingly such a phenomenon is found with older cores (2529–946 Ma)

and younger overgrowth rims (865–852 Ma).

3.4.3 Detrital zircon U–Pb ages

3.4.3.1 Sibao group and its equivalents

Two hundreds and sixty-one zircon data yield good concordance (Figure 3-4 and Table 3-3). The Sibao group and its equivalents reveal one significant peak at 853 Ma, one minor peak cluster ranging from 1900 Ma to 1500 Ma and one inconspicuous peak at ca. 2450 Ma, with the youngest age at 832 Ma (Figure 3-5).

Regarding each sample separately, the one collected in Fanjingshan (1933) yields ages in the range of 2176–834 Ma with an obvious peak at 849 Ma. The ages of samples collected in Madiyi (1400) and Sanfang (1714) range between 2645–832 Ma, and 3038–838 Ma, with distinct peaks at 861 Ma and 856 Ma, respectively. The peak clusters ranging from ca. 1000 Ma to ca. 870 look like a shoulder, lying behind the prominent peaks, and are remarkable in all of the three plots (Figure 3-4).

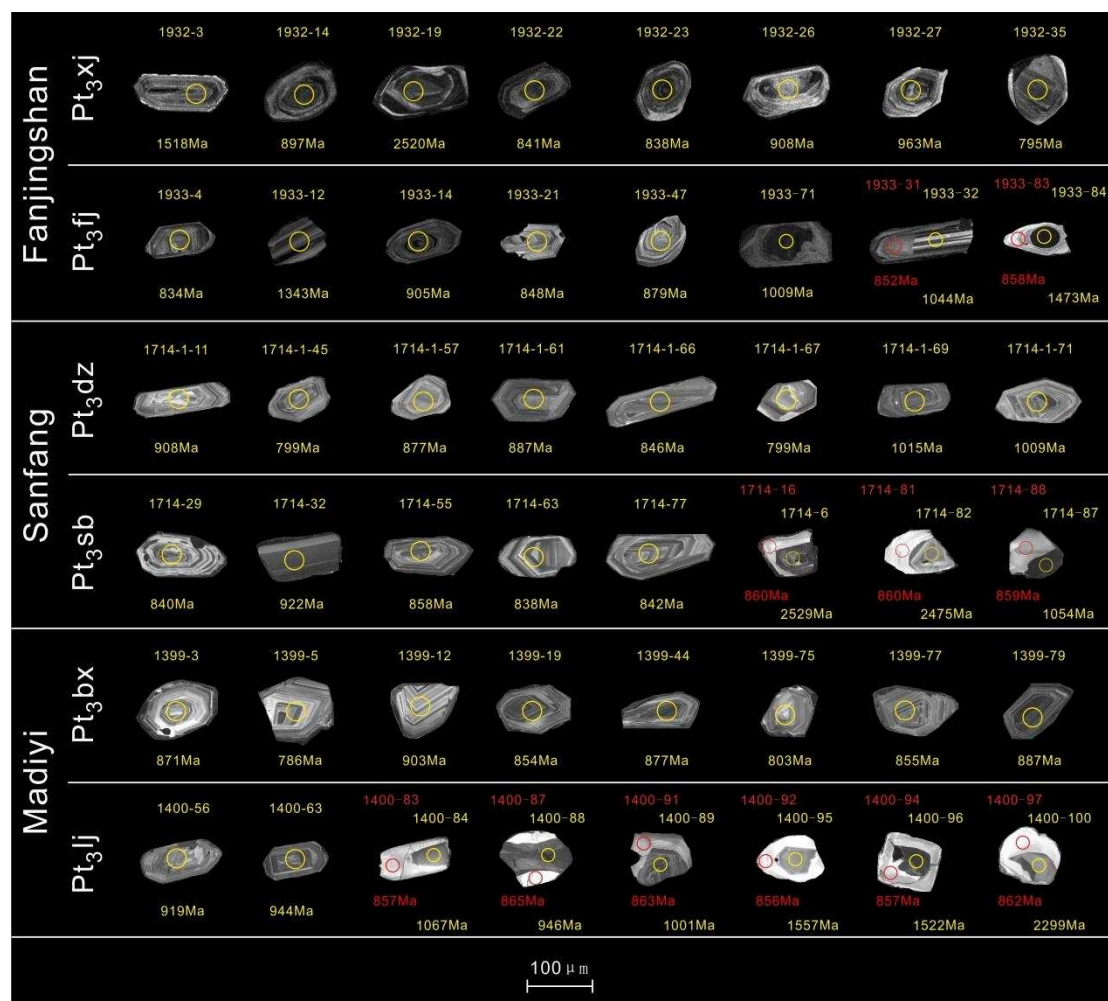


Figure 3-3. Representative cathodo-luminescence images of zircons of the samples from the Jiangnan Orogen, attached with analyzed locations and U–Pb ages.

3.4.3.2 Danzhou group and its equivalents

Totally, we got 227 zircon ages for the Danzhou group and its equivalents, most of them are concordant (Figure 3-4). In general, the age spectrum shows two obvious peaks at 850 Ma and 795 Ma, one minor peak clusters at ca. 1900–1500 Ma, and one minor peak at 2500 Ma as a whole, the relative probability plot reveals a good similarity with that of the Sibao group and its equivalents except one significant peak at 795 Ma (Figure 3-5). Moreover, there is no detrital zircon age ranging from ca. 832 Ma to ca. 803 Ma recorded in the Danzhou group and its equivalents (Figure 3-5B).

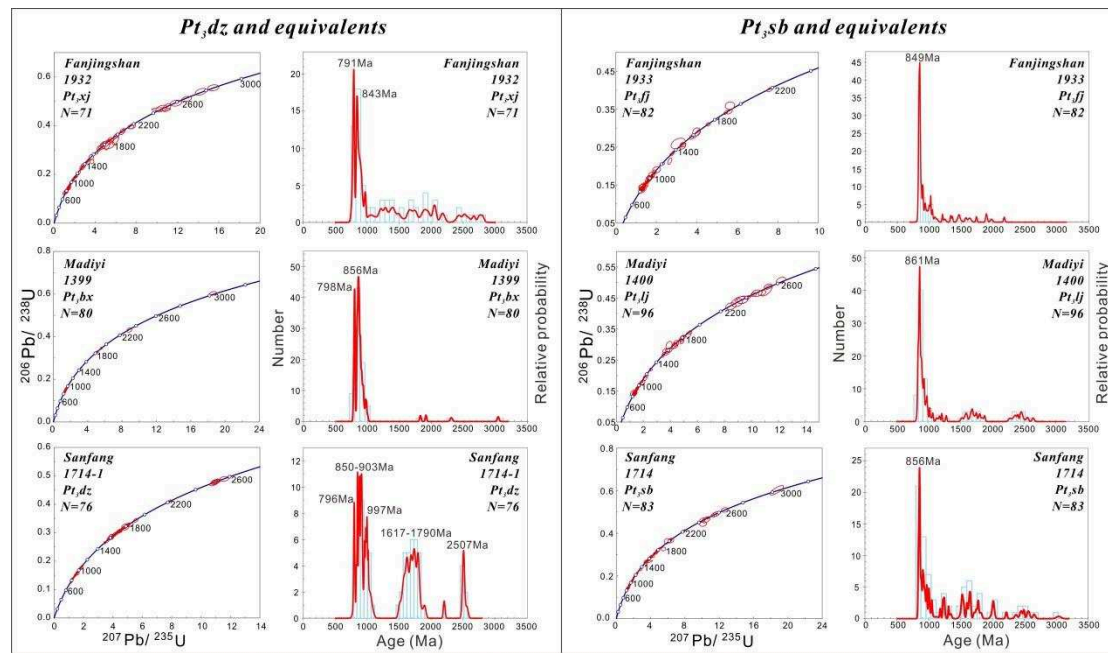


Figure 3-4. U–Pb age concordia plots and histograms and relative probability plots for the zircon of six samples from the Jiangnan Orogen.

Individually, the sample collected in Fanjingshan (1932) yields ages in the range of 2803–779 Ma. As for the sample collected in Madiyi (1399) and Sanfang (1714–1), they show ages ranging in 2997–783 Ma and 2562–796 Ma intervals, respectively. Two distinct peaks, ca. 850 Ma and ca. 795 Ma, are displayed in the relative probability plot of the sample collected from Fanjingshan and Madiyi (Figure 3-4). However, the plot of the sample collected from Sanfang reveals a different pattern and presents a significant age cluster at 903–850 Ma, two prominent peaks at 997 Ma and 796 Ma, one minor peak clusters at 1790–1617 Ma and one minor peak at 2507 Ma (Figure 3-4).

Table 3-2. Major and Trace elements data for representative samples from the western Jiangnan Orogen

Analysis	Fanjingshan				Sanfang							Madiyi	
	1932	1933	1934	1936	1942	1943	1944	1945	1952	1714-1	1714	1399	1400
	Pt3xj	Pt3fj	Pt3xj	Pt3fj	Pt3dz	Pt3dz	Pt3sb	Pt3sb	Pt3dz	Pt3dz	Pt3sb	Pt3bx	Pt3lj
SiO ₂	66.22	72.27	67.83	73.66	70.40	77.17	75.97	77.02	84.35	70.55	72.85	71.18	79.82
TiO ₂	0.86	0.70	0.89	0.47	0.43	0.32	0.47	0.45	0.23	0.79	0.67	0.44	0.55
Al ₂ O ₃	16.88	12.70	15.98	6.24	14.53	11.49	10.84	12.14	7.34	13.84	13.08	11.62	9.29
Fe ₂ O ₃ ^t	6.27	6.13	6.52	3.71	3.52	3.64	3.70	2.75	2.41	6.56	5.49	2.51	3.33
MnO	0.07	0.02	0.05	0.19	0.09	0.05	0.22	0.04	0.07	0.07	0.10	0.07	0.05
MgO	1.36	0.93	1.33	1.87	0.91	1.12	0.89	0.99	0.96	1.31	1.05	1.64	1.23
CaO	0.10	0.16	0.12	4.44	0.90	0.09	2.98	0.16	0.05	0.05	0.05	2.42	0.42
Na ₂ O	1.38	0.25	1.10	0.23	4.24	0.69	1.80	1.56	0.09	0.09	0.11	2.31	1.81
K ₂ O	3.42	3.46	3.18	1.62	1.96	2.81	1.08	2.58	1.37	3.64	3.52	2.69	1.37
P ₂ O ₅	0.07	0.11	0.05	0.09	0.06	0.06	0.10	0.08	0.02	0.04	0.05	0.07	0.13
LOI	3.25	2.72	2.85	7.22	2.54	2.21	1.33	1.98	2.26	2.96	2.77	4.69	1.51
Total	99.88	99.45	99.91	99.74	99.59	99.65	99.38	99.75	99.15	99.90	99.74	99.64	99.51
Na ₂ O+K ₂ O	4.80	3.71	4.28	1.85	6.20	3.50	2.88	4.14	1.46	3.73	3.63	5.00	3.18
La	29.90	32.40	35.20	27.80	39.00	12.50	17.60	27.10	29.10	34.00	10.60	20.60	47.30
Ce	60.80	75.90	62.80	63.90	66.00	32.00	38.60	47.40	40.00	85.80	24.00	46.10	99.10
Pr	7.60	8.53	8.52	7.02	9.43	3.91	5.24	6.66	6.76	8.16	3.63	5.30	10.40
Nd	29.20	32.70	31.50	26.20	36.30	15.30	21.20	25.00	24.60	30.60	14.50	20.10	37.60
Sm	5.66	6.28	5.67	4.76	6.97	3.59	5.08	4.66	4.38	5.98	3.00	3.94	6.85
Eu	1.01	1.09	1.03	0.90	0.80	0.35	1.15	0.76	0.58	1.14	0.51	0.85	0.82
Gd	5.02	5.18	5.13	4.17	5.80	3.16	4.80	3.95	3.52	5.27	2.76	3.59	6.12
Tb	0.82	0.79	0.85	0.61	0.91	0.58	0.90	0.62	0.47	0.78	0.52	0.58	0.88
Dy	4.75	4.46	5.09	3.28	5.12	3.81	5.51	3.51	2.37	4.30	3.20	3.43	4.80
Ho	0.98	0.92	1.09	0.65	1.01	0.85	1.09	0.73	0.48	0.87	0.65	0.71	0.96
Er	2.92	2.78	3.35	1.96	3.04	2.67	3.19	2.23	1.45	2.64	1.89	2.18	2.89
Tm	0.45	0.43	0.52	0.28	0.43	0.42	0.47	0.35	0.22	0.39	0.29	0.33	0.43
Yb	2.96	2.83	3.40	1.83	2.85	2.75	3.02	2.23	1.47	2.67	1.89	2.19	2.72
Lu	0.47	0.43	0.53	0.29	0.44	0.44	0.47	0.36	0.23	0.42	0.30	0.35	0.41
Hf	6.01	5.94	6.77	4.33	7.40	3.11	5.67	6.38	2.54	5.37	5.01	5.04	8.13
ΣREE	152.54	174.72	164.68	143.65	178.10	82.33	108.32	125.56	115.63	183.02	67.74	110.25	221.28
LREE/HREE	10.43	12.82	10.10	15.14	11.91	6.15	6.39	11.52	16.28	14.16	6.75	10.28	15.90
(La/Yb) _N	7.25	8.21	7.43	10.90	9.82	3.26	4.18	8.72	14.20	9.13	4.02	6.75	12.47
δEu	0.57	0.57	0.57	0.60	0.37	0.31	0.70	0.53	0.44	0.61	0.53	0.68	0.38
Li	63.70	33.00	73.80	21.90	10.80	31.30	9.61	13.10	32.40	48.20	42.40	19.50	25.10
Be	2.37	2.15	2.29	1.23	2.07	2.18	1.44	1.70	1.10	2.34	2.39	1.29	1.43
Sc	10.50	11.10	12.90	7.47	4.07	8.67	4.34	5.25	5.29	13.00	16.20	7.04	8.21
Ti	4971.0	4003.0	5061.0	2573.0	2496.0	1797.0	2648.0	2504.0	1251.0	4505.0	3795.0	2485.0	3090.0

V	105.00	94.40	102.00	60.60	37.00	39.10	45.00	42.70	26.40	107.00	258.00	38.20	41.90
Cr	84.30	62.50	99.40	37.00	32.80	34.50	36.20	32.40	24.60	65.20	59.40	22.20	45.00
Mn	441.0	120.0	330.0	1285.0	614.0	318.0	1481.0	293.0	443.0	422.0	526.0	457.0	297.0
Co	16.00	18.40	14.40	6.63	5.65	4.08	5.56	5.77	2.12	6.48	11.30	4.32	7.55
Ni	30.00	33.90	35.10	19.10	14.10	14.30	14.40	14.00	11.90	25.80	17.00	7.66	16.60
Cu	24.00	10.20	29.10	21.90	12.60	7.74	53.20	3.49	13.20	123.00	44.90	9.11	13.20
Zn	98.60	98.60	103.00	75.60	37.90	83.50	124.00	31.90	71.80	98.10	64.50	38.60	37.30
Ga	20.10	17.40	20.00	9.45	14.10	16.70	11.50	15.60	10.60	19.10	16.90	13.80	11.20
Rb	160.00	207.00	157.00	85.20	67.20	110.00	46.20	104.00	50.70	205.00	157.00	78.60	79.70
Sr	51.50	31.90	39.30	25.50	113.00	50.70	231.00	26.80	11.90	15.20	11.00	151.00	55.90
Y	24.60	24.00	27.10	18.30	26.30	23.50	32.00	18.80	12.10	20.00	15.10	20.30	26.50
Zr	209.00	206.00	236.00	144.00	260.00	91.70	200.00	229.00	65.40	172.00	161.00	191.00	307.00
Nb	13.30	11.50	13.90	7.70	15.90	9.75	9.67	10.00	6.43	11.70	9.14	7.37	11.40
Mo	0.08	0.08	0.07	0.29	0.48	0.06	0.09	0.03	0.05	0.04	0.06	0.20	0.28
Cd	0.01	0.03	0.04	0.94	0.04	0.04	0.27	0.05	0.04	0.02	0.04	0.09	0.05
Sn	3.32	2.76	3.21	1.61	2.03	2.01	54.30	2.08	1.24	3.07	3.02	1.16	1.67
Cs	15.90	24.20	12.80	5.18	8.27	11.50	13.30	3.27	5.90	15.10	13.90	2.35	3.86
Ba	431.00	488.00	405.00	313.00	499.00	865.00	196.00	544.00	551.00	413.00	303.00	776.00	607.00
Ta	1.07	0.96	1.13	0.63	1.17	0.57	0.77	0.79	0.43	1.03	0.89	0.51	0.99
W	2.62	1.75	2.90	1.27	0.66	0.81	0.56	2.73	0.34	5.62	9.90	0.27	1.00
Pb	10.20	5.13	15.30	15.00	19.10	12.30	70.70	4.48	5.40	33.90	57.00	9.04	16.40
Bi	0.14	0.27	0.19	0.29	0.11	0.16	31.00	0.07	0.20	0.37	1.08	0.10	0.13
Th	10.30	13.10	12.20	9.09	9.83	6.29	10.20	8.85	5.46	13.10	7.05	5.56	24.80
U	1.91	2.49	2.36	1.60	1.55	1.62	1.54	1.37	0.52	2.19	1.53	0.96	3.46

ACNK=Al₂O₃/(Na₂O+K₂O+CaO)_{Mol}; Eu/Eu*=Eu/(0.5(Sm+Gd))_n; The chondrite normalization values are from Sun S S et al.(1989), and the primitive mantle normalization values are from McDonough et al. (1992)

3.5 Discussion

3.5.1 Comparison of the age spectra between the Sibao and Danzhou groups and geological significance of the detrital zircon ages

The detrital zircon U–Pb age spectra of the Sibao and Danzhou groups and their equivalents are given in [Figures 3-4](#) and [3-5](#). In general, the age spectrum of the Sibao group and its equivalents yields a distinct peak at 853 Ma and an obvious peak cluster ranges in 1000–870 Ma as a shoulder, with two minor peaks at 1700 Ma and 2500 Ma ([Figure 3-5](#)). The age spectrum of rocks from the Danzhou group and its equivalents inherits the features of those of the Sibao group and its equivalents, but also contains a younger peak at 795 Ma.

Independently, the detrital zircon age spectra of the top sequence of the Sibao group and its equivalents collected from three localities display a good comparability with a significant peak at ca. 855 Ma and an obvious peak cluster ranging in 1000–870 Ma. The ages ranging from ca. 1500 Ma to ca. 1000 Ma are rarely recorded except for that of the sample collected from the Sanfang area ([Figure 3-4](#)). In terms of the bottom of the Danzhou group and its equivalents, the samples collected from Fanjingshan and Madiyi present two similar peaks at ca. 850 Ma and ca. 795 Ma. However, the sample collected in the Sanfang area presents a more complicated pattern that reveals a main peak cluster ranging around 903–850 Ma with two peaks at 997 Ma and 796 Ma as shoulders. The spectra from all three areas also show prominent age peaks ranging in 1790–1617 Ma and at ~2507 Ma. It is worth noting that the zircon age distribution pattern of the sample collected from the Danzhou group in the Sanfang area is different with those of the other two samples collected from Fanjingshan and Madiyi as the detrital zircon spectrum of the Danzhou group of the Sanfang area displays multiple peaks with respect to those of Fanjingshan and Madiyi. The zircon age distribution pattern of the Sanfang sample can be traced in the detrital zircon spectrum of the Cathaysia Block ([Figure 3-6C](#)). In the geographical point of view, the Sanfang area is closer to the collision boundary than the Fanjinshan and Madiyi ones ([Figure 2-1](#)),

therefore, we may infer that the detritus in the Danzhou group of the Sanfang area was partly supplied by the Cathaysia Block.

The various detrital zircon ages have different geological significances. Although no igneous rocks around 2500 Ma was reported in the Yangtze Block, some xenocrystic zircons dated at 2600–2500 Ma in the lamprophyric and basaltic rocks have been found in Hunan, Hubei and Guizhou provinces, in the eastern Yangtze Block (Wang et al., 2012b; Zheng et al., 2006). Detrital zircons with similar ages have been reported in the areas of Wuyi, southern Jiangxi and northern Guangdong provinces, Cathaysia Block (Gan et al., 1996; Yu et al., 2006, 2009). The minority of detrital zircons dated at ca. 2500 Ma in this study might correspond to the period of global continental growth at the end Archean–early Paleoproterozoic, which was already proposed by Yao et al. (2011). Similarly, the detrital zircon ages at ca. 1900–1500 Ma are interpreted to be linked with the Columbia supercontinent (Rogers & Santosh, 2002; Zhao et al., 2002). The detrital zircons ranging from 1500 Ma to 1000 Ma are abundant in the Cathaysia Block but rare in the Yangtze Block, which can be related to the Rodinia supercontinent and Grenville orogeny (Li et al., 2002). However, the detrital zircon spectra of the Yangtze Block and Jiangnan Orogen show a distinct differentiation across the time point at 1000 Ma (Figure 3-6), suggesting that a strong magmatism should have occurred after that time. Besides, igneous rocks dated at ca. 1000–870 Ma are widely reported in the Jiangnan Orogenic Belt (Xin et al., 2017 and references therein), indicating that the Jiangnan region was an active magmatic zone. Based on the geological facts and the analysis of detrital zircon age spectra in this study, we suggest that the Paleo–South China Ocean started to subduct at ca. 1000 Ma (Figure 3-7). In this study, few zircons with core–rim structure are observed (Figure 3-3), the light luminescence rims suggest a hydrothermal event (Dubińska et al., 2004; Hoskin & Schaltegger, 2003), in the range of 865–852 Ma, which are produced by a low grade metamorphism and related to the collision of the Yangtze and Cathaysia blocks. The emplacement of numerous S-type granite plutons, dated at 850–830 Ma along the

Jiangnan Orogen, formed by the melting of a continental crust, implies the ending of the orogeny. Afterwards, the absence of a magmatic activity during the interval of the 830–803 Ma may suggest that the Jiangnan Orogen was in a tectonic quiet period. The newly formed South China block began to rift around 800–780 Ma, marked by the abundant bimodal magmatism (Wang et al., 2007). The youngest zircon, dated at 779 Ma, in the bottom of the Danzhou group may record the starting time of the deposition of the Danzhou group in the Jiangnan region.

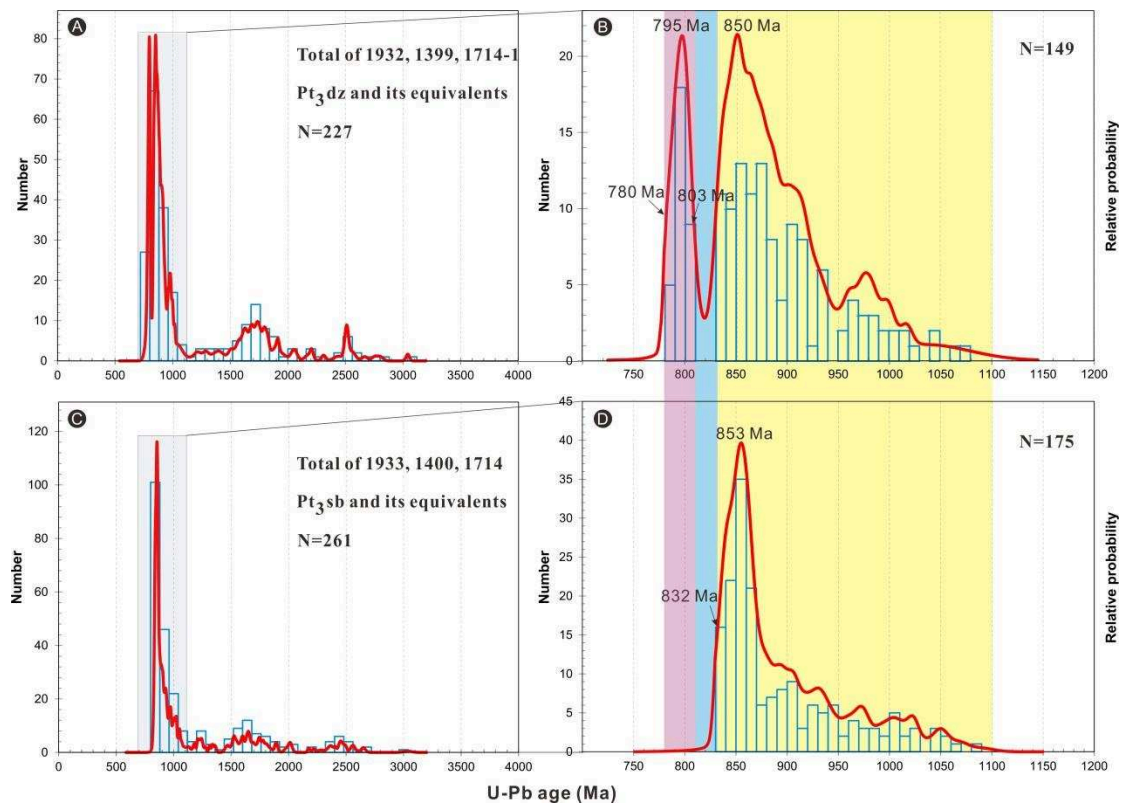


Figure 3-5. Comparison of the U–Pb age histograms and relative probability plots between the Sibao group and its equivalents and Danzhou group and its equivalents derived from the Jiangnan Orogen.

3.5.2 Comparison of the detrital zircon age spectra of the Neoproterozoic strata in the South China Block

In order to characterize the detrital zircon age spectra originated from the Neoproterozoic strata of the Yangtze Block, Jiangnan Orogen and Cathaysia Block, we collected thousands of available detrital zircon age data from early Neoproterozoic

(Sibao group and its equivalents), middle Neoproterozoic (Danzhou group and its equivalents) and late Neoproterozoic strata (Sinian and its equivalents) in three regions, mainly including the eastern Yangtze Block (northern Guizhou, northern Hunan and western Hubei provinces), whole Jiangnan Orogen (Anhui, Jiangxi, Hunan, northern Guangxi and eastern Guizhou provinces) and Cathaysia Block (Fujian, Guangdong, southeastern Hunan and southeastern Guangxi provinces).

As shown in [Figure 3-6](#), the pattern of the detrital zircon age spectrum of the Jiangnan Orogen is almost consistent with that of the Yangtze Block, but significantly different from that of the Cathaysia Block ([Figures 3-6A, 3-6B and 3-6C](#)). The most prominent peaks clustering from 1000 to 820 Ma displayed in the Yangtze Block and Jiangnan Orogen share the similar peak at ca. 840 Ma, with an increasing trend in the relative probability plot since 1000 Ma ([Figure 3-6E and 3-6F](#)). However, the contemporaneous peak cluster in the Cathaysia Block seems quite different from the former two ([Figure 3-6G](#)). Consequently, we may qualitatively infer that the Cathaysia Block was not in contact with the Yangtze Block at ca. 1000 Ma ([Figure 3-7](#)).

S-type granites, dated at 840–820 Ma, are widely distributed in the Jiangnan Orogenic Belt ([Shu, 2012; Xin et al., 2017; Yao et al., 2014b](#), and references therein). Since no contemporaneous magmatic event is known in both the Yangtze and Cathaysia blocks, these plutons formed through the melting of a continental crust emplaced at the end of the Jiangnan collision. Nevertheless, we notice the zircon age peaks at ca. 850 Ma and ca. 840 Ma in the terrigenous formations of the Yangtze and Cathaysia blocks, respectively ([Figures 3-6E and 3-6G](#)). A possible interpretation is that the Jiangnan Orogen supplied the material to the Yangtze and Cathaysia blocks. S-type granite indicates the end of the Jiangnan orogeny, thus the collision between the Yangtze and Cathaysia blocks should have occurred before 850 Ma. Furthermore, the relative probability plots of zircon age distribution from the Yangtze Block, Jiangnan Orogen and Cathaysia Block show that the proportion of the Jiangnan Orogen is approximately equal to the sum of those of the Yangtze and Cathaysia blocks in the range of 865–820

Ma ([Figures 3-6D and 3-6H](#)). This result can be interpreted as the Jiangnan Orogen was the unique source provider for the eastern Yangtze Block and western Cathaysia Block in the period from 865 to 820 Ma. In other words, we propose that the collision between the Yangtze and Cathaysia blocks probably started at 865 Ma and ended at 820 Ma. Such a 45 Myr orogenic duration is comparable with some well known orogenic belts, such as the Variscan and Himalayas. (e.g. [Charles et al., 2009](#); [Chung et al., 2005](#); [Faure et al., 2008](#); [Martinez-Catalan et al., 2014](#)).

Nevertheless, some researchers proposed that the collision took place after ca. 830 Ma, owing to the geochronology result of gabbro and diorite (850-830 Ma) in both the eastern and western parts of the Jiangnan Orogen ([Liu et al., 2015](#); [Sun et al., 2017](#); [Xia et al., 2015](#); [Zhou et al., 2009](#)). However, the CL images of the dated zircons show broad bands rather than an oscillatory zoning ([Wu & Zheng, 2004](#)), consequently, these zircons cannot be considered as magmatic ones and were probably captured, as xenocrysts from the late to post-orogenic peraluminous granites, which are widely distributed along the Jiangnan orogenic belt, during the mafic magmatism in the Neoproterozoic Nanhua rifting period.

3.5.3 Significance of the geochemistry and sedimentation record of the Sibao group

The Sibao group and its equivalents are mainly composed of phyllite, slate, greywacke, and low mature arkose. However, the Danzhou and its equivalents, unconformably covering the Sibao group and its equivalents, consist mainly of a suite of conglomerate, slate, sandstone and carbonate ([BGMRAH, 1982](#); [BGMRGX, 1985](#); [BGMRHN, 1988](#); [BGMRJX, 1984](#)). Although the weathering and metamorphism may affect the geochemical character of the source rocks, the immobile elements can be still traced as provenance indicator ([Singh, 2009](#); [Wang et al., 2012a](#)). In the Hf–La/Th plot ([Figure 3-1A](#)), most samples of the Sibao group and its equivalents cluster around the average compositions of andesite, TTG, felsic volcanic rock and granite, which are the source provider for the Sibao group and its equivalents ([Floyd & Leveridge, 1987](#)). The

tonalite–trondhjemite–granite (TTG) crust has been acknowledged as formed in a subduction zone (Hoffmann et al., 2012; Senshu et al., 2009; Zhang & Zhai, 2012). In the plot of tectonic setting discriminant, all the samples of the Sibao group and its equivalents drop in the active continental margin field (Figure 3-1B), suggesting that the Sibao group and its equivalents were more likely deposited in an active continental margin (Bhatia, 1983). The prominent trace and rare earth elements characters of the Sibao group and its equivalents show distinct enrichment in light rare earth element (LREE) with respect to heavy rare earth element (HREE), and yield strong negative Ba, Sr and Nb anomalies (Figure 3-2). These features suggest that the top sequence of the Sibao group sediments was derived from an upper crustal source. The bottom sequence of the Danzhou group was supplied from the top sequence of the Sibao group of which it inherited its geochemical features.

Considering the sedimentary process of the Sibao group and its equivalents, there are some controversial issues, such as the time span of the depositional process and the tectonic setting during the accumulation of the Sibao group and its equivalents.

The majority of researchers acknowledged that the upper limit of the Sibao group and its equivalents ranges around 835 Ma to 815 Ma (Su et al., 2018; Wang et al., 2010a, 2012a; Yao et al., 2014a; Zhang et al., 2013; Zhao & Cawood, 2012). However, there is no general agreement on the initial time of the sedimentation of the Sibao group and its equivalents. A school of researchers suggested that the Sibao group and its equivalents initiate to deposit at around 1.0 Ga according to detrital zircon trace of the Sibao group and its equivalents (Shu, 2012; Yao et al., 2014a; Zhao & Cawood, 2012). Nevertheless, some authors pointed out that the maximum depositional age of the Sibao group and equivalents is ca. 870 Ma (Su et al., 2018; Wang et al., 2007; Zhou et al., 2009) by using of the youngest detrital zircon age of the “bottom” sequence of the Sibao group. However, the sampling sites are about 2000 meters above the bottom according to their stratigraphic column. It could be a workable way to trace the bottom depositional age of the Sibao group and equivalents by analyzing the detrital zircon spectrum. In this study,

we propose that the maximum depositional age of the Sibao group is at ca. 1000 Ma, when the detrital zircon spectra become distinct (Figures 3-4, 3-5 and 3-6B).

Concerning the sedimentation setting of the Sibao group and its equivalents, most of the researchers hold the view that the Sibao group and its equivalents were accumulated in a back-arc basin (Shu, 2012; Wang et al., 2010a, 2012a; Yao et al., 2014b; Zhang & Wang, 2016), while some others proposed that they were deposited in a foreland basin (Wang et al., 2007; Zhou et al., 2009). In all these tectonic interpretations, they suggested that the collision of the Yangtze and Cathaysia blocks (i.e. the Jiangnan Orogeny) took place after the end of the sedimentation of the Sibao group and its equivalents.

However, in this study, we propose some new perspectives. As a great number of arc related magmatic rocks are exposed along the Jiangnan Orogen, we argue that the Paleo–South China Ocean started to subduct northwestwards (present coordinate) beneath the Yangtze Block since around 1000 Ma. Combined with the zircon spectra analysis of the Sibao group and its equivalents, we suggest that the Sibao group and its equivalents were formed along with the subduction of the Paleo–South China Ocean. Some oceanic crust relics were scratched and involved into the Sibao deposits during the subduction ongoing. Thus, the Sibao group is considered as an accretionary complex. Meanwhile, the mafic rocks related with arc magmatism intruded into the Sibao group and its equivalents (Chen et al., 2009; Yao et al., 2014b, 2016; Zhou et al., 1989; Zhang et al., 2013; Figure 2-1). Associated with the analysis of the geochemistry, we proposed that in the subduction period from 1.0 Ga to 865 Ma (see Sections 5.1 and 5.2), the Sibao group and its equivalents were deposited in an active continental margin zone (Figure 3-7).

The youngest detrital zircon is dated around 832 Ma in the Sibao group and its equivalents (Su et al., 2018, and this study), which is consistent with the geological fact that the Sibao group and its equivalents are intruded by the 830 ± 10 Ma granitic plutons in the Jiangnan Orogen.

Therefore, we suggest that the tectonic setting of the sedimentation of the Sibao group and its equivalents can be divided into two stages. Firstly, at 1000–865 Ma, the rocks were deposited in an active continental margin. Secondly, around 865–832 Ma, after the collision of the Yangtze and Cathaysia blocks, the Sibao group and its equivalents were accumulated during the crustal thickening. By an $\epsilon\text{Hf}(t)$ study in the Anleilin and Xiushui formations (equivalent to the Sibao group), [Li et al. \(2016\)](#) showed that the negative $\epsilon\text{Hf}(t)$ values increase along the stratigraphic sequence from the bottom to the top, indicating that the Sibao group and its equivalents received more and more crustal derived materials during its deposition in the early Neoproterozoic, which implies that the Sibao group and its equivalents had experienced a tectonic setting transition from an active continental margin to continental collision. In other words, the Sibao group and its equivalents have recorded both the subduction and collision events.

Afterwards, the Danzhou group and its equivalents began to accumulate at ca. 779 Ma. The bottom sequence inherited the bulk geochemical signature of the Sibao group and its equivalents ([Figures 3-1 and 3-2](#)), except that the rocks from the Danzhou and its equivalents present higher Al_2O_3 and lower SiO_2 contents than those from the Sibao group and its equivalents probably owing to the mechanical sorting and chemical changes related to transportation. ([Fralick & Kronberg, 1997](#)).

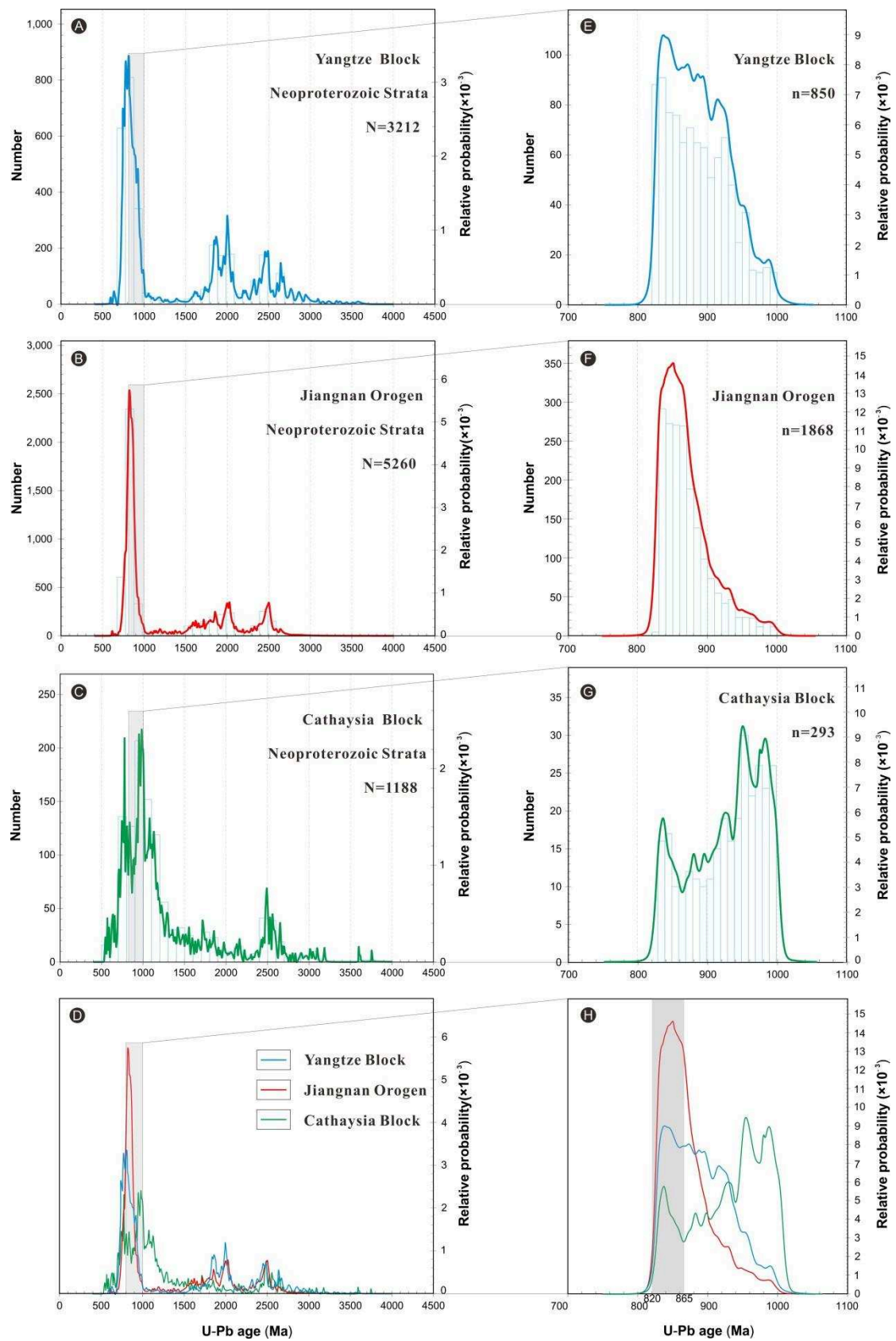


Figure 3-6. Comparison of the U-Pb age histograms and relative probability plots

derived from Neoproterozoic strata among the Yangtze Block, Jiangnan Orogen and Cathaysia Block.

3.5.4 Geodynamic evolution of the South China Block in the Early Neoproterozoic

The Jiangnan Orogenic Belt was built up due to the convergence of the Paleo–South China Ocean and the collision between the Yangtze and Cathaysia blocks (Charvet, 2013; Shu, 2012), but its geodynamic evolution process is still debated. In this study, according to the geological evidence, zircon geochronology and whole rock geochemical study of the Sibao and Danzhou groups and their equivalents, a possible spatial and temporal tectonic evolution model of the Early Neoproterozoic geological events can be suggested in the following.

As the detrital zircon spectra show a distinct differentiation across 1000 Ma (Figure 3-6), it may suggest that a significant magmatism should have occurred after that time. The gabbro in the ophiolite dated at ca. 1000 Ma in the eastern part of the Jiangnan Orogen indicates that the subduction of the Paleo–South China Ocean probably took place after that time (Zhou et al., 1989), and the mafic rocks dated at 935 Ma together with the volcanic rocks ranging in 880–870 Ma are arc related, and indicate that the subduction of the Paleo–South China Ocean was ongoing during the ca. 1000–870 Ma (Xin et al., 2017, and references therein; Yao et al., 2014b, and references therein). In addition, the spectra analysis of detrital zircon age in this study points out that the subduction of the Paleo–South China Ocean probably started at ca. 1000 Ma and ended at ca. 865 Ma. During this period, the Sibao group and its equivalents were accumulated in the active continental margin setting (Figure 3-7).

Afterwards, the Yangtze and Cathaysia blocks began to collide, the changes in temperature and fluid property possibly resulted in the metamorphism in the zircon which are traced at 865–852 Ma in this study. Abundant 840–820 Ma peraluminous late orogenic granites indicate the ending of the Jiangnan orogeny. In the period of 865–820 Ma, the upper part of the Sibao group and its equivalents were deposited in a

syn-collisional setting (Figure 3-7).

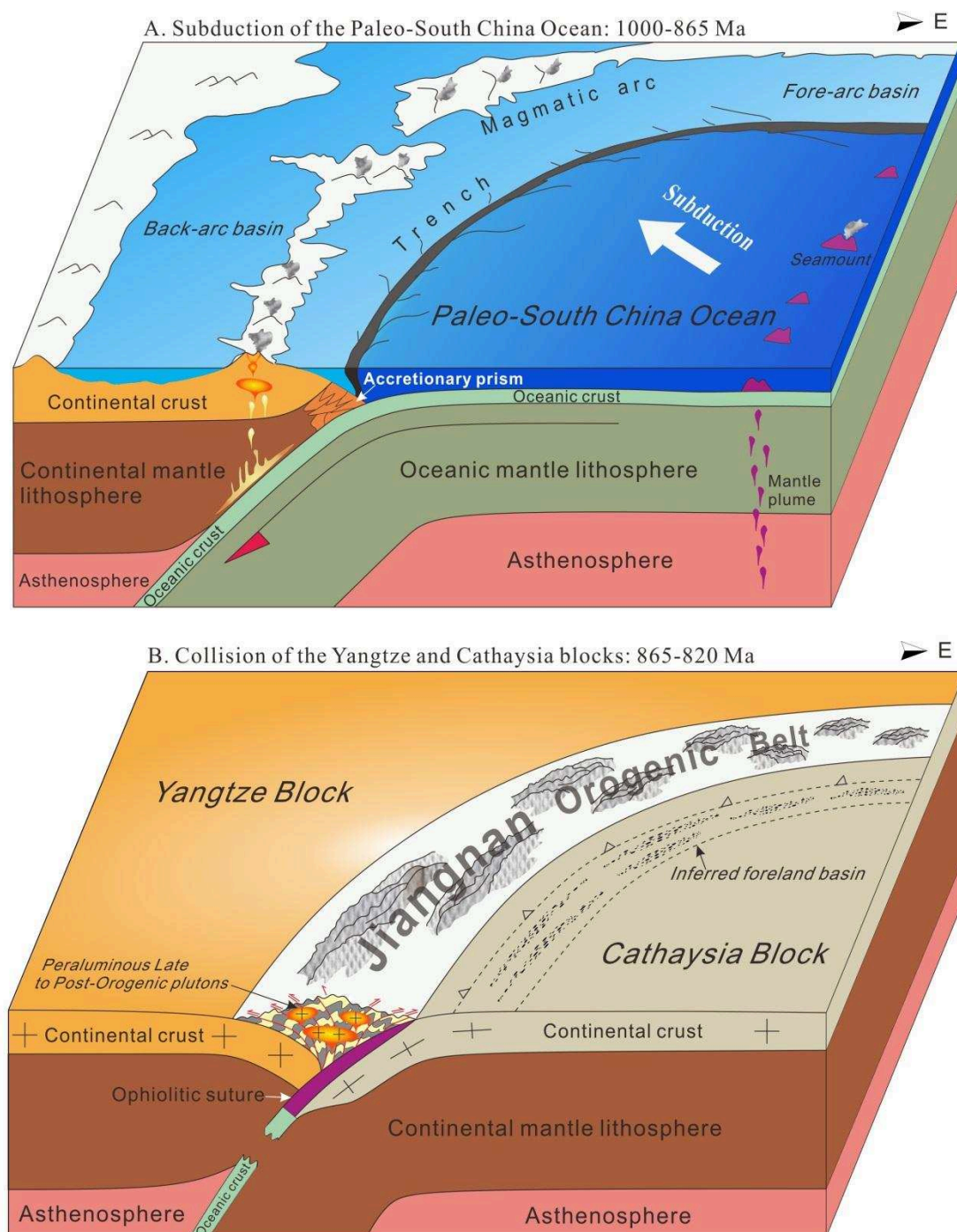


Figure 3-7. Geodynamic evolution model for the Jiangnan region in the Early Neoproterozoic. (A) Subduction of the Paleo–South China Ocean and (B) Collision of the Yangtze and Cathaysia blocks.

The fact that no magmatic imprint was traced in the 820–800 Ma period may

suggest that the Jiangnan Orogenic Belt was, at that time, probably situated in a tectonically quiet period. Then, in the 805–761 Ma period, the Nanhua rifting was accompanied by both A-type granites plutonism and mafic intrusive rocks (Li et al., 2008b; Wang et al., 2012b). The unconformity between the Sibao group (and its equivalents) and Danzhou group (and its equivalents) marks the initial time of the Nanhua rifting in the Jiangnan Orogen area. The youngest zircon age dated at 779 Ma in the bottom sequence of the Danzhou group (and its equivalents) suggests that the Danzhou group and its equivalents started their deposition at that time.

3.6 Conclusions

Integrating the new results in the detrital zircon dating, geology and geochemistry from three localities in the western part of the Jiangnan Orogen and previous ones from the Cathaysia and Yangtze blocks, we can conclude this study as following:

- (1) The subduction of the Paleo–South China Ocean started at ca. 1000 Ma and ended at ca. 865 Ma;
- (2) The Jiangnan Orogenic Belt was built up due to the assembly of the Yangtze and Cathaysia blocks between 865 and 820 Ma;
- (3) The deposition environment of the Early Neoproterozoic Sibao group and its equivalents can be divided into two stages. Firstly, the lower part of the Sibao group was deposited in an active continental margin at ca. 1000–865 Ma. Secondly, the upper part of the Sibao group accumulated in a syn-collisional setting at ca. 865–820 Ma;
- (4) The Danzhou group and its equivalents began to deposit since ca. 780 Ma in the Jiangnan Orogen area.

Table 3-3. U-Pb dating for six samples

Analysis	CORRECTED RATIOS						CORRECTED AGES (Ma)						Concordance
	207Pb/206Pb		207Pb/235U		206Pb/238U		207Pb/206Pb		207Pb/235U		206Pb/238U		
	<i>1σ</i>		<i>1σ</i>		<i>1σ</i>		<i>1σ</i>		<i>1σ</i>		<i>1σ</i>		
Sample 1932													
1932-01	0.11731	0.00568	5.16051	0.20860	0.32068	0.01661	1916	89	1846	34	1793	81	97%
1932-02	0.06823	0.00345	1.38066	0.07205	0.14492	0.00374	876	107	881	31	872	21	99%
1932-03	0.09452	0.01621	3.50162	1.28729	0.26727	0.06555	1518	350	1528	290	1527	333	99%
1932-04	0.12042	0.00385	6.03793	0.24432	0.35793	0.00983	1962	58	1981	35	1972	47	99%
1932-05	0.10396	0.00504	3.66641	0.14856	0.25298	0.00783	1696	92	1564	32	1454	40	92%
1932-06	0.11618	0.00497	5.48316	0.20595	0.34189	0.00801	1898	79	1898	32	1896	38	99%
1932-07	0.11504	0.01260	5.16103	0.56234	0.32132	0.01377	1881	205	1846	93	1796	67	97%
1932-08	0.07409	0.00248	1.46808	0.05399	0.14147	0.00283	1044	69	917	22	853	16	92%
1932-09	0.07512	0.00271	1.47696	0.04999	0.14110	0.00387	1072	74	921	20	851	22	92%
1932-10	0.07276	0.00573	1.47490	0.09475	0.14602	0.00592	1007	165	920	39	879	33	95%
1932-11	0.12619	0.00402	5.97155	0.24065	0.33846	0.01393	2046	58	1972	35	1879	67	95%
1932-12	0.07712	0.00395	2.01947	0.10055	0.18823	0.00370	1124	105	1122	34	1112	20	99%
1932-13	0.06726	0.00413	1.31528	0.06213	0.14145	0.00735	846	131	852	27	853	42	99%
1932-14	0.06839	0.00309	1.42194	0.07388	0.14922	0.00768	880	96	898	31	897	43	99%
1932-15	0.13534	0.00454	7.44220	0.23975	0.39468	0.00635	2168	60	2166	29	2144	29	98%
1932-16	0.08070	0.00200	2.13491	0.07258	0.18971	0.00314	1214	50	1160	24	1120	17	96%
1932-17	0.12718	0.00353	6.69750	0.18765	0.37923	0.00727	2059	50	2072	25	2073	34	99%
1932-19	0.16623	0.00490	10.93315	0.32278	0.47362	0.01335	2520	51	2517	27	2499	58	99%
1932-20	0.10359	0.00422	4.35804	0.16564	0.30594	0.00932	1689	77	1704	31	1721	46	99%
1932-21	0.19126	0.00565	14.25987	0.45337	0.53905	0.01127	2753	50	2767	30	2779	47	99%
1932-22	0.06671	0.00313	1.29095	0.06145	0.13940	0.00281	829	100	842	27	841	16	99%
1932-23	0.06702	0.00283	1.29844	0.06382	0.13878	0.00330	838	90	845	28	838	19	99%
1932-24	0.12682	0.00371	6.59187	0.18242	0.37422	0.00916	2054	53	2058	24	2049	43	99%
1932-25	0.06688	0.00481	1.27921	0.08879	0.13874	0.00458	834	155	837	40	838	26	99%
1932-26	0.06981	0.00367	1.46507	0.07268	0.15121	0.00303	923	111	916	30	908	17	99%
1932-27	0.06990	0.00263	1.56930	0.05988	0.16113	0.00422	925	79	958	24	963	23	99%
1932-28	0.08376	0.00193	2.61070	0.10216	0.22204	0.00626	1287	46	1304	29	1293	33	99%
1932-30	0.06933	0.00371	1.50390	0.08414	0.15526	0.00375	908	113	932	34	930	21	99%
1932-31	0.08764	0.00328	2.91676	0.11448	0.23746	0.00568	1375	74	1386	30	1373	30	99%
1932-32	0.06730	0.00226	1.30886	0.06397	0.13897	0.00885	847	72	850	28	839	50	98%
1932-33	0.06457	0.00305	1.19312	0.06195	0.13154	0.00368	760	102	797	29	797	21	99%
1932-34	0.10711	0.00684	4.86450	0.47341	0.32042	0.01659	1751	120	1796	82	1792	81	99%
1932-35	0.06566	0.00274	1.20882	0.04276	0.13132	0.00241	796	90	805	20	795	14	98%
1932-36	0.06509	0.00275	1.19087	0.04087	0.13031	0.00380	777	91	796	19	790	22	99%
1932-37	0.08023	0.00307	2.14044	0.11783	0.18886	0.00419	1203	77	1162	38	1115	23	95%
1932-38	0.06452	0.00199	1.19140	0.03970	0.13095	0.00293	759	67	797	18	793	17	99%

Oct. 2018							Chapter 3						
1932-40	0.06534	0.00407	1.20681	0.07930	0.13040	0.00330	785	134	804	36	790	19	98%
1932-41	0.08865	0.00302	2.95700	0.09796	0.23682	0.00446	1397	67	1397	25	1370	23	98%
1932-42	0.19715	0.00597	15.46332	0.43792	0.55561	0.00984	2803	51	2844	27	2848	41	99%
1932-43	0.06529	0.00239	1.19799	0.03722	0.13130	0.00331	784	79	800	17	795	19	99%
1932-44	0.10139	0.00305	4.11281	0.12424	0.28827	0.00447	1650	57	1657	25	1633	22	98%
1932-45	0.06670	0.00312	1.29532	0.06056	0.13890	0.00397	828	100	844	27	838	22	99%
1932-46	0.07090	0.00392	1.57160	0.04420	0.15882	0.00963	954	116	959	17	950	54	99%
1932-47	0.06857	0.00198	1.42739	0.04422	0.14906	0.00266	886	61	900	18	896	15	99%
1932-48	0.06938	0.00241	1.47349	0.05492	0.15233	0.00297	910	73	920	23	914	17	99%
1932-49	0.07488	0.00432	1.84196	0.10133	0.17805	0.00502	1065	119	1061	36	1056	27	99%
1932-50	0.18164	0.00527	12.84945	0.40193	0.50923	0.00884	2668	49	2669	29	2653	38	99%
1932-51	0.09313	0.00270	3.33154	0.10573	0.25826	0.00495	1491	56	1488	25	1481	25	99%
1932-52	0.10740	0.00309	4.72624	0.15147	0.31748	0.00614	1756	54	1772	27	1777	30	99%
1932-53	0.08543	0.00551	2.68817	0.16684	0.22685	0.00636	1325	128	1325	46	1318	33	99%
1932-55	0.06866	0.00385	1.31699	0.07430	0.13986	0.00331	889	119	853	33	844	19	98%
1932-56	0.06738	0.00384	1.36608	0.09822	0.14464	0.00443	850	122	874	42	871	25	99%
1932-57	0.15877	0.01140	10.38989	0.74647	0.46750	0.00490	2443	125	2470	67	2473	22	99%
1932-58	0.07404	0.00293	1.80777	0.07037	0.17540	0.00366	1043	82	1048	25	1042	20	99%
1932-60	0.06627	0.00264	1.27416	0.04914	0.13812	0.00303	815	85	834	22	834	17	99%
1932-61	0.11524	0.00503	5.36692	0.19676	0.33412	0.00817	1884	81	1880	31	1858	39	98%
1932-62	0.08986	0.00291	3.13448	0.10706	0.24884	0.00538	1423	63	1441	26	1433	28	99%
1932-63	0.06707	0.00494	1.37333	0.11672	0.14521	0.00543	840	158	878	50	874	31	99%
1932-64	0.06850	0.00414	1.40990	0.08444	0.14732	0.00330	884	128	893	36	886	19	99%
1932-65	0.08281	0.00357	2.40193	0.11787	0.20693	0.00755	1265	86	1243	35	1212	40	97%
1932-66	0.06405	0.00259	1.14520	0.04254	0.12842	0.00288	743	87	775	20	779	16	99%
1932-67	0.06511	0.01635	1.05716	0.19059	0.12980	0.01002	778	527	732	94	787	57	92%
1932-69	0.09593	0.00565	3.60203	0.18360	0.27057	0.00871	1546	114	1550	41	1544	44	99%
1932-70	0.06760	0.00281	1.33800	0.05737	0.14185	0.00337	856	89	862	25	855	19	99%
1932-72	0.06520	0.00382	1.15371	0.06507	0.12942	0.00337	781	127	779	31	785	19	99%
1932-74	0.13738	0.00483	7.58436	0.27023	0.39748	0.00833	2194	63	2183	32	2157	38	98%
1932-75	0.08565	0.00554	2.82318	0.18019	0.23525	0.00779	1330	129	1362	48	1362	41	99%
1932-76	0.06402	0.00300	1.15632	0.05396	0.13105	0.00286	742	102	780	25	794	16	98%
1932-78	0.07146	0.00365	1.62161	0.07860	0.16334	0.00358	971	107	979	30	975	20	99%
1932-79	0.17219	0.00667	11.82885	0.44531	0.49233	0.01004	2579	66	2591	35	2581	43	99%
1932-80	0.15810	0.00613	10.42393	0.45412	0.47053	0.01103	2435	67	2473	40	2486	48	99%
Sample 1933													
1933-01	0.06707	0.00224	1.28918	0.04133	0.13868	0.00232	840	71	841	18	837	13	99%
1933-02	0.06753	0.00111	1.32671	0.02215	0.14129	0.00150	854	35	857	10	852	8	99%
1933-03	0.06681	0.00189	1.28651	0.03685	0.13823	0.00175	832	60	840	16	835	10	99%
1933-04	0.06628	0.00329	1.27793	0.07242	0.13812	0.00256	815	106	836	32	834	14	99%
1933-05	0.06737	0.00173	1.30584	0.03029	0.13972	0.00204	849	55	848	13	843	12	99%

Oct. 2018							Chapter 3						
1933-06	0.06730	0.00123	1.33294	0.02391	0.14242	0.00171	847	39	860	10	858	10	99%
1933-07	0.06669	0.00249	1.28129	0.04978	0.13813	0.00290	828	80	837	22	834	16	99%
1933-08	0.06694	0.00446	1.28766	0.08321	0.13979	0.00650	836	143	840	37	843	37	99%
1933-09	0.06709	0.00145	1.31855	0.02974	0.14145	0.00253	841	46	854	13	853	14	99%
1933-10	0.06713	0.00157	1.30717	0.03373	0.13998	0.00200	842	50	849	15	845	11	99%
1933-11	0.06745	0.00215	1.31183	0.04511	0.14164	0.00312	852	68	851	20	854	18	99%
1933-12	0.08620	0.00207	2.75434	0.06665	0.23054	0.00303	1343	48	1343	18	1337	16	99%
1933-13	0.06942	0.00233	1.49114	0.04031	0.15485	0.00385	911	71	927	16	928	22	99%
1933-14	0.06936	0.00227	1.44574	0.04173	0.15076	0.00320	909	69	908	17	905	18	99%
1933-15	0.06735	0.00179	1.29842	0.03293	0.14049	0.00285	849	57	845	15	847	16	99%
1933-16	0.06689	0.00126	1.32304	0.02650	0.14231	0.00209	834	40	856	12	858	12	99%
1933-17	0.06800	0.00205	1.37953	0.04264	0.14563	0.00223	868	64	880	18	876	13	99%
1933-19	0.06744	0.00243	1.31401	0.04852	0.14057	0.00292	851	77	852	21	848	17	99%
1933-20	0.07308	0.00532	1.72450	0.15062	0.16833	0.00310	1016	152	1018	56	1003	17	98%
1933-21	0.06710	0.00319	1.30791	0.05978	0.14052	0.00344	841	102	849	26	848	19	99%
1933-22	0.06603	0.00162	1.28664	0.03419	0.13965	0.00213	807	52	840	15	843	12	99%
1933-23	0.06689	0.00147	1.29913	0.02807	0.13971	0.00219	834	47	845	12	843	12	99%
1933-24	0.06755	0.00192	1.33372	0.04008	0.14163	0.00215	855	60	861	17	854	12	99%
1933-25	0.07253	0.00171	1.73694	0.04334	0.17216	0.00252	1001	49	1022	16	1024	14	99%
1933-26	0.06850	0.00300	1.34182	0.04800	0.14165	0.00404	884	93	864	21	854	23	98%
1933-27	0.06684	0.00354	1.30177	0.06306	0.14050	0.00392	833	113	847	28	848	22	99%
1933-29	0.06652	0.00178	1.31818	0.03850	0.14247	0.00272	823	57	854	17	859	15	99%
1933-30	0.06748	0.00276	1.34601	0.06006	0.14255	0.00258	853	87	866	26	859	15	99%
1933-31	0.06739	0.00231	1.32555	0.04242	0.14135	0.00277	850	73	857	19	852	16	99%
1933-32	0.07407	0.00199	1.73279	0.09657	0.16927	0.00973	1044	56	1021	36	1008	54	98%
1933-33	0.06742	0.00229	1.33002	0.04068	0.14183	0.00205	851	72	859	18	855	12	99%
1933-34	0.06773	0.00135	1.35963	0.04885	0.14351	0.00412	860	42	872	21	865	23	99%
1933-35	0.07009	0.00137	1.51269	0.06600	0.15679	0.00686	931	41	936	27	939	38	99%
1933-36	0.07417	0.00117	1.83057	0.11687	0.17265	0.00964	1046	33	1056	42	1027	53	97%
1933-37	0.06850	0.00152	1.36538	0.03102	0.14773	0.00414	884	47	874	13	888	23	98%
1933-38	0.06747	0.00186	1.30732	0.03716	0.13959	0.00201	852	59	849	16	842	11	99%
1933-39	0.11481	0.00145	5.43353	0.08223	0.34102	0.00390	1877	23	1890	13	1892	19	99%
1933-40	0.09799	0.00224	3.74855	0.09064	0.27658	0.00515	1586	44	1582	19	1574	26	99%
1933-41	0.07207	0.00138	1.64532	0.06751	0.16489	0.00528	988	40	988	26	984	29	99%
1933-42	0.13668	0.00175	7.59934	0.11383	0.40148	0.00455	2186	23	2185	13	2176	21	99%
1933-43	0.07082	0.00104	1.57376	0.07620	0.15974	0.00698	952	31	960	30	955	39	99%
1933-44	0.06891	0.00116	1.41621	0.02326	0.14881	0.00170	896	35	896	10	894	10	99%
1933-45	0.06759	0.00108	1.32214	0.02240	0.14150	0.00167	856	34	855	10	853	9	99%
1933-46	0.06711	0.00135	1.30843	0.02492	0.14085	0.00175	841	43	849	11	849	10	99%
1933-47	0.06828	0.00187	1.38055	0.03645	0.14618	0.00195	877	58	881	16	879	11	99%
1933-48	0.06719	0.00777	1.33740	0.15808	0.14242	0.01078	844	252	862	69	858	61	99%

Oct. 2018							Chapter 3						
1933-49	0.08236	0.00149	2.35604	0.04498	0.20606	0.00264	1254	36	1229	14	1208	14	98%
1933-50	0.09036	0.00274	2.66660	0.08394	0.21289	0.00702	1433	59	1319	23	1244	37	94%
1933-51	0.06877	0.00167	1.43675	0.03649	0.14995	0.00208	892	51	904	15	901	12	99%
1933-52	0.08682	0.00165	2.83481	0.06055	0.23529	0.00339	1356	38	1365	16	1362	18	99%
1933-53	0.06744	0.00177	1.31970	0.03409	0.14119	0.00227	851	56	854	15	851	13	99%
1933-55	0.06822	0.00148	1.35745	0.03703	0.14271	0.00213	875	46	871	16	860	12	98%
1933-56	0.06660	0.00278	1.27370	0.05394	0.13815	0.00353	825	89	834	24	834	20	99%
1933-57	0.06805	0.00184	1.36457	0.03267	0.14489	0.00221	870	58	874	14	872	12	99%
1933-58	0.07217	0.00428	1.58803	0.10505	0.16448	0.00902	991	124	966	41	982	50	98%
1933-59	0.11778	0.00215	5.61321	0.11459	0.34351	0.00514	1923	34	1918	18	1904	25	99%
1933-60	0.07227	0.00457	1.49759	0.08267	0.15047	0.00448	994	132	929	34	904	25	97%
1933-61	0.07059	0.00143	1.54109	0.04707	0.15783	0.00412	946	42	947	19	945	23	99%
1933-62	0.09954	0.00441	3.98989	0.15531	0.29015	0.00865	1616	84	1632	32	1642	43	99%
1933-63	0.06716	0.00170	1.29539	0.03104	0.13925	0.00149	843	54	844	14	840	8	99%
1933-64	0.06639	0.00540	1.29760	0.12218	0.14042	0.00416	819	176	845	54	847	24	99%
1933-65	0.07375	0.00112	1.76123	0.02618	0.17222	0.00165	1035	31	1031	10	1024	9	99%
1933-66	0.07006	0.00226	1.52170	0.05654	0.15614	0.00273	930	68	939	23	935	15	99%
1933-67	0.06746	0.00114	1.30227	0.02368	0.13934	0.00207	852	36	847	10	841	12	99%
1933-68	0.10084	0.00196	3.99947	0.15228	0.28528	0.00952	1640	37	1634	31	1618	48	99%
1933-70	0.07327	0.00136	1.80432	0.03537	0.17712	0.00230	1021	38	1047	13	1051	13	99%
1933-71	0.07180	0.00476	1.68079	0.11763	0.16937	0.00425	980	139	1001	45	1009	23	99%
1933-72	0.15967	0.00503	3.61488	0.17742	0.16219	0.00558	2452	55	1553	39	969	31	53%
1933-73	0.06878	0.00206	1.42677	0.03982	0.15035	0.00253	892	63	900	17	903	14	99%
1933-74	0.06710	0.00178	1.29785	0.03233	0.13976	0.00196	841	56	845	14	843	11	99%
1933-75	0.10599	0.00199	4.55830	0.09008	0.30990	0.00377	1732	35	1742	16	1740	19	99%
1933-76	0.11490	0.00494	5.63555	0.19137	0.35918	0.00810	1878	79	1922	29	1978	38	97%
1933-78	0.06872	0.00345	1.41061	0.06251	0.14894	0.00458	890	106	893	26	895	26	99%
1933-79	0.06781	0.00218	1.33751	0.04273	0.14283	0.00204	863	68	862	19	861	12	99%
1933-80	0.07252	0.00531	1.76485	0.13547	0.17605	0.00712	1001	153	1033	50	1045	39	98%
1933-81	0.06808	0.00322	1.32275	0.05796	0.13806	0.00304	871	101	856	25	834	17	97%
1933-83	0.06801	0.00758	1.29398	0.12912	0.14234	0.00761	869	242	843	57	858	43	98%
1933-84	0.09226	0.00337	3.31957	0.11466	0.25615	0.00504	1473	71	1486	27	1470	26	98%
1933-85	0.09171	0.01082	3.07858	0.28600	0.25951	0.01139	1461	235	1427	71	1487	58	95%
1933-86	0.09334	0.00365	3.29911	0.12349	0.25274	0.00638	1495	76	1481	29	1453	33	98%
1933-87	0.07718	0.00695	2.01745	0.15689	0.19002	0.00668	1126	186	1121	53	1121	36	99%
1933-88	0.07426	0.00320	1.90937	0.07560	0.18411	0.00455	1049	89	1084	26	1089	25	99%
Sample 1714-1													
1714-1-01	0.07154	0.00178	1.61878	0.04321	0.16309	0.00254	973	52	978	17	974	14	99%
1714-1-02	0.10637	0.00183	4.55423	0.08226	0.30863	0.00373	1738	32	1741	15	1734	18	99%
1714-1-03	0.07263	0.00148	1.61866	0.03222	0.16076	0.00184	1004	42	977	12	961	10	98%
1714-1-04	0.07213	0.00141	1.67095	0.03393	0.16746	0.00220	990	41	998	13	998	12	99%

Oct. 2018							Chapter 3						
1714-1-05	0.11075	0.00193	5.00524	0.08450	0.32612	0.00325	1812	32	1820	14	1820	16	99%
1714-1-06	0.11083	0.00487	4.84952	0.20768	0.32047	0.00904	1813	82	1794	36	1792	44	99%
1714-1-07	0.13839	0.00204	7.87486	0.12141	0.41011	0.00426	2207	26	2217	14	2215	19	99%
1714-1-08	0.09393	0.00180	3.45752	0.06072	0.26479	0.00343	1507	37	1518	14	1514	18	99%
1714-1-09	0.11642	0.00254	5.54820	0.12663	0.34330	0.00524	1902	40	1908	20	1903	25	99%
1714-1-10	0.06935	0.00193	1.46627	0.03650	0.15291	0.00222	909	59	917	15	917	12	99%
1714-1-11	0.06917	0.00296	1.45002	0.06358	0.15119	0.00320	904	90	910	26	908	18	99%
1714-1-12	0.10754	0.00197	4.74606	0.08804	0.31793	0.00374	1758	34	1775	16	1780	18	99%
1714-1-13	0.10561	0.00163	4.53011	0.07520	0.30856	0.00341	1725	29	1737	14	1734	17	99%
1714-1-15	0.11013	0.00167	4.96748	0.07466	0.32484	0.00314	1801	28	1814	13	1813	15	99%
1714-1-16	0.10715	0.00178	4.65163	0.07725	0.31317	0.00355	1752	31	1759	14	1756	17	99%
1714-1-17	0.10862	0.00187	4.83633	0.08100	0.32060	0.00363	1776	32	1791	14	1793	18	99%
1714-1-18	0.16514	0.00345	10.96670	0.25254	0.47872	0.00757	2509	36	2520	21	2522	33	99%
1714-1-19	0.09902	0.00176	3.92371	0.07033	0.28502	0.00320	1606	34	1619	15	1617	16	99%
1714-1-20	0.06779	0.00208	1.30200	0.03430	0.14026	0.00205	862	65	847	15	846	12	99%
1714-1-21	0.09701	0.00179	3.73954	0.06732	0.27723	0.00310	1567	35	1580	14	1577	16	99%
1714-1-22	0.10640	0.00218	4.50465	0.08922	0.30443	0.00308	1739	38	1732	16	1713	15	98%
1714-1-24	0.09981	0.00207	3.92866	0.08100	0.28284	0.00362	1620	40	1620	17	1606	18	99%
1714-1-25	0.16622	0.00256	11.12771	0.16162	0.48188	0.00486	2520	26	2534	14	2535	21	99%
1714-1-26	0.06689	0.00163	1.22497	0.03404	0.13149	0.00238	834	52	812	16	796	14	98%
1714-1-27	0.16481	0.00247	10.97470	0.16478	0.47874	0.00501	2506	26	2521	14	2522	22	99%
1714-1-28	0.09773	0.00153	3.84900	0.06567	0.28256	0.00339	1581	30	1603	14	1604	17	99%
1714-1-29	0.06718	0.00135	1.31618	0.02582	0.14075	0.00166	843	43	853	11	849	9	99%
1714-1-30	0.10071	0.00199	4.11519	0.08588	0.29330	0.00421	1637	38	1657	17	1658	21	99%
1714-1-31	0.16435	0.00324	10.93429	0.28865	0.47680	0.00967	2501	34	2518	25	2513	42	99%
1714-1-32	0.16544	0.00301	11.05102	0.20105	0.48056	0.00677	2512	31	2527	17	2530	29	99%
1714-1-33	0.11233	0.00411	5.12774	0.21026	0.32789	0.00535	1838	68	1841	35	1828	26	99%
1714-1-34	0.09960	0.00393	3.88712	0.14221	0.28518	0.00755	1617	75	1611	30	1617	38	99%
1714-1-35	0.06876	0.00235	1.44186	0.04899	0.15061	0.00276	891	72	906	20	904	15	99%
1714-1-36	0.10937	0.00159	4.86004	0.07670	0.31913	0.00382	1789	27	1795	13	1785	19	99%
1714-1-37	0.06903	0.00189	1.43067	0.03673	0.14982	0.00195	900	58	902	15	900	11	99%
1714-1-38	0.07234	0.00145	1.72420	0.03858	0.17095	0.00206	996	42	1018	14	1017	11	99%
1714-1-39	0.10577	0.00224	4.53483	0.09435	0.30866	0.00363	1728	40	1737	17	1734	18	99%
1714-1-40	0.07327	0.00242	1.77411	0.05630	0.17437	0.00387	1021	68	1036	21	1036	21	99%
1714-1-41	0.06908	0.00255	1.45712	0.05361	0.15212	0.00281	901	78	913	22	913	16	99%
1714-1-42	0.07099	0.00298	1.55409	0.05707	0.15947	0.00273	957	88	952	23	954	15	99%
1714-1-43	0.07544	0.00214	1.63911	0.05460	0.15603	0.00406	1080	58	985	21	935	23	94%
1714-1-44	0.10363	0.00176	4.41396	0.10035	0.30589	0.00550	1690	32	1715	19	1720	27	99%
1714-1-45	0.06563	0.00186	1.20482	0.04329	0.13199	0.00375	795	61	803	20	799	21	99%
1714-1-46	0.06755	0.00146	1.34810	0.02850	0.14366	0.00150	855	46	867	12	865	8	99%
1714-1-47	0.10412	0.00251	4.40754	0.10619	0.30450	0.00438	1699	45	1714	20	1714	22	99%

Oct. 2018							Chapter 3						
1714-1-48	0.07416	0.00186	1.91731	0.06741	0.18350	0.00346	1046	52	1087	23	1086	19	99%
1714-1-49	0.07195	0.00269	1.64957	0.06023	0.16542	0.00362	985	78	989	23	987	20	99%
1714-1-50	0.06837	0.00174	1.39266	0.03539	0.14692	0.00187	880	54	886	15	884	10	99%
1714-1-51	0.06498	0.00287	1.18494	0.04805	0.13172	0.00276	774	95	794	22	798	16	99%
1714-1-52	0.07236	0.00153	1.68397	0.03651	0.16771	0.00251	996	44	1002	14	999	14	99%
1714-1-53	0.06560	0.00346	1.18368	0.07705	0.13151	0.00804	794	113	793	36	796	46	99%
1714-1-54	0.10358	0.00211	4.36014	0.10120	0.30347	0.00580	1689	38	1705	19	1709	29	99%
1714-1-55	0.10001	0.00186	3.99787	0.07343	0.28816	0.00309	1624	35	1634	15	1632	15	99%
1714-1-56	0.10292	0.00188	4.27786	0.09022	0.29983	0.00487	1677	34	1689	17	1690	24	99%
1714-1-57	0.06818	0.00136	1.37512	0.02546	0.14579	0.00161	874	42	878	11	877	9	99%
1714-1-58	0.06934	0.00188	1.46847	0.03923	0.15246	0.00228	909	57	917	16	915	13	99%
1714-1-59	0.06660	0.00159	1.27243	0.02957	0.13761	0.00193	825	51	833	13	831	11	99%
1714-1-60	0.06810	0.00142	1.36723	0.02798	0.14472	0.00179	872	44	875	12	871	10	99%
1714-1-61	0.06848	0.00266	1.40396	0.05136	0.14758	0.00224	883	82	891	22	887	13	99%
1714-1-62	0.07194	0.00176	1.64300	0.04154	0.16424	0.00221	984	51	987	16	980	12	99%
1714-1-63	0.10171	0.00265	4.17175	0.10939	0.29615	0.00424	1655	49	1668	21	1672	21	99%
1714-1-64	0.10087	0.00280	4.08594	0.11511	0.29208	0.00484	1640	53	1651	23	1652	24	99%
1714-1-65	0.06800	0.00162	1.37316	0.03154	0.14603	0.00195	869	51	878	13	879	11	99%
1714-1-66	0.06722	0.00152	1.31522	0.04045	0.14022	0.00336	845	48	852	18	846	19	99%
1714-1-67	0.06542	0.00286	1.19848	0.04931	0.13197	0.00301	788	94	800	23	799	17	99%
1714-1-68	0.17041	0.00387	11.57207	0.24727	0.48959	0.00669	2562	39	2570	20	2569	29	99%
1714-1-69	0.07303	0.00267	1.75584	0.06387	0.17327	0.00290	1015	76	1029	24	1030	16	99%
1714-1-71	0.07283	0.00196	1.76881	0.05127	0.17377	0.00293	1009	56	1034	19	1033	16	99%
1714-1-73	0.10419	0.00251	4.37509	0.09973	0.30239	0.00380	1700	45	1708	19	1703	19	99%
1714-1-74	0.06869	0.00174	1.43370	0.03611	0.14993	0.00228	889	53	903	15	901	13	99%
1714-1-75	0.11030	0.00206	5.06845	0.09288	0.32980	0.00365	1804	35	1831	16	1837	18	99%
1714-1-76	0.06767	0.00139	1.33009	0.02651	0.14126	0.00161	859	44	859	12	852	9	99%
1714-1-77	0.09760	0.00430	3.81377	0.17036	0.28025	0.00401	1579	85	1596	36	1593	20	99%
1714-1-78	0.09591	0.00193	3.62594	0.09013	0.27111	0.00509	1546	39	1555	20	1546	26	99%
1714-1-79	0.07521	0.00214	1.88673	0.04998	0.18092	0.00249	1074	59	1076	18	1072	14	99%
1714-1-80	0.06943	0.00226	1.48889	0.04734	0.15441	0.00249	912	69	926	19	926	14	99%
Sample 1714													
1714-01	0.06705	0.00215	1.33750	0.03982	0.14297	0.00216	839	68	862	17	861	12	99%
1714-02	0.06729	0.00218	1.32006	0.04064	0.14168	0.00233	847	69	855	18	854	13	99%
1714-03	0.06679	0.00302	1.33644	0.06058	0.14277	0.00282	831	97	862	26	860	16	99%
1714-04	0.09477	0.00256	3.59590	0.09064	0.27161	0.00431	1523	52	1549	20	1549	22	99%
1714-05	0.12198	0.00280	6.26301	0.13698	0.36614	0.00520	1985	42	2013	19	2011	25	99%
1714-06	0.16716	0.00415	11.38092	0.26704	0.48590	0.00800	2529	43	2555	22	2553	35	99%
1714-07	0.16884	0.00446	11.64512	0.30697	0.49069	0.00862	2546	45	2576	25	2574	37	99%
1714-08	0.09482	0.00268	3.61416	0.09737	0.27107	0.00473	1524	55	1553	21	1546	24	99%
1714-09	0.07367	0.00231	1.98579	0.18566	0.18824	0.01560	1032	65	1111	63	1112	85	99%

Oct. 2018							Chapter 3						
1714-10	0.08722	0.00400	2.84866	0.13349	0.23201	0.00642	1365	90	1368	35	1345	34	98%
1714-11	0.06857	0.00424	1.43401	0.08903	0.14916	0.00503	886	132	903	37	896	28	99%
1714-13	0.17719	0.00494	12.63911	0.32232	0.50961	0.00878	2627	47	2653	24	2655	38	99%
1714-14	0.08172	0.00305	2.41132	0.08487	0.21267	0.00463	1239	75	1246	25	1243	25	99%
1714-15	0.10603	0.00292	4.32377	0.10570	0.29200	0.00465	1732	52	1698	20	1652	23	97%
1714-16	0.06701	0.00265	1.34225	0.05843	0.14269	0.00249	838	84	864	25	860	14	99%
1714-17	0.10190	0.00213	4.08488	0.08795	0.28815	0.00419	1659	40	1651	18	1632	21	98%
1714-18	0.10908	0.00269	4.83940	0.23650	0.31784	0.01366	1784	46	1792	41	1779	67	99%
1714-19	0.10710	0.00220	4.63169	0.09171	0.31136	0.00450	1751	39	1755	17	1747	22	99%
1714-21	0.06872	0.00252	1.41639	0.05692	0.14898	0.00346	890	78	896	24	895	19	99%
1714-22	0.08146	0.00158	2.40280	0.05476	0.21255	0.00319	1233	39	1243	16	1242	17	99%
1714-23	0.06695	0.00231	1.31648	0.04830	0.14157	0.00269	836	74	853	21	854	15	99%
1714-24	0.06946	0.00139	1.47374	0.03826	0.15384	0.00368	912	42	920	16	922	21	99%
1714-25	0.09913	0.00186	3.86354	0.08272	0.28151	0.00401	1608	36	1606	17	1599	20	99%
1714-26	0.06737	0.00121	1.32085	0.02597	0.14152	0.00178	849	38	855	11	853	10	99%
1714-27	0.10090	0.00244	4.07220	0.09647	0.29190	0.00454	1641	46	1649	19	1651	23	99%
1714-28	0.08075	0.00145	2.33756	0.04336	0.20911	0.00250	1215	36	1224	13	1224	13	99%
1714-29	0.06704	0.00235	1.28559	0.04304	0.13926	0.00348	839	75	839	19	840	20	99%
1714-30	0.09552	0.00565	3.40922	0.15114	0.26217	0.00904	1538	114	1507	35	1501	46	99%
1714-31	0.06836	0.00276	1.40001	0.05903	0.14787	0.00273	880	86	889	25	889	15	99%
1714-32	0.06987	0.00185	1.47962	0.03888	0.15380	0.00292	924	56	922	16	922	16	99%
1714-34	0.09501	0.00727	3.71007	0.41324	0.26624	0.00559	1528	149	1574	89	1522	28	96%
1714-35	0.07095	0.00212	1.59036	0.04917	0.16209	0.00274	956	62	966	19	968	15	99%
1714-36	0.06818	0.00249	1.37724	0.04767	0.14635	0.00261	874	77	879	20	880	15	99%
1714-38	0.10469	0.00212	4.42844	0.11506	0.30455	0.00576	1709	38	1718	22	1714	28	99%
1714-39	0.07280	0.00272	1.67902	0.07413	0.16764	0.00483	1008	78	1001	28	999	27	99%
1714-40	0.06764	0.00248	1.34824	0.05463	0.14389	0.00322	858	78	867	24	867	18	99%
1714-41	0.15694	0.00407	10.04995	0.26762	0.46222	0.00804	2423	45	2439	25	2449	35	99%
1714-42	0.09373	0.00225	3.45187	0.09046	0.26570	0.00493	1503	46	1516	21	1519	25	99%
1714-43	0.06809	0.00249	1.37290	0.05283	0.14556	0.00279	871	78	877	23	876	16	99%
1714-44	0.12386	0.00262	6.32447	0.14668	0.36819	0.00621	2012	38	2022	20	2021	29	99%
1714-45	0.09971	0.00270	3.99757	0.11172	0.28892	0.00474	1619	52	1634	23	1636	24	99%
1714-46	0.10741	0.00263	4.71895	0.11675	0.31751	0.00509	1756	46	1771	21	1778	25	99%
1714-47	0.07067	0.00250	1.55005	0.06402	0.15775	0.00381	948	74	951	25	944	21	99%
1714-48	0.07171	0.00502	1.52822	0.09813	0.15737	0.00500	978	147	942	39	942	28	99%
1714-49	0.07190	0.00244	1.66061	0.05689	0.16761	0.00285	983	71	994	22	999	16	99%
1714-51	0.08174	0.00250	2.42479	0.10993	0.21221	0.00617	1239	61	1250	33	1241	33	99%
1714-52	0.06952	0.00193	1.47602	0.03860	0.15285	0.00190	914	58	921	16	917	11	99%
1714-53	0.07011	0.00185	1.52922	0.04126	0.15736	0.00277	932	55	942	17	942	15	99%
1714-54	0.06784	0.00227	1.34185	0.04678	0.14240	0.00302	864	71	864	20	858	17	99%
1714-55	0.06776	0.00137	1.34355	0.02616	0.14241	0.00152	861	43	865	11	858	9	99%

Oct. 2018							Chapter 3						
1714-56	0.16140	0.00246	10.63941	0.16318	0.47270	0.00478	2470	26	2492	14	2495	21	99%
1714-57	0.08408	0.00160	2.64081	0.04771	0.22579	0.00257	1294	38	1312	13	1312	14	99%
1714-58	0.10763	0.00171	4.76127	0.07868	0.31723	0.00367	1760	30	1778	14	1776	18	99%
1714-59	0.09462	0.00207	3.51678	0.07804	0.26720	0.00365	1521	42	1531	18	1527	19	99%
1714-60	0.06995	0.00237	1.49890	0.04640	0.15453	0.00308	927	71	930	19	926	17	99%
1714-61	0.10181	0.00206	4.16121	0.09753	0.29233	0.00427	1657	38	1666	19	1653	21	99%
1714-62	0.06729	0.00182	1.33047	0.03536	0.14212	0.00238	847	57	859	15	857	13	99%
1714-63	0.06706	0.00196	1.28589	0.03425	0.13888	0.00190	840	62	839	15	838	11	99%
1714-64	0.06792	0.00188	1.32237	0.04699	0.13933	0.00296	866	59	856	21	841	17	98%
1714-65	0.06728	0.00131	1.33973	0.03684	0.14248	0.00254	846	42	863	16	859	14	99%
1714-66	0.07279	0.00130	1.70383	0.03419	0.16898	0.00250	1008	37	1010	13	1006	14	99%
1714-67	0.07991	0.00205	2.24080	0.06311	0.20125	0.00323	1195	52	1194	20	1182	17	99%
1714-68	0.07342	0.00127	1.80532	0.03762	0.17674	0.00249	1025	36	1047	14	1049	14	99%
1714-69	0.09807	0.00166	3.84654	0.07401	0.28230	0.00421	1588	32	1603	16	1603	21	99%
1714-70	0.06929	0.00175	1.44490	0.03689	0.15103	0.00227	907	53	908	15	907	13	99%
1714-71	0.13857	0.00233	7.87581	0.13829	0.41069	0.00543	2209	30	2217	16	2218	25	99%
1714-72	0.07402	0.00252	1.71736	0.06068	0.17022	0.00451	1042	70	1015	23	1013	25	99%
1714-73	0.06696	0.00119	1.29508	0.02706	0.13906	0.00214	836	38	844	12	839	12	99%
1714-74	0.07091	0.00159	1.60677	0.03691	0.16284	0.00224	955	47	973	14	973	12	99%
1714-75	0.22346	0.00485	18.69396	0.65106	0.60190	0.01812	3006	36	3026	34	3038	73	99%
1714-76	0.06722	0.00156	1.31866	0.02948	0.14115	0.00195	845	49	854	13	851	11	99%
1714-77	0.06698	0.00108	1.30041	0.02466	0.13953	0.00186	837	34	846	11	842	11	99%
1714-78	0.06678	0.00224	1.30742	0.04489	0.14065	0.00240	831	72	849	20	848	14	99%
1714-79	0.07066	0.00175	1.58797	0.03824	0.16163	0.00270	947	52	965	15	966	15	99%
1714-80	0.06893	0.00113	1.44928	0.02364	0.15100	0.00161	897	35	910	10	907	9	99%
1714-81	0.06747	0.00332	1.35845	0.07264	0.14271	0.00485	852	105	871	31	860	27	98%
1714-82	0.16183	0.00584	10.11088	0.33341	0.44403	0.00923	2475	62	2445	30	2369	41	96%
1714-83	0.16004	0.00520	10.46067	0.37266	0.46327	0.01145	2456	56	2476	33	2454	50	99%
1714-84	0.11970	0.00516	5.49687	0.21507	0.32645	0.00710	1952	79	1900	34	1821	34	95%
1714-85	0.12327	0.00533	6.35889	0.27083	0.36601	0.00911	2004	79	2027	37	2011	43	99%
1714-86	0.11643	0.00638	5.88077	0.24194	0.36280	0.01070	1902	101	1958	36	1995	51	98%
1714-87	0.07445	0.00457	1.83960	0.11597	0.17692	0.00480	1054	127	1060	41	1050	26	99%
1714-88	0.06705	0.00733	1.34523	0.15398	0.14256	0.00570	839	238	865	67	859	32	99%
Sample 1399													
1399-01	0.06799	0.00217	1.39189	0.05015	0.14671	0.00233	868	68	886	21	882	13	99%
1399-02	0.07140	0.00430	1.59807	0.09124	0.16187	0.00440	969	126	969	36	967	24	99%
1399-03	0.06828	0.00154	1.37106	0.03228	0.14461	0.00180	877	48	877	14	871	10	99%
1399-04	0.06851	0.00148	1.39991	0.03334	0.14721	0.00224	884	46	889	14	885	13	99%
1399-05	0.06442	0.00227	1.15890	0.04195	0.12960	0.00218	755	76	781	20	786	12	99%
1399-06	0.06647	0.00257	1.21144	0.05247	0.13115	0.00357	821	83	806	24	794	20	98%
1399-07	0.07099	0.00147	1.62611	0.03590	0.16511	0.00192	957	43	980	14	985	11	99%

1399-08	0.06689	0.00159	1.27862	0.03052	0.13824	0.00191	834	51	836	14	835	11	99%
1399-09	0.06788	0.00167	1.34464	0.03116	0.14312	0.00169	865	52	865	13	862	10	99%
1399-10	0.06793	0.00480	1.33784	0.08738	0.14376	0.00418	866	151	862	38	866	24	99%
1399-11	0.06495	0.00296	1.16629	0.05420	0.12969	0.00291	773	98	785	25	786	17	99%
1399-12	0.06879	0.00255	1.42890	0.05014	0.15029	0.00331	892	78	901	21	903	19	99%
1399-13	0.06652	0.00131	1.27067	0.02708	0.13815	0.00199	823	42	833	12	834	11	99%
1399-14	0.06594	0.00140	1.21145	0.02619	0.13265	0.00213	805	45	806	12	803	12	99%
1399-15	0.06572	0.00205	1.18955	0.03213	0.13136	0.00268	797	67	796	15	796	15	99%
1399-16	0.06549	0.00259	1.20191	0.04488	0.13249	0.00371	790	85	801	21	802	21	99%
1399-17	0.06604	0.00142	1.21797	0.03160	0.13250	0.00170	808	46	809	14	802	10	99%
1399-18	0.06523	0.00210	1.16436	0.03400	0.12914	0.00297	782	69	784	16	783	17	99%
1399-19	0.06768	0.00131	1.32669	0.02687	0.14168	0.00181	859	41	857	12	854	10	99%
1399-20	0.06668	0.00308	1.21988	0.05047	0.13236	0.00399	828	99	810	23	801	23	98%
1399-21	0.06675	0.00177	1.22159	0.04138	0.13145	0.00240	830	56	811	19	796	14	98%
1399-22	0.06524	0.00268	1.19045	0.04737	0.13225	0.00310	782	88	796	22	801	18	99%
1399-23	0.06740	0.00137	1.32933	0.02892	0.14269	0.00208	850	43	859	13	860	12	99%
1399-24	0.06517	0.00354	1.18706	0.06527	0.13100	0.00287	780	117	795	30	794	16	99%
1399-25	0.06742	0.00128	1.31990	0.02759	0.14096	0.00188	851	40	854	12	850	11	99%
1399-26	0.06664	0.00335	1.23254	0.06852	0.13264	0.00265	827	108	815	31	803	15	98%
1399-27	0.06686	0.00131	1.28476	0.02568	0.13869	0.00190	833	42	839	11	837	11	99%
1399-28	0.07182	0.00448	1.58211	0.08574	0.16099	0.00464	981	131	963	34	962	26	99%
1399-29	0.06956	0.00345	1.47502	0.08087	0.15317	0.00463	915	105	920	33	919	26	99%
1399-30	0.11587	0.00212	5.58581	0.11254	0.34575	0.00455	1893	34	1914	17	1914	22	99%
1399-31	0.07012	0.00261	1.50997	0.05099	0.15563	0.00273	932	78	934	21	932	15	99%
1399-32	0.07130	0.00187	1.60570	0.04098	0.16294	0.00224	966	55	972	16	973	12	99%
1399-33	0.06942	0.00346	1.51326	0.08374	0.15622	0.00337	911	105	936	34	936	19	99%
1399-34	0.06931	0.00184	1.45728	0.04158	0.15158	0.00245	908	56	913	17	910	14	99%
1399-35	0.06868	0.00314	1.43852	0.07163	0.15058	0.00331	889	97	905	30	904	19	99%
1399-36	0.06794	0.00175	1.35618	0.04014	0.14394	0.00252	867	55	870	17	867	14	99%
1399-37	0.11222	0.00269	5.09496	0.13308	0.32763	0.00488	1836	45	1835	22	1827	24	99%
1399-38	0.06735	0.00226	1.31937	0.04850	0.14132	0.00299	849	71	854	21	852	17	99%
1399-39	0.07342	0.00297	1.69578	0.07264	0.16780	0.00386	1026	84	1007	27	1000	21	99%
1399-40	0.07036	0.00291	1.51314	0.06083	0.15677	0.00415	939	87	936	25	939	23	99%
1399-41	0.06979	0.00546	1.44111	0.10488	0.15162	0.00558	922	166	906	44	910	31	99%
1399-42	0.06992	0.00265	1.50563	0.06107	0.15595	0.00417	926	80	933	25	934	23	99%
1399-43	0.06721	0.00342	1.30583	0.06635	0.14069	0.00365	844	109	848	29	849	21	99%
1399-44	0.06846	0.00303	1.38103	0.05922	0.14579	0.00466	883	94	881	25	877	26	99%
1399-45	0.06789	0.00291	1.34516	0.05842	0.14318	0.00302	865	91	865	25	863	17	99%
1399-46	0.06744	0.00192	1.32420	0.03924	0.14123	0.00206	851	60	856	17	852	12	99%
1399-47	0.06848	0.00457	1.33008	0.08508	0.14180	0.00701	883	142	859	37	855	40	99%
1399-48	0.06806	0.00308	1.36937	0.05369	0.14514	0.00337	870	96	876	23	874	19	99%

Oct. 2018							Chapter 3						
1399-49	0.06641	0.00229	1.27998	0.04150	0.13851	0.00226	819	74	837	18	836	13	99%
1399-50	0.06883	0.00282	1.41768	0.05305	0.14816	0.00263	894	87	896	22	891	15	99%
1399-51	0.06933	0.00293	1.45949	0.05673	0.15132	0.00365	909	89	914	23	908	20	99%
1399-52	0.06516	0.00226	1.18446	0.03780	0.13110	0.00256	780	75	793	18	794	15	99%
1399-53	0.06769	0.00379	1.31892	0.06968	0.14337	0.00406	859	119	854	31	864	23	98%
1399-54	0.06757	0.00496	1.30490	0.08790	0.14098	0.00405	855	157	848	39	850	23	99%
1399-55	0.06877	0.00227	1.41378	0.04580	0.14795	0.00279	892	70	895	19	889	16	99%
1399-56	0.06712	0.00382	1.30268	0.07615	0.13977	0.00420	841	122	847	34	843	24	99%
1399-57	0.06888	0.00298	1.38877	0.06157	0.14757	0.00415	895	91	884	26	887	23	99%
1399-58	0.06716	0.00198	1.29235	0.03747	0.13941	0.00215	843	63	842	17	841	12	99%
1399-59	0.06755	0.00452	1.34360	0.08606	0.14363	0.00301	855	143	865	37	865	17	99%
1399-60	0.14992	0.00424	8.84926	0.24187	0.43096	0.00825	2345	49	2323	25	2310	37	99%
1399-61	0.06556	0.00595	1.20400	0.10862	0.13209	0.00318	792	198	802	50	800	18	99%
1399-62	0.06765	0.00349	1.33165	0.06248	0.14283	0.00314	858	110	860	27	861	18	99%
1399-63	0.06610	0.00286	1.19903	0.04590	0.13189	0.00234	810	93	800	21	799	13	99%
1399-64	0.06892	0.00207	1.42126	0.04447	0.14832	0.00214	896	63	898	19	892	12	99%
1399-65	0.06995	0.00278	1.48149	0.04563	0.15327	0.00330	927	84	923	19	919	18	99%
1399-66	0.22220	0.00359	18.57936	0.31601	0.60279	0.00755	2997	27	3020	16	3041	30	99%
1399-67	0.06777	0.00403	1.35426	0.08245	0.14345	0.00322	862	127	869	36	864	18	99%
1399-68	0.06826	0.00130	1.38111	0.02853	0.14542	0.00187	876	40	881	12	875	11	99%
1399-69	0.06713	0.00189	1.29386	0.03699	0.13899	0.00220	842	60	843	16	839	12	99%
1399-70	0.06708	0.00136	1.30816	0.02924	0.14002	0.00192	840	43	849	13	845	11	99%
1399-71	0.06719	0.00183	1.30581	0.03567	0.13959	0.00218	844	58	848	16	842	12	99%
1399-72	0.06724	0.00197	1.32313	0.04123	0.14140	0.00233	845	62	856	18	853	13	99%
1399-73	0.06759	0.00127	1.36365	0.02546	0.14508	0.00203	856	40	873	11	873	11	99%
1399-74	0.06597	0.00150	1.21697	0.03125	0.13219	0.00202	805	49	808	14	800	11	98%
1399-75	0.06501	0.00340	1.20334	0.06851	0.13260	0.00313	775	113	802	32	803	18	99%
1399-76	0.06876	0.00407	1.44776	0.10017	0.15027	0.00418	891	126	909	42	902	23	99%
1399-77	0.06748	0.00168	1.33417	0.03323	0.14191	0.00165	853	53	861	14	855	9	99%
1399-78	0.06792	0.00268	1.34041	0.05123	0.14456	0.00250	866	84	863	22	870	14	99%
1399-79	0.06785	0.00151	1.39198	0.02897	0.14749	0.00180	864	47	886	12	887	10	99%
1399-80	0.06740	0.00136	1.34778	0.02804	0.14317	0.00168	850	43	867	12	863	9	99%
Sample 1400													
1400-01	0.06914	0.00320	1.45335	0.05742	0.15127	0.00287	903	98	911	24	908	16	99%
1400-02	0.06766	0.00278	1.35130	0.05011	0.14328	0.00403	858	88	868	22	863	23	99%
1400-03	0.16020	0.00508	10.40726	0.30550	0.46542	0.00863	2458	55	2472	27	2463	38	99%
1400-04	0.06921	0.00207	1.46917	0.04442	0.15176	0.00348	905	63	918	18	911	19	99%
1400-05	0.06747	0.00204	1.37245	0.04043	0.14563	0.00238	852	64	877	17	876	13	99%
1400-06	0.06730	0.00272	1.34532	0.05537	0.14337	0.00340	847	86	866	24	864	19	99%
1400-07	0.06988	0.00268	1.50421	0.06083	0.15427	0.00306	925	81	932	25	925	17	99%
1400-08	0.11543	0.00352	5.32829	0.15256	0.33159	0.00684	1887	56	1873	24	1846	33	98%

Oct. 2018							Chapter 3						
1400-09	0.10023	0.00367	3.93478	0.15899	0.28188	0.00638	1628	70	1621	33	1601	32	98%
1400-10	0.07947	0.00471	2.11889	0.11093	0.19195	0.00629	1184	120	1155	36	1132	34	97%
1400-11	0.06702	0.00264	1.30086	0.05740	0.13978	0.00392	838	84	846	25	843	22	99%
1400-12	0.07105	0.00348	1.61810	0.08996	0.16347	0.00220	959	103	977	35	976	12	99%
1400-13	0.06787	0.00305	1.29956	0.04925	0.13848	0.00356	864	95	846	22	836	20	98%
1400-14	0.06783	0.00328	1.33610	0.06902	0.14199	0.00460	863	103	862	30	856	26	99%
1400-15	0.07013	0.00224	1.50873	0.04591	0.15514	0.00271	932	67	934	19	930	15	99%
1400-16	0.07221	0.00170	1.60613	0.03834	0.16026	0.00223	992	49	973	15	958	12	98%
1400-17	0.06809	0.00185	1.35935	0.03795	0.14338	0.00198	871	58	872	16	864	11	99%
1400-18	0.16555	0.00342	11.23001	0.24387	0.48677	0.00717	2513	36	2542	20	2557	31	99%
1400-19	0.06690	0.00293	1.27037	0.05091	0.13817	0.00278	835	94	833	23	834	16	99%
1400-20	0.10448	0.00403	4.41733	0.15925	0.30388	0.00762	1705	73	1716	30	1711	38	99%
1400-21	0.06651	0.00218	1.28428	0.03964	0.13854	0.00220	823	70	839	18	836	12	99%
1400-22	0.17048	0.00399	11.14558	0.32487	0.47383	0.01415	2562	40	2535	27	2500	62	98%
1400-23	0.10266	0.00297	4.24087	0.16517	0.29530	0.00900	1673	55	1682	32	1668	45	99%
1400-24	0.06820	0.00451	1.32370	0.08551	0.14246	0.00408	875	141	856	37	859	23	99%
1400-25	0.06635	0.00199	1.27839	0.03868	0.13812	0.00220	817	64	836	17	834	12	99%
1400-26	0.06713	0.00463	1.34484	0.09825	0.14317	0.00333	842	148	865	43	863	19	99%
1400-27	0.06715	0.00206	1.31693	0.03734	0.14145	0.00332	842	65	853	16	853	19	99%
1400-28	0.06909	0.00274	1.44108	0.06162	0.14945	0.00272	901	84	906	26	898	15	99%
1400-29	0.15777	0.00261	10.14962	0.17886	0.46093	0.00538	2432	29	2449	16	2444	24	99%
1400-30	0.17317	0.00380	12.19365	0.27491	0.50728	0.00805	2589	37	2619	21	2645	34	99%
1400-31	0.06653	0.00165	1.28398	0.03365	0.13864	0.00247	823	53	839	15	837	14	99%
1400-32	0.06693	0.00204	1.30523	0.03478	0.14066	0.00239	836	65	848	15	848	13	99%
1400-33	0.06779	0.00206	1.39139	0.04543	0.14719	0.00197	862	65	885	19	885	11	99%
1400-34	0.15452	0.00243	9.72375	0.16557	0.45215	0.00478	2397	27	2409	16	2405	21	99%
1400-35	0.07068	0.00146	1.59205	0.03219	0.16322	0.00211	948	43	967	13	975	12	99%
1400-36	0.06984	0.00333	1.49148	0.06226	0.15477	0.00570	924	100	927	25	928	32	99%
1400-37	0.07067	0.00255	1.50814	0.04569	0.15536	0.00240	948	76	934	18	931	13	99%
1400-38	0.10961	0.00333	4.88774	0.17672	0.32126	0.00724	1793	57	1800	30	1796	35	99%
1400-39	0.06839	0.00182	1.36767	0.04323	0.14414	0.00278	881	56	875	19	868	16	99%
1400-40	0.06756	0.00209	1.30513	0.03766	0.14011	0.00255	855	66	848	17	845	14	99%
1400-41	0.06769	0.00167	1.33974	0.03576	0.14324	0.00200	859	53	863	16	863	11	99%
1400-42	0.07927	0.00205	2.26835	0.06419	0.20654	0.00288	1179	52	1203	20	1210	15	99%
1400-43	0.06708	0.00280	1.28404	0.07522	0.13810	0.00640	840	89	839	33	834	36	99%
1400-44	0.07470	0.00186	1.77121	0.04640	0.17119	0.00222	1061	51	1035	17	1019	12	98%
1400-45	0.09705	0.00305	3.75007	0.13215	0.27922	0.00706	1568	60	1582	28	1587	36	99%
1400-46	0.07103	0.00221	1.59339	0.05200	0.16175	0.00285	958	65	968	20	966	16	99%
1400-47	0.08128	0.00327	2.24645	0.08931	0.19978	0.00428	1228	81	1196	28	1174	23	98%
1400-48	0.09398	0.00220	3.48453	0.09916	0.26652	0.00676	1508	45	1524	22	1523	34	99%
1400-49	0.08456	0.00308	2.54867	0.08482	0.21940	0.00369	1306	72	1286	24	1279	20	99%

1400-50	0.06894	0.00358	1.42175	0.06765	0.14851	0.00396	897	110	898	28	893	22	99%
1400-51	0.06936	0.00247	1.45701	0.05645	0.15059	0.00381	909	75	913	23	904	21	99%
1400-52	0.16564	0.00339	10.78816	0.22767	0.46627	0.00690	2514	35	2505	20	2467	30	98%
1400-53	0.11243	0.00277	4.85816	0.11855	0.30975	0.00622	1839	46	1795	21	1739	31	96%
1400-54	0.06723	0.00336	1.32268	0.04995	0.14247	0.00392	845	107	856	22	859	22	99%
1400-56	0.06986	0.00275	1.49350	0.06258	0.15326	0.00370	924	83	928	25	919	21	99%
1400-57	0.11007	0.00258	4.95601	0.12287	0.32333	0.00524	1801	44	1812	21	1806	26	99%
1400-58	0.10501	0.00261	4.37816	0.10608	0.29970	0.00422	1715	47	1708	20	1690	21	98%
1400-59	0.07058	0.00290	1.36641	0.07259	0.13812	0.00393	945	86	875	31	834	22	95%
1400-60	0.06848	0.00408	1.40266	0.07934	0.14711	0.00335	883	127	890	34	885	19	99%
1400-61	0.06898	0.00271	1.42549	0.05324	0.14870	0.00287	898	83	900	22	894	16	99%
1400-62	0.07539	0.00278	1.89096	0.06562	0.18036	0.00298	1079	76	1078	23	1069	16	99%
1400-63	0.07011	0.00253	1.54062	0.05488	0.15769	0.00347	932	76	947	22	944	19	99%
1400-64	0.06740	0.00206	1.33959	0.03965	0.14250	0.00227	850	65	863	17	859	13	99%
1400-65	0.06855	0.00211	1.40752	0.03831	0.14748	0.00252	885	65	892	16	887	14	99%
1400-66	0.06870	0.00309	1.39418	0.07280	0.14474	0.00337	890	95	886	31	871	19	98%
1400-67	0.11579	0.00264	5.45262	0.11789	0.33918	0.00454	1892	42	1893	19	1883	22	99%
1400-68	0.07203	0.00151	1.66491	0.03495	0.16583	0.00210	987	44	995	13	989	12	99%
1400-69	0.11018	0.00229	4.81230	0.10243	0.31282	0.00418	1802	39	1787	18	1755	21	98%
1400-70	0.06858	0.00176	1.39058	0.03387	0.14620	0.00211	886	54	885	14	880	12	99%
1400-71	0.06921	0.00288	1.45225	0.06636	0.15068	0.00380	905	88	911	27	905	21	99%
1400-72	0.06790	0.00151	1.35130	0.02975	0.14272	0.00177	865	47	868	13	860	10	99%
1400-73	0.06728	0.00130	1.34503	0.02829	0.14338	0.00206	846	41	865	12	864	12	99%
1400-74	0.06730	0.00137	1.34457	0.02598	0.14380	0.00180	847	43	865	11	866	10	99%
1400-75	0.06811	0.00229	1.34642	0.04491	0.14233	0.00260	872	71	866	19	858	15	99%
1400-76	0.06755	0.00206	1.32918	0.04096	0.14147	0.00180	855	65	859	18	853	10	99%
1400-77	0.07099	0.00294	1.52485	0.05860	0.15553	0.00281	957	87	940	24	932	16	99%
1400-78	0.06742	0.00198	1.34263	0.03912	0.14334	0.00209	851	62	864	17	863	12	99%
1400-79	0.06924	0.00186	1.42076	0.03408	0.14844	0.00177	906	57	898	14	892	10	99%
1400-80	0.06724	0.00206	1.31723	0.03924	0.14166	0.00197	845	65	853	17	854	11	99%
1400-81	0.14798	0.00658	9.24976	0.38216	0.44344	0.00896	2323	78	2363	38	2366	40	99%
1400-82	0.10379	0.00453	4.32561	0.18317	0.29553	0.00601	1693	82	1698	35	1669	30	98%
1400-83	0.06817	0.00299	1.36387	0.05840	0.14215	0.00321	874	93	874	25	857	18	98%
1400-84	0.07493	0.00649	1.87987	0.19442	0.17557	0.00602	1067	180	1074	69	1043	33	97%
1400-85	0.14236	0.00534	8.48009	0.30717	0.42374	0.00881	2256	66	2284	33	2277	40	99%
1400-87	0.06798	0.00687	1.35949	0.13182	0.14369	0.00539	868	218	872	57	865	30	99%
1400-88	0.06943	0.00389	1.54323	0.08897	0.15807	0.00516	911	119	948	36	946	29	99%
1400-89	0.07252	0.00402	1.69964	0.09472	0.16906	0.00601	1001	116	1008	36	1007	33	99%
1400-91	0.06645	0.00505	1.31174	0.10372	0.14325	0.00548	820	164	851	46	863	31	98%
1400-92	0.06825	0.00669	1.33830	0.11747	0.14209	0.00578	876	211	862	51	856	33	99%
1400-93	0.06692	0.00471	1.26485	0.08440	0.13783	0.00551	835	151	830	38	832	11	98%

Oct. 2018							Chapter 3						
1400-94	0.06759	0.00516	1.33331	0.09202	0.14223	0.00464	856	163	860	40	857	26	99%
1400-95	0.09646	0.00596	3.68582	0.21780	0.27680	0.00873	1557	119	1568	47	1575	44	99%
1400-96	0.09469	0.00473	3.89650	0.18405	0.29684	0.01093	1522	97	1613	38	1676	54	96%
1400-97	0.06727	0.01016	1.28883	0.20443	0.14302	0.00860	846	335	841	91	862	49	97%
1400-99	0.14944	0.00558	9.34571	0.34047	0.44412	0.01002	2340	65	2373	33	2369	45	99%
1400-100	0.14594	0.00563	8.92821	0.34277	0.43502	0.01066	2299	68	2331	35	2328	48	99%

Chapter 4. The construction mechanism of the Neoproterozoic S-type Sanfang-Yuanbaoshan granite plutons in the Jiangnan Orogenic Belt, South China: insights from the Geological observation, Geochronology, AMS and Bouger gravity modelling

4.1 Introduction of magmatisms of pluton emplacement and research objectives

Magmatic rock is an important constituent part of the continent crust (e.g., [de Saint-Blanquat et al., 2006](#); [Paterson, 2009](#)), and magmatic activity plays a significant role in the recycling of crustal material and crust-mantle interaction (e.g., [Faure & Pons, 1991](#); [Roman & Jaupart, 2016](#)). Therefore, it is essential to study the magmatism in order to obtain a better understanding of the magmatic process and the crustal evolution. Several aspects, such as: i) magma generation, ii) differentiation, iii) transport and ascent, and iv) emplacement, must be distinguished in the magmatic evolution (e.g., [Glazner & Bartley, 2006](#); [Hutton, 1988](#); [Pitcher, 1979](#)). The magma emplacement is the last but an essential stage of the process. During the emplacement, some features documented both in the pluton and its country rocks reflect the interaction between the magma and the country rocks as well as the space needed for the magma emplacement (e.g., [Paterson et al., 2008](#); [Stevenson et al., 2007](#)).

Previous studies showed that the features of the intrusive magma bodies are not only dominated by composition, temperature and pressure of magma, but also controlled by the rheology of the crust and synmagmatic regional tectonic setting ([Caricchi, et al., 2007](#); [Castro, 1987](#); [de Saint-Blanquat et al., 2006](#); [Glazner & Bartley, 2006](#); [Hutton, 1988](#); [Moyen et al., 2003](#); [Wei et al., 2014, 2016](#)). Consequently, deciphering the magma emplacement process, i.e., (1) the geometry of the pluton ([Cruden, 1998](#); [Cruden et al., 2017](#); [Mathieu et al., 2008](#); [O'Driscoll et al., 2006](#); [Stevenson et al., 2007](#)); (2) the style of magma channel ([Clemens & Mawer, 1992](#); [Paterson, 2009](#)); (3) the deformation and thermal conditions of the granite and its country rocks ([Byerly et al., 2017](#); [de Saint-Blanquat et al., 2001, 2006](#); [Paterson et al., 1989](#); [Žák et al., 2007](#)), can help to determine the evolution of the granite pluton and the

continental crust.

The magma emplacement has been long studied, and several models were proposed, i.e., diapirism (Paterson & Vernon, 1995), ballooning (Bateman, 1984), injection through dykes and sills (Burchardt, 2008; Gudmundsson, 1990, 2011; Morgan et al., 2017; Weinberg, 1999), stopping (Daly, 1903; Glazner et al., 2006, 2007; Paterson, 2008) and syntectonic magma emplacement (Allibon et al., 2011; de Saint Blanquat et al., 2011; Faure & Pons, 1991; Hutton, 1988; Pitcher, 1979). Liu (2017) briefly summarized these models into two groups, namely the forceful and permissive, and proposed that both the magma property and the tectonics are widely thought to be the important factors to the magma emplacement and granite pluton construction. Features of different kinds of emplacement are presented in the Table 4-1.

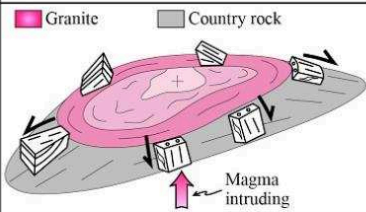
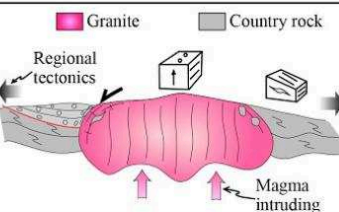
<i>Mechanism</i>		<i>Forceful</i>	<i>Permissive</i> (Passive or syn-tectonic)
<i>Features</i>			
<i>Sketch of the pluton, country rock and characteristics of emplacement</i>			
<i>Mode of pluton buliding</i>		diapirism, ballooning	dyke accretion, cauldron subsidence
<i>Deformation and fabric pattern</i>	<i>Wall rock</i>	ductile deformation around the pluton and its aureole	ductile deformation by tectonics, brittle fracturing
	<i>Pluton</i>	concordant planar and linear fabrics between the pluton and wall rocks along the contact	preferred mineral orientation corresponding to the regional tectonic regime
<i>Dynamics of pluton emplacement</i>		internal force (magma bouyancy)	external force (regional tectonics)

Table 4-1. A conclusive classification of different magma emplacement mechanisms and its associated features (Liu, 2017).

S-type granite is considered as a kind of granite produced by partial melting and crystallization of Al-rich rocks, such as crustal orthogneiss and pelitic sediments forming the lower to middle continental crust. It is commonly accepted that peraluminous magma is a syn-

to post-orogenic product formed by the melting of the thickened orogenic root (Chappell & White, 2001). However, S-type granite may also emplace in an intracontinental setting (e.g., most of the post-orogenic plutons in the Early Paleozoic orogen of SE China), and also in an active continental margin (for instance in the central Andes). In the Jiangnan Orogenic Belt, the peraluminous granite plutons crop out sporadically from east to west, including the, Xucun, Jiuling, Yuanbaoshan, Sanfang and Fanjingshan plutons (Figure 4-1). In order to better constrain the Neoproterozoic evolution of the Jiangnan Orogeny, studies on the emplacement of the Neoproterozoic granite plutons along the Jiangnan Orogenic Belt as well as the detailed consideration of the pluton construction, syn-magmatic and syn (post)-tectonic events are necessary. Consequently, we choose the Sanfang-Yuanbaoshan plutons, located in the western part of the Jiangnan Orogenic Belt, as the study target to decipher the late stage of the evolution of the Jiangnan orogeny.

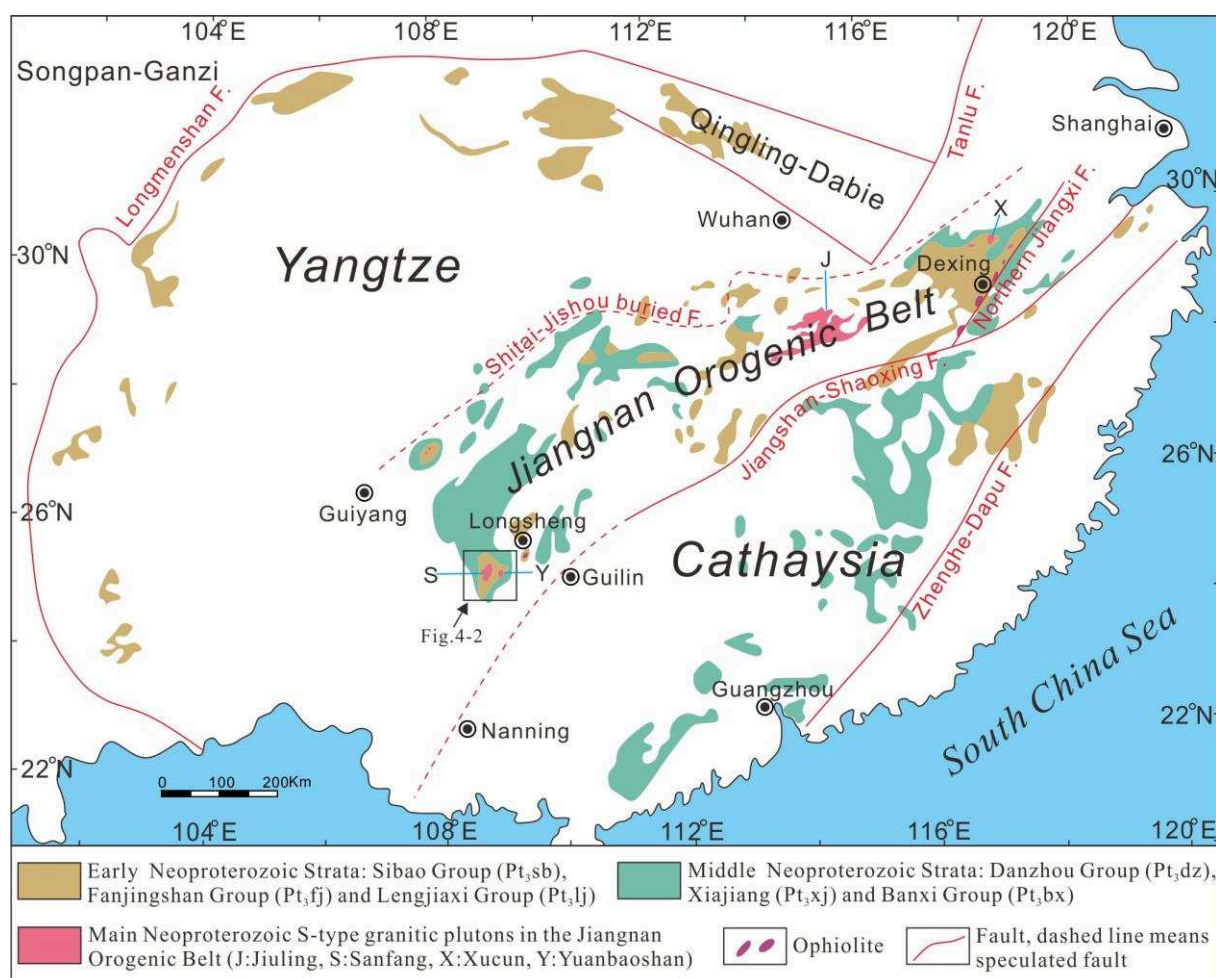


Figure 4-1. Tectonic outline of China and geological sketch map of the Yangtze and Cathaysia blocks.

4.2 Geological setting

4.2.1 The Jiangnan Orogenic Belt

The Jiangnan Orogenic Belt is an important tectonic unit in the South China Block, representing the Neoproterozoic NE–SW to E–W trending belt developed as a consequence of the collision between the Yangtze and Cathaysia blocks. The oceanic subduction of the Paleo–South China Ocean beneath the Yangtze Block since ca. 1000 Ma (Wang et al., 2007, 2008; Yao et al., 2014b) and its final closure were responsible for the formation of the Jiangnan magmatic arc, followed by the collision (or continental subduction) of Cathaysia Block (Shu, 2012; Wang et al., 2012b). Numerous ultramafic, mafic magmatic (gabbro, diorite), and volcanic rocks, interpreted as ophiolites, dated from ca. 1000 Ma to ca. 870 Ma, distribute along the suture zone (BGMRAH, 1982; BGMRJX, 1984; BGMRZJ, 1989; Xia et al., 2018).

The Precambrian basement in the Jiangnan Orogenic Belt is composed of the Sibao group and its equivalents; the Danzhou group and its equivalents unconformably cover the deformed Sibao group (refer to Chapter 2 for detailed descriptions). The Danzhou group unconformity indicates that an orogenic event had taken place in the Jiangnan Orogenic Belt before the initial deposition of the Danzhou group. The collision related orogeny led to the distinct deformation but weak metamorphism (greenschist facies) of the Sibao group and its equivalents (BGMRGX, 1985; BGMRHN, 1988; Charvet, 2013; Shu, 2012). The strata of the Sibao group were folded owing to the northwestward subduction of the Paleo South China oceanic crust below the Yangtze Block and the collision between the Yangtze and Cathaysia blocks. Northeast and north trending tight folds are widely developed in the Sibao group and its equivalents in the western part of the Jiangnan Orogenic Belt (Figure 4-2). However, the primary structure of the Danzhou group was characterised by broad and gentle folds with quite weak metamorphism or even no metamorphism (BGMRGX, 1985).

The Jiangnan Orogenic Belt was intruded by peraluminous granite plutons dated at ca.

850–830 Ma (e.g., Xucun pluton, Jiuling pluton, Yuanbaoshan pluton, Sanfang pluton; **Figure 4-1**) (Guo et al., 1989; Xin et al., 2017; Yao et al., 2014b; Zhang et al., 2013; Zhou et al., 2009).

After the formation of the South China Block, this continent started to rift probably reworking some pre-existing faults related to the Jiangnan orogeny. The NE–SW striking Nanhua rifting at ca. 800 Ma–750 Ma was coeval with the generation of bimodal igneous rocks (Li et al., 2018; Wang & Li, 2003; Xia et al., 2018; Zhang et al., 2018).

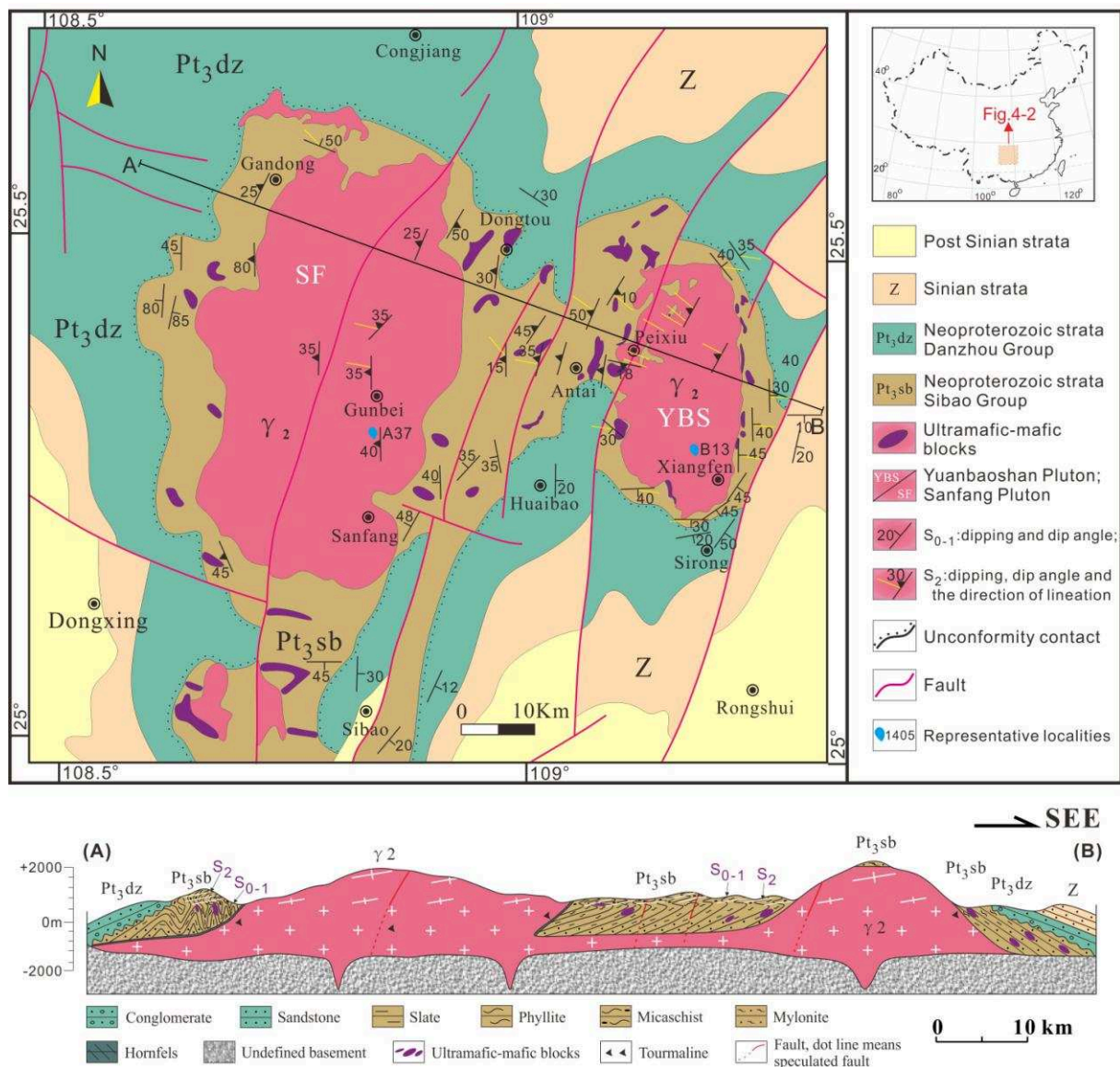


Figure 4-2. Geological sketch map and cross-section for the Sanfang-Yuanbaoshan area. For the cross-section, the contact relationships with the granite plutons and the country rocks are depicted according to the field observations, however, the deep structure of the profile is

inferred from the gravity modeling.

4.2.2 Sanfang-Yuanbaoshan granite plutons

The Sanfang and Yuanbaoshan granite plutons are located in the western part of the Jiangnan Orogenic Belt (Figure 4-1), both of these two plutons have an elliptic shaped surface with an area of ca. 1000 km² and ca. 300 km², respectively (Figure 4-2). The exposure of these two plutons show an N-S elongated geometry with aspect ratio about 2:1. Elevation of the two plutons ranges from ca. 200 meters to ca. 2000 meters.

The two granite plutons both intrude into the Sibao group which is mainly composed of bathyal to abyssal terrigenous arenaceous-argillaceous metasediments with bedded flysch (BGMRGX, 1985). Previous studies indicate that the crystallization age of the plutons varies from 823±5 Ma to 833±6 Ma with high Aluminum Saturation Index ranging in 1.15-1.40 (Yao et al., 2014b). Their geochemical feature indicates that the magma of Sanfang and Yuanbaoshan plutons were derived from supracrustal source rocks (Wang et al., 2007). The widespread tourmaline in the plutons (Li, 1999) reveals that the granites are highly evolved.

As for the deformation, Li (1999) proposed that all the granitic intrusions were deformed to varying degrees showing foliation with gneissic texture. However, Yao et al. (2014b) suggested that the granite plutons show a massive structure without evidence of metamorphism and deformation.

Faults are developed in the granite plutons as well as in the country rocks (Figure 4-2), mainly distributing in the NE-SW and N-S directions. Some kilometer to meter- scale mafic and ultramafic blocks enclosed in the mudstone-sandstone facies of the Sibao group crop out around the plutons. They are interpreted as olistoliths (BGMRGX, 1985).

4.3 Field observations

The Sanfang and Yuanbaoshan granite plutons are both shaped like N-S long and E-W narrow. These two plutons both intrude into the Sibao group which are unconformably covered by the Danzhou group. In the field, we have investigated the plutons and the country rocks, and found that some geological features are different with the descriptions of the

previous researches. Detailed field observations are presented in the following sections.

4.3.1 Granite plutons

The Sanfang pluton stands at a varying elevation ranging from ca. 200 meters to ca. 1800 meters, however, the elevation of the Yuanbao pluton attains to ca. 2000 meters. The granitic rocks of these two plutons mainly consist of quartz, plagioclase, K-feldspar, biotite and muscovite, thus they belong to a porphyritic monzogranite. However, the monzogranitic body is surrounded by a fine grain facies devoid of K-feldspar megacrysts but rich in tourmaline-plagioclase nodules. A small amount of tourmaline can be observed in some outcrops (B19, 1404; [Figures 4-3C and 4-3S](#)). We cover the two plutons as much as possible in order to obtain a good understanding of them, and according to the field observation, the granite plutons can be roughly divided into two parts, namely, undeformed and deformed ones.

For the Sanfang pluton, the undeformed granites are mostly at the elevation below 750 meters, with the magmatic texture (A51 (2065), A55; [Figures 4-3A and 4-3B](#)), distributing in the southern, southeastern, and western parts of the pluton. The quartz and feldspar are euhedral but are different in size as the elevation changed. In the northwestern part of the pluton, with the elevation of about 600 meters, the granites are massive and the quartz and feldspar grains are in the size of 1-3 millimeters (A51; [Figures 4-3A](#)). However, in the southern part of the pluton with a relative lower elevation of around 350 meters, the K-feldspar grains are in the size of 1-10 centimeters, with a preferred orientation of sub E-W (A55; [Figures 4-3B](#)). In the northeastern part of the Sanfang pluton (1404, altitude of 450 meters), the tourmaline nodules are oriented in the E-W direction within the undeformed granite. As to the Yuanbaoshan pluton, the elevation of ca. 700 meters seems like the separatrix of the undeformed and deformed granites. The undeformed ones are mainly distributed in the central to the southern part of the pluton. Similar to the features of the Sanfang granites, the grain sizes change from 1-10 centimeters to 3-5 millimeters when the elevation increases from ca. 200 to 600 meters. In the southeast, close to the east boundary between the granite and country rock, the granite is massive but the tourmaline grains are

orientated in the N-S direction (B19 ; [Figures 4-3C](#)).

The deformed granites are located in the central and northern parts of the Sanfang pluton with the elevation above 750 meters ([Figure 4-2](#)). It can be recognized that the low angle ($\sim 30^\circ$) foliations are developed, dipping to the W and SW consistently. Augen structure, gneiss structure and shear band are common in this area. The mineral and stretching lineations developed by elongated quartz grains, biotite and muscovite aggregates, and pressure shadows around the K-feldspar megacrysts are trend in the E-W direction, with the top-to-the-W kinematics (A46; [Figure 4-3D](#)).

However, in the Yuanbaoshan pluton, deformed granites are distributed in the central-northwestern part with the elevation higher than ca. 700 meters. The quartz and feldspar are deformed to augen, original magmatic structures are modified to gneiss structures (B08; [Figure 4-3E](#)). And the lineations are consistently directed in the sub E-W with gentle angle. Furthermore, in the northern part of the Yuanbaoshan pluton (2013, altitude of 2000 meters), the roof of the pluton is covered by the horizontal well-foliated Sibao group.

4.3.2 Country rocks

Neoproterozoic strata are well exposed in the Sanfang-Yuanbaoshan area, including the Sibao group, Danzhou group and Sinian strata. Generally, the Sinian strata and Danzhou group display broad and gentle folds with very low grade metamorphism or even no metamorphism ([BGMRGX, 1985](#)). However, the Sibao group shows tight folds with greenschist facies metamorphism ([BGMRGX, 1985](#)). Based on our field observations, we found that the degree of metamorphism and deformation of the Sibao group varies greatly in different sub areas:

- (1) On the west of the Sanfang pluton, close to the granite body (distance less than 2 km), the Sibao group is not metamorphic but tightly folded by upright folds. The original bedding (S_{0-1}) is nearly upright with $75-90^\circ$ angle (1442; [Figure 4-3F](#)), however, the occurrence of the Sibao group becomes gentle when it is a little bit far away (distance greater than 2 km) from the pluton, the S_{0-1} dips to the W with an angle of $30-45^\circ$ (1445; [Figure 4-3G](#)).

- Hornfels is observed in the contact boundary between the granite and the country rock (1440; [Figure 4-3H](#)) with a width of 10 meters;
- (2) On the north of the Sanfang pluton, the Sibao group is metamorphosed to schist and its foliation S_1 dips northwards with a gentle angle of 35-45°, the quartz vein interlayered in the foliated Sibao group indicates a top-to-the-N kinematic (1893; [Figure 4-3I](#));
 - (3) On the southwest of the Sanfang pluton, the foliation S_1 of the Sibao group (1447) dips to the southwest with an angle of 45°, however, when the Sibao group is far away from the pluton, the bedding planes (S_{0-1}) dip more gently to the southeast with an angle of 20° (1713; [Figure 4-3T](#));
 - (4) The Sibao group between the Sanfang and Yuanbaoshan plutons shows higher degrees of the metamorphism and deformation. In general, the sediments were metamorphosed to phyllite and micaschist. Deformation style in this area is complex: (i) the Sibao strata with flysch sequences were deformed to recumbent folds, with the folds axis plunging to the N (2050; [Figure 4-3J](#)); (ii) the primary foliations S_{0-1} were again modified by the later penetrative foliations (S_2), which are consistently dipping to the W with gentle angles of 15-45° (1406; [Figure 4-3K](#) and [4-3K'](#)). And the sigmoid quartz vein indicates a top-to-the-W kinematic (1407; [Figure 4-3L](#)); (iii) the lineations in the Sibao group are coherent with NW-SE and sub E-W directions (2051; [Figure 4-3M](#)); (iv) however, the rocks are weakly metamorphosed (1459; [Figure 4-3U](#)) at the elevation lower than 700 meters, and the foliation S_2 and lineation are un conspicuous;
 - (5) On the west of the Yuanbaoshan pluton, the foliations S_2 are dipping to the W, except the site on the SSW of the Peixiu village which may be affected by the shape of the pluton, the lineations are sub E-W directed ([Figure 4-2](#));
 - (6) On the northeast of the Yuanbaoshan pluton, the foliation S_{0-1} is dipping northeastwards and the shear bands indicate the top-to-the NE kinematics, and the lineation is sub E-W directed (2015; [Figure 4-3N](#));
 - (7) On the south and southeast of the Yuanbaoshan pluton. The Sibao group is weakly

metamorphosed, the foliations S_{0-1} are turning with the geometry of the pluton with gentle angles of 20-45°, however, the lineations are not developed (2030; [Figure 4-3O](#));

- (8) On the east of the Yuanbaoshan pluton, the protolith of the Sibao group was metamorphosed to phyllite, the foliations S_{0-1} are dipping to the E with angles of 30-50°, and the quartz veins indicate an eastward kinematics (2037, 1468; [Figures 4-3P](#) and [4-3Q](#)), the lineations are close E-W directed consistently;
- (9) In the northern part of the Yuanbaoshan pluton, at the elevation of 1800 meters, the Sibao group above on the granite, with strongly deformed to the mylonite (2013; [Figures 4-3R](#)), the foliation S_2 is horizontal with the E-W directed lineation.

In summary, the degrees of the metamorphism and deformation of the Sibao group are positively related with the elevation, and can be divided to three parts according to the elevation: (i) The Sibao group at the elevation below 200 meters display no metamorphism, which mainly consists of sandstone and mudstone. Foliation and lineation are absent, while the bedding planes of the strata are dispersed; (ii) The degrees of the metamorphism and deformation of the Sibao group at the elevation of 200-700 meters are higher than those of below the 200 meters. In this part, the foliations (S_1) of the Sibao group are the original sedimentary bedding (S_0) and distributed disorderly, however, for those close to the plutons, they are controlled by the shape of the plutons. The lineations are much developed than those of the lower part, with a sub E-W direction; (iii) For the Sibao group at the altitude higher than 700 meters, the degrees of deformation and metamorphism are totally different with the lower parts (< 800m). The original beddings (S_0) of the Sibao group are folded and even overturned as recumbent fold (S_1), with the axis gently plunging to the north. Furthermore, the later foliations S_2 penetrate the S_{0-1} , consistently dipping to the W with angles of 15-45°. Besides, the lineations are well developed in the sub E-W direction. Moreover, mylonite of the Sibao group was found above the roof of the Yuanbaoshan pluton (~ 2000m), with horizontal foliation and E-W directed lineation.

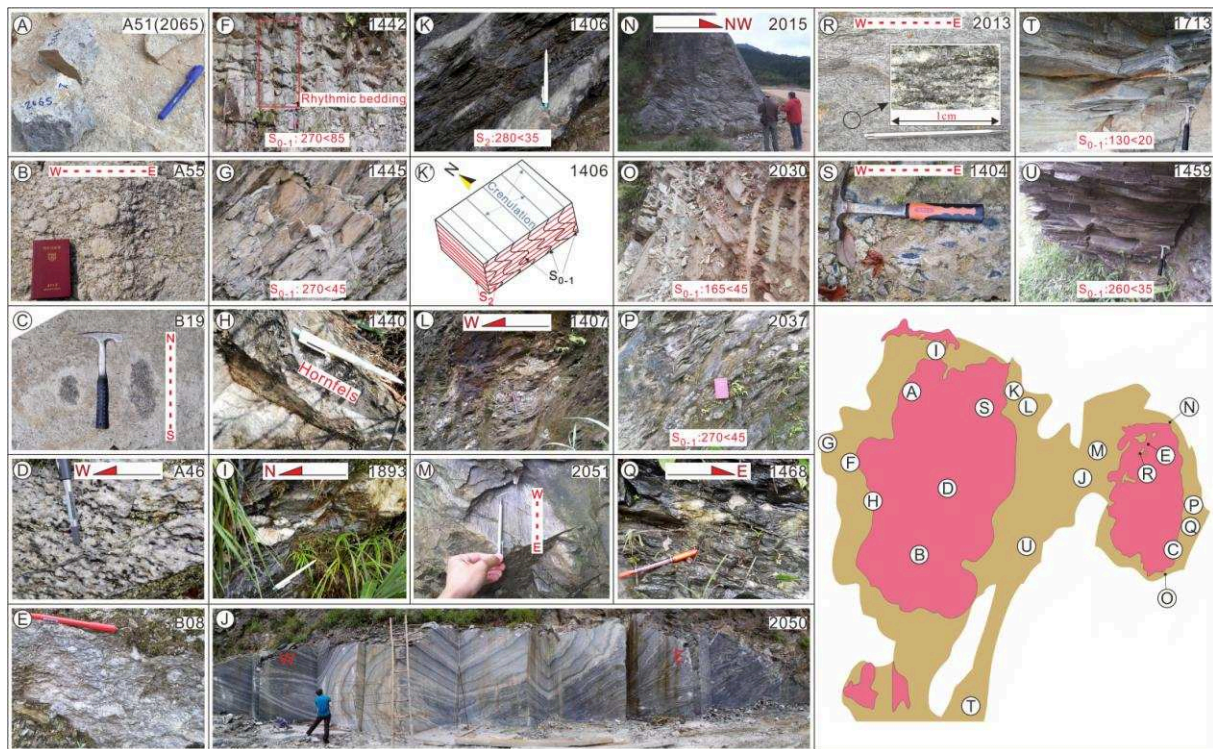


Figure 4-3. Representative field photos in the Sanfang-Yuanbaoshan area, with the geographic localities in the sketch map. (A) Massive granite; (B) Massive granite with big feldspar; (C) N-S elongated tourmalin; (D) Deformed granite with the top-to-the-W kinematics; (E) Granite with augen structures; (F) Sibao group with vertical beddings; (G) Sibao group dips to the W with steep angle; (H) Hornfels between the granites and country rocks; (I) Quartz vein showing top-to-the-N kinematics; (J) Recumbent folds in the Sibao group; (K) The primary foliations S_{0-1} were modified by the later penetrative foliations S_2 in the Sibao group; (K') Sketch of the the K; (L) Sigmoid quartz vein indicates a top-to-the-W kinematic; (M) E-W directed lineations in the Sibao group; (N) Shear bands indicate the top-to-the NE kinematics to the NE of Yuanbaoshan pluton; (O) Weakly metamorphosed dipping to the S with steep angle; (P) Foliations S_{0-1} are dipping to the E to the E of Yuanbaoshan pluton; (Q) The quartz veins indicate an eastward kinematics to the E of Yuanbaoshan pluton; (R) Mylonite on the roof of the Yuanbaoshan pluton; (S) E-W elongated tourmalin; (T) Gentle bedding planes (S_{0-1}) dipping to the southeast; (U) Weakly metamorphosed Sibao group.

4.4 Microscopic observations

As different kinds of deformation styles are observed in the field, in order to decipher the

tectonic evolution of the Sanfang-Yuanbaoshan area, we have collected both the granites and country rocks for the microscopic study.

4.4.1 Granite plutons

Tens of thin sections of the Sanfang and Yuanbaoshan granites have been investigated, and reveal that the granites are mainly composed of quartz, K-feldspar, plagioclase, biotite, muscovite and sericite (Figure 4-4). The undeformed granites from the western and southern parts of the Sanfang pluton and southern part of the Yuanbaoshan pluton display magmatic structures with euhedral crystals of quartz, feldspars and micas. The quartz grains show a slightly undulose extinction (A48, A61, A65, A55, B14, B19; Figures 4-4A to 4-4F). However, in the weakly deformed granites, the quartz are mostly recrystallized as neograins with serrated boundaries (A41, B02; Figures 4-4G and 4-4H), showing the evidence of weak high temperature deformation.

Moreover, in the highly deformed granites, the quartz and muscovite are totally recrystallized and show a preferred orientation. The myrmekites are within the feldspars (A44, A46) (Figures 4-4I and 4-4J), which indicates the granites have experienced strong dynamic metamorphism. Myrmekite is an exsolution of quartz and plagioclase due to fluid circulation during deformation. And the mica fishes from the Sanfang and Yuanbaoshan plutons both indicate the top-to-the-W kinematics (A43, B20) (Figures 4-4K and 4-4L).

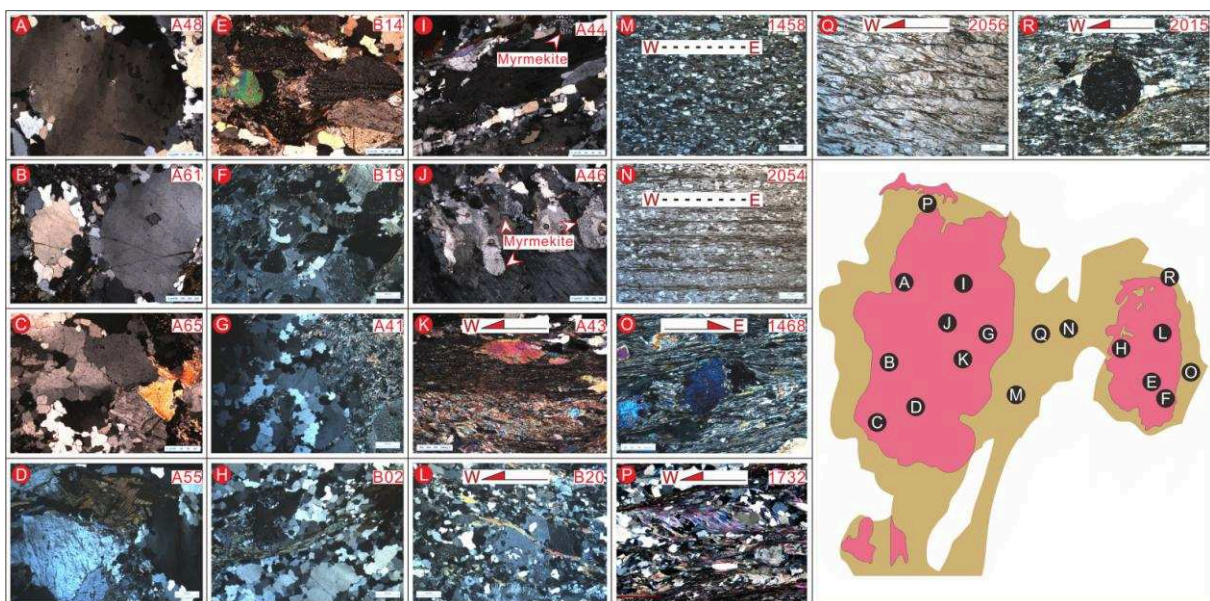


Figure 4-4. Microphotographs with the representative features in the granites and country rocks of the Sanfang-Yuanbaoshan area. (A-F): microphotographs in crossed polarized light of undeformed granites; (G-H): microphotographs in crossed polarized light of weakly deformed granites; (I-J): microphotographs in crossed polarized light of highly deformed granites showing orientated quartz and muscovite and interstitial myrmekite; (K-L): microphotographs in crossed polarized light of highly deformed granites showing top-to-the-W kinematics; (M-N): microphotographs in crossed polarized light and reflected light of the foliated country rocks of Sibao group; (O): microphotographs in crossed polarized light of top-to-the-E kinematic country rock on the east of the Yuanbaoshan pluton; (P-R): microphotographs in crossed polarized light and reflected light of the country rocks with top-to-the-W kinematics.

4.4.2 Country rocks

The microphotographs of the samples at a relative low altitude of 500-700 meters show deformed structures with orientated quartz, biotite and sericite. The quartz grains are modified to elliptical shape with smooth boundaries, and the micas are well elongated in the E-W direction but without kinematic (1458, 2054) (Figures 4-4M and 4-4N). In the micro view of 1468, on the east of the Sanfang pluton, the muscovite is altered to the sericite and strongly deformed, the pressure shadow indicates a top-to-the-E kinematic (Figure 4-4O).

However, in the microphotographs of the samples at relative high altitude of >700 meters, the indicators (e.g., mica fish, shear band, sigma structure and pressure shadows) reveal strong deformation with top-to-the-W kinematics (Figures 4-4P to 4-4R).

Therefore, the microscopic observations reinforce our field work, highlighting that the degrees of metamorphism and deformation in the granites and Sibao group in the Sanfang-Yuanbaoshan area, are positively related with the elevation.

4.5 Magma crystallization age and Hafnium isotopic analysis

The magma U-Pb crystallization age and geochemical features of the Sanfang and Yuanbaoshan plutons have been reported since the past twenty years (Li, 1999; Wang et al.,

2007; Yao et al., 2014b), however, with the development of the testing accuracy, in order to better constrain the evolution of the granite plutons, we have collected two samples, A37 (1403) and B13 (2024) (Figure 4-2), from the Sanfang and Yuanbaoshan plutons, respectively.

4.5.1 Zircon U-Pb age

Zircons were separated from the crushed rocks using heavy liquid and magnetic techniques and then handpicked under a binocular microscope. The zircon grains were mounted in epoxy resin, and then polished and coated with gold. Cathodoluminescence (CL) images of the zircons were obtained using a JEOL JXA8230 electron probe microanalyzer at the Testing Center of Shandong Bureau of China Metallurgical Geology Bureau. The laser ablation (LA)–ICP–MS analysis of zircon U–Pb isotopic compositions was performed at the Testing Center of Shandong Bureau of China Metallurgical Geology Bureau, using a ThermoX2 ICP–MS connected to a GeoLas Pro 193 nm laser ablation system. All analyses were carried out with a spot size of 30 μm or 20 μm and a laser frequency of 10 Hz. Helium was used as the carrier gas to transport the ablated material. The detailed analytical procedure is described in Liu et al. (2010). All measurements were performed using zircon 91500 as the external standard with a $^{206}\text{Pb}/^{238}\text{U}$ age of 1065.4 ± 0.6 Ma (Wiedenbeck et al., 1995). We calibrated elemental contents with NIST610 as the external standard and ^{29}Si as the internal standard. The U–Pb ages were calculated from the raw signal data using the software ICPMSDataCal (ver. 8.4). On account of the ^{204}Pb could not be measured owing to low signal and interference from ^{204}Hg in the gas supply, a common lead correction was carried out using the EXCEL program common Pb correction (Andersen, 2002). For zircons older than 1000 Ma, because of large amounts of radiogenic Pb, the $^{207}\text{Pb}/^{206}\text{Pb}$ age is more reliable than $^{206}\text{Pb}/^{238}\text{U}$, whereas for zircons younger than 1000 Ma, as a result of the low content of radiogenic Pb and uncertainty of common Pb correction, the $^{206}\text{Pb}/^{238}\text{U}$ age is more reliable.

Typical CL images of zircons are presented in Figures 4-5A and 4-5B. U–Pb results are listed in Table 4-2 and graphically illustrated in Figure 4-5. Zircons analyzed in this study range in length from 90 to 200 μm , with length/width ratio ranges from 2:1 to 3:1. All of zircon grains display oscillatory zoning (Figures 4-5A and 4-5B) and high Th/U values (average 0.35; Table

4-2), indicating their magmatic origin (Corfu et al., 2003; Hoskin and Schaltegger, 2003).

Thirty seven zircon U-Pb ages are obtained for each granite pluton (Sanfang and Yuanbaoshan), which fall in the range of 814-1150 Ma and 827-2720 Ma, respectively (Figures 4-5D and 4-5G). However, most of the data indicate ages comprised between 820 to 850 Ma (Figures 4-5E and 4-5H), with an average of 830 ± 2 Ma and 830 ± 5 Ma, respectively (Figures 4-5F and 4-5I). Some ages older than 2.0 Ga may indicate the existence of Paleoproterozoic rocks below the plutons. These grains are xenocrystals included in the granitic magma.

4.5.2 Zircon $\epsilon(\text{Hf})$ analysis

Zircon Hf isotopic composition was analyzed by Neptune MC-ICP-MS, which is a double focusing multi-collector ICP-MS and has the capability of high mass resolution measurements in a multiple collector mode. During laser ablation analyses, the isobaric interference of ^{176}Lu on ^{176}Hf is negligible due to the extremely low $^{176}\text{Lu}/^{177}\text{Hf}$ value in zircon (normally <0.002). However, the interference of ^{176}Yb on ^{176}Hf must be intensively corrected since the contribution of ^{176}Yb to ^{176}Hf . This method can provide an accurate correction of the ^{176}Yb interference on ^{176}Hf (Kemp et al., 2006). During analysis, an isotopic ratio of $^{176}\text{Yb}/^{172}\text{Yb} = 0.5887$ was applied. Standard zircon 91500 was used for the external correction, with a $^{176}\text{Hf}/^{177}\text{Hf}$ value of 0.282300 ± 8 (2σ). The detailed analytical procedure is similar to the description by Yuan et al. (2008). Initial $^{176}\text{Hf}/^{177}\text{Hf}$ values were calculated based on Lu decay constant of 1.865×10^{-11} (Scherer et al., 2001). Model ages were calculated under the assumption that the $^{176}\text{Lu}/^{177}\text{Hf}$ of average crust is 0.015, and the $^{176}\text{Hf}/^{177}\text{Hf}$ and $^{176}\text{Lu}/^{177}\text{Hf}$ ratios of chondrite and depleted mantle at the present are 0.282772 and 0.0332, 0.28325 and 0.0384, respectively (Blichert-Toft and Albarede, 1997). The model ages (TDM) provide only a minimum age for the source material of the magma from which the zircons crystallized.

More than half of the U-Pb dated zircons from the Sanfang granite were chosen for in-situ Hf isotopic analysis. The Hf analyses were executed near the fields used for U-Pb dating spots. For purpose of discussing the Hf isotopic evolution history, the initial $^{176}\text{Hf}/^{177}\text{Hf}$ values and $\epsilon\text{Hf}(t)$ were calculated using the zircon $^{206}\text{Pb}/^{238}\text{U}$ ages. The results of the Hf

isotopic analyses are presented in Table 4-3, and the $\epsilon_{\text{Hf}}(t)$ versus U–Pb age diagram is illustrated in Figure 4-5C. The sample of A37 (1403) show negative $\epsilon_{\text{Hf}}(t)$ values, ranging from -1.89 to -11.15, with an average of -4.63. Correspondingly, on the $\epsilon_{\text{Hf}}(t)$ versus U–Pb age plot, the two model ages ($T_{\text{DM}2}$) mainly concentrate on 1828–2143 Ma, while separately project at 2418 Ma (Figure 4-5C). These results indicate that the analyzed granitic rock was derived from the partial melting of Paleoproterozoic continental basement rocks. In addition, all the isotopic data are plotted under the CHUR line and suggest that the involvement of a mantle component in the granitic magma was negligible.

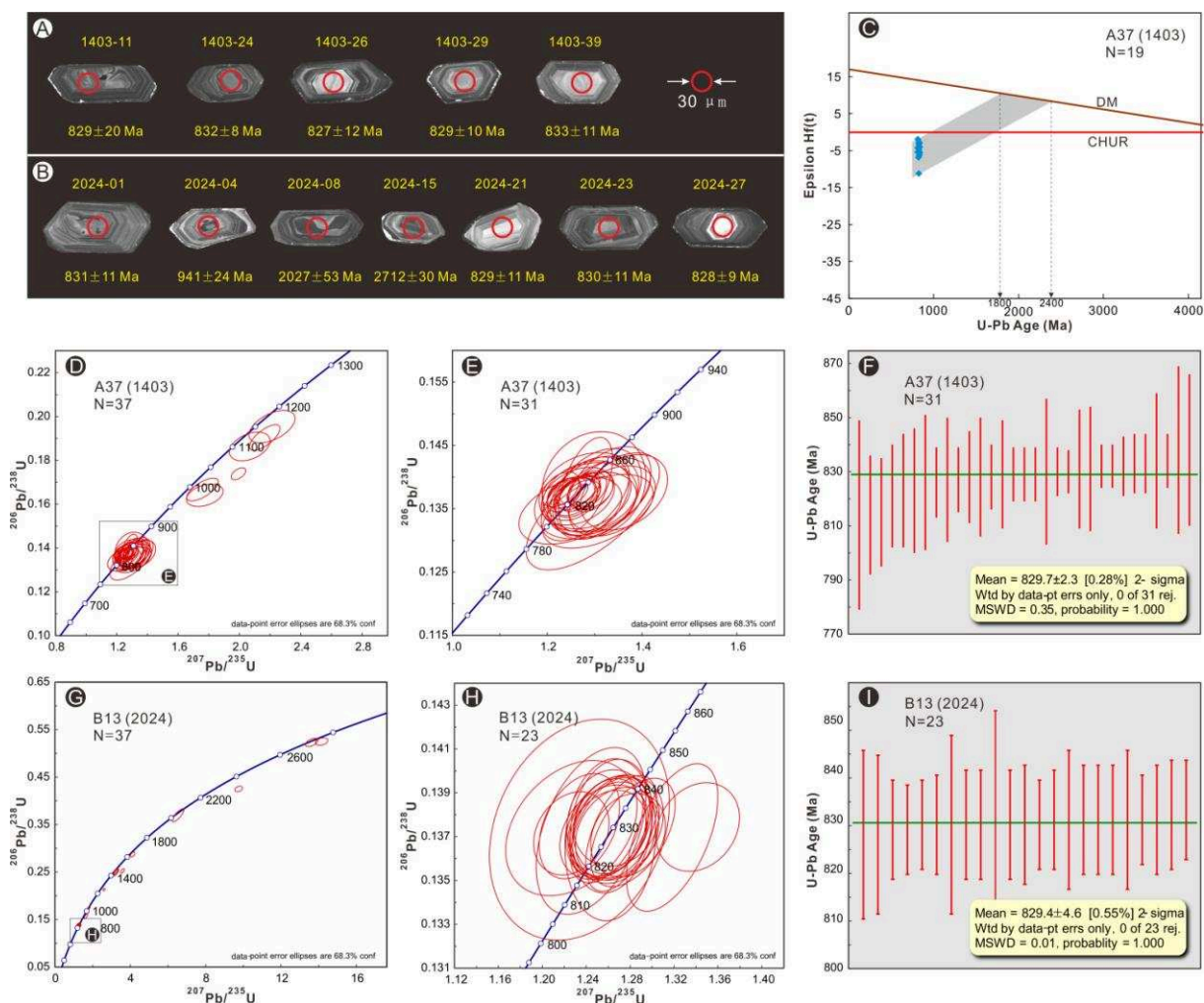


Figure 4-5. The Cathodoluminescence, U-Pb ages and epsilon Hf(t) results of the granite samples of A37 and B13 from the Sanfang and Yuanbaoshan plutons, respectively. A and B: representative cathodoluminescence images of zircons of the samples, attached with analyzed

locations and U–Pb ages; C: Plot of epsilon Hf(t) versus U–Pb age of zircons from the Sanfang pluton; D: U–Pb concordia plots for the zircons from Sanfang granite; E: Enlarged interval of the concentrated ages in the D; F: The average of the ages showed in the E; G: U–Pb concordia plots for the zircons from Yuanbaoshan granite; H: Enlarged interval of the concentrated ages in the G; I: The average of the ages showed in the H.

Table 4-2. U-Pb dating data

Analysis	CORRECTED RATIOS						CORRECTED AGES (Ma)						Th/U ratios	
	207Pb/206Pb		207Pb/235U		206Pb/238U		207Pb/206Pb		207Pb/235U		206Pb/238U	concordance		
		1σ		1σ		1σ		1σ		1σ		1σ		
Sample 1403 (A37)														
1403-1	0.064170	0.003370	1.248450	0.071490	0.134730	0.003510	747	114	823	32	815	20	99%	0.94
1403-2	0.066760	0.003550	1.296120	0.092800	0.134580	0.006090	830	114	844	41	814	35	96%	0.24
1403-3	0.067440	0.003490	1.306550	0.077200	0.134610	0.003850	851	110	849	34	814	22	95%	0.27
1403-4	0.075440	0.003150	1.773600	0.078940	0.164030	0.003350	1080	86	1036	29	979	19	94%	0.15
1403-5	0.068760	0.002930	1.337000	0.059900	0.136220	0.003670	892	90	862	26	823	21	95%	0.37
1403-6	0.079070	0.003050	2.212030	0.099380	0.195370	0.004880	1174	78	1185	31	1150	26	97%	0.56
1403-7	0.065360	0.002550	1.264680	0.050930	0.136980	0.003010	786	84	830	23	828	17	99%	0.43
1403-9	0.078520	0.003100	2.067010	0.087200	0.186330	0.004330	1160	80	1138	29	1101	24	96%	0.40
1403-10	0.067610	0.003180	1.294370	0.061930	0.135810	0.003290	856	100	843	27	821	19	97%	0.43
1403-11	0.066860	0.003240	1.283580	0.061330	0.137200	0.003550	833	103	838	27	829	20	98%	0.05
1403-12	0.067490	0.003790	1.281600	0.071510	0.136250	0.003980	853	120	838	32	823	23	98%	0.23
1403-13	0.069100	0.002910	1.331060	0.057840	0.138100	0.004430	902	89	859	25	834	25	96%	0.12
1403-14	0.067310	0.002870	1.289490	0.054860	0.136940	0.004100	847	91	841	24	827	23	98%	0.10
1403-15	0.071780	0.003150	1.362270	0.060410	0.137590	0.003940	980	92	873	26	831	22	95%	0.14
1403-16	0.067260	0.003760	1.288130	0.069470	0.137630	0.004110	846	119	840	31	831	23	98%	0.13
1403-17	0.067700	0.004320	1.298600	0.072250	0.138830	0.005520	859	136	845	32	838	31	99%	0.26
1403-18	0.066130	0.002690	1.280030	0.061390	0.136630	0.004410	811	87	837	27	826	25	98%	0.09
1403-19	0.068080	0.003100	1.317510	0.066380	0.137140	0.003870	871	97	853	29	828	22	97%	0.07
1403-20	0.067920	0.003200	1.305320	0.061680	0.137340	0.004730	866	100	848	27	830	27	97%	0.35
1403-21	0.075510	0.002170	1.759020	0.067910	0.166670	0.003440	1082	59	1030	25	994	19	96%	0.29

1403-22	0.066880	0.002100	1.280900	0.037410	0.138870	0.004890	834	67	837	17	838	28	99%	0.38
1403-23	0.064280	0.001230	1.228120	0.025780	0.138060	0.001820	751	41	813	12	834	10	97%	0.16
1403-24	0.066260	0.001240	1.264570	0.024970	0.137730	0.001430	814	40	830	11	832	8	99%	0.16
1403-25	0.064920	0.001130	1.234900	0.023080	0.137450	0.001570	772	37	817	10	830	9	98%	0.28
1403-26	0.066510	0.001570	1.263570	0.032670	0.136920	0.002160	823	50	830	15	827	12	99%	0.40
1403-27	0.065110	0.001150	1.235710	0.023980	0.137220	0.001770	778	38	817	11	829	10	98%	0.27
1403-28	0.068180	0.001240	1.297320	0.027110	0.137290	0.001830	874	38	845	12	829	10	98%	0.17
1403-29	0.066420	0.001390	1.260180	0.026490	0.137220	0.001740	820	45	828	12	829	10	99%	0.35
1403-30	0.066360	0.001400	1.263390	0.030910	0.137100	0.002120	818	45	829	14	828	12	99%	0.13
1403-32	0.081160	0.001730	2.164630	0.065780	0.190400	0.003860	1225	43	1170	21	1124	21	95%	0.09
1403-33	0.065520	0.001120	1.251830	0.022610	0.137720	0.001410	791	37	824	10	832	8	99%	0.20
1403-34	0.067610	0.001640	1.291380	0.031480	0.138000	0.002000	857	52	842	14	833	11	98%	0.63
1403-35	0.066110	0.001870	1.252750	0.034960	0.136620	0.002290	810	61	825	16	826	13	99%	0.16
1403-36	0.082480	0.001110	1.993340	0.031100	0.173880	0.001790	1257	27	1113	11	1033	10	92%	0.21
1403-38	0.066920	0.001180	1.276980	0.023200	0.137420	0.001390	835	38	836	10	830	8	99%	0.20
1403-39	0.067410	0.001330	1.284140	0.027110	0.137860	0.001900	850	42	839	12	833	11	99%	0.24
1403-40	0.066030	0.001230	1.266980	0.029430	0.137720	0.001930	807	40	831	13	832	11	99%	0.21
Sample 2024 (B13)														
2024-1	0.065500	0.001820	1.261080	0.031570	0.137580	0.002020	790	60	828	14	831	11	99%	0.76
2024-3	0.065550	0.001510	1.261460	0.026960	0.137480	0.001770	792	49	829	12	830	10	99%	0.67
2024-4	0.073800	0.002260	1.639830	0.072270	0.157100	0.004300	1036	63	986	28	941	24	95%	0.43
2024-5	0.065770	0.001710	1.267560	0.031720	0.137710	0.001680	799	56	831	14	832	10	99%	0.17
2024-6	0.065610	0.001510	1.259910	0.028700	0.137160	0.001600	794	49	828	13	829	9	99%	0.10
2024-7	0.192840	0.003750	14.152860	0.272140	0.524830	0.006440	2767	33	2760	18	2720	27	98%	0.58
2024-8	0.125120	0.002920	6.523570	0.256130	0.369490	0.011220	2031	42	2049	35	2027	53	98%	0.15

2024-9	0.066640	0.002420	1.262060	0.033830	0.136860	0.003020	826	78	829	15	827	17	99%	0.95
2024-10	0.064080	0.002440	1.226520	0.048880	0.137390	0.002520	744	82	813	22	830	14	97%	0.52
2024-11	0.066140	0.001880	1.265900	0.036240	0.137420	0.001960	811	61	831	16	830	11	99%	0.75
2024-12	0.065710	0.001680	1.256240	0.032880	0.137210	0.001760	797	55	826	15	829	10	99%	0.34
2024-13	0.065450	0.002010	1.244370	0.040780	0.137260	0.003110	789	66	821	18	829	18	98%	0.23
2024-14	0.091810	0.001810	3.232250	0.095010	0.251450	0.005490	1463	38	1465	23	1446	28	98%	0.51
2024-15	0.187020	0.003180	13.625470	0.269200	0.522990	0.007150	2716	29	2724	19	2712	30	99%	0.50
2024-16	0.065920	0.001250	1.258770	0.026960	0.137290	0.001960	804	41	827	12	829	11	99%	0.08
2024-17	0.066710	0.001660	1.268090	0.031020	0.137130	0.001730	829	53	832	14	828	10	99%	1.35
2024-18	0.067360	0.001430	1.282690	0.031340	0.137190	0.002020	849	45	838	14	829	11	98%	0.57
2024-19	0.064720	0.001490	1.233740	0.029890	0.137480	0.001960	765	50	816	14	830	11	98%	0.12
2024-20	0.065460	0.003630	1.233810	0.066950	0.137320	0.004120	789	120	816	30	829	23	98%	0.51
2024-21	0.066630	0.001730	1.265260	0.031050	0.137180	0.001890	826	56	830	14	829	11	99%	0.05
2024-22	0.074260	0.001500	1.810960	0.043730	0.175420	0.002570	1049	42	1049	16	1042	14	99%	0.55
2024-23	0.066190	0.001590	1.261210	0.030780	0.137450	0.001900	812	51	828	14	830	11	99%	0.30
2024-24	0.067000	0.001230	1.272010	0.026520	0.137150	0.002160	838	39	833	12	829	12	99%	0.25
2024-25	0.102110	0.001800	3.584060	0.079520	0.252520	0.003850	1663	33	1546	18	1451	20	93%	0.37
2024-26	0.064560	0.001480	1.226440	0.028060	0.137150	0.001550	760	50	813	13	829	9	98%	0.27
2024-27	0.067460	0.001500	1.278110	0.027800	0.137070	0.001560	852	47	836	12	828	9	99%	0.99
2024-28	0.091880	0.001830	3.249860	0.102580	0.249300	0.005470	1465	39	1469	25	1435	28	97%	0.30
2024-29	0.066310	0.001830	1.262900	0.030630	0.137480	0.002490	816	59	829	14	830	14	99%	0.16
2024-30	0.103270	0.002060	4.121880	0.093960	0.287030	0.004180	1684	38	1659	19	1627	21	98%	0.38
2024-32	0.165130	0.002750	9.749940	0.164700	0.425100	0.004890	2509	29	2411	16	2284	22	94%	0.27
2024-34	0.087950	0.001420	2.597700	0.041920	0.213070	0.002220	1381	32	1300	12	1245	12	95%	0.61
2024-35	0.067390	0.001930	1.332540	0.039080	0.142400	0.001570	850	61	860	17	858	9	99%	0.32
2024-36	0.073230	0.001920	1.663310	0.045930	0.163620	0.002090	1020	54	995	18	977	12	98%	0.13

Oct. 2018														Chapter 4
2024-37	0.073210	0.001140	1.704990	0.038310	0.167600	0.003010	1020	32	1010	14	999	17	98%	0.74
2024-38	0.070540	0.001670	1.341650	0.030980	0.137440	0.001650	944	50	864	13	830	9	96%	0.35
2024-39	0.066290	0.001430	1.262510	0.028690	0.137480	0.001860	816	46	829	13	830	11	99%	0.48
2024-40	0.069440	0.001550	1.318220	0.034040	0.136960	0.002750	912	47	854	15	827	16	96%	0.37

Table 4-3. Lu-Hf isotopic compositions

Sample	$^{176}\text{Yb}/^{177}\text{Hf}$	2σ	$^{176}\text{Lu}/^{177}\text{Hf}$	2σ	$^{176}\text{Hf}/^{177}\text{Hf}$	2σ	$\varepsilon\text{Hf}(t)$	$\varepsilon\text{Hf}(0)$	Age(Ma)	TDM1(Ma)	TDM2(Ma)	f(Lu/Hf)
Sample A37 (1403)												
1403-01.xls	0.069465	0.001329	0.002551	0.000049	0.282182	0.000018	-4.26	-20.85	815	1573	1977	-0.92
1403-02.xls	0.033276	0.002444	0.001317	0.000096	0.282133	0.000017	-5.35	-22.59	814	1591	2046	-0.96
1403-03.xls	0.052056	0.000445	0.001897	0.000020	0.282240	0.000019	-1.89	-18.82	814	1464	1828	-0.94
1403-05.xls	0.020281	0.000170	0.000823	0.000008	0.282080	0.000013	-6.79	-24.48	823	1645	2143	-0.98
1403-07.xls	0.061695	0.001249	0.002307	0.000047	0.282159	0.000038	-4.69	-21.68	828	1597	2014	-0.93
1403-10.xls	0.035740	0.000612	0.001399	0.000023	0.282159	0.000012	-4.33	-21.68	821	1558	1987	-0.96
1403-11.xls	0.015152	0.000361	0.000611	0.000014	0.282152	0.000011	-3.99	-21.94	829	1536	1971	-0.98
1403-12.xls	0.032853	0.000245	0.001274	0.000009	0.282167	0.000014	-3.95	-21.40	823	1542	1964	-0.96
1403-13.xls	0.060701	0.001586	0.002274	0.000052	0.282210	0.000017	-2.74	-19.88	834	1522	1896	-0.93
1403-14.xls	0.033084	0.001351	0.001302	0.000052	0.282124	0.000017	-5.39	-22.92	827	1603	2058	-0.96
1403-16.xls	0.031782	0.000622	0.001255	0.000024	0.282096	0.000014	-6.26	-23.89	831	1640	2116	-0.96
1403-17.xls	0.034896	0.000528	0.001431	0.000019	0.282118	0.000016	-5.43	-23.12	838	1617	2069	-0.96
1403-18.xls	0.018821	0.001017	0.000813	0.000046	0.281955	0.000025	-11.15	-28.91	826	1817	2418	-0.98
1403-19.xls	0.069655	0.001338	0.002645	0.000045	0.282206	0.000014	-3.22	-20.03	828	1544	1922	-0.92
1403-20.xls	0.043510	0.000604	0.001756	0.000024	0.282195	0.000019	-3.07	-20.41	830	1522	1914	-0.95
1403-22.xls	0.028666	0.000751	0.001136	0.000029	0.282155	0.000015	-3.96	-21.81	838	1553	1976	-0.97
1403-23.xls	0.060435	0.001617	0.002269	0.000057	0.282119	0.000015	-5.96	-23.10	834	1653	2099	-0.93
1403-24.xls	0.040540	0.001049	0.001561	0.000038	0.282197	0.000024	-2.84	-20.33	832	1511	1901	-0.95
1403-26.xls	0.033645	0.000740	0.001340	0.000028	0.282199	0.000015	-2.74	-20.25	827	1499	1891	-0.96

4.6 Rock magnetic investigation and results

4.6.1 Field sampling

A total of 352 cores from 55 sites were sampled for the AMS study, 35 and 20 for the Sanfang and Yuanbaoshan plutons, respectively (Figure 4-6). The sampling sites are expected to be homogeneously distributed in the plutons, and each site of fresh outcrop covers several tens of square meters. In the best case, the sampling sites are distanced at ~2 kilometers. For each site, at least six cores are drilled with an interval of 3 to 4 meters between each other.

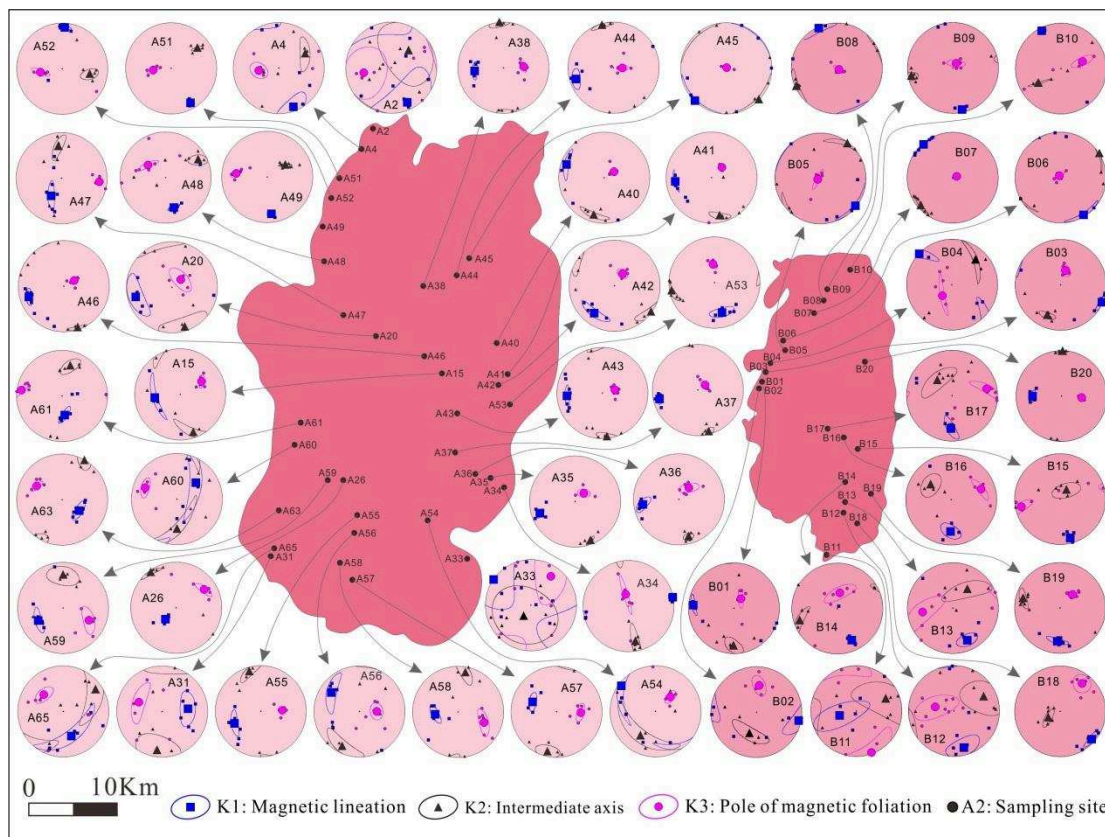


Figure 4-6. Sketch map with the sampling sites and AMS results for each sampling site.

4.6.2 Magnetic mineralogical analysis

In order to define the carriers of our Anisotropy of Magnetic Susceptibility (AMS) analysis, i.e., diamagnetic, paramagnetic and ferromagnetic minerals, we have

performed some methods: (1) a magnetic hysteresis loop characterization by using a vibrating magnetometer in the Laboratoire de Paleomagnétisme of the Institut de Physique du Globe de Paris (IPGP); (2) an isothermal remanence magnetization characterization with an IM30 pulsed magnetizer and a JR5 spinner magnetometer at the Institut des Sciences de la Terre d'Orléans (ISTO); (3) a thermomagnetic characterization by using a KLY3 kappabridge coupled with a CS3 furnace; and (4) scanning electron microscope (SEM) with the ZEISS MERLIN Compact for the minerals at the Institut des Sciences de la Terre d'Orléans (ISTO).

A total of nine samples from the Sanfang pluton were selected for magnetic mineral analysis, and the results are presented in the [Figure 4-7](#). The hysteresis curves ([Figure 4-7A](#)) present similar S-shaped hysteresis loops for the three samples with significant difference between the corrected and uncorrected curves, which suggest that both the ferromagnetic and paramagnetic minerals can be considered as the main magnetic susceptibility carriers. Rapid saturation of the isothermal magnetic remanence at about 200 mT is characteristic for the sample of A46 ([Figure 4-7B](#)), indicating the existence of ferromagnetic minerals with low magnetic coercivity. However, for the sample A48, the gradual saturation until to 1 Tesla ([Figure 4-7B](#)) highlights that the the existence of ferromagnetic minerals with high magnetic coercivity. The rates of saturation of the samples of A65 and A67 are in-between the A46 and A48 ([Figure 4-7B](#)), which reveals that both the weak and high coercive ferromagnetic minerals are existed in the granites. The thermomagnetic measurements on the samples of A10 and A23 show a rapid drop of the magnetic susceptibility at about 580°C (A10 in [Figure 4-7C](#)) and continuous drop until to 680°C (A23 in [Figure 4-7C](#)), indicateing the presence of (titano) magnetite and hematite. However, these two samples show a strong continuous increase in susceptibility during the cooling (owing to oxidation reactions) revealing that a significant mineral transformation occurred during the heating, e.g. iron sulfide to iron oxide ([Figure 4-7C](#)). The SEM investigation reveals that the existence of titanomagnetite with the mass fraction of

the TiO_2 ranged from 45.51% to 50.65%, and they are commonly intergrown or partly enclosed in biotite with the long axis parallel to the cleavage of biotite (Figure 4-7D). The Day-plot of hysteresis parameters are presented in the Figure 4-7E, revealing that (titano) magnetites of the samples are in the multidomain zone (e.g., Dunlop, 2002). It indicates that the major (elongated) axis of the magnetic susceptibility ellipsoid is concord to the major morphological axis of minerals (e.g., Borradaile & Henry, 1997).

Consequently, the magnetic susceptibility carriers in the Sanfang granite pluton are composed of ferromagnetic minerals, such as (titano) magnetite in multidomaine and hematite, with paramagnetic minerals, such as biotite, muscovite and feldspar. According to Rochette et al. (1992), the magnetic fabrics of these minerals are comparable to the petrographic ones. Therefore, the AMS measurements will be an effective way to obtain the information of the petrofabrics of granite as well as the knowledge on the pluton emplacement (Martín-Hernández et al., 2004).

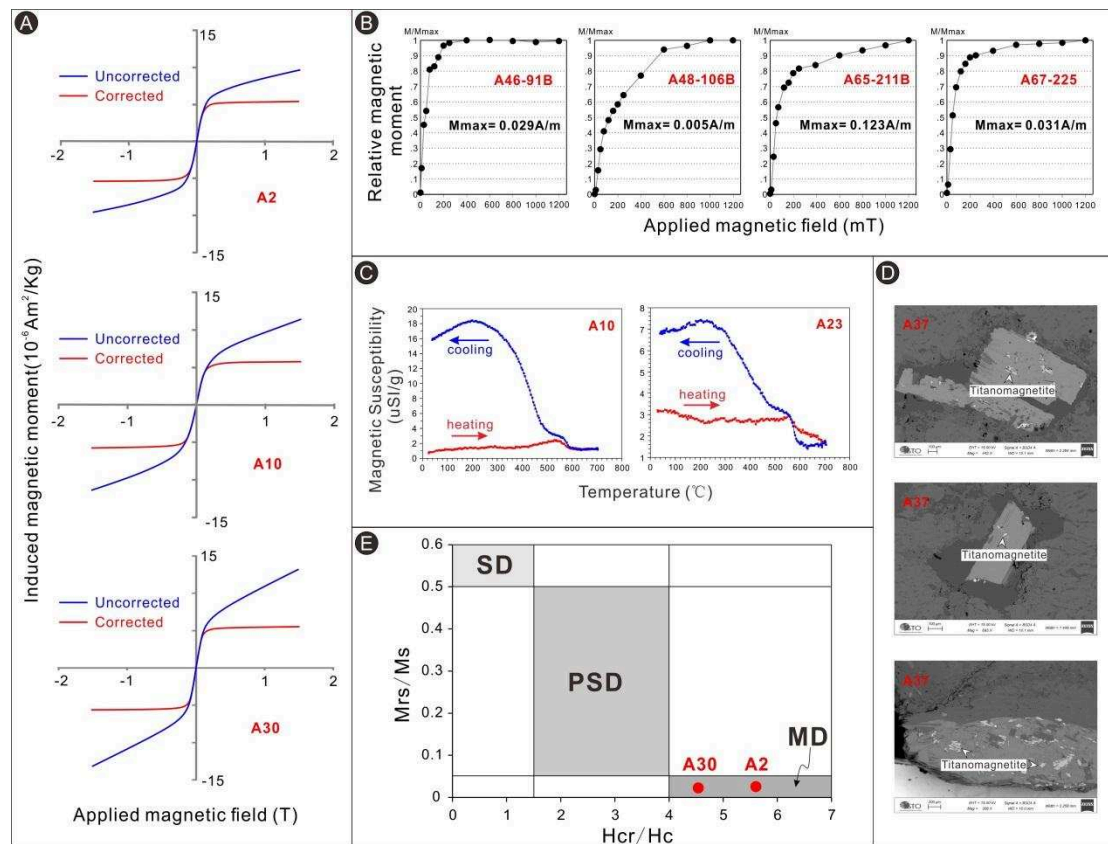


Figure 4-7. Magnetic mineralogic analyses (A-D) and Day-plot of hysteresis parameters (E) for the samples from the Sanfang pluton. SD: Single-Domain, PSD: Pseudo-Single-Domain, MD: Multidomain. Mrs: the saturation intensity of magnetic remanence, Ms: the saturation intensity of induced magnetization, Hcr: the coercivity of magnetic remanence, Hc: magnetic coercivity of the measured sample.

4.6.3 AMS parameters

The AMS measurements were carried out with a KLY3 Kapprabridge at the Institut des Sciences de la Terre d'Orléans. A total of 352 (228 and 124 from the Sanfang and Yuanbaoshan, respectively) specimens from 55 sites were prepared. Detailed informations can be found in Table 4-4. The mean bulk magnetic susceptibility (K_m) for each sampling site of the granites from the Sanfang and Yuanbaoshan plutons are varied from 27.5 to 133.0×10^{-6} SI and 32.7 to 197.0×10^{-6} SI, respectively (Figures 4-8A, 4-8B and 4-8D). The site-mean value of the degree of anisotropy (P_j) ranges in [1.017, 1.156] and [1.009, 1.172] for the Sanfang and Yuanbaoshan plutons, respectively (Figures 4-8B, 4-8C and 4-8E). The site-mean of shape parameter (T) ranges in [-0.384, 0.912] and [-0.384, 0.817] for the Sanfang and Yuanbaoshan, respectively (Figures 4-8C, and 4-8F). The degree of anisotropy and shape parameter are positively related (Figure 4-8C). Moreover, the degree of anisotropy and shape parameter are both increased with the rising of elevation (Figures 4-8E, and 4-8F).

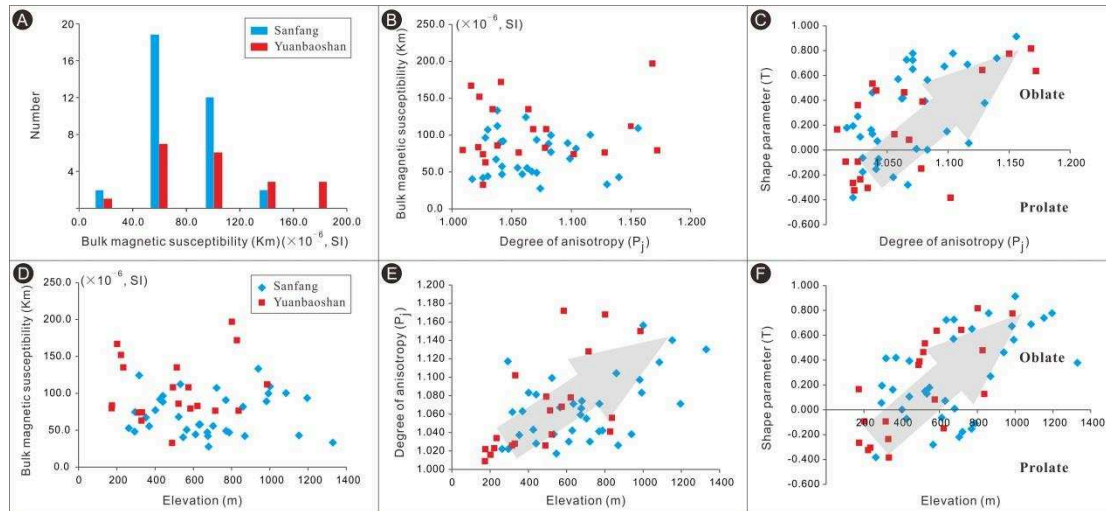


Figure 4-8. Magnetic parameters of the Sanfang-Yuanbaoshan granite plutons. (A) Distribution of the bulk magnetic susceptibility; (B) Scatter plot of the bulk magnetic susceptibility and degree of anisotropy; (C) Scatter plot of the shape parameter and degree of anisotropy with a positive correlation; (D) Scatter plot of the bulk magnetic susceptibility and elevation with a positive correlation; (E) Scatter plot of the degree of anisotropy and elevation with a positive correlation; (F) Scatter plot of the shape parameter and elevation with a positive correlation. All the data are site-mean value for each sampling site.

Table 4-4. Sampling site information and AMS site-mean results for the Sanfang-Yuanbaoshan plutons

Site	Geographic coordinates		Elv.(m)	n	Km (10 ⁻⁶ SI)	P _J	T	AMS site-mean results			
								K ₁	$\alpha_{95}(\text{max/min})$	K ₃	$\alpha_{95}(\text{max/min})$
								Dec/Inc		Dec/Inc	
								(°)	(°)	(°)	(°)
Sanfang											
A02	N25°36.269′	E108°46.973′	547	8	40.2	1.017	0.178	155.1/17.4	61.2/35.7	259.7/38.6	47.4/39.1
A04	N25°35.191′	E108°46.424′	680	6	27.5	1.074	0.007	159.2/10.1	28.2/15.6	263.1/53.5	17.6/12.7
A15	N25°22.597′	E108°49.759′	860	6	81.6	1.104	0.776	263.0/43.0	42/4.7	58.9/44.3	11.8/4.3
A20	N25°24.531′	E108°46.455′	1330	6	33.0	1.130	0.377	255.2/18.9	34.5/16.1	48.8/69.1	26.1/12.8
A26	N25°17.328′	E108°44.369′	402	6	76.9	1.083	0.000	223.2/61.7	8.7/5.4	56.9/27.6	16.5/6.2
A31	N25°13.954′	E108°40.646′	770	6	90.5	1.041	-0.155	83.9/42.4	29.7/15.0	292.0/44.0	36.5/12.5
A33	N25°13′14.7"	E108°51′33.4"	293	8	47.9	1.117	0.054	304.4/0.9	62.3/32.7	34.8/24.3	54.2/25.3
A34	N25°17′08.1"	E108°53′10.3"	263	6	52.5	1.022	-0.384	78.6/0.9	6.6/4.8	346.3/68.4	37.4/3.9
A35	N25°17′24.0"	E108°52′26.8"	370	6	55.2	1.063	0.417	251.6/19.7	11.0/4.7	46.5/68.4	11.6/7.6
A36	N25°17′44.6"	E108°51′38.9"	441	6	88.1	1.081	0.392	262.1/21.2	19.1/7.0	40.7/62.7	19/7.9
A37	N25°18′45.8"	E108°50′34.5"	524	6	67.8	1.099	0.148	256.9/14.5	7.9/4.9	54.3/74.3	11.0/3.1
A38	N25°26′07.7"	E108°48′50.7"	1153	7	42.6	1.140	0.737	263.9/36.6	14.7/4.9	86.4/53.4	10.1/4.7
A40	N25°22′52.5"	E108°54′03.7"	772	7	48.9	1.071	0.649	289.5/13.2	23.2/5.3	58.1/69.4	6.9/4.1
A41	N25°22′24.9"	E108°53′38.4"	674	6	46.9	1.059	0.569	264.2/20.8	17.3/2.6	44.9/63.9	7.3/2.6
A42	N25°21′49.1"	E108°52′57.9"	636	6	57.5	1.071	0.722	216.8/26.1	26.6/7.7	33.1/63.9	10.4/7.7
A43	N25°20′43.1"	E108°50′39.9"	993	7	99.5	1.083	0.562	265.4/23.0	16.4/4.5	76.2/66.7	6.7/4.4
A44	N25°27′23.2"	E108°50′42.3"	1085	7	100.0	1.116	0.687	253.3/14.8	15.7/9.1	91.6/74.4	10.3/5.5
A45	N25°28′15.0"	E108°51′27.9"	1001	6	109.0	1.156	0.912	224.1/1.4	37.8/3.7	30.7/88.6	7.4/0.6

A46	N25°23'25.3"	E108°49'03.4"	983	8	88.8	1.097	0.671	253.1/20.8	13.2/6.4	61.4/68.8	7.9/4.2
A47	N25°25'51.6"	E108°44'30.3"	1196	7	93.3	1.071	0.776	210.7/53.0	27.3/5.8	95.3/17.9	8.0/4.1
A48	N25°28'29.2"	E108°43'21.2"	788	8	46.6	1.042	-0.111	163.0/31.9	10.8/2.9	302.6/50.7	17.9/2.5
A49	N25°29'45.9"	E108°43'24.5"	704	8	55.5	1.055	-0.221	173.5/19.8	4.6/2.1	276.5/32.1	12.2/4.0
A51	N25°32'04.4"	E108°43'51.3"	566	6	50.3	1.067	-0.282	150.8/14.4	4.1/2.3	264.5/57.3	12.0/3.2
A52	N25°31'10.6"	E108°43'39.7"	612	6	44.0	1.030	-0.065	3.5/10.2	9.4/4.4	261.2/49.8	18.0/5.1
A53	N25°21'09.7"	E108°53'37.2"	677	6	41.9	1.066	0.725	166.0/32.7	19.9/9.0	355.4/56.9	10.1/3.7
A54	N25°15'25.5"	E108°51'46.0"	296	6	74.4	1.022	0.193	306.7/6.9	67.3/6.6	45.8/52.6	13.8/7.0
A55	N25°15'52.1"	E108°45'18.9"	317	6	124.0	1.062	0.413	245.2/36.5	22.3/6.8	87.8/51.3	8.0/6.9
A56	N25°15'03.6"	E108°45'05.5"	353	6	66.8	1.037	0.161	304.1/26.4	35.2/9.9	89.6/58.9	14.8/11.8
A57	N25°12'51.7"	E108°45'04.4"	630	5	57.3	1.042	0.071	292.5/42.4	16.1/7.1	91.9/45.7	16.2/7.1
A58	N25°13'36.6"	E108°44'15.8"	426	6	91.6	1.043	-0.073	264.2/48.0	17.4/6.9	112.2/38.5	25.3/8.5
A59	N25°17'32.8"	E108°43'37.6"	441	6	96.2	1.028	0.104	243.1/38.8	21.8/6.7	115.4/37.3	25.5/10.2
A60	N25°19'20.4"	E108°41'58.6"	870	6	41.9	1.026	0.268	49.1/44.1	68.8/10.6	289.8/26.8	16.1/8.5
A61	N25°20'23.1"	E108°42'24.2"	940	7	133.0	1.038	0.460	172.1/55.1	18.1/5.2	278.2/11.0	18.0/3.7
A63	N25°16'04.1"	E108°41'01.9"	533	7	112.0	1.038	0.128	122.9/53.3	18.6/7.2	298.1/36.6	12.0/5.2
A65	N25°14'17.1"	E108°40'46.5"	722	8	107.0	1.030	-0.178	161.9/42.6	67.4/11.4	310.7/43.0	17.9/11.2
Yuanbaoshan											
B01	N25°24'11.4"	E109°06'22.4"	494	7	108.0	1.079	0.390	274.4/11.5	16.1/4.4	36.0/68.8	17.3/4.7
B02	N25°24'00.0"	E109°06'18.9"	489	5	32.7	1.026	0.361	101.2/6.3	34.0/13.8	5.8/40.7	21.1/10.3
B03	N25°24'30.1"	E109°06'51.7"	514	6	135.0	1.064	0.464	112.8/2.0	13.5/5.9	19.0/62.8	7.6/5.1
B04	N25°25'09.4"	E109°07'23.8"	575	5	108.0	1.068	0.083	313.5/1.3	42.4/6.4	220.9/64.0	38.8/4.0
B05	N25°25'43.0"	E109°08'29.0"	715	6	76.4	1.128	0.643	128.1/2.6	32.4/3.7	249.7/85.0	20.5/3.8
B06	N25°26'11.6"	E109°08'24.6"	828	6	172.0	1.041	0.479	148.5/4.1	26.7/4.3	326.5/85.9	10.7/4.3

B07	N25°27'34.9"	E109°09'56.5"	986	7	112.0	1.150	0.775	318.9/2.9	15.4/1.6	71.1/82.3	3.7/1.5
B08	N25°28'18.0"	E109°10'32.0"	802	6	197.0	1.168	0.817	336.0/3.2	24.0/9.5	114.9/85.7	10.9/3.7
B09	N25°28'47.3"	E109°10'47.6"	622	6	82.9	1.078	-0.149	167.6/6.9	7.8/5.4	34.0/80.1	16.4/6.2
B10	N25°29'41.9"	E109°12'03.7"	332	6	74.2	1.102	-0.384	333.0/7.4	7.3/1.7	71.6/48.7	22.7/6.8
B11	N25°15'13.7"	E109°10'29.8"	173	6	79.7	1.009	0.166	255.3/58.8	58.1/18.9	159.5/3.2	46.7/18.8
B12	N25°17'24.2"	E109°11'45.9"	202	8	167.0	1.016	-0.094	165.0/17.7	27.5/18.6	282.4/55.3	43.4/18.5
B13	N25°18'06.9"	E109°11'52.2"	222	6	152.0	1.023	-0.325	155.9/23.4	16.9/12.4	262.5/33.4	48.7/15.3
B14	N25°19'08.4"	E109°11'46.9"	234	6	135.0	1.034	-0.305	155.4/24.6	13/3.4	8.9/61.3	31.6/10.5
B15	N25°20'35.0"	E109°12'26.6"	315	6	74.0	1.026	-0.094	165.5/12.6	14.0/3	258.8/14.4	26.7/6.8
B16	N25°21'03.0"	E109°11'38.0"	523	5	85.9	1.038	0.534	181.2/30.4	19.7/11.8	70.5/31.1	21.4/6.6
B17	N25°21'46.0"	E109°10'43.3"	837	8	76.3	1.056	0.127	182/28.5	26.1/6.5	78.5/23.2	33.7/6.8
B18	N25°16'45.0"	E109°12'38.5"	175	6	83.6	1.022	-0.265	131.6/8.3	14.8/5.7	38.1/22.9	18.8/13.9
B19	N25°18'12.6"	E109°13'29.7"	329	7	63.0	1.028	-0.235	184.9/27.2	18.1/5.7	42.5/57	8.8/4.8
B20	N25°25'02.7"	E109°12'54.6"	585	6	79.3	1.172	0.636	269.7/36.4	10.5/4.1	94.4/53.5	5.9/1.2

Note: Alt.: Altitude, n: number of specimens at sampling site, Km: bulk magnetic susceptibility P_J : degree of susceptibility anisotropy, T: shape parameter of the AMS ellipsoid, K1:

Magnetic lineation, K3: The pole of the magnetic foliation, Inc.: Inclination, Dec.: Declination, α_{95} (max/min): the long and short axes of the confidence ellipsoid at 95% level.

4.6.4 AMS results

The AMS results for all sampling sites are given in Figure 4-6. And the distribution of the magnetic foliations and lineations are presented in Figure 4-9.

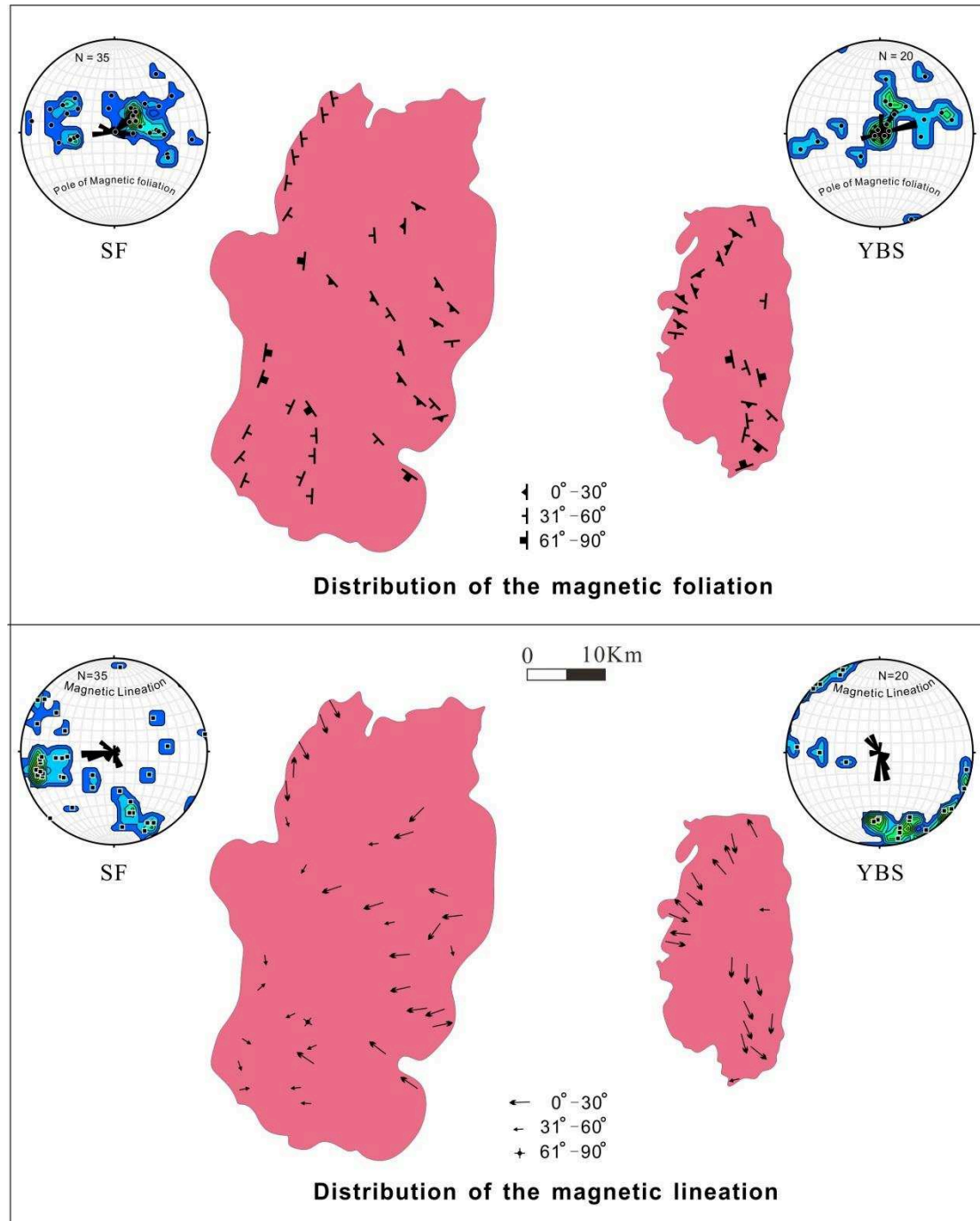


Figure 4-9. Distribution of the site-mean magmatic foliations and magnetic lineations for the Sanfang (SF) and Yuanbaoshan (YBS) plutons, with the density diagrams of

poles of magnetic foliations and magnetic lineations for these two plutons.

Generally, the main strikes of the magnetic foliations are NW-SE and N-S directed for the Sanfang pluton. And the predominant direction of the magnetic lineations is NEE-SWW, with a subordinate direction of the NNW-SSE. However, for the Yuanbaoshan pluton, the main strikes of the magnetic foliations are sub N-S and NW-SE, and the magnetic lineations are mainly N-S and NW-SE directed (Figure 4-9).

Considering the magnetic foliation and lineation, degree of anisotropy and shape parameter, the studied areas in the Sanfang-Yuanbaoshan plutons can be divided to six sub zones (Figure 4-10).

In the western part of the Sanfang pluton, the magnetic foliations consistently dip to the E with the inclination ranged from 33 to 79 degrees, but the magnetic lineations are mainly E-W and N-S. Almost all the specimens with P_j value lower than 1.1, which suggests that the magnetic fabric is a magmatic one (Borradaile and Henry, 1997), and with an even shape parameters between oblate ($T > 0$) and prolate ($T < 0$) (Zone 1). In the southern part of the Sanfang pluton, the magnetic foliations dip to the W with the inclination from 31 to 63 degrees, and the magnetic lineations are nearly E-W directed. 94% of the specimens have the P_j value lower than 1.1 and the ratio between the oblate and prolate is about 2:1 (Zone 2). However, in the central-northeastern part of the Sanfang pluton, the P_j value, with the range from 1.041 to 1.187, is much higher than other zones in the Sanfang pluton. 37% of the specimens with the P_j value higher than 1.1, suggesting that the magnetic fabric could be modified in the post-solidus state (Tarling and Hrouda, 1993). The magnetic foliations gently dip to the SW, with coherent NEE-SWW directed magnetic lineations. More than 95% of the shape parameters of the specimens are greater than zero, i.e., prolate shape (Zone 3). The remained part of the Sanfang pluton displays

the gentle magnetic foliations with dispersed magnetic lineations. All the P_j values are lower than 1.1 and the ratio of shape parameter between the oblate and prolate is about 2:1 (Zone 4).

As to the Yuanbaoshan pluton, the central-northwestern part is similar to Zone 3 of the Sanfang pluton, highlighting higher P_j value ranging from 1.017 to 1.183 and 57% of sites in this zone are higher than 1.1, with a positive value of shape parameter for almost all sites. It shows moderate magnetic foliations dipping ranging from 4 to 27°, with consistent NW-SE directed magnetic lineations (Zone 5). In the central-southern part and a fraction of the northern part, the strikes of the magnetic foliations are sub N-S with relative steep inclinations of 35 to 76°, and the magnetic lineations are always north- and southward. Most of the P_j values are lower than 1.1, and the ratio between the oblate and prolate shapes is about 1:1 (Zone 6). However, some localities close to the boundary between the granite plutons and country rocks, i.e., A33 and B11 in Figure 4-10, are quite different with others, suggesting that they were probably affected by the country rocks during the magma emplacement.

According to the anisotropy degree (P_j), these six zones can be, moreover, subgrouped into two units, namely, zone with magmatic fabrics and zone with tectonic ones (Figure 4-10), which correspond to the undeformed and deformed granites, respectively.

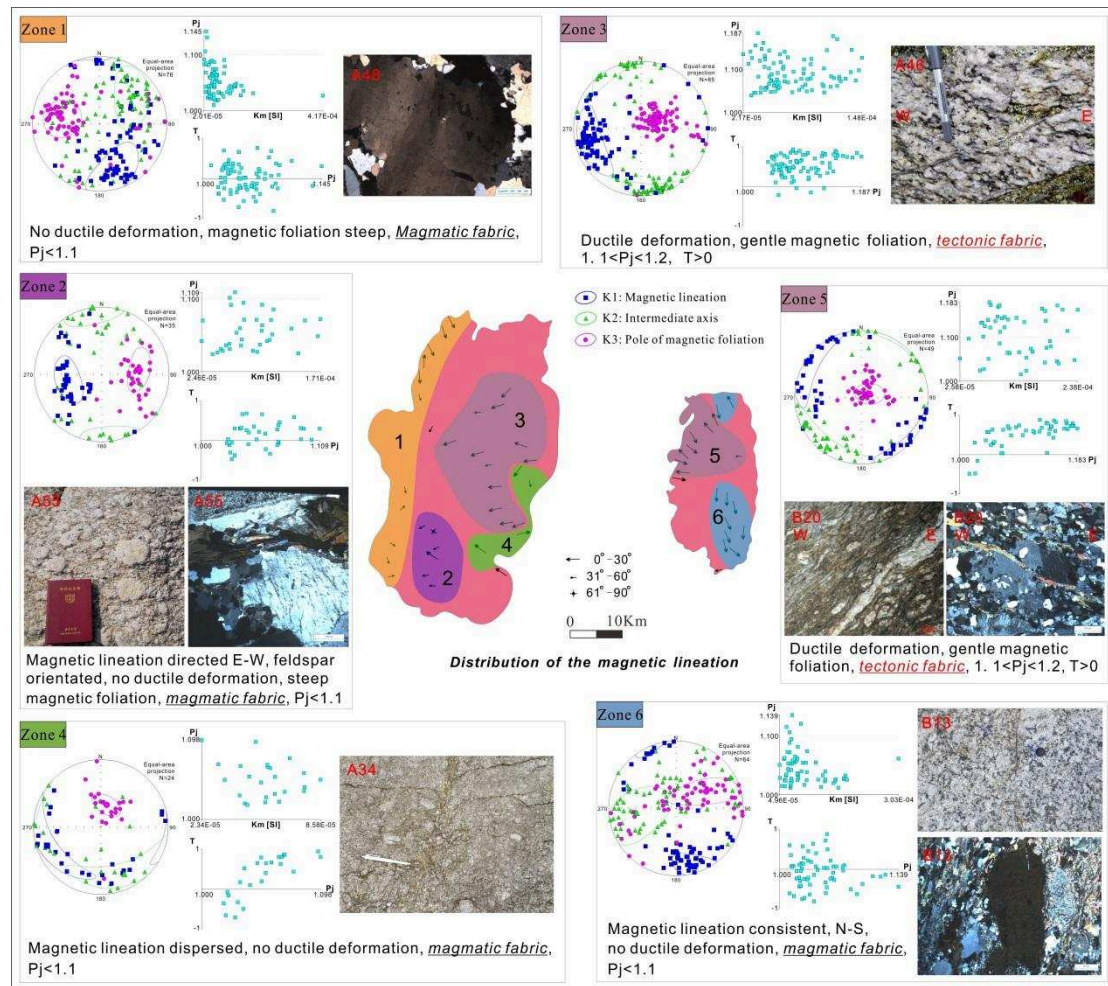


Figure 4-10. Six sub-zones for the Sanfang-Yuanbaoshan plutons defined by the degree of anisotropy, magnetic foliation and magnetic lineation, with representative macroscopic and microscopic pictures.

4.7 Gravity modeling

The regional gravity anomaly reflects the density architecture of the underground, hence, the proper decipherment of the gravity anomaly data can help to reveal the construction of the geological units in the deep (e.g., [Martelet et al., 2013](#)). Especially for the intrusive geological bodies which are usually in large density contrast with respect to the country rocks. Consequently, the gravity modeling method is applied to deduce the Sanfang and Yuanbaoshan pluton shapes within the Sibao strata. The 1:200,000 original Bouguer gravity anomaly map for the Sanfang-Yuanbaoshan area

is from the Chinese Bouguer gravity anomaly database which covers the Sanfang and Yuanbaoshan plutons exposure and their surrounding areas. The Digital Elevation Model (DEM) for the Sanfang-Yuanbaoshan area, with a resolution of 90 m at the equator, is downloaded from the website of <http://srtm.csi.cgiar.org/>.

We collected both the granites and country rocks for the measurement of their density. They were measured at the University of Nanjing by using the Matsuhaku Electronic Densimeter GH-300. For each sample, we measured twice and take the average value at a precision of 0.001g/cm³. Detailed density data for the samples from the granites, Sibao group, Danzhou group and Sinian strata can be referred in [Table 4-5](#). As the post Sinian strata is poorly exposed, so we take it as same as the density of the Sinian strata. Besides, the density of the mafic-ultramafic block is referred to the geological survey of the Guangxi province ([BGMRGX, 1985](#)) ([Figure 4-12](#)).

In the original Bouguer gravity data, both the regional and long wavelength signals are involved, which reflect the surface and deep signatures, respectively. Thus the long wavelength signals need to be removed in order to get suitable gravity anomaly information just produced by the sub-surface geological body. After removing the long wavelength signals from the original gravity anomaly data, the rest normally is residual gravity anomaly data. Several low-pass Butterworth filters are tested for removing the long wavelength signals with cutoff wavelengths of 10 km, 20 km, 30 km... to 130 km, 140 km and 150 km. Through the comparison between the residual gravity anomaly data and geological boundaries, the residual gravity anomaly data with the cutoff of wavelength of 130 km is the most suitable one, which matches best with surface geological features ([Figure 4-11](#)).

The residual Bouguer gravity anomaly map shows two obvious negative anomaly centers in the southern and central parts of the Sanfang and Yuanbaoshan plutons, respectively ([Figure 4-11](#)). The negative anomaly regions for these two

plutons are both N-S directed, which are concur with the geometry of the two plutons. According to the residual Bouguer gravity anomaly data and regional tectonic features, five profiles of gravity modeling are performed: two of them are perpendicular to the regional tectonic line (WE 1 and WE 2), and three are parallel with the regional structures (NS 1, NS 2 and NS 3).

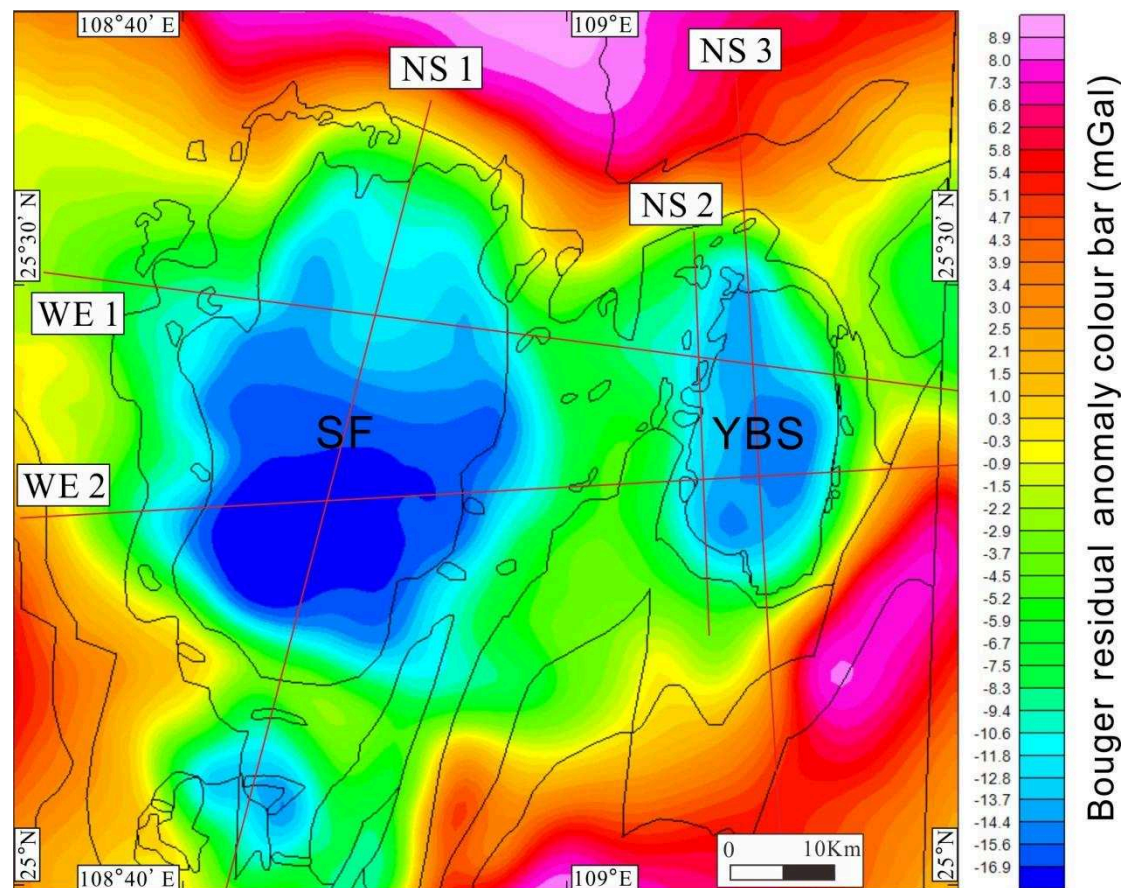


Figure 4-11. The residual Bouguer gravity anomaly of the Sanfang and Yuanbaoshan plutons and their surrounding areas.

Five interpreted profiles are presented in Figure 4-12. The contact relationships between the granite plutons and the country rocks are depicted according to the field observations and geological maps, however, the deep structures of profiles are modeled with the gravity data. According to the residual Bouguer gravity anomaly modeling along these profiles, we can characterize these two plutons as following (1)

Negative gravity anomalies are N-S orientated within the Sibao group; (2) The roots of the granite plutons are presented in a N-S orientated dyke shape; (3) In the E-W direction, two plutons are in a tongue shape; (4) For the Sanfang pluton, the deepest root of ca. 5.3 km (dyke) is located in its southern part, the depth is progressively decreased northwards with the shallowest depth of ca. 0.5-1 km in the northern part; (5) For the Yuanbaoshan pluton, the deepest part is ca. 5.3 km (dyke), the thickness in the N-S direction does not change significantly; (6) The Sanfang and Yuanbaoshan plutons seem to be connected in the deep.

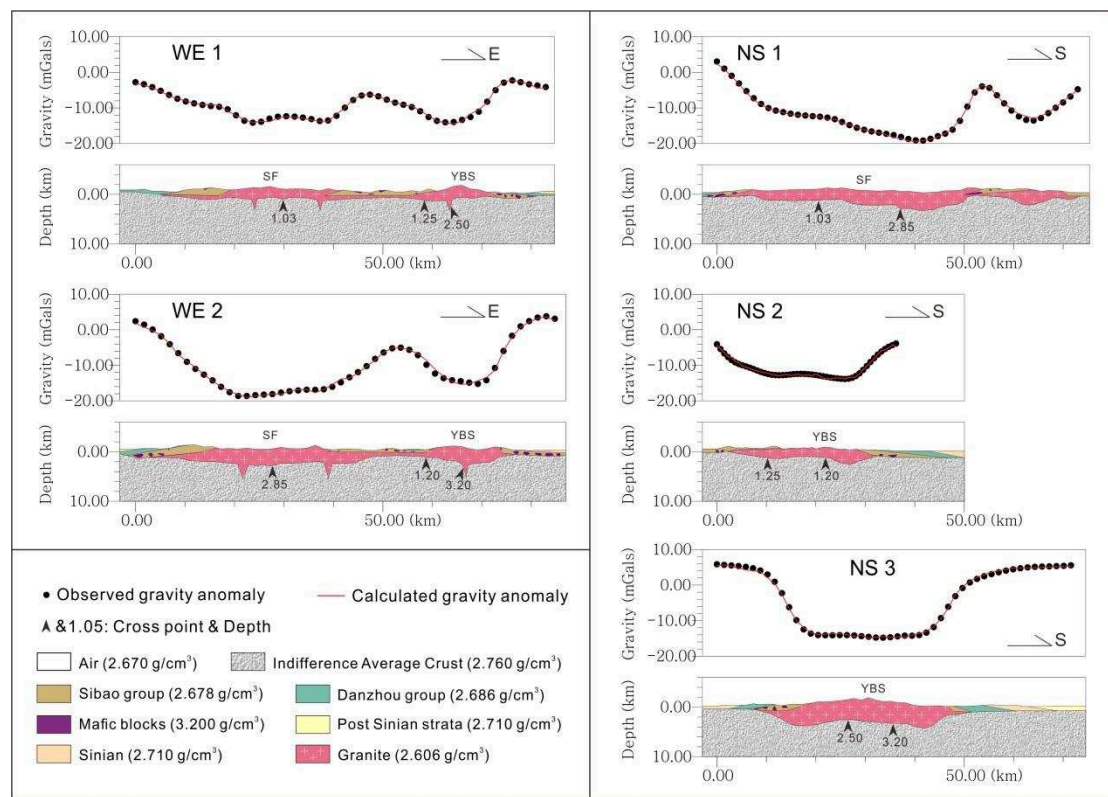


Figure 4-12. Interpreted profiles of the residual Bouguer gravity anomaly of the Sanfang and Yuanbaoshan plutons and their surrounding areas. The contact relationships between the granite plutons and the country rocks are depicted according to the field observations and geological maps.

Table 4-5. The density of the Sanfang-Yuanbaoshan granites and country rocks

Strata/Rock	Lithology	Sampling number	Density of each sample (g/cm ³)	Average of measured density (g/cm ³)	Standard derivation
γ_2 Sanfang	Granite	1404	2.630	2.606	0.0425
		A35	2.534		
		A37	2.586		
		A38	2.601		
		A39	2.663		
		A40	2.549		
		A42	2.559		
		A45	2.670		
		A46	2.671		
		A48	2.592		
		A49	2.615		
		A51	2.591		
		A52	2.622		
		A55	2.673		
		A57	2.576		
		A58	2.648		
		A59	2.534		
		A62	2.582		
		A63	2.631		
		A65	2.602		
		A66	2.587		
γ_2 Yuanbaoshan	Granite	B07	2.597	2.606	0.0129
		B09	2.594		
		B02	2.621		
		B05	2.623		
		B19	2.591		
		B20	2.612		
Sibao Group	Slate	1406	2.741	2.678	0.0577
	Slate	1415	2.673		
	Slate	1419	2.664		
	Slate	1422	2.757		
	Slate	1425	2.740		
	Sandstone	1427	2.648		

	Sandstone	1429	2.684		
	Slate	1439	2.706		
	Slate	1447	2.679		
	Slate	1451	2.622		
	Sandstone	1453	2.763		
	Sandstone	1458	2.568		
	Slate	1459	2.763		
	Slate	1460	2.681		
	Slate	1468a	2.692		
	Slate	1469	2.754		
	Slate	2002	2.696		
	Slate	2003	2.601		
	Sandstone	2004	2.671		
	Sandstone	2006	2.545		
	Sandstone	2007	2.655		
	Sandstone	2020	2.628		
	Slate	2031	2.678		
	Slate	2051	2.584		
	Slate	2052	2.700		
	Slate	2054	2.722		
	Slate	2055	2.685		
Danzhou Group	Sandstone	1420	2.756		
	Sandstone	1461	2.734		
	Sandstone	2000-1	2.528		
	Sandstone	2001	2.738	2.686	0.0851
	Sandstone	2064	2.704		
	Blastopsammite	2066	2.585		
	Sandstone	2067	2.759		
Sinian		2040	2.715		
	Sandstone	2040-1	2.714	2.710	0.0066
		2040-2	2.701		

4.8 Discussion on the construction process of the Sanfang-Yuanbaoshan plutons

In order to have a comprehensive understanding of the construction process of the Sanfang and Yuanbaoshan plutons, several scientific problems are discussed in the following section: (1) The origin of the magma and its crystallization age; (2) The origin of the magnetic fabrics of two plutons; (3) the emplacement mechanism of the granitic plutons through the 3-D pluton reconstruction; and (4) records of the post-orogenic tectonic event.

4.8.1 Origin of the magma and its crystallization age

A number of studies have addressed the origin and petrogenesis of the Neoproterozoic granites in the Jiangnan Orogenic Belt (e.g., Li, 1999; Wang et al., 2007; Wu et al., 2006; Xue et al., 2010; Yao et al., 2014b; Zhong et al., 2005). The granites in the western part of Jiangnan Orogenic Belt (i.e., Sanfang and Yuanbaoshan plutons) perform high Aluminum Saturation Index (ASI) ranging in 1.15-1.40 (Yao et al., 2014b) and low initial ϵ_{Nd} values of -4.8 to -7.6 with high enrichment in Rb, K and Th and relatively low Zr, Hf and higher rare earth elements (Li, 1999). All the geochemical features indicate that the granites were derived from supracrustal source rocks (Wang et al., 2007). All the granites show the zircon U-Pb crystallization ages in the range of 850 to 820 Ma, with a peak at 830 Ma. Thus, it was proposed that the granites in Sanfang and Yuanbaoshan were generated by the upper crustal materials during the post orogenic event at around 830 Ma.

In this study, the new zircon results from the Sanfang and Yuanbaoshan granites indicate that the mean ages of these two plutons are at 830 ± 2 Ma and 830 ± 5 Ma, respectively (Figures 4-5F and 4-5I). However, few zircon grains give ages older than 2.0 Ga (Figure 4-5G), indicating that a Paleoproterozoic basement is probably existed below the supracrust in this area, and the zircons were captured during the magma ascent. The cathodoluminescence (CL) images (Figures 4-5A and 4-5B) show the zircons with clear oscillatory zoning, revealing the typical feature of the zircon from

the acidic magma.

The geochemical results of this study indicate that the samples collected from the Sanfang and Yuanbaoshan plutons support crustal sources for the genesis of the granitic magma. Petrologically, the granite samples are K-feldspar megacryst riched (Figure 4-3B). Isotopically, all 19 isotopic results from the Sanfang granite are under the CHUR line (Figure 4-5C), which is compatible with the melting of a continental basement with little or no input of juvenile crust. Two-stage continental crust model ages of the analyzed zircon grains show a group of age at ca. 1800–2400 Ma ages, suggesting the possible existence of Paleoproterozoic rocks probably beneath the Jiangnan Orogenic Belt. Furthermore, the relatively homogeneous lithological features of the granites plutons may suggest that the source of magma chamber was derived from a mono-component chamber.

4.8.2 Origins of magnetic fabrics and its tectonic implications

According to magnetic investigation and macro-microscopic observations, the investigated areas in the Sanfang and Yuanbaoshan plutons can be divided into two fabric domains, namely, the magmatic and post-solidus ones. We roughly constrain the transition zone between the magmatic and post-solidus fabric units at the elevation range of 700-800 meters.

The magmatic domain concerns the zone with the elevation below 700 meters. In this domain, the granites are "nearly isotropic" (Figure 4-10, zones 1, 2, 4 and 6), though relatively coherent fabrics have been evidenced in this domain by AMS studies. The microscopic study shows that the quartz grains are euhedral with very slightly undulose extinction (Figure 4-4). The biotites in the granites are magmatic without any post-solidus deformation. These evidence suggest that the granite did not suffer a post-solidus deformation. Furthermore, 96% of the P_j values lower than 1.1, which indicates that the magnetic fabrics are acquired during the magma crystalization (Borradaile and Henry, 1997), in agreement with the macroscopic and microscopic studies presented above. Therefore, we propose that the magnetic fabrics

in these domain are primary ones, i.e. without any post-solidus overprint of posterior geological events. The shape parameters indicate both oblate and prolate shapes with equivalent proportion, which indicates that the magnetic foliation and lineation developed almost equally, and thus we can propose that the original magma probably flowed in a weak stress field.

On the contrary, in the post-solidus domains (Zones 5 and 6 in [Figure 4-10](#)) at altitudes above 800 meters, the granites are well foliated with augen gneissic structures, and shear bands. Microscopic studies reveal that the quartz grains are mostly recrystallized as neograins with serrated boundaries, showing the evidence of high temperature and high strain rate deformation. A top-to-the-W kinematics is indicated macroscopically by the sigmoidal augen structure and shear bands, and microscopically by mica fish and pressure shadows. In addition, the P_j values of these two zones are higher than 1.1, i.e., higher than other four zones of the magmatic domain, suggesting that the magnetic fabrics are acquired after the magma cristalization which may be related to a posterior tectonic event ([Tarling and Hrouda, 1993](#)). Thus, the evidence above reveal that the magnetic fabrics of this domain are secondary ones and the synmagmatic ones are overprinted. These post-solidus fabrics might have been developed during the ending stage of the magma emplacement and crystallization and/or during a regional tectonic events that post-dated the plutons emplacement. Moreover, it is worthy to note that almost all the shape parameters for the specimens in this domain are greater than zero ([Figure 4-10](#)), indicating the planar magnetic fabric is more developed than the linear magnetic ones probably due to a tectonic event.

4.8.3 Space creation and the mechanism of the magma emplacement

The Jiangnan Orogeny took place at 850-830 Ma (see Chapter 3), resulted in the deformation of the Sibao group with N-S trending tight folds, and probably N-S and NE-SW directed faults ([Figure 4-2](#)) ([BGMRGX, 1985](#); [BGMRHN, 1988](#); [Yan et al., 2015](#)). The field investigation shows that the granite plutons have a N-S elongated

shape with a ratio of 2:1 (Figure 4-2). The gravity modeling displays that these two plutons are also N-S elongated at depth (Figures 4-12 and 4-13). Consequently, we propose that the magma were generated from the crustal materials and then intruded into the well-folded Sibao group, ascending probably along the previously existing tectonic weak zones, i.e., the fault planes, and fold hinges. However, the depth of emplacement is unclear (Figure 4-13B).

The AMS study indicates that the magnetic fabrics are magmatic ones for the samples collected in zones 1, 2, 4, and 6 observed at altitudes below ca. 700 meters (Figures 4-9 and 4-10), therefore, they can be utilized for the interpretation of the magma flow and emplacement process (Tarling and Hrouda, 1993). In Zone 1, the magmatic foliations are consistently dipping to the E with steep angles (31-60 degrees), even near vertical angles (61-90°) for 2 sites. However, the magmatic lineations in this zone can be divided into two units, i.e., the southern one mainly plunging in the E-W with steep angle, and the northern one mostly plunging in the N-S with gentle angles (0-30°) (Figure 4-9). It may reflect that the magmatic lineations in the southern part are mainly dominated by the vertical and E-W vectors, while those of the northern unit by the horizontal and meridional vectors. In Zone 2, about five kilometers east to Zone 1, the westward dipping magmatic foliations with steep angles and mainly W-dipping lineation may imply that the magma dominantly flowed steeply and accreted in the E-W direction. In Zone 6 of the Yuanbaoshan pluton, the strikes of the magmatic foliations are almost N-S directed with steep and even vertical angles, whereas the magmatic lineations are consistently N-S directed with gentle angles (Figure 4-9), suggesting that the magma might vertically ascend and gently or horizontally flow in the N-S direction (present coordinates). In addition, the shape parameter plot shows the ratio between the oblate and prolate shapes is about 1:1, indicating the magmatic foliations and lineations were developed at a weak stress field, and thus we can speculate that the magma migrated equally in the vertical and horizontal (N-S) directions. Moreover, the residual Bouguer gravity anomaly data

show that the roots of the Sanfang and Yuanbaoshan plutons are located in their southern and central parts, respectively (Figure 4-11). The interpreted profiles suggest that the roots of the two plutons are constructed by some dykes and the shape of two plutons are both oblate in the E-W but are prolate in the N-S. For both of these two plutons, the thickest part of granite pluton is in the south and gradually decreases northward, which seems like tongues and sills (Figures 4-12 and 4-13).

Consequently, we propose that the magma: (1) intruded into probably pre-existing tectonically weak zones in the Sibao group; (2) ascended with steep to vertical angle and E-W laterally accumulated by N-S oriented dykes; (3) dominantly flowed from south to north with gentle angle to form the tongue- and/or sill-shaped plutons (present coordinates) (Figure 4-13B).

4.8.4 A top-to-the-W tectonic event

In the post-solidus fabric domain (Zones 3 and 5 in Figure 4-10), the degrees of metamorphism and deformation of the granites and country rocks are positively related with the elevation in the Sanfang and Yuanbaoshan areas (Figure 4-2).

These granites change from the massif body (elevation at ca. 200-700 m) (Figures 4-3A and 4-3B) to the gneissic one (elevation at ca. 800-1600 m) (Figures 4-3D and 4-3E). Equivalently, in the microscopic view, the quartz and micas are transformed from euhedral to anhedral (Figures 4-4A to 4-4L), indicating that these granites have suffered high temperature deformation. Moreover, the myrmekite as those found in samples A44 and A46 (Figures 4-4I and 4-4J), typically occurs in the metamorphic orthogneisses, forming under metasomatic conditions (Castle and Lindsley, 1993; Garcia et al., 1996). Therefore, it is usually recognised as the products of progressive fluid-assisted deformation in molten rocks (Simpson and Wintsch, 1989). Furthermore, the AMS results also indicate that the fabrics of these granites were overprinted by a tectonic event (Figure 4-10).

However, the lithology of the Sibao group varies from weakly metamorphosed

rocks (elevation below ca. 700 m) (sandstone, slate) to relative highly metamorphosed ones (elevation above ca. 800 m) (phyllite, micaschist) (Figure 4-2). The sandstone and slate are located at the lower altitude preserve primary stratigraphic dispersed bedding (S_{0-1}) (Figures 4-3F, 4-3G, 4-3O, 4-3T and 4-3U). Nevertheless, the phyllite and micaschist at the higher elevation display complex deformation styles. Recumbent folds with subhorizontal N-S axes are developed in the rhythmic bedding of turbidite (S_{0-1}) (Figure 4-3J). The primary surface (S_{0-1}) is folded by a secondary one (S_2) which dips to the W and axial planar to these folds (Figure 4-3K). In the monzogranite, augen orthogneiss exhibits an E-W striking mineral and stretching lineation (Figures 4-3L and 4-3M). The microscopic study of these rocks show the quartz grains and micas are consistently orientated in the E-W direction (Figures 4-4N, 4-4P and 4-4Q). Moreover, the mylonite is observed on the roof and the western margin of the Yuanbaoshan pluton (Figure 4-3R), with strongly deformed feldspar and biotite E-W orientated.

By integrating the field observations and microscopic investigations, we conclude that the foliations consistently dip to the W in both of the granites and country rocks, with coherent lineations directed in the sub E-W. All of the kinematic indicators, i.e., shear band, augen structure, mica fish, S-C fabric and pressure shadows (Figures 4-3D, 4-3L, 4-4K, 4-4Q and 4-4R), reveal the top-to-the-W sense of shear. Consequently, we propose that a ductile shearing event took place within the posterior fabric domain in the Sanfang-Yuanbaoshan area, with a thickness of at least 1.5 km (Figure 4-13C). However, the timing of this ductile shearing event is poorly constrained. Our Ar-Ar measurements of muscovite from the Sanfang and Yuanbaoshan plutons show an age cluster at 440-400 Ma (see Chapter 5), indicating that the ductile shearing event should, at least, be not younger than this period. Therefore, we can deduce that the ductile shearing event took place in a time interval comprised between 830-400 Ma. Under this premise, we propose two possible interpretations.

1) The ductile shearing event took place at the end of the Jiangnan orogeny shortly after the plutons emplacement. Late to post-orogenic collapse might be the driving mechanism. However, evidence of crustal thickening in this part of the Jiangnan orogen is not documented neither by structural nor metamorphic features. Furthermore, the Sanfang-Yuanbaoshan area was located in the upper plate of the orogen, that is to say, in a region where crustal thickening should be limited. In this interpretation, it is also necessary to assume that the plutons and their country rocks remain buried at depth, or where reheated in the Middle Paleozoic.

2) The ductile shearing event took place in the 440-400 Ma period. This period correspond to the late stage of the intracontinental Early Paleozoic orogeny of SE China (e.g., [Charvet, 2013](#); [Faure et al., 2009](#); [Shu et al., 2008](#)). Although crustal melting represented by numerous ca 400 Ma plutons and migmatites, from Zhejiang to NE Vietnam, N-directed structures that might account for the reworking of the Neoproterozoic rocks are rare all along the Early Paleozoic belt. N or NW dipping foliations have been documentd near Chongren in Jiangxi Province, (e.g., [Faure et al., 2009](#)). However, in particular such a NW-directed ductile shearing of ca 400 Ma age that would rework the Jiangan Orogenic Belt has never been recognized before..

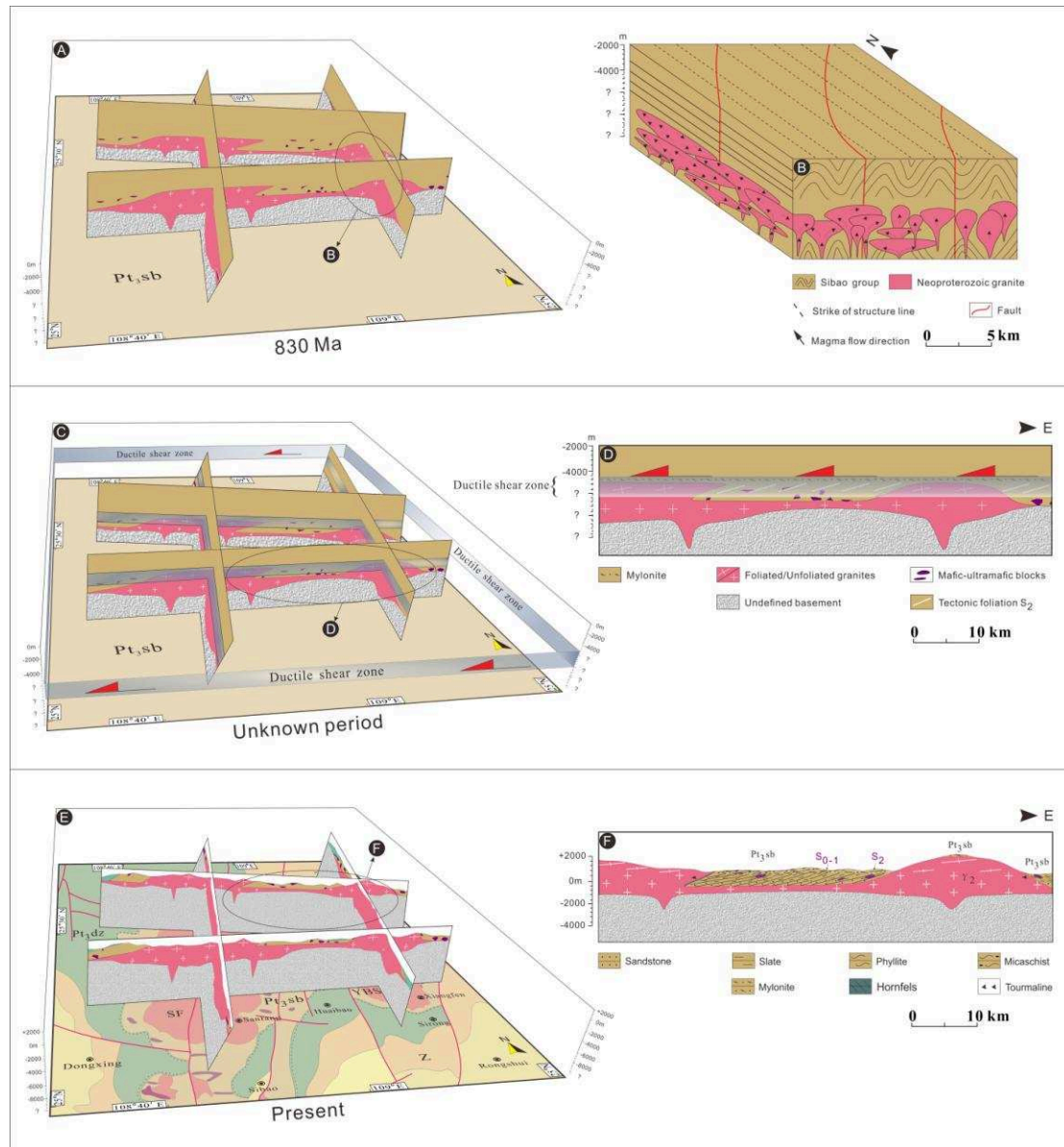


Figure 4-13. 3-D sketch models of the magma emplacement (A), regional ductile shearing event (C), and current geological features (E) for the Sanfang and Yuanbaoshan plutons; (B) Detail 3-D modeling of the magma emplacement in the E-W and N-S directions; (D) Sketch map of the ductile shearing in the granite plutons and country rocks; (F) Sketch map of the current geological signatures of the Sanfang and Yuanbaoshan plutons and country rocks. All of the models are in the present coordinate.

4.9 Conclusions

Through multidisciplinary studies, the formation and evolution of the Neoproterozoic S-type Sanfang-Yuanbaoshan granite plutons in the Jiangnan Orogenic Belt can be concluded as following:

(1) The magma source of the plutons is derived from the melting of crustal material and crystallized at 830 Ma;

(2) The magnetic fabrics can be divided into two groups, namely, an early primary magmatic fabric developed in a magmatic stage during the plutons emplacement, and secondary post-solidus one related to the development of planar and linear fabrics;

(3) The magma intruded into the tectonic weak zones in the Sibao group, with E-W lateral accumulated by N-S oriented dykes, and dominantly flowed from south to north horizontally to construct the tongue- and/or sill-shaped plutons;

(4) A top-to-the-W ductile shearing event took place after the magmatic emplacement, however, the timing of this event is unclear.

Chapter 5. Early Paleozoic to Triassic geological events in the Sanfang-Yuanbaoshan, western Jiangnan region: the Argon isotopic record

5.1 Introduction

The western Jiangnan Orogenic Belt is considered as the product of the collision of the Yangtze and Cathaysia blocks at ca. 865 Ma and this orogeny is ended at ca. 830 Ma as suggested by the emplacement of late orogenic peraluminous magma. The field observation shows that the upper part of the S-type granite of the Sanfang-Yuanbaoshan plutons have been well deformed, even mylonitized, however, its lower part keeps its magmatic state (see Chapter 4). As this evident post-solidus deformation did not attract any attention before, the study area was regarded as without obvious deformation by the tectonic event since Nanhua rifting and subsequent Early Paleozoic and Triassic orogenies. Therefore, it naturally leads us to wonder about the age of this post-solidus deformation. Consequently, we take the advantage of Argon-Argon thermochronology method.

The $^{40}\text{Ar}/^{39}\text{Ar}$ geochronological technique has significantly contributed to the study of crustal deformation (Kelley, 2002; Scaillet, 1996), and was proved to be an efficient one to date the deformed rocks by potassium-bearing minerals, e.g., muscovite, biotite, sericite and amphibole (Mcdougall & Harrison). $^{40}\text{Ar}/^{39}\text{Ar}$ dating relies on neutron irradiation from a nuclear reactor to convert a stable potassium (^{39}K) into the radioactive ^{39}Ar . As long as a standard sample of known age is co-irradiated with unknown samples, it is possible to use a single measurement of argon isotopes to calculate the $^{40}\text{K}/^{40}\text{Ar}^*$ ratio, and thus to calculate the age of the unknown sample. $^{40}\text{Ar}^*$ refers to the radiogenic ^{40}Ar , i.e. the ^{40}Ar produced from radioactive decay of ^{40}K . $^{40}\text{Ar}^*$ does not include atmospheric argon adsorbed to the surface or inherited through diffusion and its calculated value is derived from measuring the ^{36}Ar (which is assumed to be of atmospheric origin) and assuming that ^{40}Ar is found in a

constant ratio to ^{36}Ar in atmospheric gases (Scaillet, 1998). $^{40}\text{Ar}/^{39}\text{Ar}$ geochronology assumes that a rock retains all of its ^{40}Ar after cooling past the closing temperature. The closure temperature concept (Dodson, 1973) is based on the volume circulation of a diffusing chemical element in the host mineral and temperature, for fixed realistic cooling rate and mineral grain-size. This concept is defined as a transitional temperature range, at which the diffusion of a daughter isotope evolved from fully open state (continuous equilibrium) to virtually closed behaviour (frozen equilibrium).

Different minerals have different closure temperatures, like the biotite, muscovite and hornblende, with the ranges of 260-350 °C, 360-420 °C and 450-550 °C, respectively (Chiaradia et al., 2013). Consequently, it can be used for estimating the thermal history of the rocks.

5.2 Geological setting (Late Proterozoic to Triassic)

After the Neoproterozoic Orogeny, the whole South China Block entered into a rifting period at 800-750 Ma (Shu, 2012), and then the sediments were deposited in a marine environment over a long period until the Silurian. The Phanerozoic tectonic evolution of South China is characterized by two distinct orogenic cycles, including early Paleozoic and Triassic orogenies, respectively (Charvet, 2013; Li et al., 2016a; Shu, 2012).

As recognized since 1920's (Grabau, 1924), the fact that the Middle Devonian terrigenous rocks unconformably cover Early Paleozoic folded rocks and granitoids document an Early Paleozoic tectono-magmatic event widespread in the Cathaysia Block. The Early Paleozoic orogeny is characterized by: i) the regional absence of Silurian strata, ii) the unconformity between the middle Devonian terrigenous (conglomerate, sandstone) and limestone sequences and Ordovician terrigenous deposits, iii) a greenschist to amphibolite facies metamorphism coeval with a ductile deformation, iv) a decollement layer between an underlying metamorphic unit and an overlying fold-and-thrust belt unit; and v) the occurrence of migmatites, and numerous

S-type granitic plutons (Faure et al., 2009). From a geodynamic point of view, the Early Paleozoic orogeny of the South China Block was interpreted as the consequence of the rift closure in the Late Ordovician to Early Silurian. Therefore, the orogeny corresponds to an intracontinental event accommodated by the continental subduction of the southern part of the rift below its northern one. During the exhumation, the metamorphic rocks experienced retrogression and partial melting at ca. 444–420 Ma represented by migmatite and granitoid (Faure et al., 2009). However, it was widely accepted that the Early Paleozoic intracontinental orogeny was not well developed in the Jiangnan region, and the Cambrian and Ordovician strata are not metamorphosed, only showing brittle deformation (Shu, 2012).

The Triassic deformation is widespread in the entire South China. A middle Triassic orogeny (called Indosinian) was originally defined by a late Triassic unconformity in Vietnam (e.g., Deprat, 1914; Fromaget, 1932). Geodynamically, the Indosinian orogeny results from the continental collision of the South China block with the Indochina Block. Furthermore, other Triassic belts such as the Xuefengshan, Longmenshan, Dabashan, recognized in the South China Block (Figure 5-1) are intracontinental orogens. The link between the Indosinian collision and the intracontinental orogens is unclear yet (see for instance Faure et al., 2016). The Triassic Deformation is well recognized in the entire South China (Figure 5-1), including the Triassic plutonism, ductile shearing, thrusting, folding, and greenschist-facies metamorphism (e.g., Wang et al., 2005, 2007b, c; Lin et al., 2008; Shu et al., 2009; Zhang and Cai, 2009; Xu et al., 2011). The Triassic orogeny resulted in important intracontinental deformation with intensive folds and thrusts in the South China block (Figure 5-1), especially in the areas of Wuyi, Nanling, Yunkai and Xuefengshan (Chu et al., 2012; Lin et al., 2008; Wang et al., 2005, 2007b; Figure 5-1). The current agreement is that these events occurred within an intracontinental setting (Chu et al., 2012; Wang et al., 2005; Shu et al., 2015). Whereas, several competing models have been proposed to describe the mechanics of Triassic intracontinental

structures, for example the flat subduction of the Paleo-Pacific plate (Li and Li, 2007) or continental subduction (Chu et al., 2012).

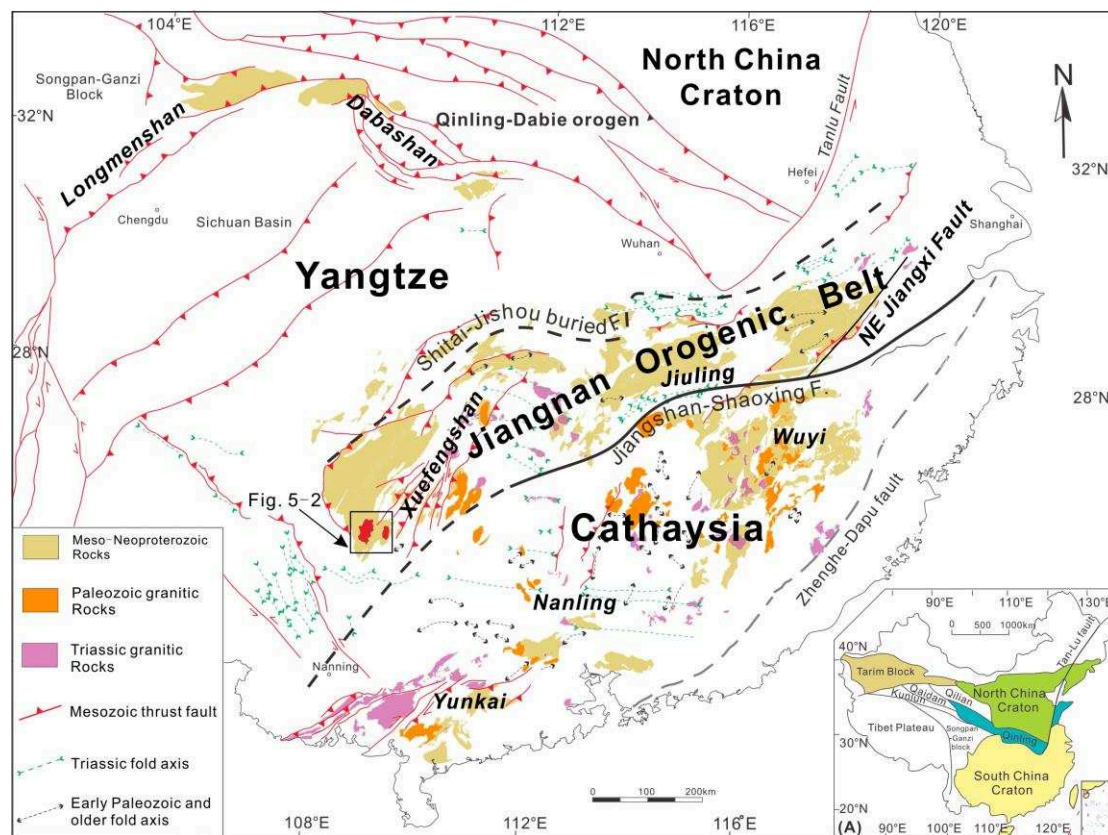


Figure 5-1. Sketch map of South China delineating the distributions of Paleozoic and Triassic structures, igneous rocks, and Neoproterozoic strata. The red bodies in the square are Sanfang (left) and Yuanbaoshan (right) plutons, respectively (modified after Li et al., 2016a).

5.3 Sample collection, description and analytical procedures

5.3.1 Sample collection

A great volume of granite is exposed in the Sanfang and Yuanbaoshan plutons, therefore, they are suitable targets for probing into the thermal history of the plutons. Besides, the plutons possibly divided into sub-solidus magmatic and post-solidus deformation (see Chapter 4). Moreover, the Sibao group located between the Sanfang and Yuanbaoshan plutons was strongly deformed, even mylonitized, and metamorphosed with a higher grade than in the west or south of Sanfang.

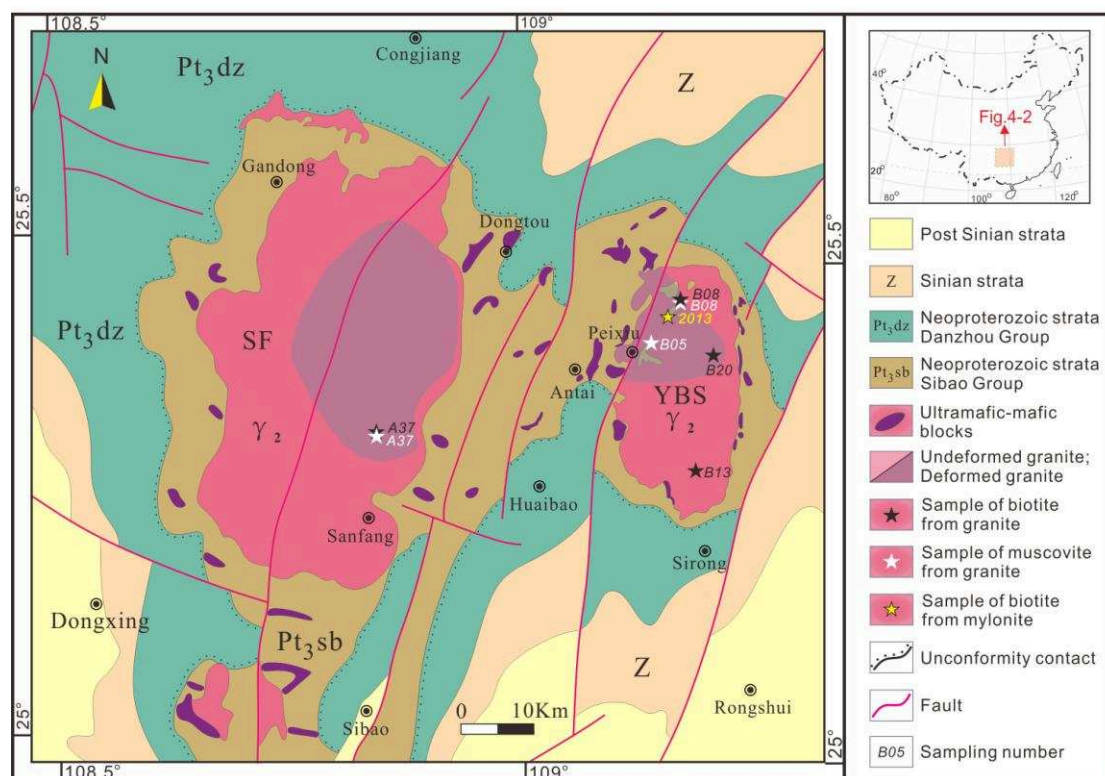


Figure 5-2. Sketch map of the Sanfang and Yuanbaoshan plutons with sampling localities.

In the Yuanbaoshan pluton, we have collected fresh granite samples at altitudes from ca. 200 m to ca. 900 m, including the deformed and undeformed ones (Figure 5-2). As mentioned in Chapter 4, the transition zone between the deformed and undeformed granites is at the altitude of 500-700 meters. In the Sanfang pluton, we have collected one sample (A37, at an altitude of 560 m) in the transition zone between deformed and undeformed granite. Furthermore, a mylonite of country rocks (2013) with fresh biotite was also targeted for the analysis. Details are provided in Table 5-1.

Table 5-1. Sample list for the Ar-Ar age analysis on the micas from SF and YBS

Sample	GPS	Num. run	Num. analysis	Petrology	Mineral	El. (m)	Age (Ma)
In situ UV laser							
A37	N 25°18'45"E108°50'35"	N71	126	Slightly deformed granite	Bio	560	R: [240, 420]
		N86	23		Bio		R: [240, 420]
		N86	45		Mus		R: [400, 450]
		N87	28		Bio		R: [290, 420]
		N88	16		Bio		R: [330, 420]
		N89	12		Bio		R: [310, 420]
Step heating							
B08	N 25°28'18"E109°10'32"	N121	17	Deformed granite	Mus	803	PA: 413.0±1.2
		N122	25		Bio		TGA: 409.6±5.1
B05	N 25°25'43"E109°08'29"	N123	17	Deformed granite	Mus	688	PA: 406.6±1.1
B13	N 25°18'06"E109°11'52"	N125	19	Undeformed granite	Bio	222	PA: 392.2±0.8
B20	N 25°25'03"E109°12'54"	N144	16	Deformed granite	Bio	585	PA: 404.4±0.8
2013	N 25°27'03"E108°09'33"	N141	14	Mylonite, country rock	Bio	1112	PA: 407.8±0.9

Note: El. (m): elevation; R: age range; TGA: total gas age; PA: plateau age; Bio: biotite; Mus: muscovite

5.3.2 Sample description

Six samples have been selected for the argon isotopic analysis, including the deformed granites, undeformed granites and one mylonite sample from country rocks. The granite sample (A37) from the Sanfang pluton is in transition zone between deformed and undeformed granites. In the hand sample, the biotite and muscovite surround the sigmoidal feldspar (**Figure 5-3A**), with the top-to-the-W kinematic. However, another one, the biotite is euhedral, with self-structured quartz and feldspar

(Figure 5-3B).

The deformed granites collected in the Yuanbaoshan pluton show that the mica, quartz and feldspar are elongated in a preferred E-W orientation, with well developed foliations, indicating that they have experienced a ductile shearing deformation. Meanwhile, the indicators, e.g., mica fish and augen structure, yield the top-to-the-W kinematics (Figures 5-3C, D, E and F).

In the undeformed sample (B13) picked in the south part of the Yuanbaoshan pluton, the granite is massive, and the biotite, quartz, and feldspar are all euhedral (Figures 5-3G and H).

Moreover, in the mylonite sample from country rocks and collected on the roof of the Yuanbaoshan pluton, the biotites and feldspars are strongly stretched in the E-W direction, however, the kinematic is not obvious (Figures 5-3I).

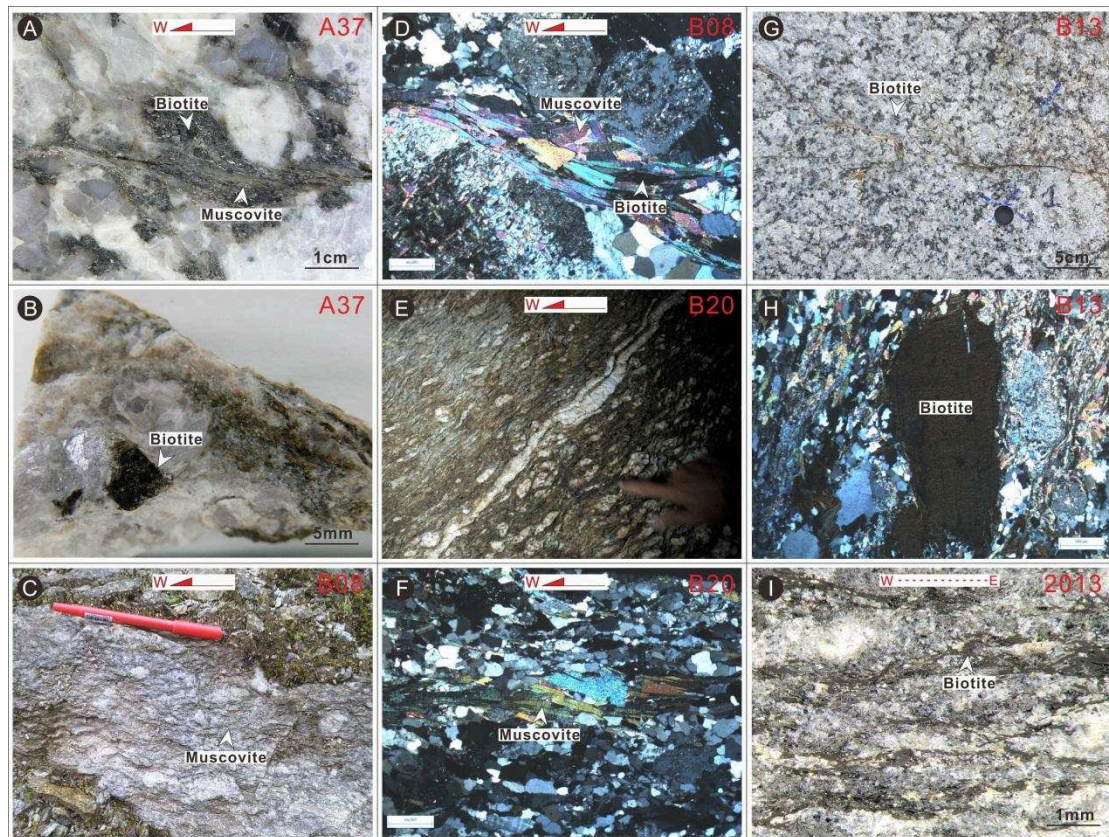


Figure 5-3. Photos of hand-sample and thin-section of the samples collected from the Sanfang, Yuanbaoshan plutons and the country rocks. (A) Hand-sample of the granite from the Sanfang pluton, with sigmoid feldspar and stretched biotite and muscovites; (B) Hand-sample of the granite from the Sanfang pluton, with euhedral biotite aggregate; (C) Foliated granite from the Yuanbaoshan pluton, with top-to-the-W kinematics (D) thin-section in crossed polarized light of the B08 sample, the stretched micas and sigmoidal k-feldspar indicate top-to-the-W kinematics (E) Gneissic granite with top-to-the-W kinematic; (F) thin-section in crossed polarized light of the B20 sample, recrystallized quartz and stretched muscovite are distributed along the foliation, with the top-to-the-W kinematics; (G) Massive granite of B13; (H) Thin-section of the massif granite in the crossed polarized light of B13, with undeformed biotite; (I) Mylonite sample from the country rocks on the roof of the Yuanbaoshan pluton, with strongly stretched biotite and feldspar, but unclear kinematic sense.

5.3.2 Analytical procedure

The $^{40}\text{Ar}/^{39}\text{Ar}$ dating approach combines both conventional CO_2 laser step-heating technique on biotite and muscovite single grains, and in situ analyses on biotite and muscovite from rock-chips by high-resolution UV laser technique. Biotite grains were extracted by gently crushing the samples and hand-picking the coarsest produced fraction. They were firstly imaged using a high-resolution ($\times 20$ to $\times 60$) binocular microscope to screen out suspect (altered or broken) specimens. All grain sizes were between 0.125-0.25 mm. For in situ analyses, microstructures were drilled on samples, cut and polished to obtain 1.0-1.5 mm \times 10 mm circular rock-chips. Rock-chips and separated single grains were then washed in acetone, ethanol and de-ionised water in ultrasonic bath, dried at 50 °C in oven, weighted and finally microscopically analysed and photographed. After weighing using a high-precision (± 0.001 mg) micro-balance, the individual samples and rock chips were wrapped in aluminium foil and coaxially stacked in an irradiation package about 2.5 cm and 4.5 cm

long, respectively, along with sanidine standard FCS (28.02 ± 0.28 Ma, [Renne et al., 1998](#)). The batch was irradiated for 10 hours in CLICIT (Corvallis irradiation center, OSU, USA). Afterwards, the samples were analysed at the Argon Geochronology Laboratory, Orléans University (France). $^{40}\text{Ar}/^{39}\text{Ar}$ geochronology of biotite and muscovite were conducted by Helix SFT™ Split Flight Tube Noble Gas Mass Spectrometry combining continuous-wave CO_2 ($10.6\text{ }\mu\text{m}$) lasers with very-low background extraction systems at the $^{40}\text{Ar}/^{39}\text{Ar}$ Lab housed at Institut des Sciences de la Terre d'Orléans (ISTO), France. After about 100 days of post-irradiation cooling, the single grains were loaded into a differentially-pumped sample holder connected to the ultra-high vacuum extraction and purification system and baked out at $180\text{ }^\circ\text{C}$ for 48 hours.

Laser spot analyses were performed on single grains of biotite and muscovite using a continuous carbon dioxide laser beam. They were individually step-heated with a nominal step increase of 0.5 % of the total output laser power until total fusion (single-grain analysis). Each measurement included one blank every consecutive sample extraction step. Purification prior to expansion into the MS consisted in 6 min static exposure to a cold trap ($-127\text{ }^\circ\text{C}$) and two hot ($250\text{ }^\circ\text{C}$) GP-50 St-101 SAES® getters, followed by static MS peak-hopping of the five argon isotopes plus ^{35}Cl (blank: 5 peak-hopping cycles; sample: 10 cycles). Raw blanks for each isotope were fitted using a 3rd to 4th-order polynomial across the daily session, and each assigned a respective error corresponding to the empirical mean average deviation from the best fit trend. Typical blank values were $5 \cdot 10^{-1}$, $7 \cdot 10^{-3}$, $2 \cdot 10^{-3}$, $2 \cdot 10^{-2}$, $7 \cdot 10^{-3}$ fA at $m/e = 40, 39, 38, 37, 36$, respectively. Corrections applied include (1) static blanks, (2) mass-bias and isobaric interferences, (3) post-irradiation ^{39}Ar , ^{37}Ar , and ^{36}Cl decay, (4) neutron-flux gradient and monitoring, and (5) K, Ca, and Cl isotopic interferences following [Scaillet \(2000\)](#). Ages were calculated using isotopic constants quoted in [McDougall & Harrison \(1999\)](#). TGA refers to total-gas ages calculated by summing all volumes of gaz (i.e., Ar beam intensity) extracted for each isotope till fusion with an error derived

by quadratic error propagation of all individual error terms involved in the age calculation. This corresponds to a formal K-Ar age. WMA are weighted-mean ages calculated by pooling and inverse-variance weighing the $^{40}\text{Ar}^*/^{39}\text{Ar}$ ratios included in the mean, with a final error corresponding to the maximum-likelihood estimate (MLE) of the error of the mean ($^{40}\text{Ar}^*$ = radiogenic ^{40}Ar). WMA errors basically differ from TGA errors by the effect of the $1/\sqrt{N}$ error-reduction rule typical of pooled MLE. PA are plateau ages calculated as the WMA, but for which the empirical MSWD score (MSWD = Mean Square Weighted Deviation) fall in the fiducial interval for the corresponding degrees of freedom according to CHI-2 statistics.

Whereas, in situ ablation analyses on rock chips were performed using a pulsed UV laser beam. After laser spot analysis, the gas was extracted into the transfer line, and the next steps were same to those of step heating as described above.

5.4 Analytical results

The argon isotopic analyses on the biotite and muscovite put high resolution $^{40}\text{Ar}/^{39}\text{Ar}$ time-constraints using both conventional step heating and in situ UV laser techniques.

5.4.1 Step heating

Six single grains were analysed by $^{40}\text{Ar}/^{39}\text{Ar}$ step heating, including three granite biotite, two muscovite and one mylonite biotite (Figure 5-4, Table5-1). All the samples show well defined plateau ages with more than 70% of ^{39}Ar released, except one biotite grain, B08, which yield no plateau age (PA), however, the total gas age (TGA) spectrum is flat with small fluctuation, hence, we can regard the TGA as a reliable one (Laurent et al., 2017). All of the six ages are distributed in the range of 414-392 Ma. The sample of B08 analysed for both of the muscovite and biotite displays the ages of 413.8 ± 1.2 Ma and 409.6 ± 5.1 Ma, respectively. The sample of B05 yields an age of 406.6 ± 1.0 Ma with 10/17 (valid steps/total steps) steps. However, the results of samples B13 and B20 are more convincing, with more than 90% of ^{39}Ar

released gas. Furthermore, the mylonite sample (2013), collected from the country rocks on the roof of the Yuanbaoshan pluton, yield the biotite age of 407.8 ± 0.9 Ma with high precision.

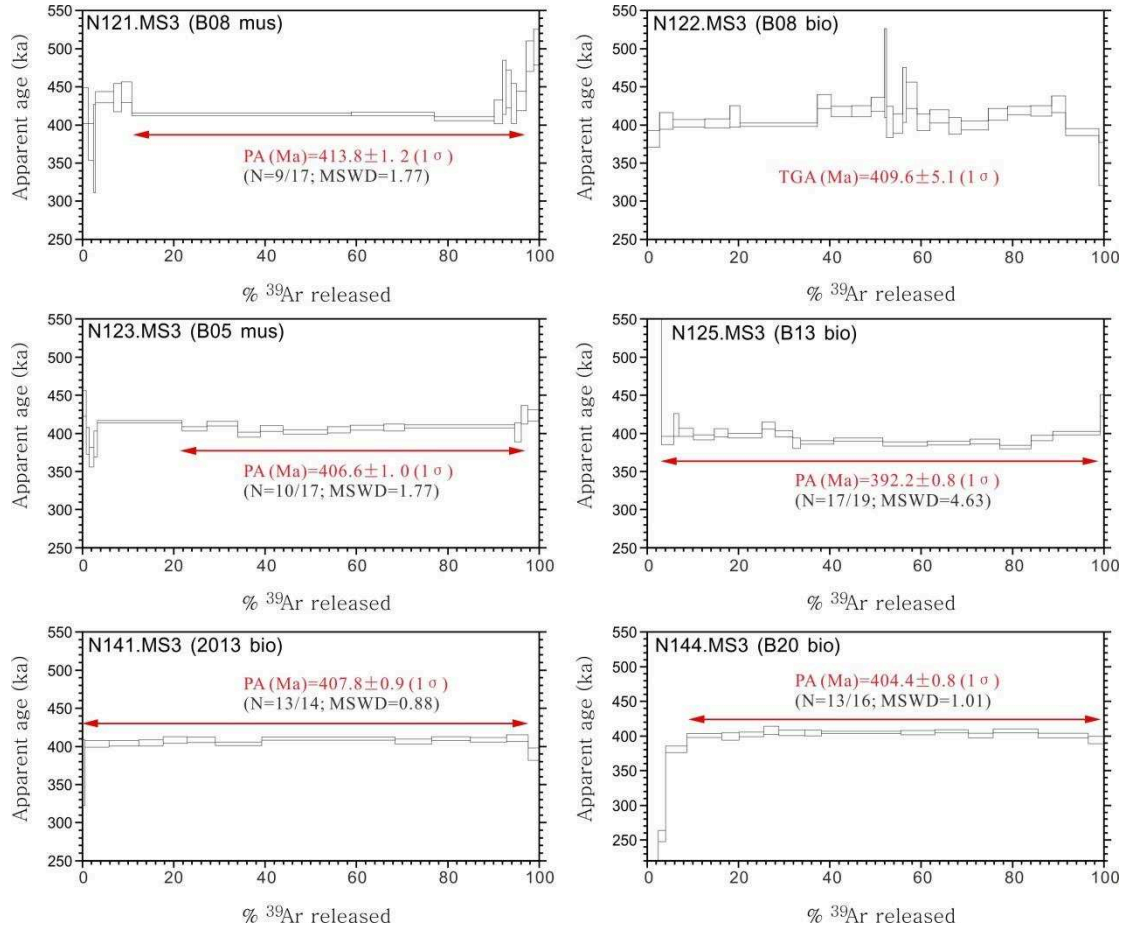


Figure 5-4. $^{40}\text{Ar}/^{39}\text{Ar}$ age spectra obtained on single grain from samples of the Yuanbaoshan granites and mylonite (2013) of the Sibao group. PA: plateau age; TGA: total gas age.

5.4.2 In situ UV laser

Six runs have been carried on the rock-chips and biotite aggregations of the sample A37 collected from the Sanfang pluton, including the deformed and undeformed micas (Figure 5-5A).

126 data of the undeformed biotites have been acquired from the rock-chip N71, which yield a broad staircase-shaped age cluster, ranging from 420 Ma to 240 Ma,

with a steady declining trend (Figure 5-5B). Quite similarly, the deformed biotite of the rock-chip N86 indicate a same age range of 420-240 Ma, and the decreasing behaviour of the age is almost coincident with that of N71. However, the stretched muscovite (45 data) yield a relative narrow age range of 450-400 Ma, with a flat age interval between 420 Ma and 400 Ma (Figure 5-5B). Meanwhile, the biotite aggregations (N87 and N88) and rock-chip N89 yield a similar age range of ca. 420-300 Ma with analogous declining trend (Figure 5-5B).

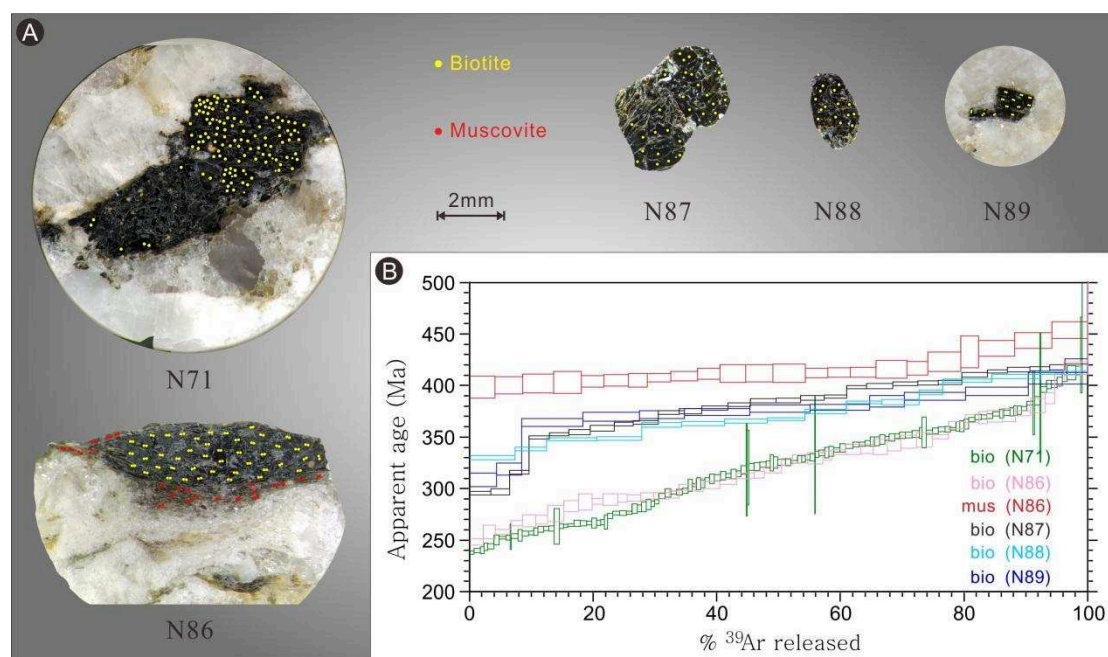


Figure 5-5. $^{40}\text{Ar}/^{39}\text{Ar}$ analyses for the sample of A37, from Sanfang pluton, by in situ UV laser ablation technique. (A) Photos of rock-chips and biotite aggregations. The samples are all undeformed except the chip N86. The yellow spots means the analyses on the biotite, while the red spots on the muscovite; (B) Results of the analyses on each samples.

5.5 Discussion

Sampling was designed as to explore the behaviour of the $^{40}\text{Ar}/^{39}\text{Ar}$ system at two different scales: (1) a nearly one kilometre vertical thickness shows the distribution of ages across the upper part of Yuanbaoshan pluton by the single mica grains; (2) millimetre-scale shear zones and euhedral crystals were examined with the

in situ UV laser method on rock-chips and biotite aggregations. Totally, we got six results from step heating and six others from in situ analyse. Based on the geological setting and previous studies, we can discuss the significance of these Ar isotopic data as following:

5.5.1 Comparison of $^{40}\text{Ar}/^{39}\text{Ar}$ ages from the biotite and muscovite

In total, we have got 12 groups of ages, by two analytical techniques, namely, the step heating and in situ UV laser ablation methods. Both biotite and muscovite were analysed by each method.

For the sample of B08 from the Yuanbaoshan pluton, both of the muscovite and biotite grains (125-250 μm) were analysed by step heating technique, and yield apparent $^{40}\text{Ar}/^{39}\text{Ar}$ ages of 413.8 ± 1.2 Ma and 409.6 ± 5.1 Ma, respectively (Figure 5-4). The age of the muscovite is obviously, but slightly, older than that of the biotite in the same sample. The samples of B05, B13, B20 and 2013 yield well defined apparent ages of 406.6 ± 1.0 Ma, 392.2 ± 0.8 Ma, 404.4 ± 0.8 Ma and 407.8 ± 0.9 Ma, respectively (Figure 5-4).

As to the in situ method, all of the analyses were on the sample of A37, collected from the Sanfang pluton. The sample targets were made as rock-chips and biotite aggregations. Five runs were carried on the biotite, whereas one run was conducted in the stretched muscovite (Figure 5-5A). The biotite shows the broad age ranges from 420 Ma to ca. 300 Ma (N87, N88, N89) and 240 Ma (N71, N86), with staircase shaped decreasing trend. However, the muscovite mostly yield a flat release pattern at ca. 420 Ma, whereas only a small fraction of ages display the spectrum like the staircase with the maximum age of 450 Ma (Figure 5-5B). Moreover, the maximum age of the biotite is as same as the most frequency ages of the muscovites at 420 Ma. This also indicates that the muscovite is always older than the biotite in the same sample.

5.5.2 Comparison of the results with previous $^{40}\text{Ar}/^{39}\text{Ar}$ thermochronological studies

Many works on $^{40}\text{Ar}/^{39}\text{Ar}$ have been done across the SE South China Block in the continental scale, including the Wuyi, Yunkai, Jiuling and Xuefengshan areas (Figure 5-6). The details can be referred to Table 5-2.

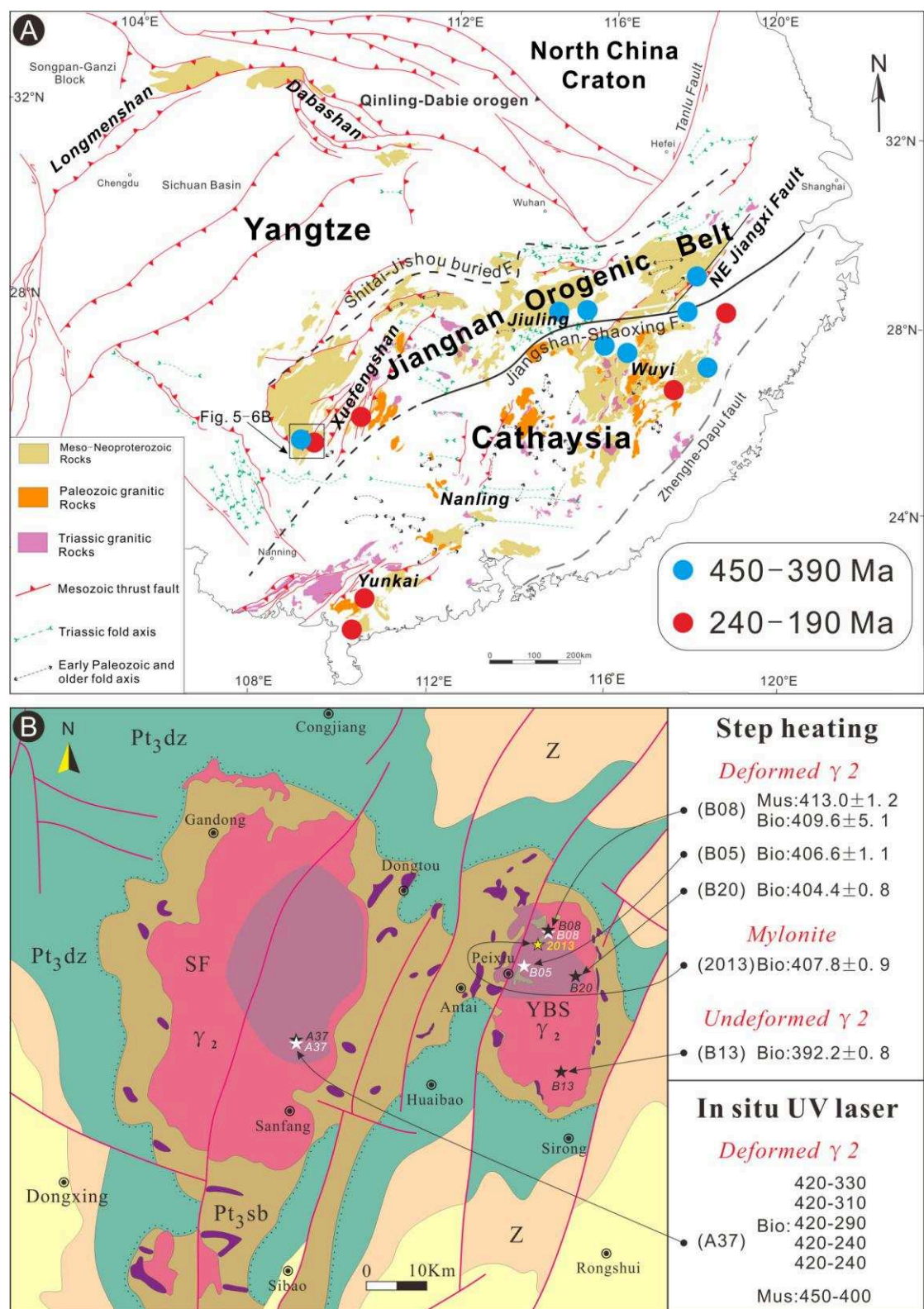


Figure 5-6. (A) Previous studies and this study on the $^{40}\text{Ar}/^{39}\text{Ar}$ results in the Jiangnan and Cathaysia regions; (B) Sampling localities with detailed $^{40}\text{Ar}/^{39}\text{Ar}$ results of this study.

In the previous studies, the argon isotopic thermochronological method has been utilized to the micaschist, gneiss and mylonite, and yield two significant age ranges, i.e., 450-390 Ma and 238-194 Ma (Figure 5-6). It was widely accepted that these two groups of $^{40}\text{Ar}/^{39}\text{Ar}$ thermochronological data are related with the Silurian intracontinental orogeny and Triassic intracontinental tectonic events in the SE South China (Cathaysia Block) (e.g., Faure et al. 2009; Li et al., 2016a; Shu et al., 1999, 2008; Wang et al., 2007b; Xu et al., 2011, 2015). However, it was commonly believed that the western Jiangnan region (this study areas) was not affected by the early Paleozoic intracontinental event. The influence of the Triassic tectonic event in this area is still debated. Some researchers proposed the intraplate deformation event was well developed in the Xuefengshan, western Jiangnan region (Chu et al., 2012). Whereas, some people hold the view that the Phanerozoic sedimentary sequences are not ductilely deformed, and therefore proposed that the Triassic intraplate event did not affect at least this study area (Wang et al., 2007b).

However we traced the $^{40}\text{Ar}/^{39}\text{Ar}$ information of the Paleozoic and Mesozoic ages. By comparison, we found the $^{40}\text{Ar}/^{39}\text{Ar}$ ages of the muscovite in the shear band (N86) yield similar ages with the previous results (Figure 5-7). The distinct difference is that our results show the flat release pattern at ca. 420 Ma, while the previous results reveal the most flat distribution at ca. 430 Ma (Figure 5-7). Moreover, both of our and previous studies yield quite similar decreasing trend from 450 Ma to 390 Ma. Nevertheless, the biotite rock-chips and aggregations display complex age distribution patterns, which reveal two groups of staircase shaped age spectra, i.e., the 420-ca. 390 Ma and 420-240 Ma. The decreasing patterns are smooth without sudden break. Besides, it is apparent to note that the minimum age of our biotite is coeval with the maximum age of the Mesozoic aged mica (Figure 5-7). Furthermore, the previous Mesozoic aged $^{40}\text{Ar}/^{39}\text{Ar}$ data display a smooth and flat spectrum which is quite different with biotite behavior in our study.

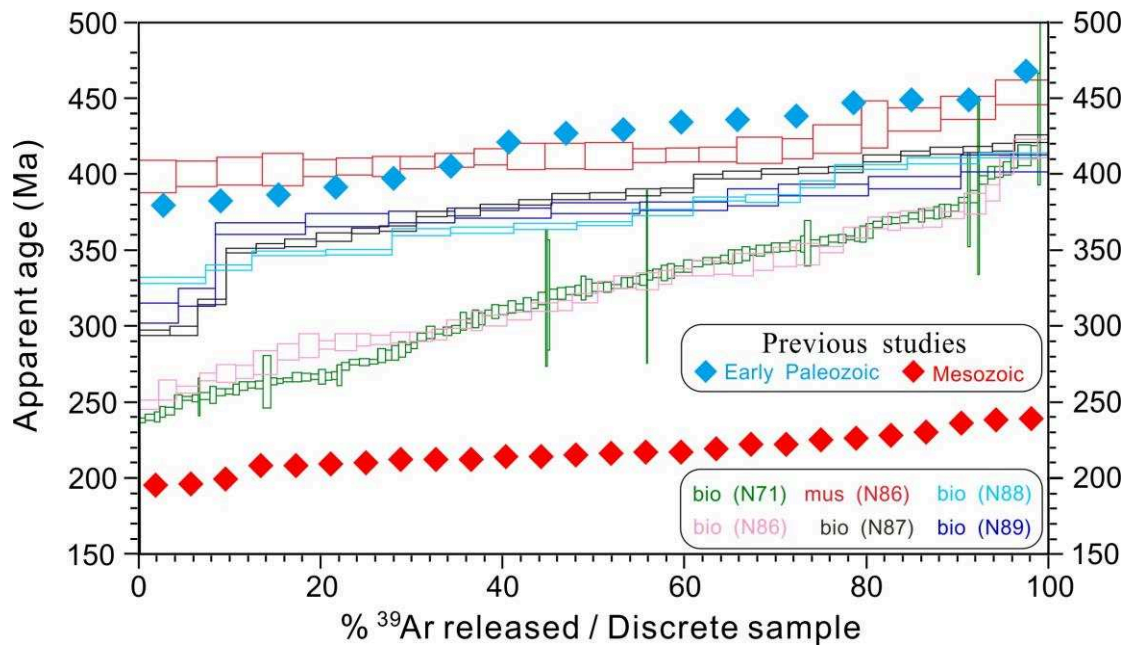


Figure 5-7. Comparison of the $^{40}\text{Ar}/^{39}\text{Ar}$ results between this study and previous studies. Note that, the results of this study are distributed according to the ^{39}Ar released, however, the previous studies results are discrete samples which are equispaced arranged.

Table 5-2. Previous studies on the $^{40}\text{Ar}/^{39}\text{Ar}$ results in the Jiangnan and Cathaysia regions

Region	Rock type	Age (Ma)	Mineral	Method	Reference
Early Paleozoic					
Zhenghe-Dapu Fault	Marble	391.4±3.0	Muscovite	Step heating	Shu et al., 1999
Jiangshan-Shaoxing Fault	Mylonitic granite	421.3±7.8	Muscovite	Step heating	Shu et al., 1999
Nanfeng-Yintang shear zone	Mylonite	427.7±3.7	Muscovite	Step heating	Wang et al., 2007a
Ductile décollements	Micaschist	405.0±4.0	Muscovite	Step heating	Faure et al., 2009
Ductile décollements	Micaschist	397.0±4.0	Biolite	Step heating	Faure et al., 2009
Jiuling	Mylonite	468.0±12.0	Muscovite	Step heating	Chu et al., 2014
Jiuling	Mylonite	379.0±4.0	Muscovite	Step heating	Chu et al., 2014
Jiuling	Mylonite	386.0±6.0	Biolite	Step heating	Chu et al., 2014
Jiuling	Mylonite	382.0±2.0	Biolite	Step heating	Chu et al., 2014
Northeast Jiangxi Fault	Micaschist	449.3±4.4	Sericite	Step heating	Xu et al., 2015
Northeast Jiangxi Fault	Micaschist	429.0±3.4	Sericite	Step heating	Xu et al., 2015
Eastern Jiuling	Mylonite	447.0±3.0	Muscovite	Step heating	Li et al., 2016a
Eastern Jiuling	Mylonite	439.0±2.0	Muscovite	Step heating	Li et al., 2016a
Eastern Jiuling	Mylonite	435.0±4.0	Muscovite	Step heating	Li et al., 2016a
Eastern Jiuling	Mylonitic gneiss	449.0±3.0	Biolite	Step heating	Li et al., 2016a
Eastern Jiuling	Mylonitic granite	434.0±1.0	Muscovite	Step heating	Li et al., 2016a
Mesozoic					
Mylonite in SW Zhejiang	Mylonite	221.0±10.0	K-feldspar	Step heating	Zhu et al., 1997
Mylonite in SW Zhejiang	Mylonite	237.6±1.3	Muscovite	Step heating	Zhu et al., 1997
Xuefengshan tectonic belt	Mylonite	194.7±0.3	Whole rock	Step heating	Wang et al., 2005
Xuefengshan tectonic belt	Mylonite	216.9±0.3	Biolite	Step heating	Wang et al., 2005
Xuefengshan tectonic belt	Mylonite	215.3±0.8	Muscovite	Step heating	Wang et al., 2005
Xuefengshan tectonic belt	Mylonite	213.5±0.2	Sericite	Step heating	Wang et al., 2005
Xuefengshan tectonic belt	Mylonite	207.2±0.2	Sericite	Step heating	Wang et al., 2005
Yunkai tectonic belt	Mylonite	229.9±0.5	Biolite	Step heating	Wang et al., 2007b
Yunkai tectonic belt	Mylonite	227.9±0.3	Biolite	Step heating	Wang et al., 2007b
Yunkai tectonic belt	Mylonite	225.4±0.3	Biolite	Step heating	Wang et al., 2007b
Yunkai tectonic belt	Mylonite	224.7±0.4	Biolite	Step heating	Wang et al., 2007b
Yunkai tectonic belt	Mylonite	221.8±0.4	Biolite	Step heating	Wang et al., 2007b
Yunkai tectonic belt	Mylonite	218.4±0.3	Biolite	Step heating	Wang et al., 2007b
Yunkai tectonic belt	Mylonite	216.9±0.3	Biolite	Step heating	Wang et al., 2007b
Yunkai tectonic belt	Mylonite	214.2±0.4	Biolite	Step heating	Wang et al., 2007b
Yunkai tectonic belt	Mylonite	211.5±0.5	Biolite	Step heating	Wang et al., 2007b
Yunkai tectonic belt	Mylonite	211.1±0.2	Biolite	Step heating	Wang et al., 2007b
Yunkai tectonic belt	Mylonite	209.0±0.2	Sericite	Step heating	Wang et al., 2007b
Yunkai tectonic belt	Mylonite	208.9±1.4	Sericite	Step heating	Wang et al., 2007b
Yunkai tectonic belt	Mylonite	207.8±0.2	Biolite	Step heating	Wang et al., 2007b
Hepu-Hetai shear zone	Mylonite	198.9±1.2	Muscovite	Step heating	Zhang and Cai, 2009
Hepu-Hetai shear zone	Mylonite	195.2±1.3	Muscovite	Step heating	Zhang and Cai, 2009

Hepu-Hetai shear zone	Mylonite	213.0±4.0	Muscovite	Step heating	Zhang and Cai, 2009
Hepu-Hetai shear zone	Mylonite	211.6±3.4	Muscovite	Step heating	Zhang and Cai, 2009
Ductile shear zone in Wuping	Mylonite	238.5±2.8	Muscovite	Step heating	Xu et al., 2011
Ductile shear zone in Wuping	Mylonite	235.3±2.8	Biolite	Step heating	Xu et al., 2011

5.5.3 Significance of the $^{40}\text{Ar}/^{39}\text{Ar}$ thermochronology: two stage events

In metamorphic rocks, the transport of radiogenic ^{40}Ar is mainly conducted by four physicochemical mechanisms: (1) solid-state volume circulation; (2) recrystallization enhanced by deformation and fluid diffusion; (3) fluid advection; and (4) grain-boundary flow and diffusion (Scaillet, 1998). Consequently, $^{40}\text{Ar}/^{39}\text{Ar}$ ages are often regarded as cooling ages following the closure temperature Dodson (1973). Also, they can be interpreted as crystallization ages constrained by different tectonometamorphic events, or intermediate mixed ages reflecting the interaction of all these mechanisms (e.g., Agard et al., 2002; Forster and Lister, 2016; Laurent, 2017; Lister and Baldwin, 1996; Ruffet et al., 1997; Scaillet et al., 1992; Scaillet, 1998; Villa, 1998; Wijbrans et al., 1990). The biotite and muscovite hold different closure temperatures with the ranges of 260-350°C and 360-420°C, respectively (Chiaradia et al., 2013). Therefore, they can be applied to estimate the thermal history, and even the tectonic stories of the rocks. In this study, the muscovite and biotite display significantly different age spectra, they should correspond to distinct geological events, the reasonable interpretations are given as following:

5.5.3.1 Stage I: ductile shearing or crustal uplift in the Early Paleozoic

The older age range of 450-400 Ma from the muscovite located in the shear band plays a first-order importance in both number and quality of our Ar-Ar dating though it is not over the entire rock-chip (Figure 5-7). Such age range has been also defined by previous study in ductile décollements and shear zones in the Cathaysia block (see Table 5-2), which were interpreted as the consequence of the Early Paleozoic intracontinental orogeny. Figure 5-7 shows the good compatibility of our results with previous ones in the Cathaysia block and eastern Jiangnan region. Therefore, it is reasonable to assume that the muscovite (in our study region, the western Jiangnan Orogenic Belt) were deformed during the same period as those in the Cathaysia block and eastern Jiangnan region. However, up to now, few people in favour of this perspective due to undeformed and unmetamorphosed Cambrian and Ordovician

strata, these authors reject the idea that the Jiangnan Orogenic Belt region has been reactivated by the Silurian tectonic event (Wang et al., 2007b).

Nevertheless, Xu et al., (2015) and Li et al., (2016) recently reported the early Paleozoic aged micas (449-429 Ma) in the Neoproterozoic strata in the eastern Jiangnan region, e.g., the NE Jiangxi fault belt and eastern Jiuling area. This challenges the idea that the Jiangnan Orogenic Belt has escaped the Early Paleozoic tectonic event .

To consider our results, the ductilely deformed muscovite yield apparent $^{40}\text{Ar}/^{39}\text{Ar}$ ages of 450-400 Ma, with a distinct flat pattern at 420 Ma (Figure 5-7). As previous study showed, the deformation can reduce the effective grain-size and favour the mobility of argon, which increase the kinetics of recrystallization, facilitating new grains formation (recrystallization) and to resetting of the K/Ar isotopic system (Scaillet, 1998). Besides, the fluid circulation can be possibly channelized within major tectonic structures, it can significantly influence the open vs. closed behaviour of the argon system (Proyer, 2003). Therefore, in this way, we propose that the 420 Ma age may be considered as an important period for ductile shearing partly superimposed on the neoproterozoic structures.

However, how to match this Paleozoic age with the undeformed Cambrian and Ordovician sedimentary sequence?

Many researchers have investigated the rigidity of the Jiangnan Orogenic Belt and Cathaysia block (e.g., Liu, 2017; Shu, 2012; Yu et al., 2009), and reached an agreement that the Cathaysia block was made up by several sub-unit blocks with relatively weak rigidity, this is the reason why the 420 Ma Ar-Ar results cover almost all Cathaysia block. It seems that the case is different for the Jiangnan Orogenic Belt. Geophysical investigations show that the Jiangnan Orogenic Belt is underlain by the relatively homogeneous and rigid Yangtze basement (Deng et al., 2014). That is probably why we observe rarely the highly metamorphic and strongly deformed rocks

in the Jiangnan Orogenic Belt. All Ar-Ar data showing ca. 420 Ma ages within Proterozoic rocks are located along the Jiangnan Orogenic structures (Figure 5-6). This may indicate that the Jiangnan Orogenic Belt has been modified by the Paleozoic orogenic event, but locally instead of pervasively. In other words, the Paleozoic deformation is just localised in the limited zones, probably the old structures.

The alternative way to explain the age range at about 420 Ma by Ar-Ar dating may consider that this age concerns just a thermal phenomenon instead of deformation one. As the deformation of this age is still rarely observed in the Jiangnan Orogenic Belt, moreover, these observed ages are from or near the Proterozoic plutons. The deformation is quasi localised around or in the plutons. One of scenario may be proposed as following. During the emplacement of these post-orogenic plutons, the upwelling magma may push the already crystallised granite and/or the country rocks away to create the space. This may evoke a relative movement within plutons as well as in the country rocks, and produce a shearing band(s) near or on the top of the pluton. All of this may take place in a depth where the temperature is higher than the mica closure ones. The later Paleozoic orogenic event exhumed plutons (why not also all the Jiangnan Orogenic Belt), and consequently the age of ca. 420 Ma was recorded by mica when they passed their closure temperature (Figures 5-9A and 5-9B). In other words, the deformation of the shearing band was produced during the construction of the plutons, i.e., the syn-emplacement deformation. This hypothesis may be tested by more Ar-Ar investigations in different tectonic and geological units.

5.5.3.2 Stage II: slow exhumation after the Early Paleozoic

However, to consider our in-situ biotite results (one sample), intermediate $^{40}\text{Ar}/^{39}\text{Ar}$ ages are progressively distributed between 420 and 240 Ma (Figure 5-8A). They probably imply the mixed signature of partial inheritance and partial thermal overprint of mica. As the results showed, the progressively decreasing ages of biotite go down until to the range of 330-240 Ma (Figure 5-8A). Generally, the closure temperatures of the biotite range from 350-260°C (Chiaradia et al., 2013), with a

90-degree interval. Assuming that the argon isotopic system in biotite was reset during the period of isobaric cooling, then we can quantitatively estimate the cooling rate of biotite. Using the interval of cooling temperatures (90°C) divided by the age differences (90 and 180 Ma, respectively), we can get the cooling rates of 1.00°C/Ma and 0.50°C/Ma, respectively.

Moreover, the step heating of single mica grains (different samples) yield a positive correlation between the $^{40}\text{Ar}/^{39}\text{Ar}$ age and elevation. Assuming that the closure temperature of the micas were completely induced by the geothermal, and therefore we can make an estimation of cooling rate by the formula with a constant geothermal gradient value of 30°C/Km:

$$R(T) = \frac{\Delta\text{Height}}{\Delta\text{Age}} \times 30 \text{ (}^\circ\text{C} \cdot \text{Km}^{-1}\text{)}$$

where the ΔHeight is the height difference, while the ΔAge is the difference of the $^{40}\text{Ar}/^{39}\text{Ar}$ age. In this way, we get the cooling rates of the biotite and muscovite at 0.97°C/Ma and 0.58°C/Ma (Figure 5-8B), respectively, which are comparable to those of the biotite aggregations.

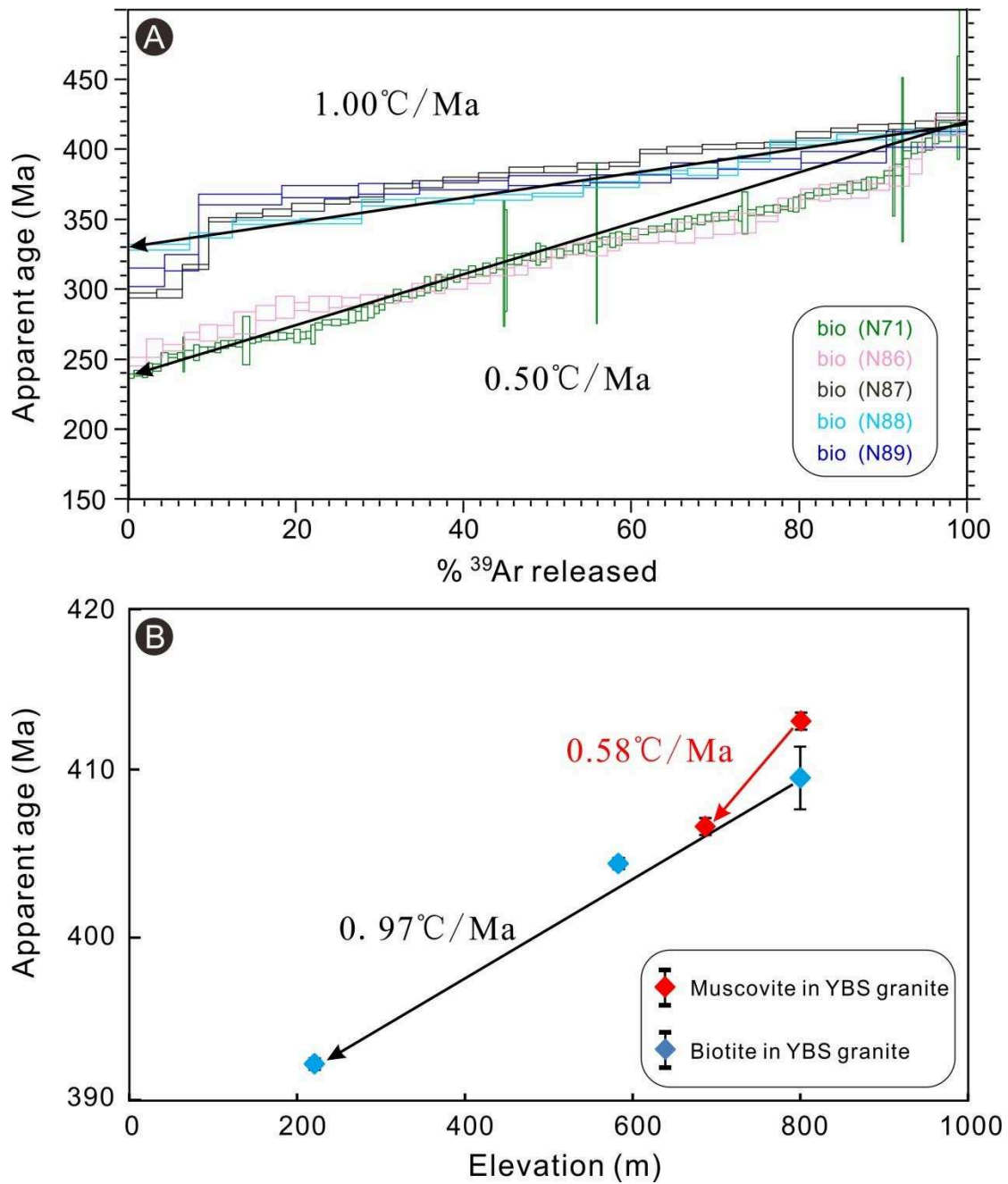


Figure 5-8. (A) Distribution of the biotite ages analyzed by the in-situ UV laser technique, with qualitative cooling rates of the biotite. (B) Distribution of both muscovite and biotite single grain ages analyzed by the step heating method, versus the elevation plot, with cooling rates of the muscovite and biotite.

Such progressive decreasing apparent age spectra indicate that the study area was exhumed with a so low rate that this exhumation doesn't like to be produced by tectonic events since 420 Ma. As the tectonism was negligible, we can ignore the

influence by the tectonic event and active fluid diffusion, hence, it is suggested that the heat was almost sourced from geothermal. According to the slow cooling rates, therefore, we can furthermore infer that the exhumation of the crust was quite slow accommodated by isostatic re-equilibration due to erosion with an average rate interval of 16.7-33.3 meters per million years (Figures 5-9C to 5-9F; Fitzgerald et al., 1995).

Nevertheless, the geological significance of the mica $^{40}\text{Ar}/^{39}\text{Ar}$ ages are still not well constrained by (1) the intrinsic parameters controlling argon transport kinetics in nature (volume diffusion, thermal-pressure-compositional effects), and (2) the effects of deformation and fluid circulation on crystal-scale ^{40}Ar distributions.

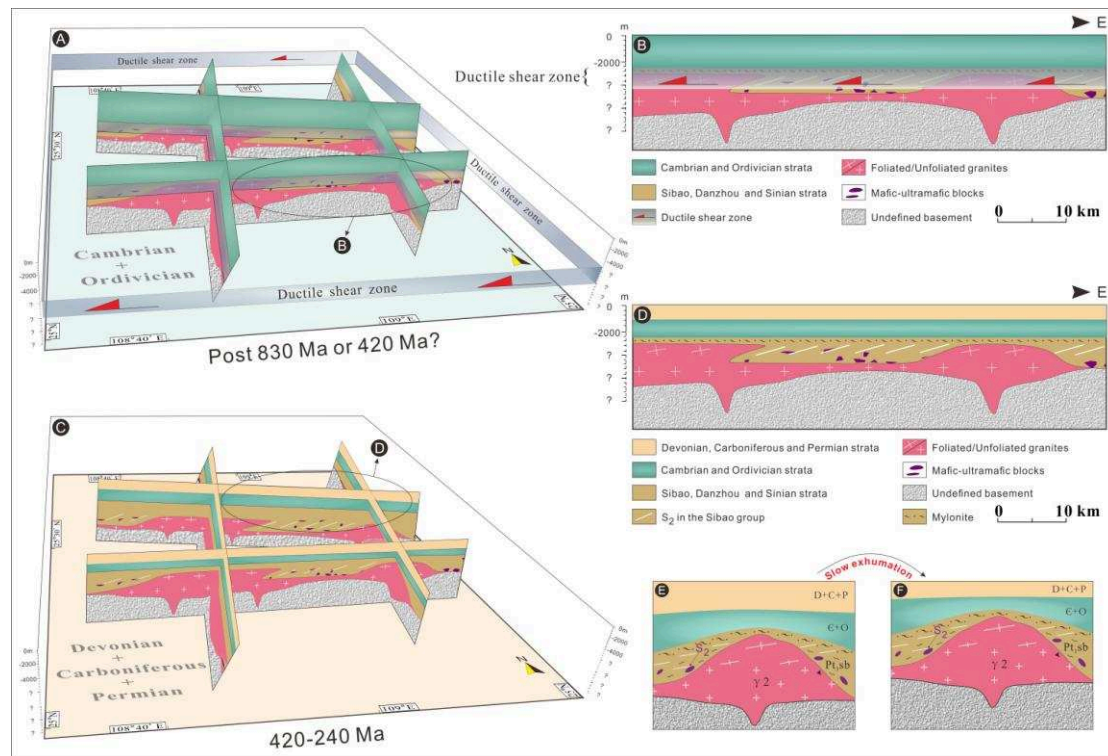


Figure 5-9. (A): 3-D sketch model of the early Paleozoic ductile shearing event in the Sanfang and Yuanbaoshan areas; (B): Sketch map of the ductile shearing in the granite plutons and country rocks; (C): 3-D sketch model of the upper crust in the Sanfang and Yuanbaoshan areas during the 420-240 Ma; (D): Sketch map of the crust when it exhumed during the 420-240 Ma; (E) and (F): Sketch sections of the slow exhumation

during the 420-240 Ma.

5.6 Conclusions

Through the $^{40}\text{Ar}/^{39}\text{Ar}$ analyses on the both deformed and undeformed muscovite and biotite from the Sanfang-Yuanbaoshan plutons, the early Paleozoic to Triassic geological events in this area can be concluded as following:

(1) Ar-Ar dating provides a signification age range at ca. 420 Ma from the Sanfang-Yuanbaoshan plutons and their roof. This age may imply that (1) the shearing band on the upper part of plutons and their roof may be the consequence of the reactivation of Proterozoic structures reactivated by the Paleozoic orogeny or (2) the exhumation of the study areas by the Paleozoic orogeny;

(2) During the 420 Ma to 240 Ma period, the study areas have experienced a slow rate of exhumation which may correspond to the isostatic crustal re-equilibration.

Chapter 6. Conclusions and perspectives

6.1 Conclusions: tectonic evolution of the western Jiangnan Orogenic Belt

The Jiangnan Orogenic Belt locates in the southeastern margin of the Yangtze Block, tracing the northwestward subduction of the Paleo–South China Ocean and the collision between the Yangtze and Cathaysia blocks. This study focuses on the western part of Jiangnan region, where Neoproterozoic unconformity and S-type granite plutons are exposed. Depending on the significant geological facts, we have carried out: i) an overview of the Jiangnan Orogenic Belt with detailed field investigation; ii) the detrital zircon age spectra analyses between the Neoproterozoic strata on both sides of the unconformity, as well as the detrital zircon age spectra analyses of the Neoproterozoic strata among the Yangtze, Jiangnan and Cathaysia regions; iii) the geochronology, geochemistry, structural analysis, anisotropy of magnetic susceptibility and gravity measurements on the Sanfang and Yuanbaoshan plutons; and iv) argon isotopic analyses on the micas from the Sanfang and Yuanbaoshan plutons. Here, we outline the conclusive results of our studies and propose a tentative model from the subduction to collision and then the construction mechanism of the granite plutons as well as the tectonic events posterior to the peraluminous magma emplacement, that can adequately answer most of the geological phenomena.

(1) In the regional view, the subduction of the Paleo–South China Ocean started at ca. 1000 Ma and ended at ca. 865 Ma (Figure. 6-1A). Afterwards, the Jiangnan Orogenic Belt was built up due to the assembly of the Yangtze and Cathaysia blocks between ca. 865 and 820 Ma (Figure. 6-1B). During the subduction-collision period, the deposition environment of the early Neoproterozoic Sibao group and its equivalents can be divided into two stages. Firstly, the lower part of the series deposited in an active continental margin in the period of ca. 1000–865 Ma. Then, the upper part was accumulated in a collisional setting in the period of ca. 865–820 Ma. After the Neoproterozoic orogeny, the Danzhou group and its equivalents began to deposit since

ca. 780 Ma in the western Jiangnan region;

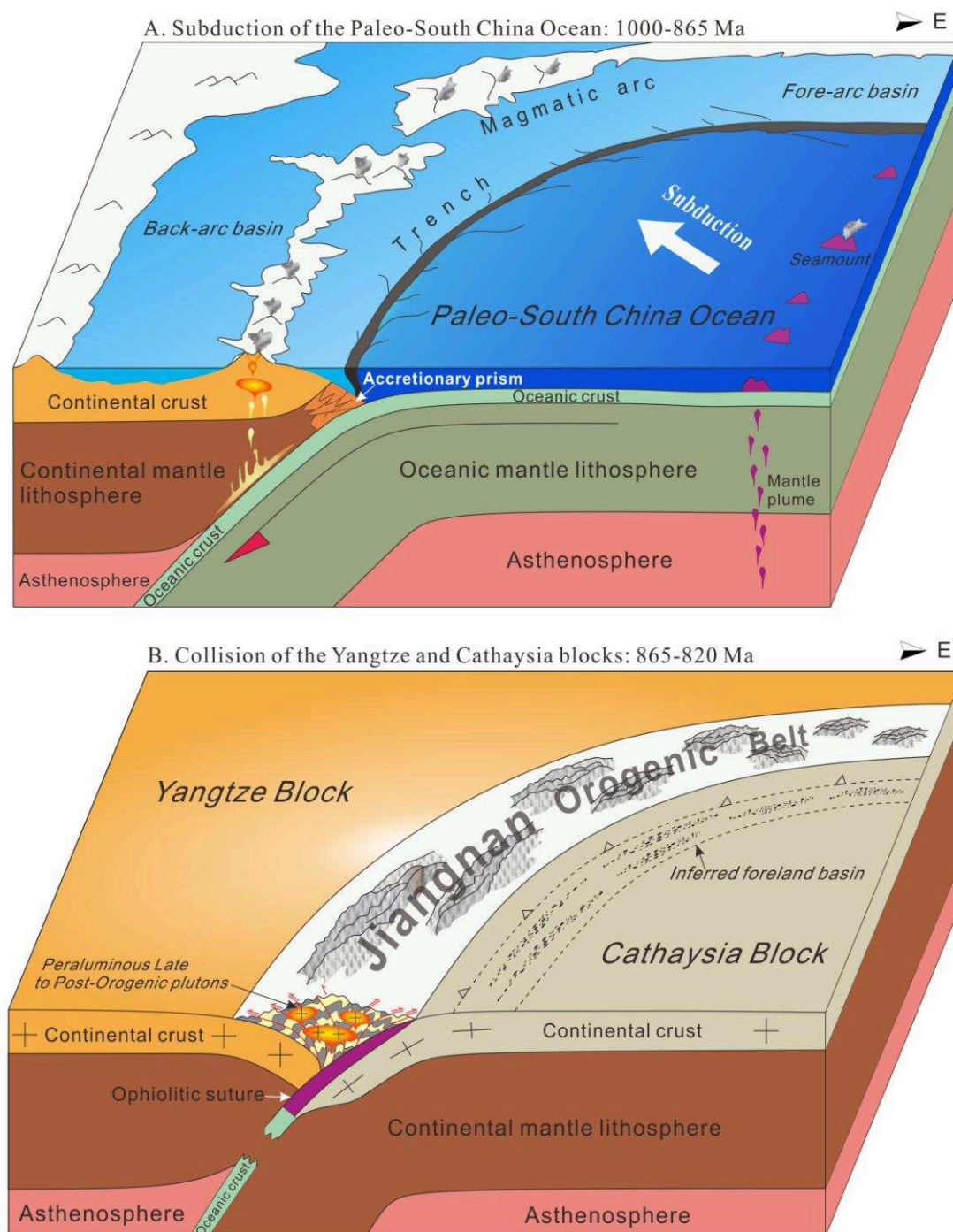


Figure 6-1. Geodynamic evolution model for the Jiangnan region in the Early Neoproterozoic. (A) Subduction of the Paleo–South China Ocean; and (B) Collision of the Yangtze and Cathaysia blocks.

(2) The parental magma of the Sanfang and Yuanbaoshan plutons was derived

from the melting of crustal material, and crystallized at ca. 830 Ma, which indicates the ending of the Jiangnan Orogeny (Figure 6-2A). According to the field, microscope-scale texture, AMS and gravity studies, the granitic fabrics can be divided into two groups, the first one is a magmatic fabric developed in a subsolidus stage during the plutons emplacement. The second one is post-solidus one developed after the crystallisation of granite. According to multidisciplinary results, it seems that the granitic magma intruded into the pre-existing tectonic fold/fault structures in the Sibao group, the tongue- and/or sill-shaped plutons were constructed by an E-W lateral accumulation of N-S oriented dykes with a dominantly northward horizontal magma flow from south to north (Figure 6-2B);

(3) A top-to-the-W ductile shearing event (Figures 6-2C and 6-2D) has been identified at the top of the plutons and their sedimentary roof by the macro and microscopic scales kinematic studies and the secondary post-solidus magnetic fabric related to the development of planar and linear fabrics. Moreover, a coherent mica age of ca. 420 Ma has been obtained from the deformed muscovites of the Sanfang plutons by Ar-Ar dating. Two hypotheses may be proposed to explain these new results. a) The emplacement of pluton occurred at a deeper depth where the temperature is higher than the mica closure ones. The ductile deformation took place locally during the emplacement. During the Paleozoic orogeny, the study area is uplifted and the mica passed their closure temperature and record this event; b) The ductile shearing took place after the magmatic emplacement by the Paleozoic orogeny along the ancient structures in the study area.

(4) Afterwards, the rather slow cooling process revealed from Ar-Ar dating of biotite and muscovite from both Sanfang-Yuanbaoshan plutons during the 420-240 Ma period in this area (Figures 6-2E and 6-2F), which may correspond to the isostatic crustal re-equilibration. The final uplift and erosion of this part of the South China crust led to the present exposures (Figures 6-2G and 6-2H).

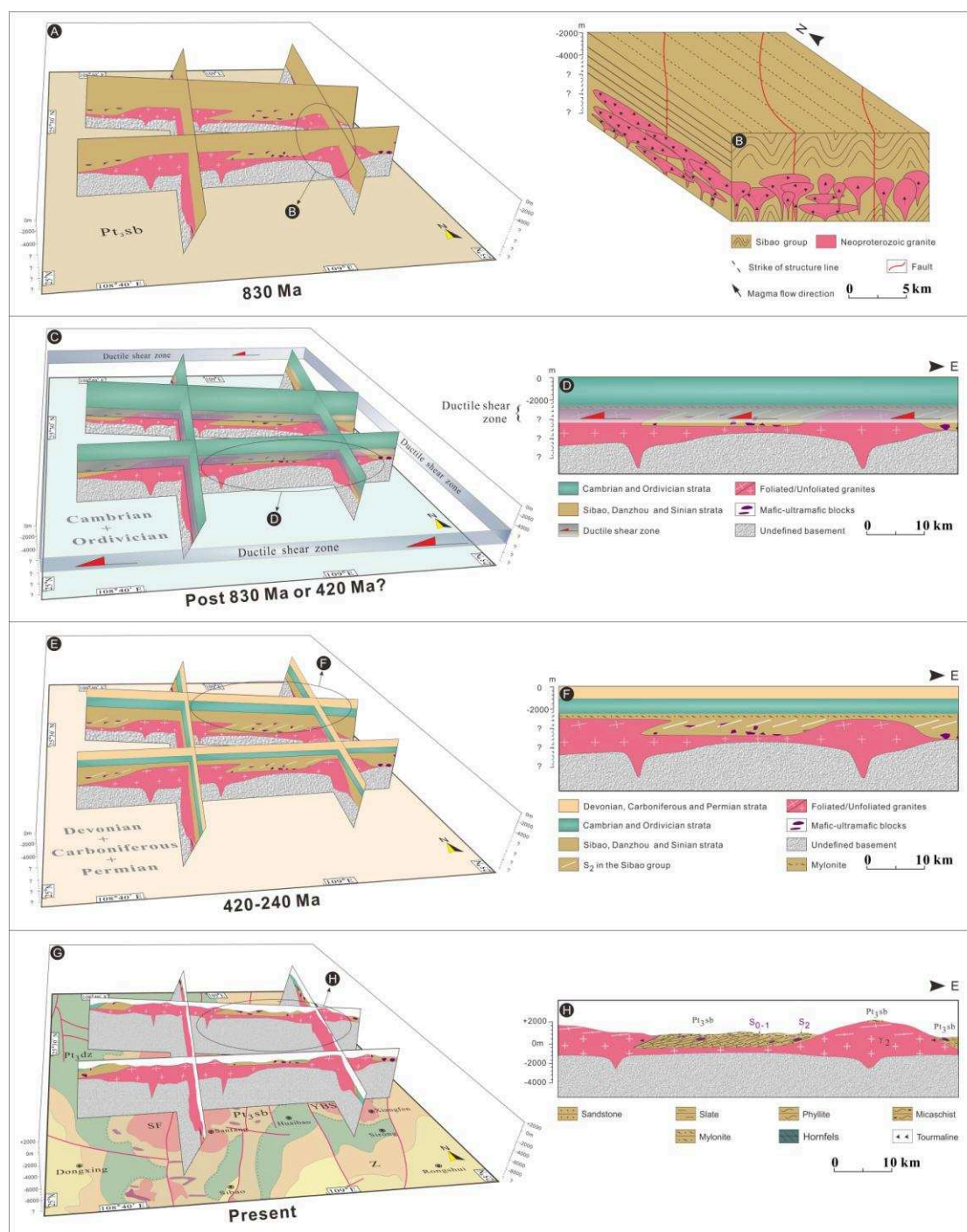


Figure 6-2. Tectonic evolution model of the Sanfang and Yuanbaoshan areas since the end of the orogeny. (A) 3-D model of the granite plutons intruded into the Sibao group and crystallized at 830 Ma; (B) Emplacement mechanism of the peraluminous magma of the Yuanbaoshan pluton; (C) A top-to-the-W ductile shearing event took place at ca. 420 Ma in the Sanfang-Yuanbaoshan area; (D) Sketch section of the ductile shearing

in the granite plutons and country rocks; (E) 3-D sketch model of the upper crust in the Sanfang and Yuanbaoshan areas during the 420-240 Ma; (F): Sketch section of the crust when it uplifted during the 420-240 Ma; (G) 3-D model of the current shape of the Sanfang and Yuanbaoshan plutons with the country rocks; (H) Current geological cross section of the two granite plutons and their country rocks in the Sanfang and Yuanbaoshan areas.

6.2 Perspectives

In order to better constrain the tectonic evolution of the western Jiangnan Orogenic Belt or even the whole Jiangnan region, more details need to be clarified. Such as the depositional history of the Sibao group and its equivalents, what were the source of the sediments and how the sediments were transported and then deposited? These answers are of great importance to get a bulk understanding of the subduction of the Paleo-South China Ocean. Besides, the metamorphic study of the sedimentary rocks, including the Sibao and Danzhou groups and their equivalents, and Sinian strata, would provide a more comprehensive vision on exploring the significance of the ductile shearing event. Of course, to visit the eastern part of the Jiangnan Orogenic Belt is necessary if we want to have a bulk understanding of the tectonic evolution history of the whole Jiangnan Orogenic Belt.

References

- Agard, P., Monié, P., Jolivet, L., Goffé, B. (2002). Exhumation of the Schistes Lustrés complex: in situ laser probe $^{40}\text{Ar}/^{39}\text{Ar}$ constraints and implications for the Western Alps. *Journal of Metamorphic Geology* 20, 599–618.
- Allibon, J., Bussy, F., Lewin, E., Darbellay, B. (2011). The tectonically controlled emplacement of a vertically sheeted gabbro–pyroxenite intrusion: feeder–zone of an ocean–island volcano (Fuerteventura, Canary Islands). *Tectonophysics*, 500(1), 78–97.
- Andersen, T. (2002). Correction of common Pb in U–Pb analyses that do not report ^{204}Pb . *Chemical Geology*, 192, 59–79.
- Bateman, R. (1984). On the role of diapirism in the, segregation, ascent and final emplacement of granitoid magmas. *Tectonophysics*, 110(3–4), 211–231.
- Beltrando, M., Lister, G.S., Forster, M., Dunlap, W.J., Fraser, G., Hermann, J. (2009). Dating microstructures by the $^{40}\text{Ar}/^{39}\text{Ar}$ step–heating technique: deformation–pressure– temperature–time history of the Penninic units of the Western Alps. *Lithos* 113, 801–819.
- BGMRAH (Bureau of Geology and Mineral Resources of Anhui Province). (1982). Regional Geology of Anhui Province [in Chinese with English Abstract]. Geological Publishing House, Beijing, pp. 1–715.
- BGMRFJ (Bureau of Geology and Mineral Resources of Fujian Province). (1985). Regional Geology of Fujian Province [in Chinese with English Abstract]. Geological Publishing House, Beijing, pp. 7–564.
- BGMRGX (Bureau of Geology and Mineral Resources of Guangxi Province). (1985). Regional Geology of Guangxi Autonomous Region [in Chinese with English Abstract]. Geological Publishing House, Beijing, pp. 1–853.
- BGMRGZ (Bureau of Geology and Mineral Resources of Guizhou Province). (1984).

- Regional Geology of Guizhou Province [in Chinese with English Abstract]. Geological Publishing House, Beijing, pp. 1–698.
- BGMRHN (Bureau of Geology and Mineral Resources of Hunan Province). (1988). Regional Geology of Hunan Province [in Chinese with English Abstract]. Geological Publishing House, Beijing, 6–664.
- BGMRJX (Bureau of Geology and Mineral Resources Jiangxi Province). (1984). Regional Geology of Jiangxi Province [in Chinese with English Abstract]. Geology Publishing House, Beijing, pp. 2–725.
- BGMRZJ (Bureau of Geology and Mineral Resources Jiangxi Province). (1989). Regional Geology of Jiangxi Province [in Chinese with English Abstract]. Geology Publishing House, Beijing, pp. 5–575.
- Bai, L.X., & Zhu, R.X. (1996). A review of the tectonic evolution and paleomagnetic research for the Yangtze Block during Paleozoic. *Progress in Geophysics*, 11(3), 109–116 (in Chinese with English abstract).
- Bhatia, M. R. (1983). Plate tectonics setting of sandstones and geochemical composition of sandstones. *J. Geol.*, 91(6), 611–627.
- Blichert-Toft, J., Albarede, F. (1997). The Lu–Hf isotope geochemistry of chondrites and the evolution of the mantle–crust system. *Earth and Planetary Science Letters*, 148, 243–258.
- Borradaile, G. J., and B. Henry. (1997). Tectonic applications of magnetic susceptibility and its anisotropy, *Earth–Science Reviews*, 42(1), 49–93, doi:[http://dx.doi.org/10.1016/S0012-8252\(96\)00044-X](http://dx.doi.org/10.1016/S0012-8252(96)00044-X).
- Burchardt, S. (2008). New insights into the mechanics of sill emplacement provided by field observations of the Njardvik Sill, Northeast Iceland. *Journal of Volcanology and Geothermal Research*, 173(3), 280–288.
- Byerly, A., Tikoff, B., Kahn, M., Jicha, B., Gaschnig, R., Fayon, A. K. (2017). Internal

- fabrics of the Idaho batholith, USA. *Lithosphere*, 9(2), 283–298.
- Caricchi, L., Burlini, L., Ulmer, P., Gerya, T., Vassalli, M., Papale, P. (2007). Non-Newtonian rheology of crystal-bearing magmas and implications for magma ascent dynamics. *Earth and Planetary Science Letters*, 264(3), 402–419.
- Castle, R. O., & Lindsley, D. H. (1993). An exsolution silica-pump model for the origin of myrmekite. *Contributions to Mineralogy and Petrology*, 115, 58–65.
- Castro, A. (1987). On granitoid emplacement and related structures. A review. *Geologische Rundschau*, 76(1), 101–124.
- Chappell, B.W., & White, A.J.R. (2001). Two contrasting granite types: 25 years later. *Australian Journal of Earth Sciences*, 48(4), 489–499.
- Charles, N., Faure, M., Chen, Y. (2009). The Montagne Noire migmatitic dome emplacement (French Massif Central): new insights from petrofabric and AMS studies. *Journal of Structural Geology*, 31(11), 1423–1440.
- Chu, Y., W. Lin, M. Faure, Q. C. Wang, W. B. Ji. (2012), Phanerozoic tectonothermal events of the Xuefengshan Belt, central South China: Implications from U–Pb age and Lu–Hf determinations of granites, *Lithos*, 150, 243–255.
- Chu, Y., & Lin, W. (2014). Phanerozoic polyorogenic deformation in southern jiuling massif, northern south china block: constraints from structural analysis and geochronology. *Journal of Asian Earth Sciences*, 86(3), 117–130.
- Chiaradia, M., Schaltegger, U., Spikings, R., Wotzlaw, J. F., Ovtcharova, M. (2013). How accurately can we date the duration of magmatic–hydrothermal events in porphyry systems?—an invited paper. *Economic Geology*, 108(4), 565–584.
- Corfu, F., Hanchar, J.M., Hoskin, P.W.O., Kinny, P. (2003). Atlas of zircon textures. *Reviews in Mineralogy and Geochemistry*, 53, 469–500.
- Charvet, J. (2013). The neoproterozoic–early paleozoic tectonic evolution of the South China Block: an overview. *Journal of Asian Earth Sciences*, 74, 198–209.

- Charvet, J., Shu, L.S., Faure, M., Choulet, F., Wang, B., Lu, H.F., Breton N.L. (2010). Structural development of the Lower Paleozoic belt of South China: Genesis of an intracontinental orogen. *Journal of Asian Earth Sciences*, 39, 309–330.
- Chen, J. F., Foland, K. A., Xing, F., Xu, X., Zhou, T. (1991). Magmatism along the southeastern margin of the Yangtze block: Precambrian collision of the Yangtze and Cathaysia block of China. *Geology*, 19, 815–818.
- Chen, X., Wang, X. L., Wang, D., Shu, X. J. (2018). Contrasting mantle–crust melting processes within orogenic belts: implications from two episodes of mafic magmatism in the western segment of the Neoproterozoic Jiangnan orogen in South China. *Precambrian Research*, 309, 123–137.
- Chen, Z.H., Guo, K.Y., Dong, Y.G., Chen, R., Li, L.M., Liang, Y.H., Li, C.H., Yu, X.M., Zhao, L., Xing, G.F. (2009). Possible early Neoproterozoic magmatism associated with slab window in the Pingshui segment of the Jiangshan–Shaoxing suture zone: Evidence from zircon LA–ICP–MS U–Pb geochronology and geochemistry. *Science in China Series D: Earth Sciences*, 52, 925–939.
- Chung, S. L., Chu. M. F., Zhang, Y. Q., Xie. Y. W., Lo, Q. H., Lee, T. Y., et al. (2005). Tibetan tectonic evolution inferred from spatial and temporal variations in post–collisional magmatism. *Earth Science Reviews*, 68(3), 173–196.
- Clemens, J. D., & Mawer, C. K. (1992). Granitic magma transport by fracture propagation. *Tectonophysics*, 204(3–4), 339–360.
- Cruden, A. R. (1988). Deformation around a rising diapir modeled by creeping flow past a sphere. *Tectonics*, 7(5), 1091–1101.
- Cruden, A. R., McCaffrey, K. J. W., Bunger, A. P. (2017). Geometric scaling of tabular igneous intrusions: Implications for emplacement and growth. DOI: 10.1007/11157_2017_1000
- Daly, R. A. (1903). The mechanics of igneous intrusion. *American Journal of Science*,

- (88), 269–298.
- Dubińska, E., Bylina, P., Kozłowski, A., Dörr, W., Nejbert, K., Schastok, J., Kulicki, C. (2004). U–Pb dating of serpentinization: hydrothermal zircon from a metasomatic rodingite shell (Sudetic ophiolite, SW Poland). *Chemical Geology*, 203(3), 183–203.
- de Saint Blanquat, M., Law, R.D., Bouchez, J.–L., Morgan, S.S. (2001). Internal structure and emplacement of the Papoose Flat pluton: An integrated structural, petrographic, and magnetic susceptibility study. *Geological Society of America Bulletin*, 113, 976–995.
- de Saint Blanquat, M., Habert, G., Horsman, E., Morgan, S. S., Tikoff, B., Launeau, P., Gleizes, G. (2006). Mechanisms and duration of non–tectonically assisted magma emplacement in the upper crust: the Black Mesa pluton, Henry Mountains, Utah. *Tectonophysics*, 428(1), 1–31.
- de Saint Blanquat, M., Horsman, E., Habert, G., Morgan, S., Vanderhaeghe, O., Law, R., Tikoff, B. (2011). Multiscale magmatic cyclicity, duration of pluton construction, and the paradoxical relationship between tectonism and plutonism in continental arcs. *Tectonophysics*, 500(1), 20–33.
- Deng Y.F., Zhang Z.J., José B., Fan W.M. (2014). 3–D density structure under South China constrained by seismic velocity and gravity data. *Tectonophysics*, 627, 159–170.
- Deprat, J. (1914). Etude des plissements et des zones de cisaillement de la moyenne et de la basse Rivière Noire, *Mem. Serv. Geol. Indochine*, 3, 59.
- Dodson, M.H. (1973). Closure temperature in cooling geochronological and petrological systems. *Contributions to Mineralogy and Petrology*, 40, 259–274.
- Dunlop, D. J. (2002). Theory and application of the Day plot (Mrs/Ms versus Hcr/Hc) 2. Application to data for rocks, sediments, and soils, *Journal of Geophysical*

- Research: Solid Earth, 107(B3), EPM 5–1–EPM 5–15, doi:10.1029/2001JB000487.
- Faure, M., Pons, J. (1991). Crustal thinning recorded by the shape of the Namurian–Westphalian leucogranite in the Variscan belt of the northwest Massif Central. *France Geology*, 19, 730–733.
- Faure, M., Bé Mézème, E., Cocherie, A., Rossi, P., Chemenda, A., Boutelier, D. (2008). Devonian geodynamic evolution of the Variscan Belt, insights from the French Massif Central and Massif Armoricaïn, *Tectonics*, 27. <https://doi.org/10.1029/2007TC002115>
- Faure, M., Shu, L.S., Wang, B., Charvet, J., Choulet, F., Monié, P. (2009). Intracontinental subduction: a possible mechanism for the Early Paleozoic Orogen of SE China. *Terra Nova*, 21, 360–368.
- Faure, M., Lin, W., Yang, C., Lepvrier, C. (2016). Triassic tectonics of the southern margin of the South China Block. *C. R. Geosci*, 328, 5–14.
- Fitzgerald, P. G., Sorkhabi, R. B., Redfield, T. F., Stump, E. (1995). Uplift and denudation of the central alaska range: a case study in the use of apatite fission track thermochronology to determine absolute uplift parameters. *Journal of Geophysical Research Solid Earth*, 100(B10), 20175–20191.
- Floyd, P., & Leveridge, B. (1987). Tectonic environment of the Devonian Gramscatho basin, south Cornwall: framework mode and geochemical evidence from turbiditic sandstones. *Journal of the Geological Society*, 144, 531–540.
- Forster, M.A., & Lister, G.S. (2004). The interpretation of $^{40}\text{Ar}/^{39}\text{Ar}$ apparent age spectra produced by mixing: application of the method of asymptotes and limits. *Journal of Structural Geology*, 26, 287–305.
- Fralick, P. W., & Kronberg, B. I. (1997). Geochemical discrimination of clastic sedimentary rock sources. *Sedimentary Geology*, 113, 111–124.

- Fromaget, J. (1932). Sur la structure des Indosinides, C. R. Hebd. Seances Acad. Sci., 195, 538.
- Garcia, D., Pascal, M-L., and Roux, J. (1996). Hydrothermal replacement of feldspars in igneous enclaves of the Velay granite and the genesis of myrmekite. *European Journal of Mineralogy*, 8, 703–711.
- Gan, X. C., Zhao, F. Q., Jin, W. S., Sun, D. Z. (1996). The U–Pb ages of early Proterozoic–Archean zircons captured by igneous rocks in Southern China [In Chinese with English abstract]. *Geochimica*, 25(2), 112–119.
- Gao, J., Klemd, R., Long, L.L., Xiong, X.M., Qian, Q. (2009). Adakitic signature formed by ractional crystallization: An interpretation for the Neo–Proterozoic meta–plagiogranites of the NE Jiangxi ophiolitic mélange belt, South China. *Lithos*, 110, 277–293.
- Ge, W. C., Li, X. H., Li, Z. X., Zhou, H. W. (2001). Mafic intrusions in Longsheng area: age and its geological implications [in Chinese with English abstract]. *Chinese Journal of Geology*, 36, 112–118.
- Glazner, A. F., & Bartley, J. M. (2006). Is stoping a volumetrically significant pluton emplacement process?. *Geological Society of America Bulletin*, 118(9–10), 1185–1195.
- Glazner, A. F. (2007). Thermal limitations on incorporation of wall rock into magma. *Geology*, 35(4), 319–322.
- Greentree, M. R., Li, Z. X., Li, X. H., Wu, H.C. (2006). Late Mesoproterozoic to earliest Neoproterozoic basin record of the Sibao orogenesis in west South China and relationship to the assembly of Rodinia. *Precambrian Research*, 151, 79–100.
- Gudmundsson, A. (1990). Emplacement of dikes, sills and crustal magma chambers at divergent plate boundaries. *Tectonophysics*, 176(3–4), 257–275.
- Gudmundsson, A. (2011). Deflection of dykes into sills at discontinuities and

- magma–chamber formation. *Tectonophysics*, 500(1), 50–64.
- Guo, L. H., & Gao, R. (2018). Potential–field evidence for the tectonic boundaries of the central and western Jiangnan belt in South China. *Precambrian Research*, 309, 45–55.
- Guo, L. Z., Shi, Y. S., Ma, R. S., Lu, H. F., Ye, S. F., Ding, Y. W. (1984). On terrane—A latest concern in the study of plate tectonics [In Chinese with English abstract]. *Bulletin of the Chinese Academy of Geological Sciences*, 10, 27–34.
- Guo, L. Z., Shi, Y. S., Ma, R. S., Dong, H. G., Yang, S. F. (1989). The pre–Devonian tectonic patterns and evolution of south China. *Journal of Southeast Asian Earth Sciences*, 3, 87–93.
- Harrison, T.M., Célérier, J., Aikman, A.B., Hermann, J., Heizler, M.T. (2009). Diffusion of ^{40}Ar in muscovite. *Geochimica et Cosmochimica Acta*, 73, 1039–1051.
- Hoffmann, J. E., Münker, C., Nagel, T. J., Næraa, T., Polat, A., Rosing, M.T. (2012). The tholeiite–TTG connection during Eoarchean crust formation in Isua, southern West Greenland: the role of subduction processes. EGU General Assembly Conference. EGU General Assembly Conference Abstracts, vol 14, pp.8217.
- Hoskin, P. W. O., & Schaltegger, U. (2003). The composition of zircon and igneous and metamorphic petrogenesis. *Reviews in mineralogy and geochemistry*, 53(1), 27–62.
- Hutton, D.H.W. (1988). Granite emplacement mechanisms and tectonic controls: inferences from deformation studies. *Earth and Environmental Science Transactions of the Royal Society of Edinburgh*, 79, 245–255.
- Kelley, S., 2002. Excess argon in K–Ar and Ar–Ar geochronology. *Chemical Geology* 188, 1–22.
- Kemp, A.I.S., Hawkesworth, C.J., Paterson, B.A., Kinny, P.D. (2006). Episodic growth

- of the Gondwana supercontinent from hafnium and oxygen isotopes in zircon. *Nature*, 439, 580–583.
- Laurent, V. (2017). Localisation de la déformation au sein de zones de cisaillement haute–pression basse–température et enregistrement isotopique $^{40}\text{Ar}/^{39}\text{Ar}$. Ph.D thesis, Université d'Orléans.
- Laurent, V., Huet, B., Labrousse, L., Jolivet, L., Monie, P., Augier, R. (2017). Extraneous argon in high–pressure metamorphic rocks: distribution, origin and transport in the cycladic blueschist unit (greece). *Lithos*, 272–273, 315–335.
- Li, J.H., Dong, S.W., Zhang, Y.Q., Zhao, G.C., Johnston, S. T., Cui, J., et al. (2016a). New insights into phanerozoic tectonics of south china: part 1, polyphase deformation in the jiuling and lianyunshan domains of the central jiangnan orogen. *Journal of Geophysical Research Solid Earth*, 121(4), 3048–3080.
- Li, J. Y., Wang, X. L., Zhang, F. F., Zhou, X. H., Shu, X. J. (2016b). A rhythmic source change of the Neoproterozoic basement meta–sedimentary sequences in the Jiangnan Orogen: Implications for tectonic evolution on the southeastern margin of the Yangtze block. *Precambrian Research*, 280, 46–60.
- Li, L. M., Lin, S. F., Xing, G. F., Jiang, Y., Xia, X. P. (2018). Geochronology and geochemistry of volcanic rocks from the Jingtian Formation in the eastern Jiangnan Orogen, South China: constraints on petrogenesis and tectonic implications. *Precambrian Research*, 309, 166–180.
- Li, W. X., Li, X. H., Li, Z. X. (2005). Neoproterozoic bimodal magmatism in the Cathaysia Block of South China and its tectonic significance. *Precambrian Research*, 136, 51–66.
- Li, W. X., Li, X. H., Li, Z. X., Lou, F. S. (2008a). Obduction–type granites within the NE Jiangxi Ophiolite: Implications for the final amalgamation between the Yangtze and Cathaysia Blocks. *Gondwana Research*, 13, 288–301.

- Li, X. H., Zhou, G., Zhao, J., Fanning, C. M., Compston, W. (1994). SHRIMP ion microprobe zircon U–Pb age of the NE Jiangxi ophiolite and its tectonic implications [in Chinese with English abstract]. *Geochimica (Beijing)*, 23(2), 125–131.
- Li, X.H., Zhao, J.X., Mculloch, M.T., Zhou, G.Q., Xing, F.M. (1997). Geochemical and Sm–Nd isotopic study of Neoproterozoic ophiolites from southeastern China: petrogenesis and tectonic implication. *Precambrian Research*, 81, 129–144.
- Li, X. H. (1999). U–pb zircon ages of granites from the southern margin of the yangtze block: timing of neoproterozoic jinning: orogeny in se china and implications for rodinia assembly. *Precambrian Research*, 97(1), 43–57.
- Li, X.H., Li, Z.X., Ge, W.C., Zhou, H.W., Li, W.X., Liu, Y., Wingate, M.T.D. (2003a). Neoproterozoic granitoids in South China: crustal melting above a mantle plume at ca. 825 Ma? *Precambrian Research*, 122, 45–83.
- Li, X. H., Li, W. X., Li, Z. X., Liu, Y. (2008b). 850–790 Ma bimodal volcanic and intrusiverocks in northern Zhejiang, South China: a major episode of continental rift magmatism during the breakup of Rodinia. *Lithos*, 102, 341–357.
- Li, X. H., Li, W. X., Li, Z. X., Lo, C. H., Wang, J., Ye, M. F., Yang, Y. H. (2009). Amalgamation between the Yangtze and Cathaysia blocks in South China: Constraints from SHRIMP U–Pb zircon ages, geochemistry and Nd–Hf isotopes of the Shuangxiwu volcanic rocks. *Precambrian Research*, 174, 117–128.
- Li, X. H., Li, Z. X., Li, W. X. (2014). Detrital zircon U–Pb age and Hf isotope constrains on the generation and reworking of Precambrian continental crust in the Cathaysia Block, South China: A synthesis. *Gondwana Research*, 25 (3), 1202–1215.
- Li, Z. X., Li, X. H., Zhou, H., Kinny, P. D. (2002). Grenville–aged continental collision in South China: new SHRIMP U–Pb zircon results and implications for Rodinia configuration. *Geology*, 30, 163–166.

- Li, Z.X., Li, X.H., Kinny, P.D., Wang, J., Zhang, S., Zhou, H.W. (2003b). Geochronology of Neoproterozoic syn–rift magmatism in the Yangtze Craton, South China and correlations with other continents: evidence for a mantle superplume that broke up Rodinia. *Precambrian Research*, 122, 85–109.
- Li, Z.X., & Li, X.H., (2007). Formation of the 1300–km–wide intracontinental orogen and post–orogenic magmatic province in mesozoic south china : a flat–slab subduction model. *Geology*, 35(2), 179–182.
- Li, Z.X., Wartho, J.–A., Occhipinti, S., Zhang, C.L., Li, X.H., Wang, J., Bao, C. (2007). Early history of the eastern Sibao orogen (South China) during the assembly of Rodinia: new mica $^{40}\text{Ar}/^{39}\text{Ar}$ dating and SHRIMP U–Pb detrital zircon provenance constraints. *Precambrian Research*, 159 (1–2), 79–94.
- Li, Z.X., Bogdanova, S.V., Collins, A.S., Davidson, A., De Waele, B., Ernst, R.E., Fitzsimons, I.C.W., Fuck, R.A., Gladkochub, D.P., Jacobs, J., Karlstrom, K.E., Lu, S., Natapov, L.M., Pease, V., Pisarevsky, S.A., Thrane, K., Vernikovsky, V. (2008b). Assembly, configuration, and break–up history of Rodinia: A synthesis. *Precambrian Research*, 160, 179–210.
- Lin, W., Wang, Q.C., Chen. K. (2008). Phanerozoic tectonic of South China block: New insights from the polyphase deformation in the Yunkai massif, *Tectonics*, 27, TC6004, doi:10.1029/2007TC002207.
- Lister, G.S., & Baldwin, S.L. (1996). Modelling the effect of arbitrary PTt histories on argon diffusion in minerals using the MacArgon program for the Apple Macintosh. *Tectonophysics*, 253, 83–109.
- Liu, H. S. (2017). Emplacement mechanism of the Jurassic granitic magma in South China and its geodynamic implications. Ph.D thesis, Nanjing University.
- Liu, Y. S., Gao, S., Hu, Z. C., Gao, C. G., Zong, K. Q., Wang, D. B. (2010). Continental and oceanic crust recycling–induced melt–peridotite interactions in the trans–north china orogen: U–Pb dating, Hf isotopes and trace elements in zircons

- from mantle xenoliths. *Journal of Petrology*, 51, 537–571.
- Liu, Z., Jiang, Y. H., Wang, G. C., Ni, C. Y., Qing, L., Zhang, Q. (2015). Middle Neoproterozoic (~845 Ma) continental arc magmatism along the northwest side of the Jiangshan–Shaoxing suture, South China: geochronology, geochemistry, petrogenesis and tectonic implications. *Precambrian Research*, 268, 212–226.
- Martelet, G., J. Perrin, C. Truffert, and J. Deparis (2013). Fast mapping of magnetic basement depth, structure and nature using aeromagnetic and gravity data: combined methods and their application in the Paris Basin, *Geophysical Prospecting*, 61(4), 857–873, doi:10.1111/1365–2478.12024.
- Martín–Hernández, F., Lüneburg, C. M., Aubourg, C., Jackson, M. (2004). Magnetic fabric: methods and applications—an introduction. Geological Society, London, Special Publications, 238(1), 1–7.
- Martinez–Catalan, J. R., Rubio Pascual, F. J., Díez Montes A., Díez Fernández, R., Gómez Barreiro, J., Dias Da Silva, I., et al. (2014). The late Variscan HT/LP metamorphic event in NW and central Iberia: Relationships with crustal thickening, extension, orocline development, and crustal evolution. In « The Variscan Orogeny: Extent, Timescale and the Formation of the European Crust », Schulmann, K., Martínez Catalán, J. R., Lardeaux, J. M., Janousek, V. Oggiano, G. (eds). Geological Society, London, Special Publications, 405, 289–311.
- Mathieu, L., De Vries, B. V. W., Holohan, E. P., Troll, V. R. (2008). Dykes, cups, saucers and sills: Analogue experiments on magma intrusion into brittle rocks. *Earth and Planetary Science Letters*, 271(1), 1–13.
- McDougall, I., & Harrison, T.M. (1999). *Geochronology and Thermochronology by the $^{40}\text{Ar}/^{39}\text{Ar}$ Method*, Oxford University Press, Oxford, 252 pp.
- Morgan, S., Jones, R., Conner, J., Student, J., Schaner, M., Horsman, E., de Saint Blanquat, M. (2017). Magma sheets defined with magnetic susceptibility in the Maiden Creek sill, Henry Mountains, Utah, USA. *Geology*, 45(7), 599–602.

- Moyen, J. F., Martin, H., Jayananda, M., Auvray, B. (2003). Late Archaean granites: a typology based on the Dharwar Craton (India). *Precambrian Research*, 127(1), 103–123.
- O'Driscoll, B., Troll, V. R., Reavy, R. J., Turner, P. (2006). The Great Eucrite intrusion of Ardnamurchan, Scotland: Reevaluating the ring–dike concept. *Geology*, 34(3), 189–192.
- Paterson S. R., Vernon R. H., Tobisch O. T., (1989). A review of criteria for the identification of magmatic and tectonic foliations in granitoids[J]. *Journal of structural geology*, 11(3): 349–363.
- Paterson, S.R., & Vernon, R.H., (1995). Bursting the bubble of ballooning plutons: A return tonested diapirs emplaced by multiple processes. *Geological Society of America Bulletin*, 107, 1356–1380.
- Paterson, S. R., Pignotta, G. S., Farris, D., Memeti, V., Miller, R. B., Vernon, R. H., Žák, J. (2008). Is stoping a volumetrically significant pluton emplacement process?: Discussion. *Geological Society of America Bulletin*, 120(7–8), 1075–1079.
- Paterson, S. R. (2009). Magmatic tubes, pipes, troughs, diapirs, and plumes: Late–stage convective instabilities resulting in compositional diversity and permeable networks in crystal–rich magmas of the Tuolumne batholith, Sierra Nevada, California. *Geosphere*, 5(6), 496–527.
- Pitcher, W.S., (1979). The nature, ascent and emplacement of granitic magmas. *Journal of the Geological Society*, 136, 627–662.
- Proyer, A. (2003). Metamorphism of pelites in NKFMASH—a new petrogenetic grid with implications for the preservation of high–pressure mineral assemblages during exhumation. *Journal of metamorphic Geology*, 21, 493–509.
- Renne, P.R., Swisher, C.C., Deino, A.L., Karner, D.B., Owens, T.L., DePaolo, D.J.

- (1998). Intercalibration of standards, absolute ages and uncertainties in $^{40}\text{Ar}/^{39}\text{Ar}$ dating *Chem. Geol.*, 145, 117–152.
- Rochette, P., Jackson, M., Aubourg, C. (1992). Rock magnetism and the interpretation of anisotropy of magnetic susceptibility. *Reviews of Geophysics*, 30, 209–226.
- Rogers, J. J. W., & Santosh, M. (2002). Configuration of Columbia, a Mesoproterozoic Supercontinent. *Gondwana Research*, 5, 5–22.
- Roman, A., & Jaupart, C. (2016). The fate of mafic and ultramafic intrusions in the continental crust. *Earth and Planetary Science Letters*, 453, 131–140.
- Ruffet, G., Gruau, G., Ballèvre, M., Féraud, G., Philippot, P. (1997). Rb/Sr and $^{40}\text{Ar}/^{39}\text{Ar}$ laser probe dating of high-pressure phengites from the Sesia zone (Western Alps): underscoring of excess argon and new age constraints on the high-pressure metamorphism. *Chemical Geology*, 141, 1–18.
- Scaillet, B., Pichavant, M., Roux, J., Humbert, G., Lefevre, A. (1992). Improvements of the Shaw membrane technique for measurement and control of f_{H_2} at high temperatures and pressures. *American Mineralogist*, 77, 647–655.
- Scaillet, S. (1996). Excess ^{40}Ar transport scale and mechanism in high-pressure phengites: A case study from an eclogitised metabasite of the Dora-Maira nappe, western Alps. *Geochim Cosmochim Acta*, 60, 1075–1090.
- Scaillet, S. (1998). K–Ar ($^{40}\text{Ar}/^{39}\text{Ar}$) geochronology of ultrahigh pressure rocks, in: *When Continents Collide: Geodynamics and Geochemistry of Ultrahigh-Pressure Rocks*. Springer, pp. 161–201.
- Scaillet, S., (2000). Numerical error analysis in $^{40}\text{Ar}/^{39}\text{Ar}$ dating, *Chem. Geol. (Isot. Geosci. Sec.)*, 162, 269–298.
- Scherer, E., Munker, C., Mezger, K. (2001). Calibration of the Lutetium–Hafnium clock. *Science* 293, 683–687.
- Senshu, H., Maruyama, S., Rino, S., Santosh, M. (2009). Role of

- tonalite–trochilite–granite (TTG) crust subduction on the mechanism of supercontinent breakup. *Gondwana Research*, 15(3–4), 433–442.
- Shu, L.S. (2012). An analysis of principal features of tectonic evolution in South China Block. *Geological Bulletin of China*, 31 (7), 1035–1053 (in Chinese with English abstract).
- Shu, L.S., Zhou, W.Q., Shi, Y.S., Yin, J. (1993). Study of high pressure metamorphic blueschist and its late Proterozoic age in the eastern Jiangnan belt. *Chin. Sci. Bull.*, 38, 1879–1882 (in Chinese with English Abstract).
- Shu, L. S., Zhou, G. Q., Shi, Y. S., Yin, J. (1994). Study on the high pressure metamorphic blueschist and its Late Proterozoic age in the Eastern Jiangnan belt. *Chinese Science Bulletin*, 39, 1200–1204.
- Shu, L. S., Shi, Y. S., Guo, L. Z., Charvet, J., Sun, Y. (1995). Plate Tectonic Evolution and the Kinematics of Collisional Orogeny in the Middle Jiangnan, Eastern China [in Chinese with English abstract]. Publishing House of Nanjing University, pp. 1–174.
- Shu, L. S., & Charvet, J. (1996). Kinematic and geochronology of the Proterozoic Dongxiang–Shexian ductile shear zone (Jiangnan region), South China. *Tectonophysics*, 267(1–4), 291–302.
- Shu, L.S., Lu, H.F., Jia, D., Charvet, J., Faure, M. (1999). Study of the $^{40}\text{Ar}/^{39}\text{Ar}$ isotopic age for the early Paleozoic tectonothermal event in the Wuyishan region, South China. *J. Nanjing Univ. Nat. Sci.*, 35 (6), 668–674 (in Chinese with English abstract).
- Shu, L.S. (2006). Pre–Devonian tectonic evolution of South China: from Cathaysia Block to Caledonian period folded Orogenic Belt. *Geological Journal of China Universities (Earth Sci.)* 12 (4), 418–431 (in Chinese with English abstract).
- Shu, L.S., Yu, J.H., Jia, D., Wang, B., Shen, W.Z., Zhang, Y.Q. (2008). Early Paleozoic

- orogenic belt in the eastern segment of South China. *Geological Bulletin of China*, 27 (10), 1581–1593 (in Chinese with English abstract).
- Shu, L.S., Jahn, B.M., Charvet, J., Santosh, M., Wang, B., Xu, X.S., Jiang, S.Y. (2014). Early Paleozoic depositional environment and intracontinental orogeny in the Cathaysia Block (South China): implications from stratigraphic, structural, geochemical and geochronologic evidence. *American Journal of Science*, 314 (1), 154–186.
- Shu, L.S., Wang, B., Cawood P.A., Santosh, M., Xu, Z.Q. (2015). Early Paleozoic and early Mesozoic intraplate tectonic and magmatic events in the Cathaysia Block, South China. *Tectonics*, 34 (8), 1600–1621.
- Simpson, C. and Wintsch, R. P. (1989). Evidence for deformation–induced K–feldspar replacement by myrmekite. *J. Metam. Geol.*, 7, 261–275.
- Singh, P. (2009). Major, trace and REE geochemistry of the Ganga River sediments: Influence of provenance and sedimentary processes. *Chemical Geology*, 266, 242–255.
- Stevenson, C. T., Owens, W. H., Hutton, D. H., Hood, D. N., Meighan, I. G. (2007). Laccolithic, as opposed to cauldron subsidence, emplacement of the Eastern Mourne pluton, N. Ireland: evidence from anisotropy of magnetic susceptibility. *Journal of the Geological Society*, 164(1), 99–110.
- Sun, W.H., Zhou, M.F., Gao, J.F., Yang, Y.H., Zhao, X.F., Zhao, J.H. (2009). Detrital zircon U–Pb geochronological and Lu–Hf isotopic constraints on the Precambrian magmatic and crustal evolution of the western Yangtze Block, SW China. *Precambrian Research*, 172, 99–126.
- Su, H. M., Jiang, S. Y., Mao, J. W., Zhang, D. Y., Wu, X. K., Qin, H. F. (2018). U–Pb Ages and Lu–Hf Isotopes of Detrital Zircons from Sedimentary Units across the Mid–Neoproterozoic Unconformity in the Western Jiangnan Orogen of South China and Their Tectonic Implications. *Journal of Geology*, 126, 207–228.

- Sun, J. J., Shu, L. S., Santosh, M., Wang, L. S. (2017). Neoproterozoic tectonic evolution of the Jiuling terrane in the central Jiangnan orogenic belt (South China): Constraints from magmatic suites. *Precambrian Research*, 302, 279–297.
- Sun, S. S., & McDonough, W. F. (1989). Chemical and isotopic systematics of oceanic basalts: implication for mantle composition and processes. *Geological Society of London*, 42(1), 313–345.
- Tarling, D., & F. Hrouda. (1993). *Magnetic anisotropy of rocks*, Springer Science & Business Media.
- Taylor, S. R., & McLennan, S. M. (1981). The composition and evolution of the continental crust: rare earth element evidence from sedimentary rocks [and discussion]. *Philosophical Transactions of the Royal Society A*, 301(1461), 381–399.
- Villa, I.M. (1998). Isotopic closure. *Terra Nova–Oxford*, 10, 42–47.
- Wang, J., & Li, Z. X. (2003). History of Neoproterozoic rift basins in South China: implications for Rodinia break-up. *Precambrian Research*, 122, 141–158.
- Wang, M., Dai, C. G., Wang, X. H., Chen, J. S., Ma, H. Z. (2011). In-situ zircon geochronology and Hf isotope of muscovite-bearing leucogranites from Fanjingshan, Guizhou Province, and constraints on continental growth of the Southern China block [in Chinese with EnglishAbstract]. *Earth Science Frontiers*, 18 (5), 213–223.
- Wang, W., Wang, F., Chen, F., Zhu, X., Xiao, P., Siebel, W. (2010a). Detrital zircon ages and Hf–Nd isotopic composition of Neoproterozoic sedimentary rocks in the Yangtze block: constraints on the deposition age and provenance. *The Journal of Geology*, 118, 79–94.
- Wang, W., Zhou, M. F., Yan, D. P., Li, J. W. (2012a). Depositional age, provenance, and tectonic setting of the Neoproterozoic sibao group, southeastern Yangtze

- block, South China. *Precambrian Research*, 192(1), 107–124.
- Wang, X. C., Li, X. H., Li, W. X., Li, Z. X. (2009). Variable involvements of mantle plumes in the genesis of mid–neoproterozoic basaltic rocks in south china: a review. *Gondwana Research*, 15(3), 381–395.
- Wang, X.L., Zhou, J.C., Qiu, J.S., Zhang, W.L., Liu, X.M., Zhang, G.L. (2006). LA–ICP–MS U–Pb zircon geochronology of the Neoproterozoic igneous rocks from Northern Guangxi, South China: implications for petrogenesis and tectonic evolution. *Precambrian Research*, 145 (1–2), 111–130.
- Wang, X.L., Zhou, J.C., W.L. Griffin, Wang, R.C., Qiu, J.S., S.Y. O’Reilly, Xu, X.S., Liu, X.M., Zhang, G.L. (2007a). Detrital zircon geochronology of Precambrian basement sequences in the Jiangnan orogen: dating the assembly of the Yangtze and Cathaysia Blocks. *Precambrian Research*, 159 (1–2), 117–131.
- Wang, X. L., Zhao, G. C., Zhou, J. C., Liu, Y. S., Hu, J. (2008). Geochronology and Hf isotopes of zircon from volcanic rocks of the Shuangqiaoshan Group, South China: Implications for the Neoproterozoic tectonic evolution of the eastern Jiangnan orogen. *Gondwana Research*, 14, 355–367.
- Wang, X. L., Shu, L. S., Xing, G. F., Zhou, J. C., Tang, M., Shu, X. J., et al. (2012b). Post–orogenic belt extension in the eastern part of the Jiangnan Orogenic belt: evidence from ca 800–760 Ma volcanic rocks. *Precambrian Research*, 222–223, 404–423.
- Wang, Y. J., Y. H. Zhang, W. M. Fan, and T. P. Peng. (2005), Structural signatures and $^{40}\text{Ar}/^{39}\text{Ar}$ geochronology of the Indosinian Xuefengshan transpressive belt, south China interior, *J. Struct. Geol.*, 27, 985–998.
- Wang, Y., W. Fan, P. A. Cawood, S. Ji, T. Peng, and X. Chen. (2007b), Indosinian high–strain deformation for the Yunkaidashan tectonic belt, south China: Kinematics and $^{40}\text{Ar}/^{39}\text{Ar}$ geochronological constraints, *Tectonics*, 26, TC6008, doi:10.1029/2007TC002099.

- Wang, Z., Xu, D., Hu, G., Yu, L., Wu, C., & Zhang, Z., et al. (2015). Detrital zircon U–Pb ages of the Proterozoic metaclastic–sedimentary rocks in Hainan province of south china: new constraints on the depositional time, source area, and tectonic setting of the shilu Fe–Co–Cu ore district. *Journal of Asian Earth Sciences*, 113, 1143–1161.
- Wei, W., Chen, Y., Faure, M., Shi, Y.H., Martelet, G., Hou, Q.L., Lin, W., Le Breton, N., Wang, Q.C. (2014). A multidisciplinary study on the emplacement mechanism of the Qingyang–Jiuhua Massif in Southeast China and its tectonic bearings. Part I: Structural geology, AMS and paleomagnetism. *Journal of Asian Earth Sciences*, 86, 76–93.
- Wei, W., Chen, Y., Faure, M., Martelet, G., Lin, W., Wang, Q., Yan, Q., Hou, Q. (2016). An early extensional event of the South China Block during the Late Mesozoic recorded by the emplacement of the Late Jurassic syntectonic Hengshan Composite Granitic Massif (Hunan, SE China). *Tectonophysics*, 672–673, 50–67.
- Weinberg, R. F. (1999). Mesoscale pervasive felsic magma migration: alternatives to dyking. *Lithos*, 46(3), 393–410.
- Wiedenbeck, M., Alle, P., Corfu, F., Griffin, W.L., Meier, M., Oberli, F., et al. (1995). Three natural zircon standards for U–Th–Pb, Lu–Hf, trace element and REE analyses. *Geostand. Newslett.*, 19(1), 1–23.
- Wijbrans, J.R., Schliestedt, M., York, D. (1990). Single grain argon laser probe dating of phengites from the blueschist to greenschist transition on Sifnos (Cyclades, Greece). *Contributions to Mineralogy and Petrology*, 104, 582–593.
- Wu, R. X., Zheng, Y. F., Wu, Y. B., Zhao, Z. F., Zhang, S. B., Liu, X. M., Wu, F. Y. (2006). Reworking of juvenile crust: Element and isotope evidence from Neoproterozoic granodiorite in South China. *Precambrian Research*, 146, 179–212.
- Wu, Y. B., & Zheng, Y. F. (2004). Zircon genetic mineralogy study and constraint on

- the interpretation of the U–Pb age. *Chinese Science Bulletin*, 16(49), 1589–1604.
- Wu, T., Zhou, J. X., Wang, X. C., Li, W. X., Wilde, S. A., Sun, H. R., et al. (2018). Identification of ca. 850 Ma high–temperature strongly peraluminous granitoids in southeastern Guizhou Province, South China: A result of early extension along the southern margin of the Yangtze Block. *Precambrian Research*, 308, 18–34.
- Xia, Y., Xu, X. S., Zhao, G. C., Liu, L. (2015). Neoproterozoic active continental margin of the Cathaysia block: Evidence from geochronology, geochemistry, and Nd–Hf isotopes of igneous complexes. *Precambrian Research*, 269, 195–216.
- Xia, Y., Xu, X. S., Niu, Y. L., Liu, L. (2018). Neoproterozoic amalgamation between Yangtze and Cathaysia blocks: The magmatism in various tectonic settings and continent–arc–continent collision. *Precambrian Research*, 309, 56–87.
- Xin, Y., Li, J., Dong, S., Zhang, Y., Wang, W., Sun, H. (2017). Neoproterozoic post–collisional extension of the central Jiangnan Orogen: Geochemical, geochronological, and Lu–Hf isotopic constraints from the ca. 820–800 Ma magmatic rocks. *Precambrian Research*, 294, 91–110.
- Xu, X. B., Zhang, Y. Q., Shu, L. S., Jia, D., Wang, R. R., Xu, H. Z. (2010). Precambrian geochronology and stratigraphy in the Wuyishan area, South China [in Chinese with English abstract]. *Journal of Stratigraphy*, 34(3), 254–267.
- Xu, X., Li, Y., Tang, S., Xue, D., Zhang, Z. (2015). Neoproterozoic to early Paleozoic polyorogenic deformation in the southeastern margin of the Yangtze block: constraints from structural analysis and $^{40}\text{Ar}/^{39}\text{Ar}$ geochronology. *Journal of Asian Earth Sciences*, 98, 141–151.
- Xu, X.S., O'Reilly, S.Y., Griffin, W.L., Wang, X., Pearson, N.J., He, Z. (2007). The crust of Cathaysia: age, assembly and reworking of two terranes. *Precambrian Research* 158, 51–78.
- Xue, H. M., Ma, F., Song, Y. Q., Xie, Y. P. (2010). Geochronology and geochemistry of

- the Neoproterozoic granitoid association from eastern segment of the Jiangnan orogen, China: Constraints on the timing and process of amalgamation between the Yangtze and Cathaysia blocks [in Chinese with English abstract]. *Acta Geologica Sinica*, 26, 3215–3244.
- Xue, Z., Martelet, G., Lin, W., Faure, M., Chen, Y., Wei, W., et al. (2017). Mesozoic crustal thickening of the longmenshan belt (ne tibet, china) by imbrication of basement slices: insights from structural analysis, petrofabric and magnetic fabric studies, and gravity modeling. *Tectonics*, 36 (12), 3110–3134.
- Yan, C. L., Shu, L. S., Santosh, M., Yao, J. L., Li, J. Y., Li, C. (2015). The Precambrian tectonic evolution of the western Jiangnan Orogen and western Cathaysia Block: Evidence from detrital zircon age spectra and geochemistry of clastic rocks. *Precambrian Research*, 268, 33–60.
- Yan, C. L., Shu, L. S., Faure, M., Chen, Y., Li, C. (2017). Early Paleozoic intracontinental orogeny in the Yunkai domain, South China Block: New insights from field observations, zircon U–Pb geochronological and geochemical investigations. *Lithos*, 268–271, 320–333.
- Yang, C., Li, X. H., Wang, X. C., Lan, Z. (2015). Mid–neoproterozoic angular unconformity in the yangtze block revisited: insights from detrital zircon u–pb age and hf–o isotopes. *Precambrian Research*, 266, 165–178.
- Yao, J. L., Shu, L. S., Santosh, M. (2011). Detrital zircon U–Pb geochronology, Hf–isotopes and geochemistry–new clues for the Precambrian crustal evolution of Cathaysia block South China. *Gondwana Research*, 20, 553–567.
- Yao, J.L., Shu, L.S., M. Santosh, Li, J.Y. (2012). Precambrian crustal evolution of the South China Block and its relation to supercontinent history: Constraints from U–Pb ages, Lu–Hf isotopes and REE geochemistry of zircons from sandstones and granodiorite. *Precambrian Research*, 208–211, 19–48.
- Yao, J.L., Shu, L.S., M. Santosh, Li, J.Y. (2013). Geochronology and Hf isotope of

- detrital zircons from Precambrian sequences in the eastern Jiangnan Orogen: Constraining the assembly of Yangtze and Cathaysia Blocks in South China. *Journal of Asian Earth Sciences*, 74, 225–243.
- Yao, J.L., Shu, L.S., M. Santosh, Zhao, G.C. (2014a). Neoproterozoic arc-related mafic-ultramafic rocks and syn-collision granite from the western segment of the Jiangnan Orogen, South China: Constraints on the Neoproterozoic assembly of the Yangtze and Cathaysia Blocks. *Precambrian Research*, 243, 39–62.
- Yao, J.L., Shu, L.S., Santosh, M., Zhao, G.C. (2014b). Neoproterozoic arc-trench system and breakup of the South China Craton: Constraints from N-MORB type and arc-related mafic rocks, and anorogenic granite in the Jiangnan orogenic belt. *Precambrian Research*, 247, 187–207.
- Yao, J., Shu, L., Santosh, M. (2014c). Neoproterozoic arc-trench system and breakup of the south china craton: constraints from n-morb type and arc-related mafic rocks, and anorogenic granite in the jiangnan orogenic belt. *Precambrian Research*, 247(247), 187–207.
- Yao, J. L., Cawood, P. A., Shu, L. S., Santosh, M., Li, J. Y. (2016a). An early Neoproterozoic accretionary prism ophiolitic Mélange from the Western Jiangnan Orogenic Belt, South China. *Journal of Geology*, 124, 587–601.
- Yao, J., Shu, L., Cawood, P. A., Li, J. (2016b). Delineating and characterizing the boundary of the cathaysia block and the jiangnan orogenic belt in south china. *Precambrian Research*, 275, 265–277.
- Yao, J.L., Shu, L.S., Cawood, P.A., Li, J.Y. (2017). Constraining timing and tectonic implications of neoproterozoic metamorphic event in the cathaysia block, south china. *Precambrian Research*, 293, 1–12.
- Ye, M. F., Li, X. H., Li, W. X., Liu, Y., Li, Z. X. (2007). SHRIMP zircon U–Pb geochronological and whole-rock geochemical evidence for an early Neoproterozoic Sibaoan magmatic arc along the southeastern margin of the

- Yangtze Block. *Gondwana Research*, 12, 144–156.
- Yu, J. H., Wang, L. J., Zhou, X. M., Jiang, S. Y., Wang, R. C., Xu, X. S., Qiu, J. S. (2006). Compositions and formation history of the basement metamorphic rocks in northeastern Guangdong province [In Chinese with English abstract]. *Earth Science*, 31, 38–48.
- Yu, J.H., Wang, L.J., O'Reilly, S.Y., Griffin, W.L., Zhang, M., Li, C.Z., Shu, L.S. (2009). A Paleoproterozoic orogeny recorded in a long-lived cratonic remnant (Wuyishan terrane), eastern Cathaysia Block, China. *Precambrian Research*, 174, 347–363.
- Yuan, H.L., Gao, S., Dai, M.N., Zong, C.L., Günther, D., Fontaine, G.H., Liu, X.M., DiWu, C.R. (2008). Simultaneous determinations of U–Pb age, Hf isotopes and trace element compositions of zircon by excimer laser ablation quadrupole and multiple collector ICP–MS. *Chemical Geology*, 247 (1–2), 100–118.
- Žák, J., Paterson, S. R., Memeti, V. (2007). Four magmatic fabrics in the Tuolumne batholith, central Sierra Nevada, California (USA): implications for interpreting fabric patterns in plutons and evolution of magma chambers in the upper crust. *Geological Society of America Bulletin*, 119(1–2), 184–201.
- Zhang, C. L., Santosh, M., Zou, H. B., Li, H. K., Huang, W. C. (2013). The Fuchuan ophiolite in Jiangnan Orog Geochemistry, zircon U–Pb geochronology, Hf isotope, implications for the Neoproterozoic assembly of South, China. *Lithos*, 179, 263–274.
- Zhang, F. F., Wang, X. L., Sun, Z. M., Chen, X., Zhou, X. H., Yang, T. (2018). Geochemistry and zircon–apatite U–Pb geochronology of mafic dykes in the Shuangxiwu area: constraints on the initiation of Neoproterozoic rifting in South China. *Precambrian Research*, 309, 138–151.
- Zhang, K.J., & Cai, J.X. (2009). NE–SW–trending Hepu–Hetai dextral shear zone in southern China: penetration of the Yunkai Promontory of South China into

- Indochina. *J. Struct. Geol.*, 31, 737–748.
- Zhang, S.B., Zheng, Y.F., Wu, Y.B., Zhao, Z.F., Gao, S., Wu, F.Y. (2006). Zircon U–Pb age and Hf–O isotope evidence for Paleoproterozoic metamorphic event in South China. *Precambrian Research*, 151, 265–288.
- Zhang, Q., & Zhai, M. G. (2012). What is the Archean TTG? *Acta Petrologica Sinica*, 28(1), 3446–3456.
- Zhang, Y. Z., & Wang, Y. J. (2016). Early Neoproterozoic (~840 Ma) arc magmatism: geochronological and geochemical constraints on the meta–basites in the Central Jiangnan orogenic belt. *Precambrian Research*, 275, 1–17.
- Zhao, G. C., Cawood, P. A., Wilde, S. A., Sun, M. (2002). Review of global 2.1–1.8 Ga collisional orogens and accreted cratons: a pre–Rodinia supercontinent? *Earth Science Reviews*, 59, 125–162.
- Zhao, G.C., & Cawood, P.A., (2012). Precambrian geology of China. *Precambrian Research* 222, 13–54.
- Zhao, J. H., Zhou, M. F., Zheng, J. P. (2013). Constraints from zircon U–Pb ages, O and Hf isotopic compositions on the origin of Neoproterozoic peraluminous granitoids from the Jiangnan Fold Belt, South China. *Contributions to Mineralogy and Petrology*, 166, 1505–1519.
- Zheng, J.P., Griffin, W.L., O'Reilly, S.Y. (2006). Widespread Archean basement beneath the Yangtze craton. *Geology*, 34, 417–420.
- Zheng, Y. F., Wu, R. X., Wu, Y. B., Zhang, S. B., Yuan, H. L., Wu, F. Y. (2008). Rift melting of juvenile arc–derived crust: geochemical evidence from Neoproterozoic volcanic and granitic rocks in the Jiangnan orogen, South China. *Precambrian Research*, 163, 351–383.
- Zhong, Y. F., Ma, C. Q., She, Z. B., Lin, G. C., Xu, H. J., Wang, R. J., et al. (2005). SHRIMP U–Pb zircon geochronology of the Jiuling granitic complex batholith in

- Jiangxi Province [in Chinese with English abstract]. *Earth Science–Journal of China University of Geosciences*, 30, 685–591.
- Zhou, J.B., Li, X.H., Ge, W.C., Li, Z.X. (2007). Age and origin of middle neoproterozoic mafic magmatism in southern yangtze block and relevance to the break-up of rodinia. *Gondwana Research*, 12(1), 184–197.
- Zhou, J.C., Wang, X.L., Qiu, J.S., Gao, J.F. (2004). Geochemistry of meso- and neoproterozoic mafic-ultramafic rocks from northern guangxi, china : arc or plume magmatism?. *Geochemical Journal Gj*, 38(2), 139–152.
- Zhou, J.C., Wang, X.L., Qiu, J.S. (2009). Geochronology of Neoproterozoic mafic rocks and sandstones from northeastern Guizhou, South China: Coeval arc magmatism and sedimentation. *Precambrian Research*, 170, 27–42.
- Zhou, X. M., Zhou, H. B., Yang, J. D., Wang, Y. X. (1989). Sm–Nd isochron age of the ophiolite suite in Shexian county, Anhui province and its geological significance. *Chinese Science Bulletin*, 35, 208–212.
- Zhu, B.Q., Wang, Y.X., Wang, H.F., Chen, D.G., Chen,, D.f. (1997). Huangshan–Wenzhou geochemical section and its corridor area of lithosphere in southeast China. *Geochimica*, 26 (2), 1–13 (in Chinese with English abstract).

Publications

1. **Yan, C. L.**, Shu, L. S., Santosh, M., Yao, J. L., Li, J. Y., Li, C. (2015). The Precambrian tectonic evolution of the western Jiangnan Orogen and western Cathaysia Block: Evidence from detrital zircon age spectra and geochemistry of clastic rocks. **Precambrian Research**, 268, 33–60.
2. **Yan, C. L.**, Shu, L. S., Faure, M., Chen, Y., Li, C. (2017). Early Paleozoic intracontinental orogeny in the Yunkai domain, South China Block: New insights from field observations, zircon U–Pb geochronological and geochemical investigations. **Lithos**, 268–271, 320–333.
3. **Yan, C. L.**, Shu, L. S., Faure, M., Chen, Y., Huang, R. B. (2018). Time constraints on the closure of the Paleo–South China Ocean and the Neoproterozoic assembly of the Yangtze and Cathaysia blocks: insight from new detrital zircon analyses. **Tectonics** (Under review).
4. **Yan, C. L.**, Shu, L. S., Chen, Y., Faure, M. (2018). The construction mechanism of the Neoproterozoic S-type Sanfang-Yuanbaoshan granite plutons in the Jiangnan Orogenic Belt, South China: insights from the Geological observation, Geochronology, AMS and Bouger gravity modelling (In preparation).
5. **Yan, C. L.**, Shu, L. S., Scaillet, S., Chen, Y., Faure, M. (2018). Early Paleozoic to Triassic geological events in the Sanfang-Yuanbaoshan, western Jiangnan region: the Argon isotopic record (In preparation).

Evolution tectonique Néoproterozoïque de la chaîne de Jiangnan Occidental et sa réactivation au Paléozoïque inférieur-Mésozoïque

La chaîne de collision d'âge néoproterozoïque de Jiangnan, orientée NE-SW, marque la limite entre les blocs du Yangtze et de Cathaysia. Son évolution tectonique reste encore débattue. Une des questions les plus controversées est l'âge de la collision entre les deux blocs. Afin d'acquérir une meilleure compréhension de ce problème, nous avons collecté des échantillons dans les couches sédimentaires situées au dessus et au dessous de la discordance dans le but de comparer les spectres d'âge des zircons détritiques et aussi de les confronter à ceux décrits dans les séries néoproterozoïques des régions du Yangtze, Jiangnan et Cathaysia. En outre, nous nous sommes intéressés aux plutons granitiques d'âge néoproterozoïque de Sanfang et Yuanbaoshan, de type-S, situés dans la partie occidentale de la chaîne de Jiangnan afin de tracer l'évolution tectonique de la région depuis 830 Ma par la mise en œuvre de méthodes pluridisciplinaires: géologie structurale, géochronologie U-Pb, AMS, modélisation gravimétrique et thermochronologie Argon.

Notre étude montre les résultats suivants: (i) La chaîne de Jiangnan s'est formée par la collision des blocs de Yangtze et Cathaysia entre ca. 865 and 830 Ma; (ii) Les intrusions granitiques de 830 Ma se sont mises en place dans des formations encaissantes du groupe Sibao plissées et faillées. Les plutons ont été construits par accumulation latérale E-W de filons N-S, avec un écoulement horizontal du magma du sud vers le nord; (iii) Un cisaillement ductile du haut vers l'Ouest a été reconnu dans la partie supérieure des plutons. Des âges Ar/Ar vers 420 Ma obtenus sur plusieurs grains de muscovite et biotite déformés impliquent que le cisaillement ductile peut être: a) formé pendant l'orogénèse du Paléozoïque inférieur de Chine du Sud, ou b) pendant la mise en place des plutons au Néoproterozoïque dans une croûte chaude, sous la température de fermeture du chronomètre argon, puis lors de l'orogénèse du Paléozoïque inférieur, ce domaine crustal de Chine du Sud est passé au dessous de 350°C; (iv) Durant la période 420-240 Ma, la région de Sanfang-Yuanbaoshan a connu un refroidissement lent qui pourrait correspondre au ré-équilibre isostatique de la croûte.

Mots clés: Orogène de Jiangnan, Discordance Néoproterozoïque; granite de type S; AMS; Modélisation gravimétrique; datation Ar-Ar.

The Neoproterozoic tectonic evolution of the western Jiangnan Orogenic Belt and its early Paleozoic-Mesozoic tectonic reworking

The Jiangnan Orogenic Belt is a NE-SW trending Neoproterozoic collisional suture, marking the boundary between the Yangtze Block and the Cathaysia Block. Its tectonic evolution is still debated. One of the most controversial questions is the timing of the collision between the Yangtze and Cathaysia blocks. In order to have a better understanding of this problem, we have collected the sedimentary rocks from the strata both overlying and underlying the Neoproterozoic unconformities to compare the detrital zircon age spectra between them, as well as to compare the detrital zircon spectra of Neoproterozoic sequences among the Yangtze, Jiangnan and Cathaysia regions. Moreover, we paid attention to the Neoproterozoic S-type granite plutons located in the western Jiangnan region in order to trace the crustal evolution in the Sanfang-Yuanbaoshan area since 830 Ma by multidisciplinary methods, including structural geology, geochronology, AMS, gravity modelling and Argon isotopic dating.

Our study shows that: (i) The Jiangnan Orogenic Belt was built up due to the assembly of the Yangtze and Cathaysia blocks between ca. 865 and 830 Ma; (ii) The 830 Ma granitic magma intruded into the pre-existing folds and faults in the Sibao group, the tongue- and/or sill-shaped plutons were constructed by an E-W lateral accumulation of N-S oriented dykes with a dominantly northward horizontal magma flow from south to north; (iii) A top-to-the-W ductile shear band has been identified on the top of plutons, (iv) the coherent mica Ar-Ar age of ca. 420 Ma, obtained from the deformed muscovite, implies that this shearing may be formed either a) during the Early Paleozoic orogeny, or b) during the Neoproterozoic plutons emplacement, then the plutons were exhumed by the Paleozoic orogeny; (iv) During the 420-240 Ma period, the Sanfang-Yuanbaoshan area has experienced a slow cooling rate, which may correspond to the isostatic re-equilibration of the crust.

Keywords: Jiangnan Orogenic Belt, Neoproterozoic unconformity; S-type granite; AMS; Gravity modelling; Ar-Ar dating